Cryo-electron microscopy structural characterization of outer dynein arm and the role of post-translational modification in eukaryotic cilia

by

© Shun Kai Yang (Sky) 楊舜凱

Department of Anatomy and Cell Biology

McGill University, Montreal

A thesis submitted to McGill University in partial fulfillment of the requirements for the Degree of Doctor of Philosophy in Anatomy and Cell Biology

on

Table of Contents

Abstract

Cilia are microtubules-based organelles that protrude outside of almost every eukaryotic cells. Cilia are the main players in many cellular functions, such as motility, signal transduction, and embryonic development. The building and maintenance of cilia are achieved by many proteins working together in a process called intraflagellar transport (IFT). During IFT, tubulins, the building block of cilia, are carried into the cilium to construct doublet microtubules. Big subcomplex such as axonemal outer dynein arm (ODA) complex is pre-packed in the cytoplasm before being transported into the cilia for assembly.

ODA comprises dynein heavy chains (HCs), intermediate chains, and light chains responsible for ATP-dependent force production that leads to cilia bending. Recently, it was shown in *Tetrahymena thermophila* that a regulatory protein, Shulin, packs together three dyneins HCs of ODA to keep the HC heads in an inactive pre-powerstroke conformation during IFT. To uncover how the inactive form of ODA becomes activated, we obtained the cryo-EM structure of the active ODA bound onto the doublet microtubule via the docking complex. Using molecular dynamic simulation, we propose a model of ODA attachment to doublet microtubule to induce remodelling and activation of the ODA. The motility rate of ODA could be regulated by post-translational modification (PTM) within the cilia, such as acetylation of the doublet microtubules (DMT).

PTMs of ciliary proteins, such as acetylation, polyglutamylation, and phosphorylation, maintain and regulate ciliary functions. Tubulin becomes acetylated by α-tubulin acetyltransferase-1 (αTAT1) after being assembled into the doublet microtubules (DMT). One of the main sites for acetylation is within the lumen of DMT, on lysine 40 (K40) of α-tubulin. The K40 loop is structurally flexible and disordered during in vitro reconstitution. In *Tetrahymena thermophila*, cells carrying a K40R substitution in α-tubulin show loss of acetyl-α-tubulin, while αTAT1 knock-out cells (MEC-17) show complete loss of acetyl-α-tubulin in cilia that led to short and labile cilia. To understand the effect of acetylation in the cilia, we obtained 3.5 Angstrom resolution cryo-EM structures of doublet microtubules from wild type (WT) and mutants (K40R and MEC-17) that have un-acetylated tubulins. The K40 loops were visible in both mutants and the WT. Using molecular dynamics, the inner junction region of the WT structure shows lower energy and better stability when acetylated, suggesting that acetylation may play a role in microtubule inner protein interaction and stability. Our mass spectrometry results identified kinase, phosphatase, and polyglutamylation-related enzymes that are downregulated in the acetylation mutants. We propose a model that, shifting the balance of one type of PTM may initiate a compensatory effect by another type of PTM to maintain cilia function.

Résumé

Les cils cellulaires sont des organites à base de microtubules qui s'étendent de presque toutes les cellules eucaryotes. Les cils sont les principaux acteurs de nombreuses fonctions cellulaires, telles que la motilité, la transduction du signal et le développement embryonnaire. La construction et le maintien des cils sont réalisés par de nombreuses protéines travaillant ensemble dans le transport intraflagellaire (IFT). Au cours de l'IFT, les tubulines, la pierre angulaire des cils, sont transportées dans le cil pour construire des microtubules doublets. Un grand sous-complexe tel que le complexe du bras de dynéine externe axonémal (ODA) est pré-emballé dans le cytoplasme avant d'être transporté dans les cils pour l'assemblage.

L'ODA comprend des chaînes lourdes (HC) de dynéine, des chaînes intermédiaires et des chaînes légères responsables de la production de force dépendante de l'ATP qui conduit à la flexion des cils. Récemment, il a été montré dans *Tetrahymena thermophila* qu'une protéine régulatrice, Shulin, regroupe trois dynéines HC d'ODA pour maintenir les têtes HC dans une conformation inactive avant la puissance pendant l'IFT. Pour découvrir comment la forme inactive de l'ODA est activée, nous avons obtenu la structure cryo-EM de l'ODA active liée au microtubule doublet via le complexe d'amarrage. En utilisant la simulation dynamique moléculaire, nous proposons un modèle d'attachement de l'ODA au microtubule doublet pour induire le remodelage et l'activation de l'ODA. Le taux de motilité de l'ODA pourrait être régulé par une modification post-traductionnelle (PTM) dans les cils, telle que l'acétylation des microtubules doublets (DMT).

Les PTM de protéines ciliaires, telles que l'acétylation, la polyglutamylation et la phosphorylation, maintiennent et régulent les fonctions ciliaires. La tubuline est acétylée par la -tubuline acétyltransférase-1 (αTAT1) après avoir été assemblée en DMT. L'un des principaux sites d'acétylation se trouve dans la lumière du DMT, sur la lysine 40 (K40) de la -tubuline. La boucle K40 est structurellement flexible et désordonnée lors de la reconstitution in vitro. Chez *Tetrahymena thermophila*, les cellules portant une substitution K40R dans la -tubuline montrent une perte d'acétyl-α-tubuline, tandis que les cellules knock-out αTAT1 (MEC-17) montrent une perte complète d'acétyl-α-tubuline dans les cils qui ont conduit à des cils courts et labiles. cils. Pour comprendre l'effet de l'acétylation dans les cils, nous avons obtenu des structures cryo-EM avec une résolution de 3,5 angströms de microtubules doublet de type sauvage (WT) et de mutants (K40R et MEC-17) qui ont des tubulines non acétylées. Les boucles K40 étaient visibles à la fois chez les mutants et dans le WT. En utilisant la dynamique moléculaire, la région de jonction interne de la structure WT montre une énergie plus faible et une meilleure stabilité lorsqu'elle est acétylée, ce qui suggère que l'acétylation peut jouer un rôle dans l'interaction et la stabilité des protéines internes des microtubules. Nos résultats de spectrométrie de masse ont identifié des enzymes liées à la kinase, la phosphatase et la polyglutamylation qui sont régulées à la baisse dans les mutants

d'acétylation. Nous proposons un modèle qui, en déplaçant l'équilibre d'un type de PTM peut initier un effet compensatoire par un autre type de PTM pour maintenir la fonction des cils.

Acknowledgments

Please allow me first to acknowledge my parents and grandparents, especially, **Jie Chen** (陳潔), **YuXian Wang** (王玉仙), **LiHua Sun** [孫麗華], **XinRong Chen** [陳新榮], and **Hua Yang** (楊華) for supreme support and heavenly love. I also like to thank my family members, Na Yang (楊娜), Gaetan L'italien, Jun Zhang (張雋), BaoYuan Chen (陳寶媛), Ling Tang (唐齡), PeiLan Chen (陳佩蘭), LingSheng Zhou [周領生], QuanKun Chen (陳全昆), JinYan Ni (倪金燕), Fu'An Zhang (張福安), and Gilles L'italien for guidance and care during my years in Montréal. Thanks to my cousins Lei Zhang (張蕾), YanLi Xu (徐燕黎), LeiLei Tang (唐磊磊), WeiJia Zhang (張薇嘉), Ling Zhang (張嶺), JunHan Chen (陳俊翰), ShengHua Yan (阎晟驊), and Li Gao (高立) for being like my sisters and brothers for supporting me through M.Sc. and Ph.D. I cannot express how lucky and grateful I am for being born into such a loving family within a fascinating nation that was rich in culture, virtues, arts, and history.

To my family, I was too busy and had to miss many important family events during my Ph.D. Please accept my deepest regrets for not attending and caring for my family members who are sick. My father, Hua Yang (stroke) and my grandmother, YuXian Wang (stroke and myocardial infarction), have been under intensive care since September 2017 to this day. My deepest regrets to my grandmother LiHua Sun and my uncle LingSheng Zhou who were deeply ill and passed away; I cannot come to see you one last time and attend your funeral in person.

During these hardships, many friends helped me tremendously to endure and transit through the pain of passing and not able to see the sick ones, namely, **Jeannie Mui, Dr. Kelly Sears, LongJi Deng** (鄧隆基), **Kai Sheng** (盛開), **Dylan Dai** (戴海軍), **Stephen Li** (李禧琛/李鵬飛), **Jason Cao** (曹鉞), **Jeo Gai** (蓋俊鵬), **Qianli Xu** (徐千里), **Yang Xiao** (肖揚), **Weawkamol Leelapornpisit**, **Corbin Black**, and **Dr. Khanh Huy Bui**. Dr. Khanh Huy Bui is also my Ph.D. supervisor, and I am grateful for his understanding, emotional support and counselling during these six years (and eight years if counting M.Sc. at McGill).

My supervisor Dr. Bui has given me a lot of guidance and advice on all the research projects I worked on during my Ph.D. Along with past and current lab members, especially, Melissa Valente-Paterno, Dr. Muneyoshi Ichikawa (市川宗厳), Corbin Black, Kubo Shintaroh (久保新太郎), Katya Peri, Dinan Liu (刘迪南), Daniel Dai (戴晨), Amin Maghrebi, for all your support in the laboratory. Members at the **Facility of Electron Microscope Research (FEMR)**, namely, **Jeannie Mui, Dr. Kelly Sears, Dr. Kaustuv Basu, Weawkamol Leelapornpisit** for operation with electron microscopes and the Thermo Fisher CorrSight.

A big thank you goes explicitly out to **Dr. Bui** for taking me as the first Ph.D. student for the Bui lab. We have gone through many difficulties at the beginning for grants applications, setting up, managing the lab. It was time-consuming for me, in the beginning, to help operate/organize the lab and order/resupply chemicals, but you were there to have my back when I needed you the most. In 2019, Melissa joining the lab as lab manager helped take a huge burden from me, and I am grateful for that! You're an excellent advisor as you're always patient and meticulous. Your way of social interactions and being humble has taught me many life skills outside of research. Especially in developing a relationship with everyone around us, your actions helped me fully realize Matthew 6:19-23 and Diamond Sutra 26. We also had a lot of fun going to restaurants and watching World Cup games together, and I hope this friendship will last a lifetime! It was a great pleasure to be learning from you about cryo-EM and reconstruction, and I would love to know more from you in the future.

During my Ph.D., I received guidance and constructive criticism feedbacks from professors and primary investigators from around the world. Some of these professors include Dr. Jacek Gaertig, Dr. Karl Lechtreck, Dr. Masahide Kikkawa, Dr. Haruaki Yanagisawa, Dr. Muneyoshi Ichikawa, Dr. Isabelle Rouiller, Dr. Javier Vargas, Dr. Bhushan Nagar, Dr. Craig Mandato (and Dr. Eric Boucher), Dr. Dieter Reinhardt, Dr. Joaquin Ortega, Dr. Susanne Bechstedt, and Dr. Justin Kollman. I want to acknowledge my advisory committee members: Dr. Chantal Autexier, Dr. Nathalie Lamarche-Vane, Dr. John Presley, Dr. Alba Guarné, and Dr. Elitza Tocheva (2015-2018).

In the August of 2017, I had the opportunity to travel to the University of Tokyo for a one-month exchange program. I like to thank the Department of Anatomy and Cell Biology **(Joelle Denomy-Hasilo)** and Graduate and Postdoctoral Studies **(Dr. Elaine Caroline Davis)** at McGill for processing the funding application. I am grateful and indebted to **Professor Masahide Kikkawa** (吉川雅英) and **Dr. Haruaki Yanagisawa**-sensei (柳澤春明) for taking me into their lab and helping me hand-to-hand with the cloning and making of *Chlamydomonas reinhardtii* cell strains for use with BioID2, IFT-BCCP, IFT-GFP purification and visualization. These strains helped tremendously in my IFT project, but they will not be discussed in this thesis.

I like to extend acknowledgement to all collaborators that I have worked with in the past. **Dr. Jie Xu**, for all the chocolates and food. **Dr. Alexei Gorelik**, now a postdoctoral fellow, you are hardworking and talented! **ZiXian Li**, for all the laughter and invitation to your place for dinner. Besides, Dr. Alexei, ZiXian, Ahmad Gebai, and Sarah Sabboobeh always invited me to join board game nights at the Department of Biochemistry, and they were memorable experiences of a lifetime!

In the end, please allow me to say thank you to all the students I met as a teaching assistant and lecturer during the ANAT542 Course: Electron Microscopy. You are lovely students, I enjoyed teaching so much because of you, and I wish you all the best in your career path. Some of the students went on to research projects involving electron microscopy, and I am very proud of you for that! I also hoped that we forged a friendship during graduate school and may your future career be bright as stars in the sky: Daniel Dai, Ian Noel Costas Cancelas, Johanan Idicula, Daniel Buss, Klaudia Bednarz, Jill Lauren, Logine Ghadban, JingYu Sun, Ahmad Khalifa, Katya Peri, Aaron Ju, Quentin Basiren, and Penelope Neocleous. Your presence and laughter added spices to my Ph.D., and I enjoyed teaching so much because of your ingenuity.

Preface

Many people have asked this, why doing a Ph.D. in cell biology/biochemistry/biophysics?

Short Answer: I love to explore scientific mechanisms in nature. Many devastating diseases need to be studied, and I wish to understand them to be free of pain and suffering from diseases. By checking the sciences underlying these diseases, I wish to contribute to the scientific advancement of knowledge to benefit humankind.

Long Answer:
I have had a profound fascination with nature since childhood. A childhood growing up in Yunnan, located within a subequatorial zone with altitudes ranging from 1500 to 3000 meters, allowed me to interact with a vast niche of plants, fungi, and animals. It was also one of the least industrialized and urbanized places in China, so I exercised my curiosity by collecting all the seeds I could find from plants, feeding every animal in the zoo and wild, and learning all the constellations in the night sky. When I was five, my mother bought me special glasses to watch a solar eclipse, and my father bought me binoculars to observe comets. I enjoyed observing my grandfather's two giant fish tanks and counting meteoroids with my paternal grandmother in the suburbs. My happiest childhood moments were for picking wild berries and mushrooms in the mountains with both of my parents. My maternal grandmother was a swimming gold medalist, and I adored exploring new pools and lakes. My grandmother bought me the fanciest amateur telescope for my tenth birthday, and my mother bought me Dr. Stephen Hawking's Chinese translation *of A Brief History of Time* and *The Universe in a Nutshell*. Since then, I have been indulging in the study of natural sciences, especially in the subjects of astronomy and biology.

Good times do not last, as it was difficult being an immigrant when I was 12 years old to Canada. Learning new cultures and languages was one thing but dealing with discrimination was another. I was bullied and looked down on by some students and even teachers/administration during high school. My mother's dentist credentials were not recognized in Canada, so we had difficult times incorporating into this new country. My mother wanted to maintain a good living standard for a better learning environment, so we declined social assistance, affordable housing, and government welfare programs. My single-parent mother and I were working and studying full-time to earn our living. Despite constant discrimination at school from students and teachers, I still maintained a very high grade (~95/100), but my emotional health was declining, and I developed a severe sleeping illness.

When God closes a door, He opens a window. During my mother's teaching at New Brunswick Community College, she met Carole Findlay and Alexandra Langley. Carole was a kind and caring individual who oversaw the Atlantic Cooperative Youth Leadership, a program to reach out to empower youth to become leaders in their community. In this program, I met Carole and young individuals who inspired and helped me overcome my difficulties and renew my resolve. Finally, I walked out of the shadow of discrimination and participated in many high school societies.

I became the co-editor of my high school yearbook, working with photos and layout designs. I also wanted to see the outside world, so I volunteered in a few community charity organizations such as YMCA, Red Cross, and non-profit co-operatives. By Carole's referral, I gained the opportunity to volunteer at YMCA by teaching math and English to young children in the evenings. It touches my heart to see that these students were also being judged at school, but many warm-hearted volunteers helped them. So, I developed life-bonding connections and sympathy with these students. Even during the coldest winter, I remember I bundle up myself and running 3 kilometres every day to YMCA so I won't miss any opportunity to help my students. After teaching finished, I would quickly jog home, not losing any toes to the bitter cold. Teaching and volunteering at YMCA renewed my hope in our society. Even if there will be discrimination and prejudice against us, we can always make our community a better place by helping others in need. But helping these students at YMCA was not a long-term solution, as many were suffering from learning disabilities or developmental disorders. However, we cannot find a cure to treat them. It made me think about becoming a doctor or medical researcher to help find a cure.

In grade 11, I got sick due to stomach bleeding and stayed at home for recovery for two months. After that, Alexandra Langley, a stranger my mom met, visited me weekly and subscribed to the monthly *National Geographic Magazine* and *Science Magazine* as birthday gifts for many years. Reading these magazines allowed me to see the outside natural world once more as if my childhood curiosity had once again returned to me. Alexandra also took us out to skiing and dining and her cottage in Shediac, basically treating me as if I was her child. Her action touched me, and it was as if kindness is a ripple effect, promoting people to perform more acts of kindness when the ripple propagates outwards. This time, I have gathered a solid resolve to do a Ph.D. to research in the biological sciences because I, too, believe that my efforts can help other people in biomedical research. Besides, I can explore the natural universe as I once did with my parents and grandparents.

My involvement in the community quickly came to the attention of the Mayor of Moncton at the time, George LeBlanc. He recruited me into his Youth Advisory Committee. Every two weeks or month, I would sit down with 7 other youth from Moncton and Mr. LeBlanc to discuss outstanding issues in our city concerning young citizens. For two years, I had this great opportunity to help my city by speaking out for the youth population and publishing our results bi-yearly via press conference. I graduated high school with scholarships and bursaries from the Canadian Millenium Scholarship Foundation, Atlantic Coop, Wal-Mart, and Dalhousie University.

At Dalhousie University, I met Melissa MacKay, the Residence Education Coordinator, during my undergraduate years. She offered me a position to welcome and enrich undergraduate students with

the fun of science in Dalhousie residences. I enjoyed these times as I would design various interesting (and safe) science experiments for students in my residence. With help from Melissa, I took the initiative to start the Spread the Net fundraising campaign for Dalhousie University. Our fundraising was a success and matched up to top Canadian universities, such as McGill and Toronto, for the total amount of bednets raised for African nations to protect against malaria. This successful campaign strengthened my resolve to pursue a science education in graduate school.

I joined Dr. Bui's laboratory interested in learning cryo-electron microscopy, a technique that had a recent revolutionary breakthrough for direct electron detectors to help determine the structure of proteins at atomic resolution. Attending conferences and workshops worldwide has allowed me to meet many individuals affected by ciliopathies and diseases associated with cilia. For example, in July of 2017, I attended a cilia conference in Phoenix, Arizona, and I met many families affected by ciliopathies in a gathering across the road. After the conference, I wanted to explore the Grand Canyons, so I drove to Page, Arizona. Unfortunately, during my stay at a hotel, the owner's granddaughter was affected by an unknown form of ciliopathy, leading to defects in neural tube development. Doctors are unsure what the cause was but suspect cilia-related Sonic Hedgehog signalling problems, and there is not enough basic research to give a definitive answer. The hotel owner and family were amiable and social people, so it saddens my heart to see good family and kind people affected by such a devastating disease with limited knowledge.

In December 2019, our lab received two mutant strains of *Tetrahymena* K40R and MEC17. Dr. Bui and I discussed a new side project by using cryo-EM to study the ciliary structure of these two mutant strains and compare them with that of the wildtype (CU428). Unlike previous strains we worked with (SB255-mucous less strain), the strains of CU428, K40R, and MEC17 were difficult to grow and purify axoneme because they had much mucous. Nevertheless, I overcame these difficulties by innovating new purification approaches, with a fire in my heart that our work would help answer medical questions that could eventually benefit people’s lives. This fire in my heart also kept me optimistic during the times when SARS-CoV-2 struck, which encouraged me to complete data analysis and two paper manuscripts in two years.

In the end, I am deeply inspired by parents and friends, believing kindness is a ripple effect on relatives and strangers around me. Therefore, I strive to make my life meaningful by making a difference in others' lives. In my Ph.D., I chose to study cilia, a highly conserved cellular organelle found on almost every cell in the human body. It was previously thought to be a vestigial organelle. Still, recent research has revealed many functions of this tiny structure and the diseases it can cause if a mutation is reported. Perhaps due to cilium's high conservation across eukaryotic organisms, mutations in its structural components can cause ciliopathies. I hope my research can benefit many people, especially those suffering from ciliopathies. I believe we could also explore many mysteries and knowledge by researching nature's beautiful and wonderous design. "**Call to Me,**

and I will answer you, and show you great and mysterious things, which you do not know." (**Jeremiah 33:3** TSPM).'

I remember another quote from the movie *The Hobbits: An Unexpected Journey*, based on the same name novel by John Ronald Reuel Tolkien:

> "Saruman believes it is only great power that can hold evil in check, but that is not what I have found. It is the small everyday deeds of ordinary folk that keep the darkness at bay. Small acts of kindness and love. Why Bilbo Baggins? Perhaps because I am afraid, and he gives me courage."
>
> ― Peter Jackson via *Gandalf the Gray*

In my heart, no matter how difficult life is, I know that my everyday kindness can cause a ripple effect to affect more people. This act of kindness will brighten up someone who had a bad day or has been having rollercoaster life experiences. Whatever path we may take, know that the stars will always shine to guide us should we all make a difference in another's life, no matter how small or big. I wish that every individual will find the right path to their success and that our civilization will one day reach peace, harmony and prosperity by understanding and helping one another.

Contribution to Original Knowledge

In this manuscript-based thesis, I used cryo-EM to obtain a 3.5 Å high-resolution electron density map and atomic model of the doublet microtubules from K40R and MEC17 *Tetrahymena* mutants. The manuscripts described are:

1. Kubo, S., **Yang, S.K.**, Black, C.S., Dai, D., Valente-Paterno, M., Gaertig, J., Ichikawa, M., Bui, K.H. (2021). Remodeling and activation mechanisms of outer arm dyneins revealed by cryo-EM. *EMBO Report*, 22: e52911. doi:10.15252/embr.202152911

2. **Yang, S.K.**, Kubo, S., Peri, K., Black, C.S., Dai, D., Fan, Z., Valente-Paterno, M., Bui, K.H. (2021). Effect of alpha tubulin acetylation on the doublet microtubule structure and microtubule inner proteins.

My cryo-EM maps are the first to show MIPs densities in MIP1-7, which was distinct enough to show certain side-chains to allow atomic modelling and identification of individual proteins and laid the framework for another manuscript in preparation Kubo et al. (2022) for the identification of MIPs in *Tetrahymena* CU428. In addition, I helped with the processing of the CU428 cryo-EM map.

For the first manuscript, the ODA cryo-EM maps I prepared show the ODA in its native state that was bound to doublet microtubules. Kubo was able to help us use molecular dynamic simulation to derive a model. Together, the cryo-EM map and molecular dynamic simulation generated a molecular model for understanding the conformational change of ODA from its inactive state into an active state.

For the second manuscript, I specifically modelled visible and partially visible αK40 loop region in the cryo-EM electron density maps of CU428, K40R, and MEC17 *Tetrahymena* species. These maps show that MIPs are intact within the lumen for both WT and acetylation mutants and that there is no structural difference for the αK40 loops. However, we see that the αK40 loops interact with MIPs and become stabilized via MIPs interactions. Furthermore, we show that the αK40 loops are stable in places with many MIPs, and together with our molecular dynamics simulation, we show that acetylated αK40 loops have lower energy and are less flexible. I prepared the samples for mass spectrometry for CU428, K40R, MEC17, Rib72a, Rib72ab *Tetrahymena* species. Our mass spectrometry identified kinase, phosphatase, and glutamylation-related proteins downregulated in the acetylation mutants to suggest a balance and crosstalk between types of post-translational modifications within the eukaryotic cilia.

Contribution of Authors

1. Kubo, S., **Yang, S.K.**, Black, C.S., Dai, D., Valente-Paterno, M., Gaertig, J., Ichikawa, M., Bui, K.H. (2021). Remodeling and activation mechanisms of outer arm dyneins revealed by cryo-EM. *EMBO Report*, 22: e52911. DOI:10.15252/embr.202152911

Contribution of S.K. Yang: Growth of cells, purification of cilia, purification of doublet microtubule. Optimization, preparation, vitrification and screening of negative-staining and cryo-EM grids. Cryo-EM data collection, reconstruction, and its analysis. Including Figures 2.1, 2.2, 2.3, 2.6, 2.9, 2.11.

2. **Yang, S.K.**, Kubo, S., Peri, K., Black, C.S., Dai, D., Fan, Z., Valente-Paterno, M., Bui, K.H. (2021). Effect of alpha tubulin acetylation on the doublet microtubule structure and microtubule inner proteins.

Contribution of S.K. Yang: Growth of cells, purification of cilia, purification of doublet microtubule. Optimization, preparation, vitrification and screening of negative-staining and cryo-EM grids. Cryo-EM data collection, reconstruction, and its analysis. Preparation of samples for mass spectrometry. Analysis of mass spectrometry results with Katya. All of the figures and tables except for: Fig 3.6A,B,C.

Publications

Here is a list of research papers (published or in preparation) that are included in this thesis:

Kubo, S. [Ψ], **Yang, S.K. [Ψ]**, Black, C.S., Dai, D., Valente-Paterno, M., Gaertig, J., Ichikawa, M., Bui, K.H. (2021). Remodeling and activation mechanisms of outer arm dyneins revealed by cryo-EM. *EMBO Report*, 22: e52911. DOI:10.15252/embr.202152911

Yang, S.K. [Ψ], Kubo, S. [Ψ], Peri, K., Black, C.S., Dai, D., Fan, Z., Valente-Paterno, M., Bui, K.H. (2021). Effect of alpha tubulin acetylation on the doublet microtubule structure and microtubule inner proteins.

[Ψ] These authors contributed equally

Here is a list of papers published or in preparation during my doctoral studies that are not included in this thesis:

Gorelik, A., Illes, K., **Yang, S.K**., Basu, K., Bui, K.H., Nagar, B. (2022). Structures of the mannose-6-phosphate pathway enzyme, GlcNAc-1-phosphotransferase. *Sciences Advance: In Press*

Khalifa, A.A.Z., Ichikawa, M., Dai, D., Kubo, S., Black, C.S., Peri, K., McAlear, T.S., Veyron, S., **Yang, S.K**., Vargas, J., Bechstedt, S., Trempe, J., Bui., K.H. (2020). The inner junction complex of the cilia is an interaction hub that involves tubulin post-translational modifications. *Elife*: 9:e52760. DOI: 10.7554/eLife.52760

Leary, A., Sim, S., Nazarova, E., Shulist, K., Genthial, R., **Yang, S.K**., Bui, K.H., Francois, P., Vogel, J. (2019). Successive Kinesin-5 Microtubule Crosslinking and Sliding Promote Fast, Irreversible Formation of a Stereotyped Bipolar Spindle. *Current Biology*: 29, (22), p3825-3837.

Imhof, S., Zhang, J., Wang, H., Bui, K.H., Nguyen, H., Atanasov, I., Hui, W.H., **Yang, S.K**., Zhou, Z.H., Hill, K.L. (2019). Cryo electron tomography with volta phase plate reveals novel

structural foundations of the 96-nm axonemal repeat in the pathogen *Trypanosoma brucei*. *Elife*: 8:e52058. DOI: 10.7554/eLife.52058

Usluer, G., Dimaio, F., **Yang, S.K**., Hansen, J.M., Polka, J.K., Mullins, D., Kollman, J., (2018). Cryo-EM structure of the AlfA filament reveals the basis for assembly of a bacterial actin missing a canonical subdomain. PNAS: 115, (13), p3356-3361. DOI:10.1073/pnas.1715836115

Ichikawa, M., Liu, D., Katritis, P., Basu, K., Hsu, T.C., **Yang, S.K**., Bui, K.H. (2017). . Subnanometer-resolution structure of the doublet microtubule reveals new classes of microtubule-associated proteins. Nature Communications (8), 15035.

List of Figures and Tables

List of Abbreviations

α: Alpha, e.g., α-tubulin

Å: Angstrom, 10 Angstrom = 1 nanometer

ATP: Adenosine triphosphate

Avg: Average

β: Beta, e.g., β-tubulin

C. elegans: Caenorhabditis elegans

Chlamydomonas: Chlamydomonas reinhardtii

C. reinhardtii: Chlamydomonas reinhardtii

Cryo-EM: Cryo electron microscopy / Electron cryo-microscopy

CU428: Cornell University Strain 428 (wild-type *Tetrahymena thermophila*)

Doublet, DMT: Doublet microtubules

FAP: Flagella-associated protein

GTP: Guanosine triphosphate

HDAC6: Histone deacetylase 6

H. sapien: Homo sapien, humans

IDA: Inner dynein arm

IFT: Intraflagellar transport

K40: Lysine 40 of α-tubulin

MAP: Microtubule associate protein

MIP: Microtubule inner protein

MT: Microtubules

MEC17: MEC-17, Mechanosensory abnormality protein 17

ODA: Outer dynein arm / outer arm dynein

PACRG: PArkin-CoRegulated Gene

PCD: Primary cilia dyskinesia

PTM: Post-translational modification

R40: Arginine 40 of α-tubulin

SIRT2: nicotinamide adenine dinucleotide-dependent deacetylase sirtuin 2

αTAT: Alpha-tubulin N-acetyltransferase

Tetrahymena: Tetrahymena thermophila

T. thermophila: Tetrahymena thermophila

TTLL: tubulin tyrosine ligase-like

WT: wild-type

Zebrafish*: Danio rerio*

Introduction

"No problem can stand the assault of sustained thinking."

Voltaire (François-Marie Arouet), French author, 1694 – 1778 C.E.

«Aucun problème ne peut résister à l'assaut de la pensée soutenue. »

Voltaire (François-Marie Arouet), auteur français, 1694 - 1778 E.C.

I. Aim of the thesis

This thesis compiles two research papers, with one already published and another in manuscript form. These two papers study the near-atomic-resolution structures of ciliary proteins, aiming to reveal their molecular mechanism of action. In these studies, cilia from *Tetrahymena thermophila* was selected as a model system for which cryo-electron microscopy, molecular dynamics, and mass spectrometry were adopted as the main techniques of choice.

Chapter One will provide a literature review to comprehensively analyze the past and recent research on the subject area.

Chapter Two will be **Paper I,** which is "Remodeling and activation mechanisms of outer arm dynein revealed by cryo-EM." This study proposed a model for activating the outer dynein arm complex from inactive to active forms.

Chapter Three will be for **Paper II**, a manuscript ready to be submitted for review. This paper studies the compensatory effects and mechanisms of post-translational modification, particularly acetylation in doublet microtubules. In this study, we presented a near-atomic model of the doublet microtubules from wild-type and de-acetylated mutants. In addition, we performed a molecular dynamics simulation to study the effect of acetylation on doublet microtubules in cilia.

Chapter Four will provide a general summary and discussion of the two papers, including plans for projects and the conclusion of this thesis.

II. Project background

Cilia and flagella are appendage-like organelles protruding from most eukaryotic cells' surfaces (DuJardin, 1841; Müller, 1786). Cilia and flagella are different vocabularies for the same structure. Historically, the term flagellum was used for a single structure on the cell, such as sperm. The term was also used in bacterial flagellum, which is different from the eukaryotic ones. The term cilia were used in cases where many structures are present on the cell body, such as cilia in the respiratory tract.

Cilia are highly conserved between humans and lower eukaryotes. Cilia from the model organism *Tetrahymena thermophila* and *Chlamydomonas reinhardtii* were often used in cilia-related research because these organisms have been the subject of extensive proteomic and genomic research. In addition, *Tetrahymena thermophila* is inexpensive to genetically manipulate and fast to cultivate, as the growth time takes no more than three days at 30 ^{o}C temperature (Cassidy-Hanley, 2012).

A eukaryotic cilium is constructed by 500~700 different unique proteins (Hiroaki Ishikawa, Thompson, Yates, & Marshall, 2012; Gregory J. Pazour, Agrin, Leszyk, & Witman, 2005). The main backbone of every eukaryotic cilium is tubulin, which builds into doublet microtubules that physically support the cilium. There are a series of proteins inside the doublet microtubules' lumen, called microtubule inner proteins (MIPs) which may help structurally support the doublet microtubules (Ichikawa et al., 2017; Norrander, A.M., Brown, Porter, & Linck, 2000). The cilium then carries out many essential functions for the cell, such as motility, sensory, and cellular

signalling. Cilia that carry out motile functions are known as motile cilia, and these cilia are composed of nine doublet microtubules surrounding a pair of microtubules at the center of the cilium. The non-motile cilia are known as primary cilia, such as in light-sensitive photoreceptor cells (De Robertis, 1956, 1960; Sjostrand, 1953; Tokuyasu K - Yamada & Yamada, 1959) or renal epithelial cells (Kotsis et al., 2007; Yoder, 2007), and they are composed of nine doublet microtubules only. There are some exceptions, such as the motile nodal cilia, which are found in the development of embryos and spin in a circular pattern to create the nodal flow to establish the left-right asymmetry (Hirokawa, Tanaka, Okada, & Takeda, 2006). Surprisingly, nodal cilia do not have central apparatus perform spinning motion in a circular pattern to activate nodal signalling. The production of movements such as waveform and bending motion in cilia are mediated by the dynein arm complexes (C. J. Brokaw & Kamiya, 1987; D.R. & Rosenbaum, 1985; Kamiya & Okamoto, 1985).

III. Research Question #1: How does outer arm dynein becomes activated to facilitate cilia bending?

Dynein arms complexes (also known as arm dynein) are important protein complexes inside cilia that help to generate propulsive force, and they could be categorized into inner dynein arms (IDA) and outer dynein arms (ODA). The IDA is important to produce waveform motion in cilia. At the same time, the ODA is responsible for the sliding of doublet microtubules that translates into the ciliary bending, which dictates beat frequency (C. J. Brokaw & Kamiya, 1987; D.R. & Rosenbaum, 1985; Kamiya & Okamoto, 1985). Defects in ODA can lead to abnormal motility and hence, diseases such as primary ciliary dyskinesia (PCD), infertility, and situs inversus.

In *Tetrahymena thermophila*, ODA comprises three dynein heavy chains (HCs), intermediate chains, and numerous light chains responsible for ATP-dependent force production that leads to cilia bending. It was shown in *Tetrahymena* that Shulin, a regulatory protein, packs together three dynein HCs of ODA to keep the heads in an inactive pre-powerstroke conformation (Mali et al., 2021b). A cryo-EM structure was produced to show this inactive form before it is transported into the cilium. *However, it is still unclear how the inactive form translates into the active conformation and is bound onto the doublet microtubule.*

IV. Research Question #2: How do post-translational modifications in cilia regulate cilia's elongation, shrinking, and functions?

The motility rate of ODA on doublet microtubules could be regulated by acetylation and deacetylation of the doublet microtubules. Acetylation of lysine-40 (K40) increased the motility of ODA, while deacetylation by Nicotinamide Adenine Diphosphate (NAD)-dependent deacetylase sirtuin 2 (SIRT2) decreased the motility (Alper, Decker, Agana, & Howard, 2014). This finding is interesting because the site of acetylation K40 is located inside the lumen of the doublet microtubules. However, a previous cryo-EM study of reconstituted microtubules could not detect a significant structural change that may affect ODA between acetylated and non-acetylated tubulins.

Acetylation of tubulin happens when tubulin becomes assembled into doublet microtubules in cilia. Acetylation was first discovered in cilia and serve as one of the post-translational modifications (PTMs) to maintain ciliary functions (M. & Piperno, 1987; S.W. & Rosenbaum, 1983). For cytoplasmic singlet microtubules, acetylation exists as a mechanism to help stabilize microtubules when there are cracks in the lattice so the structure could have time to repair. The primary acetylation enzyme in cilia is known as, α-tubulin acetyltransferase 1 (αTAT1, also known as MEC17), helps to acetylate doublet microtubules K40 of α-tubulin from within the lumen (Jin et al., 2010; Loktev et al., 2008; Shida, Cueva, Xu, Goodman, & Nachury, 2010; Y. Zhang et al., 2002). In doublet microtubules, deacetylation of acetyl-K40 by SIRT2 or histone deacetylase 6 (HDAC6) would promote disassembly by destabilizing the doublet microtubule lattice.

The K40 loop is structurally flexible and disordered, but acetylation may help to restrict motion and lower the disorder by changing the electrostatic interaction energy (Eshun-Wilson et al., 2019). It was shown that motor proteins have higher binding and transport affinity to acetylated microtubules (Garnham & Roll-Mecak, 2012; Reed et al., 2006). Mice that lack αTAT1 have defective flagellar beat (Kalebic et al., 2013; Kim, L., Ghorbani, You, & Yang, 2013), *Caenorhabditis elegans* become touch insensitive without αTAT1 (Akella et al., 2010), and in humans, acetylation of tubulin may be involved with Parkinson's and Alzheimer's diseases (Esteves et al., 2019; F. Zhang et al., 2015). *Tetrahymena thermophila* mutant cells with an α-tubulin-K40R substitution have normal gross phenotypes but show loss of acetyl-α-tubulin under fluorescent light microscopy (Akella et al., 2010). The αTAT1/MEC17 knock-out *Tetrahymena thermophila* mutant cells show complete loss of acetyl-α-tubulin and more labile doublet microtubules. It has been shown that in *Tetrahymena thermophila* mutants deficient in tubulin glycylation, the acetylated-K40 levels increased (Wloga et al., 2009). In human cell lines, increasing the acetylation level by inhibition of SIRT2 could lead to a decrease in Tau phosphorylation and an increase in binding of microtubule associated proteins Tau and alpha-synuclein to tubulin (Esteves et al., 2019). There might exist such a crosstalk or compensatory mechanism for acetylation mutants with other types of PTMs and could probably help to explain the mild consequences of the loss of acetylation in some organisms. *The exact structural effects of acetylation in doublet microtubule in vivo are unknown, as previous studies examined acetylation in vitro studies and could not visualize the K40 loop. It would be interesting to discover the structural changes to other PTMs and MIPs inside the lumen when acetylation is switched on or off.*

V. Rationale & Objectives

There are many unanswered questions about dynein arms and the acetylation of doublet microtubules. Therefore, the objectives of this thesis are to:

1. Previously, Mali et al. (2021) showed that the preassembled ODA complex could be transported from the *Tetrahymena* cell body into the cilia via IFT. However, the ODA shown was in its inactive form, and it remains unclear how ODAs are bound to the doublet microtubules and how they are later activated. Since the activation mechanism is unclear, we also don't know how ODA activation drives the bending of cilia, which is significant because cilia bending takes part in many biological processes. It was also unclear how Shulin has a regulatory role by keeping the ODA inactivated and how Shulin leaves as ODA is being activated.

To help understand this transition from inactive and active ODA complexes, the active form of *Tetrahymena* ODA complexes already bound to doublet microtubules would be cryogenically preserved. Performing cryo-EM would help produce a structure of the active conformation of ODA compared to the inactive form with Shulin bound that was previously described by Mali et al. (2021). This new structure would allow us to propose a working model to explain the full mechanism of ODA's functional significance in cilia bending.

2. Previously, cryo-EM of reconstituted doublet microtubules by Eshun-Wilson et al. (2019) could not visualize the K40 loop. Still, the molecular dynamic simulation suggested that acetylation could restrict the motion of the K40 loop while deacetylated K40 loop extends

deeper into the lumen to likely influence lateral contacts. It was also shown that deacetylation of microtubules in cilia destabilize the lattice (Cueve 2012). It is unclear how acetylation of K40 could have a structural effect on the stability of doublet microtubules in whole, how it forms lateral contacts with the lattice, and if it interacts with MIP inside the lumen. To understand these questions, wild-type and acetylation mutant cilia from *Tetrahymena* would be purified and cryogenically preserved. Cryo-EM would be used to gain high-resolution structures of the K40 loop in acetylated and deacetylated states. By comparing, we could propose a model for the structural effect of acetylation and de-acetylation K40 *in vivo*.

Chapter One

"[One should] study extensively, inquire prudently, think critically, distinguish clearly, and practice sincerely."

Doctrine of the Mean, ZiSi (Ji Kong, grandson of Confucius), 483 – 402 B.C.E.

"博學之，審問之，慎思之，明辨之，篤行之"

《中庸》, 子思(孔伋), 前 483 年－前 402 年

1.1 Cilia and flagella

1.1.1 The history of cilia

In the past, the word "flagella" was a general term used to describe any hair-like appendages extending away from the cells found in bacteria, archaea, and eukaryotes. However, the word used for flagella to encompass any organelle that resembles a hair is not accurate. The eukaryotic flagellum is a different structure from the prokaryotic flagellum. Although they may share a few similar functions, such as motility and attachment, the fundamental mechanisms and proteins are completely different. It is also worth noting that not all hair-like appendages are flagella, such as microvilli of the intestine. In this literature review, only eukaryotic flagella and cilia would be the main focus. These two words, "cilia and flagella," and their adjectives may be used interchangeably to describe the same structure.

Cilia and flagella are hair-like eukaryotic organelles found in eukaryotic organisms and almost all cells. Historically, cilia were considered vestigial until many recent studies suggest their importance in cell motility, signalling, and embryonic development. The word cilium came from Latin, meaning "eyelash," and was probably first coined by Otto Friedrich Müller in 1786 C.E. (Müller, 1786). In 1674 C.E. Leeuwenhoek was the first to observe and describe the multiciliated cells that were swimming under his primitive light microscope. The word flagellum was attributed to Félix Dujardin in 1841 C.E. (DuJardin, 1841), with its Latin name meaning "whip". By the mid-19th century, the word flagellum was usually used when a cell has a single or only a few numbers of the organelle. In contrast, the word cilia are used when a cell has many numbers the organelles, such as those found in *Tetrahymena thermophila* (Figure 1.1A). This notation is

carried on to this day, where we call the distal part of the single tail of sperm as flagellum (Figure 1.1B) and call tracheal epithelial cilia since it has hundreds of cilia on a single cell.

Cilia and flagella can be classified by motile and non-motile status, which can be further defined by the arrangement of their axonemal microtubules (Figure 1.1C). In motile cilia, axonemal microtubules come in a 9+2 pattern with dynein arms (Figure 1.1D), meaning that nine outer doublet microtubules surround a pair of central microtubules. In non-motile cilia, axonemal microtubules come in a 9+0 pattern without dynein arms and are missing the central pair of microtubules (Figure 1.1D). The nine doublet microtubules pattern is related to the nine-fold symmetry pattern of the basal body, which is part of the centriole and will be reviewed in Section 1.1.4 under Ciliogenesis. However, there are exceptions to this classification, such as eel sperm and nodal cilia, which are mostly in a 9+0 pattern. In addition, nodal cilia can spin themselves in a circular motion without the central pair because they possess dynein arms. The role of dynein arms will be further reviewed in Section 1.4.

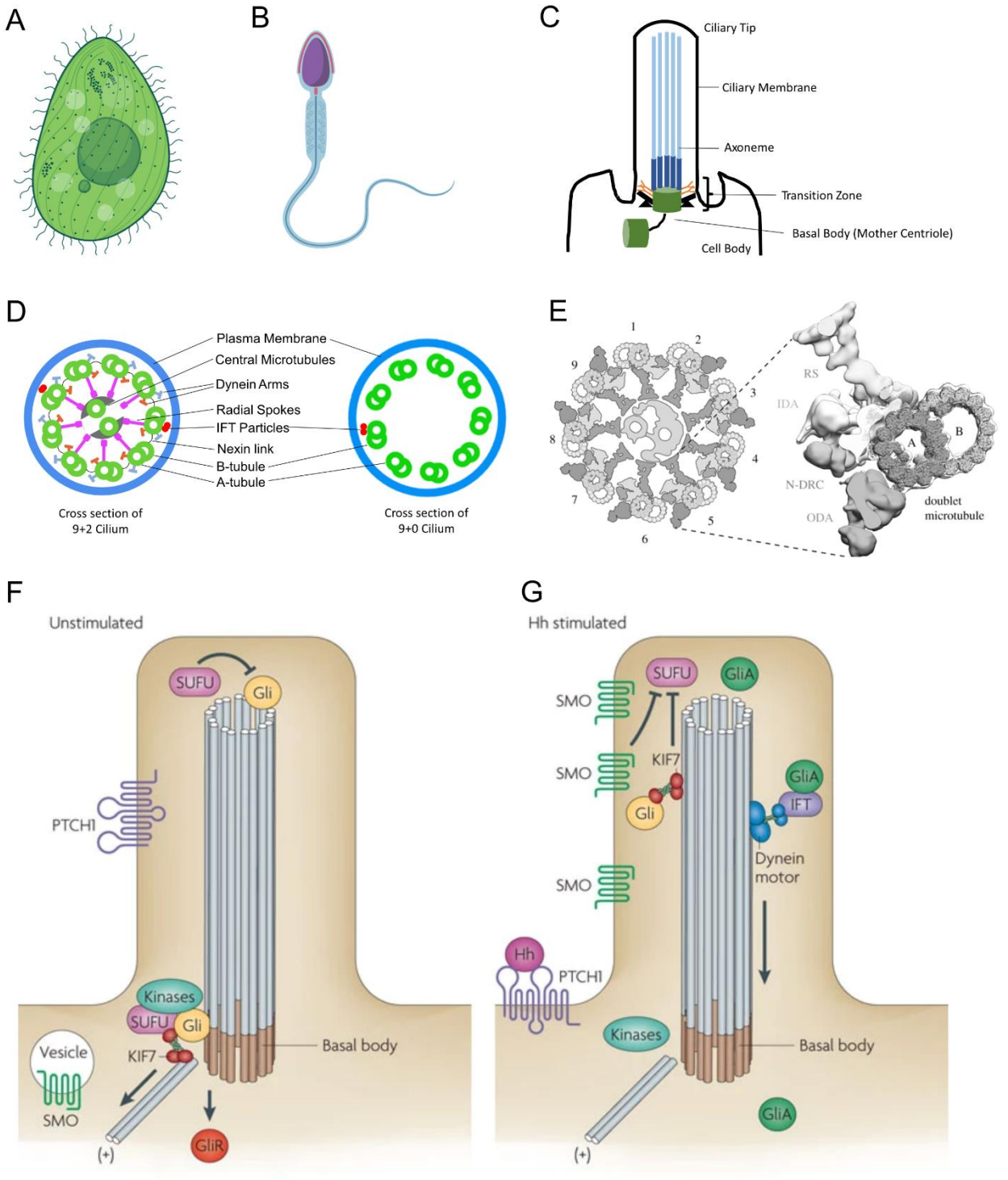

Figure 1.1 Pictures of cilia and flagella and the Hedgehog pathway.

A. Cartoon representation of *Tetrahymena thermophila* cell, showing cilia covering the cell, source: Biorender under usage license.

B. Sperm cell cartoon, showing flagellum as the tail, source: Biorender under usage license.

C. Cartoon drawing of eukaryotic cilia longitudinal section, showing basal body, transition zone, and doublet microtubules.

D. Cartoon representation of 9+2 cilium (left) and 9+0 cilium (right).

E. (Left) Diagram of *Chlamydomonas reinhardtii* cross section cilium, (right) showing Outer Dynein Arm (ODA), Inner Dynein Arm (IDA), Radial Spoke (RS), Nexin-Dynein Regulatory Complex (N-DRC), and with doublet microtubules. Image from Dutcher SK. 2019, Phil. Trans. R. Soc. B, usage under license with permission.

F. When the ligand is missing, PTCH1 blocks SMO entry into primary cilia. KIF7 localize to the base and form a complex with Gli proteins.

G. After the Hh pathway is activated, SMO localize to the ciliary membrane, and KIF7 enters the primary cilia to block SUFU. IFT and dynein motors transport activated Gli out of cilia.

F-G images are from Goetz, S. C., & Anderson, K. V. (2010). The primary cilium: a signalling centre during vertebrate development. Nature reviews. Genetics, 11(5), 331–344. The using of these images were done with permission.

1.1.2 The ultrastructure of cilia

The ultrastructure of cilium itself is mostly well conserved across eukaryotic organisms. Cilia are usually found on the apical side of the cell. A pair of centrioles is located near the cell membrane and comes in triplet microtubules that help to extend outside the epithelium (Figure 1.1C). This part of the cilia serves as the building foundation and is called the basal body (Wallace F. Marshall, 2008). The centriole that directly extends outside the membrane is the mother centriole, and the other centriole is the daughter centriole (Nigg & Raff, 2009). The ciliary pocket usually accompanies the basal body (Molla-Herman et al., 2010). Where the cell membrane forms a pocket-like pattern by folding back its membranes, the exact mechanism of this formation is unclear, but actin filaments at the pocket have been observed (Molla-Herman et al., 2010), and the shape of this pocket may be contributed to the actin cytoskeleton dynamics in the cell. This ciliary pocket helps isolate the cilia from the nearby cell membrane, so that entry to the cilium can be better regulated and controlled in a transition zone (Jensen et al., 2015). The distal appendages from the centriole would mature into transition fibres, which may help to anchor to the cell membrane, so the cilium is stable (Tanos et al., 2013).

At the base of the cilia, a series of Y-shaped ciliary necklaces are located in the transition zone above the transition fibres (Figure 1.1C). The ciliary necklaces are several parallel strands of particles that occupy part of the transition zone . While these ciliary necklaces' identity and protein composition are unknown, they may help control entry and exit from the cilium by either diffusion or transport (Reiter, Blacque, & Leroux, 2012). All the transition zone components may act as a selective barrier for the cilium, but this selective role function is not well understood. There are

hypotheses for a gate that may resemble the nuclear pore due to the presence of RAs-related nuclear protein (RAN) inside cilium and that protein import into the cilium may be mediated by a GTP gradient (Dishinger et al., 2010). There is also evidence for the existence of a diffusion barrier at the base of the cilium, as septins-membrane associated proteins were present to form a barrier for lateral diffusion during cytokinesis (Hu et al., 2010).

Above the transition zone is the axoneme, where the most function of the cilia is carried out. A density of proteins that separates the transition zone from the axoneme region of the cilia is known as the basal plate (Doolin & Birge, 1966). The axonemal region comprises hundreds of individual proteins, with microtubules extending from the basal body as the backbone of the axoneme (Figure 1.1B). Human and *Tetrahymena* cilia axoneme will be mostly constituted by doublet microtubules. In some organisms, the triplet microtubule from centriole will extend well into the cilium, such as in sea urchin sperm. In other cases, the doublet microtubule will become a singlet microtubule, as in *Caenorhabditis elegans* cilia. The doublet microtubules are further constructed by adding tubulin subunits to extend the cilium outwards such that receptors and channels on cilium may be more easily accessed and used for signalling, motility, and functions.

1.1.3 Components of the 9+2 axoneme

The ciliary axoneme contains many components that work together to carry out cilium's functions. The cilium is surrounded by plasma membranes which are derived and extended from the cell membrane. In the 9+2 structure, each doublet microtubule contains dynein arms that extend outward and inward from the central pair (Figure 1.1D and E). Each doublet microtubule is connected by the nexin-dynein regulatory complex that helps stabilize the axoneme and is also a hub for regulating dynein-driven ciliary motility. Each doublet microtubule also has an extension protein known as radial spoke that has a stalk and head region, which extends towards the inner sheath that covers the central pair of microtubules. These structures that are essential for motility have a periodicity repeat of 96 nanometers.

1.1.4 Ciliary functions

Due to cilia's important functions, the main structure of cilium is conserved throughout the evolution of eukaryotic species. A well-established function for cilia is locomotion. In primitive protozoan *Tetrahymena thermophila* and algae *Chlamydomonas reinhardtii,* their motile cilia serve as a locomotion function. *Chlamydomonas reinhardtii* is a photosynthetic organism that uses its two flagella for moving towards and away from light sources. *Tetrahymena thermophila* uses its cilia to move as it is attracted by chemokinesis, usually peptide or protein attractants (Per Hellung-larsen, 1986).

In higher eukaryotes, the motile cilia could be found in many tissues. For example, the uterine tube (Fallopian tube) in mammals and the oviduct in avians and amphibians have epithelial cells lined with motile cilia. The ciliated uterine tube helps to move the egg cell out towards the uterus to help with fertilization. In hens, the ciliated oviduct helps to move the developing shelled egg towards excretion. For lungfish and amphibians, the ciliated oviduct is lined with mucus-secreting glands to surround the ovum in a jelly. In sperm, cilium, more commonly referred to as the flagellum, helps drive the sperm forward to fertilize the egg.

Cilia are predicted to have sensory functions for the cell as early as 1898, when Karl Wilhelm Zimmermann studied primary cilia (Zimmermann, 1898). Primary cilia have 9+0 axoneme, and they are stationary (Figure 1.1D). A sensory function was speculated for participating in signalling pathways. In the eye, cilia from photoreceptors (rod and cone cells) are the only connection between the outer and inner segments of the photoreceptors (De Robertis, 1956, 1960; Sjostrand,

1953; Tokuyasu K - Yamada & Yamada, 1959). Cilia contain proteins such as transducin, arrestin, visual pigment opsin, cGMP-phosphodiesterases, and cyclic nucleotide-gated channel to function in phototransduction cascade in the retina with the help of intraflagellar transport proteins (Khanna, 2015). Primary cilia are also present on the renal epithelium in kidneys, extending into the lumen of the renal tubules for detecting fluid flow as a mechanosensor for calcium signalling (Kotsis et al., 2007; Yoder, 2007).

The primary cilium is specialized for Hedgehog (Hh) signalling pathway (Figure 1.1 F and G), which is carried in and out of cilia via intraflagellar transport (IFT) (D. Huangfu et al., 2003). Mutation in IFT proteins can result in loss of Hh phenotypes in the neural tubes and gain of function Hh in the limb (Haycraft et al., 2005; Danwei Huangfu & Anderson, 2005). For example, IFT88 could regulate hedgehog signalling to result in misaligned kinocilium (C. F. Chang & Serra, 2013; Moon et al., 2020). Inside the cilia (Figure 1.1 F and G), Sonic hedgehog (Shh) interacts with Patched homolog 1 (Ptc1) that represses Smoothened (Smo), allowing Smo to enter the cilium and Ptc1 to leave the cilium (Corbit et al., 2005; Rohatgi, Milenkovic L - Scott, & Scott, 2007), such that Smo can repress Suppressor of Fused (SuFu) that could be found at the tip of cilium (Figure 1.1 F and G). Furthermore, because SuFu represses glioma-associated oncogene (Gli), Smo's repression of SuFu could liberate Gli to be post-translationally modified to Gli activator form (GliA). GliA could then be transported out of cilium to allow activation of downstream target genes in the nucleus. The quantitative changes of the levels of GliA and its repressed form GliR inside the nucleus could result in developmental defects such as polydactyly, hypothalamic hamartoma, and vertebrate limb malformations (Hill, B, & Rüther, 2007; Kang, Jr, Olney, & Biesecker, 1997; B. Wang, Fallon, & Beachy, 2000).

Motile cilia can also partake in signalling. Forkhead Box Protein J1 (Foxj1) helps to form long cilia. Foxj1 modifies the cellular response to Shh by decreasing the level of Gli transcriptional factors for patterning neural tube floor plate during development (Cruz et al., 2010). Tracheal epithelial cells, which help sweep mucus out of the lung by generating synchronous metachronal waves, have T2R-family bitter taste receptors (A. S. Shah, Ben-Shahar, Moninger, Kline, & Welsh, 2009). Chemical agonists could increase intracellular Ca^{2+} concentration and the beating of these cilia, suggesting that tracheal epithelial cilia have motile and sensory functions. Interestingly, cilia from *Tetrahymena thermophila* were discovered to express epidermal-growth factor receptor-like molecules, but the function of these molecules in terms of sensory function is not understood (Csaba, Kovács P - Pállinger, & Pállinger, 2004).

1.1.5 Ciliogenesis

Ciliogenesis is a process for the building and deconstruction of cilia in several stages (S. Sorokin, 1962; S. P. Sorokin, 1968). The synthesis of cilium-specific proteins may regulate ciliogenesis as several hundreds of genes are upregulated during cilia construction. Before ciliogenesis, axonemal precursors must be produced in the cytoplasm. Initially, the pair of centrioles migrate towards the apical side of the cell and attach to the cell membrane (Figure 1.2A). The mother centriole, which is closest to the membrane, attaches via appendages. The daughter centriole, which is further away, remains attached to the mother centriole via a structure called root. The mother centriole would now be known as the basal body, which fuses with the membrane and form the ciliary pocket by folding back the cell plasma membrane and later becomes part of the ciliary membrane (Figure 1.2B). However, the ciliary membrane is different from the cell plasma membrane in part due to its ability for signalling. When the mother centriole anchor to the cell membrane, triplet microtubules extend away from the basal body and form into the cilia (Figure 1.2C). Diffusion of material is sufficient to construct a small length of cilia (Craft Van De Weghe, Harris, Kubo, Witman, & Lechtreck, 2020), but additional length is required with help from IFT that carries building blocks to a farther distance.

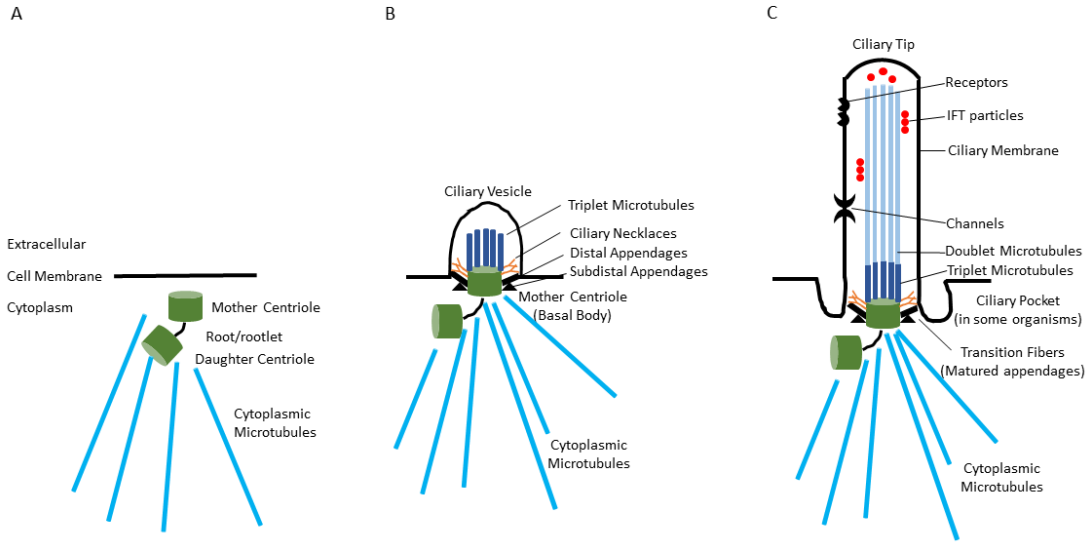

Figure 1.2 Simplified cartoon showing ciliogenesis of cilia in eukaryotic cells.

A. After cell division, the cell have no cilium and the mother centriole would localize close to the cell membrane, usually at the apical side of the cell. The mother centriole is supported by cytoplasmic microtubules that form a part of the cytoskeleton with actin and intermediate filaments.

B. The mother centriole move closer to the cell membrane, and grows microtubules in triplets which helps to extend and protrude out of the cell to form a ciliary vesicle with part of the cell membrane becoming ciliary membrane. The mother centriole is rooted by appendages to the plasma membrane, and with ciliary necklaces forming to create a transition zone between the ciliary vesicle and cell body.

C. The cilia grows as doublet microtubules extend outwards away from the cell, which can be further supported by IFT transport. At this stage, the cilium carries out many cellular functions such as signal transduction or locomotion. The cilium gets absorbed into the cell prior to mitosis.

Ciliogenesis usually occurs during the G1 or G0 phases in normal dividing cells. Cilia usually disassemble before mitosis, as noticed by Zimmermann in 1898 (Zimmermann, 1898) and Meves

in 1899 (Meves, 1899), but only reported by Ladislaus Walter in 1929 (L. Walter, 1929). Multiciliated cells do not go through the ciliogenesis cycle since they are post-mitotic and terminally differentiated. The cilium is removed prior to mitosis probably because centrioles are needed for the proper formation of the mitotic spindle. One mechanism to remove the cilium is katanin-mediated microtubule severing by cutting off doublet microtubules between the transition zone and the basal body (Parker et al., 2010). Without the structural support of doublet microtubules (or triplet microtubules as speculated in *Chlamydomonas*), the cell will lose the cilium.

Another mechanism by which cilia are disassembled is by resorption into the cell body (Pan, Q., & Snell, 2004; Pan & Snell, 2005; Piao et al., 2009), and be regulated by two proteins known as Pitchfork (Kinzel et al., 2010) and Human enhancer of filamentation 1 (Pugacheva, Jablonski, Hartman, Henske, & Golemis, 2007). Both proteins interact with Aurora A kinase, which in turn positively regulate tubulin deacetylase histone deacetylase 6 (HDAC6) (Hubbert et al., 2002; Pugacheva et al., 2007). Deacetylation of α-tubulin subunits will reduce the stability of doublet microtubules and lead to ciliary resorption.

1.2 Doublet microtubules

1.2.1 Components of the doublet microtubule

Doublet microtubules can be categorized into A-tubule and B-tubule (Figure 1.1D, and Figure 1.3A). The A-tubule comprises 13 protofilaments of α- and β-tubulin dimers interacting laterally, forming a hollow tube (Figure 1.3A). The B-tubule contains ten protofilaments, with protofilament B1 continuing clockwise to B10 at the inner junction (looking from the plus end). Nomenclature-wise, the region where protofilament B1 connects to A10 and A11 is known as the outer junction, as it faces towards the outside of the cilia (Figure 1.3B). On the opposite side of the outer junction, the first protofilament of the A-tubule (A1) is the one that is closest to a small gap to the B-tubule; this region is known as the inner junction, which faces towards the center of the cilia (Figure 1.3C). The inner junction contains several proteins depending on species to help the B-tubule form indirect contact with the A-tubule (Figure 1.3E).

In the A-tubule, the first to the thirteenth protofilament is counted in a clockwise pattern when looking from the plus end. As such, the B-tubule directly contacts the A-tubule at protofilament A10 and A11 (the outer junction). The first protofilament of the B-tubule, B1 is contacting PFs A10 and A11, and the tubulin interface is strong enough to maintain B-tubule attachment (Ichikawa et al., 2017). It is hypothesized that there might be a favourable angle for the protofilaments such that B1 can bind specifically to A10 and A11 due to high curvature in a non-canonical tubulin-tubulin interaction (Ichikawa et al., 2017).

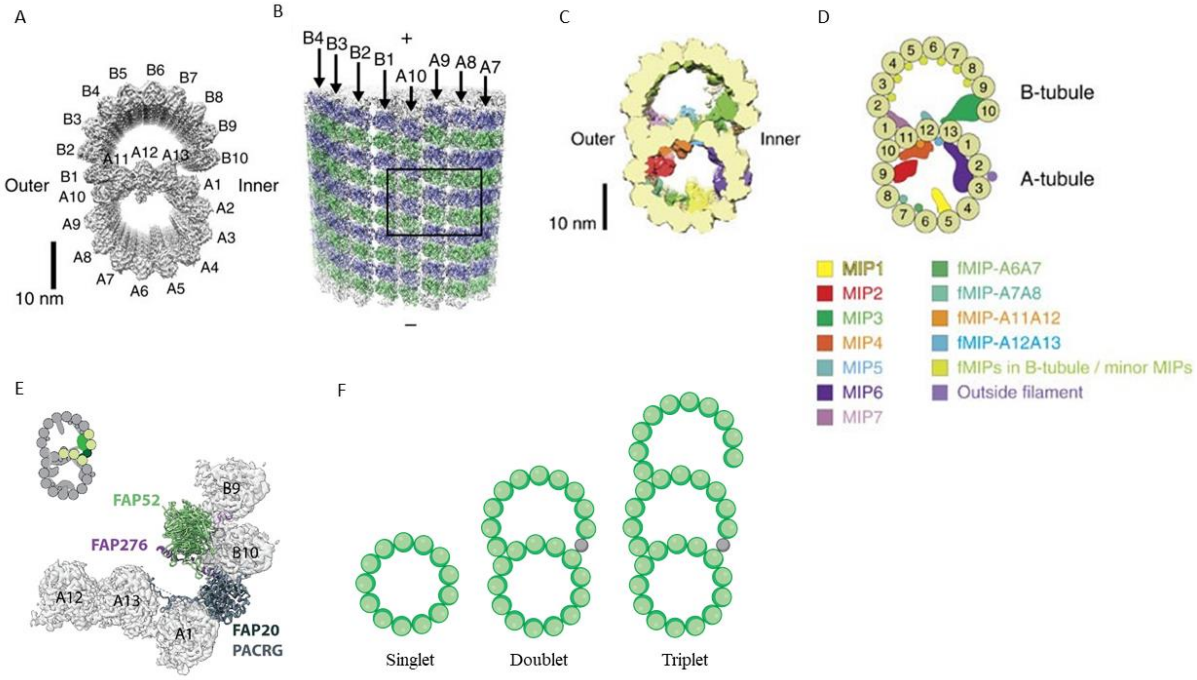

Figure 1.3 Models to show the doublet microtubules in cilia.

A. Surface rendering of electron density map 8 nm repeat of *Tetrahymena* thermophila doublet microtubule, viewed from the plus end of cilia, showing each protofilament, inner and outer junctions.

B. Surface rendering view of density map from the outer junction side of *Tetrahymena* doublet, α-tubulin: green; β-tubulin: cornflower blue.

C and D show surface rendering of density map (D) and cartoon (E) of 48 nm repeat of *Tetrahymena* doublet, with MIPs and MAPs colored.

E. Surface rendering view of density map of the inner junction region from *Chlamydomonas reinhardtii* doublet microtubules, with FAP52 in light green, FAP276 in purple, FAP20 in dark green, PACRG in gray, and tubulin in transparent gray.

F. Cartoon representation of singlet, doublet and triplet microtubules, with small grey ball representing the inner junction.

Panels ABCD were borrowed from Ichikawa et al., 2017, Nature Communication, under Creative Common permission. Panels E was borrowed from Khalifa et al, 2020, Elife, with Creative Common permission.

The doublet microtubules contain proteins outside and inside the structure. The cavity inside the microtubule is known as the lumen. Luminal proteins inside the doublet microtubules are collectively called microtubule inner proteins (MIPs), as shown in Figure 1.3D. The proteins on the outside of the microtubule, such as Outside filament in Figure 1.3D, or proteins associated with the microtubule are collectively known as microtubule-associated proteins (MAPs). To avoid confusion, because MIPs also interact with the doublet microtubules, MIPs can also be categorized into MAPs.

Proteins inside and outside the doublet microtubule usually contribute to the stability of the structure. In cytoplasmic microtubules, MAPs such as MAP2, MAP4, and tau helps to stabilize the lattice of singlet microtubules by binding on the outside (Dehmelt & Halpain, 2005). In doublet microtubules, a few filamentous proteins were be discovered in Chapter 3 of this thesis. However, the functions are unclear and may help to stabilize the doublet microtubule in some way.

Some of the MIPs in doublet microtubules, such as Rib43a (shown in position of fMIP-A12A13 in Figure 1.3D), is known to help stabilize the doublet microtubule, which forms into a network of longitudinal and lateral interactions (Ichikawa et al., 2017; Norrander et al., 2000). The MIPs can bind be as globular when they bind to the surface of tubulin on the inside, or they can be as filamentous and run along the doublet microtubule lengthwise. Each MIP usually have a specific periodicity repeat for every a few nanometers, so they may provide extra stability along the doublet structure to prevent dynamic instability and catastrophe as seen in cytoplasmic microtubules. This

periodicity is reasonable since motile cilia are required for motility, and extra stability is required for sustained functions. Besides, during ciliary motility and bending, doublet microtubules may undergo extensive distortion and shear force, so MIPs may help prolong the protofilaments' lifespan.

An additional hypothesis for the function of MIPs is that their binding may induce conformational changes of protofilaments. As the A-tubule becomes assembled, MIP7 (microtubule inner protein 7) binds to protofilament A11 to induce local distortion. MIP7 may also help recruit tubulin between protofilament A10 and A11 as tubulin subunits bind to the outside of microtubule lattice by non-canonical tubulin-tubulin interaction (Ichikawa et al., 2017). Together, these may help to assemble the outer junction and ensure that B-tubule formation is rigid.

1.2.2 Inner junction

The inner junction is the region between protofilaments A1 and B10, making it one of the two places for the B-tubule to connect with the A-tubule. However, unlike the outer junction with non-canonical tubulin-tubulin interaction between the A-tubule and B-tubule, the inner junction indirectly facilitates this connection via many proteins. Depending on the species, different proteins are present in the inner junction, but Parkin Co-Regulated Gene (PACRG), Flagella Associated Protein 20 (FAP20), and Flagella Associated Protein 52 (FAP52) and their homolog would be present in most eukaryotic species (Dymek et al., 2019; Khalifa, 2020; Yanagisawa et al., 2014). Figure 1.3E shows the inner junction proteins in *Chlamydomonas reinhardtii*. In some species, such as *Tetrahymena*, two copies of the same protein would be present, namely, PACRG-A and PACRG-B. These inner junction proteins help stabilize both the B-tubule, which in turn help to stabilize the A-tubule and doublet microtubule as a whole. In *Chlamydomonas,* mutation loss in these PACRG or FAP20 results in cell motility defects and reduced microtubule sliding velocities *in vitro* (Dymek et al., 2019).

Furthermore, loss of FAP52 and FAP20 cause detachment of B-tubule from the A-tubule and short flagellum (Owa et al., 2019). These results suggest that the inner junction proteins stabilize the ciliary axoneme, and the inner junction help to modulate dynein-driven microtubule sliding via the nexin-dynein regulatory complex. Diseases are also caused by loss and mutation of inner junction proteins, which will be discussed in Section 1.6.

The inner junction may serve as a scaffold to assemble the beak structure (Yanagisawa et al., 2014). The beak structure could be found on protofilaments B5 and B6 of doublet microtubules 1, 5, and 6 *in vivo* (Khanh Huy Bui, Yagi, Yamamoto, Kamiya, & Ishikawa, 2012; Yanagisawa et al., 2014). The beak structure may be involved in the asymmetric bending of the flagella.

PACRG and FAP20 contacts with the C-terminus of β-tubulin from protofilament A1 could stabilize the β-tubulin by forming a helical turn (Khalifa, 2020). However, without PACRG and FAP20, this would not be present due to the flexibility of residues E432-F436 at the C-terminus. As such, the protofilament A1 interaction with the N-terminus of PACRG appears to result from steric proximity (Khalifa, 2020).

1.2.3 Singlet, doublet, and triplet microtubules

Singlet microtubules could usually be found in the cytoplasm of a cell, though they are also present at the tip of cilia in some organisms as an extension from the doublet microtubules (as in *Caenorhabditis elegans*). Cytoplasmic microtubules are formed by tubulin dimers binding to two molecules of GTP into protofilaments. After assembly, the GTP becomes hydrolyzed into GDP. Usually, 13 protofilaments are found, but the number of protofilaments could change in a small population of different species. One of the key features of singlet microtubules in the cytoplasm is dynamic instability, as they could undergo assembly and disassembly simultaneously. It is commonly assumed that a cap of GTP tubulin sits at the tip of the growing microtubule for stabilization. If the cap is hydrolyzed, a catastrophe occurs by microtubules falling apart (Brouhard & Sept, 2012; Drechsel & Kirschner, 1994). It has been speculated that this constantly growing and shrinking of microtubules is advantageous in mitosis, as microtubules can grow and look for kinetochore attachment (Blackwell et al., 2017). Doublet and triplet microtubules do not undergo dynamic instability and catastrophe, partly due to adding an extra tubule for added stability.

Doublet microtubules are the backbone of all cilia. The cilia, being a structure that constantly undergoes mechanical stress, would benefit from doublet microtubules that are more stable than a single microtubule. Doublet microtubules form a ring structure that outlines the cilia. Like singlet microtubules, it is also formed by tubulin dimers binding to GTP molecules and has additional proteins that associate with the structure to provide stability (Ichikawa 2017). However, doublet microtubules have an additional tubule, known as the B-tubule, which has ten protofilaments. The

inner junction proteins help stabilize B-tubule binding, which helps the stability of the doublet microtubule.

In the triplet microtubule, there is an additional C-tubule (Figure 1.3F). The C-tubule is presumed to attach to the B-tubule via non-tubulin proteins (S. Li, Fernandez, Marshall, & Agard, 2012). The C-tubule cannot attach directly to the B-tubule as in the outer junction because curvature on the B-tubule is small (Ichikawa et al., 2017). The triplet microtubule only runs short in most organisms, growing away from the mother centriole towards the ciliary tip.

1.3 Intraflagellar transport

1.3.1 Components of intraflagellar transport complex

Intraflagellar transport (IFT) is an important process for the functions of the cell. IFT was initially observed as granule-like particles that move bidirectionally along the cilium (Kozminski, K.A., Forscher, & Rosenbaum, 1993). However, IFT could also be seen as electron-dense particles sandwiched between ciliary membrane and doublet microtubules using electron microscopy (EM) (Kozminski et al., 1993). These electron-dense particles have been nicknamed "IFT train" and were isolated using sucrose density gradient to be complexes of transport proteins and molecular motors, kinesin-2 and cytoplasmic dynein-2.

The main proteins responsible for IFT are IFT proteins, which had names given initially according to their approximate molecular weight in kilodaltons. A group of proteins, known as BBSome proteins, also contribute to the transport process. The IFT complex could be separated into at least two subcomplexes, IFT-A and IFT-B subcomplexes (Figure 1.4). Subcomplex IFT-A contains six protein components, IFT43, IFT121, IFT139, IFT122, IFT140, and IFT144 (Figure 1.4A). IFT-A has a molecular mass of about 750 kDa, with the first three proteins forming an auxiliary domain and the last three forming a core domain. Subcomplex IFT-B has at least 15 individual peptides, with IFT20, IFT38, IFT56, IFT57, IFT64, IFT80, and IFT172 forming an auxiliary domain (Figure 1.4B). IFT22, IFT25/27, IFT46, IFT52, IFT70, IFT74, IFT81, and IFT88 forming a core domain of the IFT-B subcomplex (Figure 1.4B). IFT-B has a predicted molecular mass of at least 1 MDa.

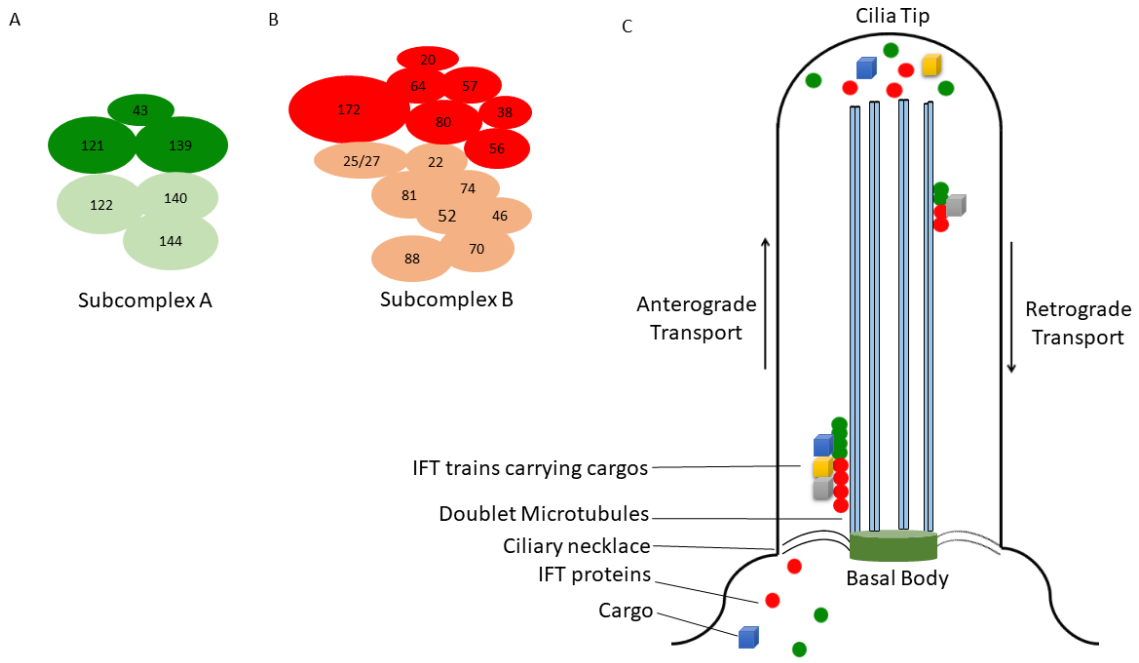

Figure 1.4 Cartoon showing anterograde and retrograde intraflagellar transport.

A. Schematic of IFT subcomplex A, with darker green showing the IFT proteins forming the auxiliary domain and light green showing the core domain.

B. Schematic of IFT subcomplex B, with red showing the IFT proteins forming the auxiliary domain, and orange showing the principal domain.

C. Diagram showing the anterograde and retrograde process of IFT.

IFT is a fast and dynamic process that helps to carry cargo in and out of the cilium. IFT uses kinesin-2 as the motor for transport into the cilia and dynein-2 out of the cilium, and this is known as anterograde and retrograde transport, respectively (Figure 1.4C). It was measured that anterograde transport can go to 2.0 μm/sec and retrograde transport is 3.5 μm/sec in *Chlamydomonas* (H. Ishikawa & Marshall, 2017). The processivity and velocity of kinesin-2 could be further increased by the enzymatic addition of glutamate residues to stimulate

polyglutamylation of reconstituted porcine α- and β-tubulin (Sirajuddin, Rice, & Vale, 2014). In *Caenorhabditis elegans*, the velocity of Osm3 kinesin-2 could be increased on hyper-glutamylated doublet microtubules lacking cytosolic carboxypeptidase 1 (CCP1), a microtubule deglutamylase (O'Hagan et al., 2011).

Anterograde and retrograde transport probably will not collide, with supporting data from detyrosination of tubulin in the B-tubule (discussed in 1.5.4) (Johnson, 1998; Sirajuddin et al., 2014). In addition, fluorescence microscopy and cryo-electron tomography suggest that anterograde trains travel on B-tubule, and retrograde trains travel on A-tubule (Jordan & Pigino, 2019; Stepanek & Pigino, 2016). Exactly how IFT trains disassemble and remodel at the tip of cilia is unknown, but IFT172 is involved with the transition between anterograde and retrograde IFT trains (Pedersen et al., 2005; Tsao & Gorovsky, 2008).

Though many of the IFT proteins were solved by X-ray crystallography, the current resolution of the native and active IFT complex is low, and the exact mechanism is yet to be validated. The exact stoichiometry of each IFT component and its associated proteins is unknown. Furthermore, there is limited information on which IFT proteins are responsible for the anterograde and retrograde transport and interaction with motors. Recently, it was shown that IFT54 might be a central component as it could directly interact with IFT dynein subunit D1bLIC and kinesin-II. Deleting IFT54 residues 342-356 showed reduced anterograde traffic of IFT, while IFT complex and motors accumulated in the proximal region of cilia. Deletion of IFT54 residues 261-275

reduced entry of dynein into the cilia, while the IFT complex started to accumulate at the tip of the cilium (Zhu, Wang, Li, Lechtreck, & Pan, 2021).

1.3.2 Components of the BBSome

The BBSome is a protein complex that is an adaptor to the IFT complex. BBsome proteins are named based on Bardet-Biedl syndrome (BBS) proteins: BBS1, BBS2, BBS4, BBS7, BBS8, and BBS9. Like the IFT complex, the BBSome complex is also well conserved in ciliated organisms and its function as an adaptor to the IFT complex by loading ciliary membrane proteins. However, BBSome mainly functions as an adaptor for the removal of ciliary signalling proteins such as protein phospholipase D (PLD) and Sonic Hedgehog (Y. X. Liu et al., 2021; Q. Zhang, Seo, Bugge, Stone, & Sheffield, 2012). For example, in *Chlamydomonas*, BBS3 protein enters the cilium in a GTP-bound state and arrives at the cilia's tip by diffusion. GTP-bound BBS3 recruits the BBSome to the ciliary membrane to load signalling protein PLD and then loads onto the IFT train for retrograde transport across the transition zone (Y. X. Liu et al., 2021).

1.3.3 Functional significance of intraflagellar transport

In *Chlamydomonas*, diffusion of tubulin into the cilium probably contributes most of the requirement for axonemal assembly (Craft Van De Weghe et al., 2020). However, under diffusion-only conditions, the ciliary growth speed and length would be both reduced. Thus, IFT is a tool to augment the supply of tubulin to growing cilia by maintaining a critical concentration (Craft Van De Weghe et al., 2020).

The transition zone is a selective barrier, and not all proteins can enter or exit the cilium freely by diffusion. For example, PLD can enter cilia by diffusion and IFT but must exit via IFT train. Activated ciliary G protein-coupled receptors (GPCRs) Smoothened and Somatostatin Receptor 3 (SSTR3) also require IFT out of cilia (Ye, Nager, & Nachury, 2018). Altered GPCR signalling would likely result in obesity. Signals in the photoreceptors also need to be transported via IFT train, which would be evolutionarily advantageous, rather than diffusion, to avoid time delay in processing life-threatening visual cues.

As such, even though diffusion may seem to be sufficient for ciliogenesis (Craft Van De Weghe et al., 2020), mutations in the signaling adaptor BBSome demonstrate a mild phenotype. The important role of IFT is indispensable in terms of maximizing full ciliary functions. During the anterograde transport, IFT may selectively transport cargos through the diffusion barrier and the selective gate resembling nuclear pore. With IFT's high velocity in the cilium, cargos could be transported to the tip of cilia most efficiently since a growing cilium requires much more axonemal

precursors at the tip than during a steady-state (W. F. Marshall, H., Rodrigo Brenni, & Rosenbaum, 2005). Although the regulation of size, speed, periodicity of IFT trains remains is unknown, the IFT process would also be a key regulator of ciliogenesis in higher eukaryotes. Indeed, mutation of most IFT results in devastating phenotypes and diseases in humans to exemplify the functional significance of IFT.

1.4 Dynein arms

1.4.1 Dynein arm species

Dynein was initially isolated from *Tetrahymena* cilia in 1963-1965 and was the first microtubule motor protein described capable of producing force (I. R. Gibbons, 1963; I. R. Gibbons & Rowe, 1965). Axonemal dynein arms are huge molecular complexes composed of many individual protein components (Figure 1.5A). There are two axonemal dynein arms populations: the outer dynein arms (ODAs) and inner dynein arms (IDAs). Various types of dynein proteins work together to carry out the beating and bending of cilia. For example, in the *Chlamydomonas* axoneme, three heavy chains (HCs) constitute the outer dynein arm, and eight heavy chains exist in IDA.

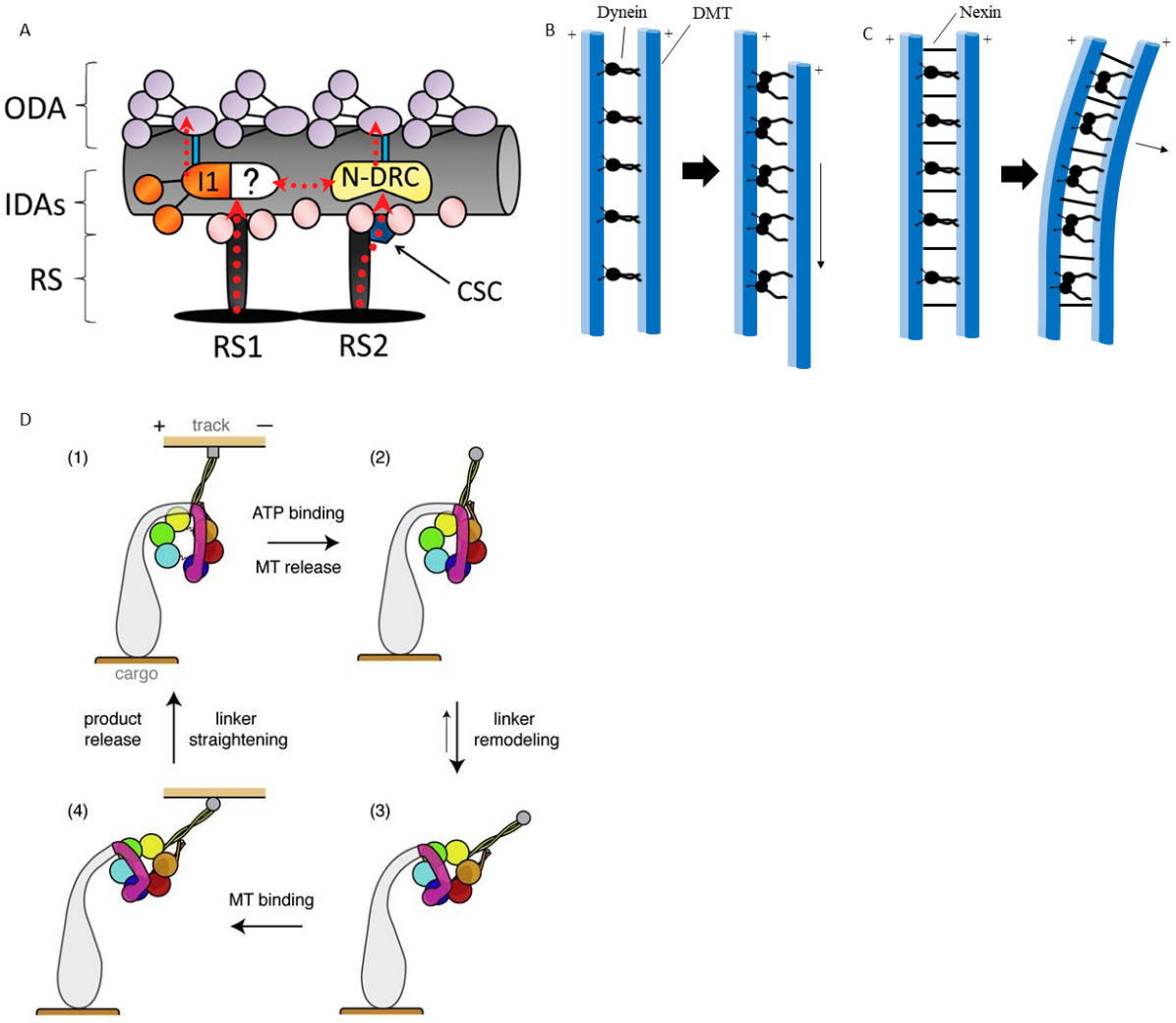

Figure 1.5 Outer and inner dynein arm illustration

A. Doublet 96-nm repeat diagram showing Outer Dynein Arm (ODA), Inner Dynein Arm (IDA), Radial Spoke (RS), Nexin-Dynein Regulatory Complex (N-DRC), calmodulin- and spoke-associated complex (CSC), and with doublet microtubules in grey. Picture taken from Yamomoto et al., 2013, J. Cell Biol. with permission.

B, C. Dynein alone will result in sliding of doublet microtubules, but when nexin is crosslinked as in C, the cilia will produce a bending motion.

D. A schematic of dynein with 6 AAA domain & ATP hydrolysis.

(1) Dynein is tightly bound to the microtubule without ATP.

(2) ATP binding result in closing of the gap between AAA1 and AAA2 to dislodge the linker and neck.

(3) ATP induce a slow conformational change of the linker to hinge toward the base.

(4) The stalk attaches to a new location on the microtubule. And to allow release of hydrolysis product from AAA1 so that the linker could move toward the stalk. Figure borrowed from Roberts et al., 2012, Structure, under Creative Commons License.

1.4.2 How cilia beat

All doublet microtubules in the cilium are oriented, with the minus end towards the cell body and the plus end towards the ciliary tip. Hydrolysis of ATP allows dynein arms to move towards the minus end of an adjacent doublet microtubule (Numata et al., 2008). This motion results in a sliding force such that the doublet microtubules slide apart from one another (Figure 1.5B). When dynein arms on one side are activated, doublet microtubules slide. However, dynein arms on the other side of the cilium must be inactive for cilia bending to occur (Figure 1.5C). Then, the activation and inactivation of the two sides of dynein must switch to oscillate a beat down the axoneme. It is unclear what controls or regulates this mechanism, but computer simulations have hypothesized that curvature of the cilium could help regulate dynein arm activation (Charles J. Brokaw, 2009). In theory, modifying how much distance the doublets slide between each other could also regulate the dynein arm activity for generating self-organized oscillations (C. J. Brokaw, 1975; Charles J. Brokaw, 2009), as in a mechanical spring. Therefore, a mechanism such as this would be able to allow continuous cilia bending and beating.

In *Chlamydomonas*, ODA and IDA mutant cells swim slower than the wild type due to different reasons. It was found that *oda* mutants swim slower because of decreased beat frequency (D.R. & Rosenbaum, 1985; Kamiya & Okamoto, 1985), while *ida* mutant swim slower due to reduced amplitude of bending waves (C. J. Brokaw & Kamiya, 1987). These results suggest that ODA regulates the beating frequency, and the IDA regulates the waveform of bending motion.

1.4.3 Dynein arm heavy chain and ATP hydrolysis

The HC in dynein arms is composed of three distinct structures, the N-terminal tail, the head, and the stalk (Burgess, Ml, Sakakibara, Knight, & Oiwa, 2003). The stalk is an elongated apparatus with a coiled-coil structure with a globular tip to bind to doublet microtubules (Gee, Heuser Je - Vallee, & Vallee, 1997). There is a slender tail at one-third of the N-terminal of the heavy chain, and this is responsible for heavy chain dimerization, binding of peptides, and cargo (Habura, I, Chisholm, & Koonce, 1999; Tynan, Gee, & Vallee, 2000). In the C-terminal of the heavy chain, approximately 380 kD residues were identified as the motor domain, which could drive the translocation of doublet microtubules (Numata et al., 2008). The C-terminal portion of the heavy chain is also composed of six tandemly linked AAA+ molecules that fold into a ring-like head (Ogawa, 1991; Samso, Radermacher, Frank, & Koonce, 1998). To generate ciliary propulsion, axonemal dynein arms hydrolyze ATP within this ring-like head. The dynein HC has six AAA+ modules with a single heavy chain, with AAA1-AAA4 containing nucleotide-binding and hydrolyzing sites. The rest of the two modules, AAA5 and AAA6, does not contain a nucleotide-binding and hydrolyzing site (Numata et al., 2008).

ATP hydrolysis of dynein occurs with its six AAA domains. Initially, dynein is tightly bound to the microtubule without ATP (Figure 1.5D). Then, the binding of ATP to dynein result in closing of the gap between AAA1 and AAA2 to dislodge the linker and neck. This is followed by ATP inducing a slow conformational change of the linker to hinge toward the base. Lastly, the stalk attaches to a new location on the microtubule which then allows the release of hydrolysis product from AAA1 so that the linker could move toward the stalk.

1.4.4 Inner dynein arm proteins

The IDA heavy chain also contains the ring-like head for ATP hydrolysis, B-terminal tail, and stalk (Burgess et al., 2003). In *Chlamydomonas*, there are three population of inner dynein arm, IDA1, IDA2, and IDA3. IDA1 has four dynein heavy chains, but IDA2 and IDA3 each have two dynein heavy chains, with this arrangement of IDAs repeating once every 96 nm. There is a strap-like link between the inner and outer dynein arms, nexin, to the next B-tubule (Burgess, Da, Dover, & Woolley, 1991).

The IDA is composed of one heterodimeric and six monomeric dyneins. The heterodimeric dynein is known as dynein f, which is located close to the A-tubule. The six monomeric dyneins are dynein a, b, c, d, e, and g, and their AAA+ rings are colinear to form three dyads around two radial spokes (K. H. Bui, H, Movassagh, Oiwa, & Ishikawa, 2008). RS2 could form a coupled association with IDA subform c to suggest that motor activity could be regulated by the mechanical signal via radial spokes (M. Gui, Ma, et al., 2021). Each of the formed dyads is composed of two heavy chains, and a radial spoke. Therefore, IDA monomers work as functional dimers in the axoneme, and the combination of dyneins is necessary for the axoneme's function. The N-terminal tail of the six heavy chains orients towards the tip of the cilium, at the distal side of the AAA+ rings. The α and β rings of IDA and ODA could contact the adjacent B-tubule through their stalks, but the IDA probably have different handedness or AAA rings in a different orientation compare to ODA (K. H. Bui et al., 2008).

1.4.5 Inner and outer dynein arm communication

The IDA can functionally communicate with ODA via intermediate chain 2 (IC2). Intermediate chain 2 from ODA can interact with the nexin-dynein regulatory complex to become part of a connection is known as the outer-inner dynein (OID) linker (Oda, Yagi, Yanagisawa, & Kikkawa, 2013). The OID linker could control both the ODAs and IDAs, which in turn modulate flagellar beating. Using biotinylation experiments, IC2 was identified as a hub between IDAs and ODAs. The addition of a biotinylation tag to the amino terminus of IC2 resulted in an altered waveform, corresponding to the altered activity of IDA (Oda et al., 2013). IC2 mutant also showed enhanced ATPase activities of ODA. These results suggest a functional connection between the IDA and ODA via IC2 (Oda et al., 2013).

As shown in Figure 1.5A, the 96-nm periodic repeat of axoneme contains four outer arms, one inner arm I1/f, six monomeric inner arms, and two radial spokes (three in *Tetrahymena*). The N-DRC complex (Heuser, M, Krell, Porter, & Nicastro, 2009) and the modifier of inner arms (MIA) complex (Yamamoto et al., 2013) are included in the periodic repeat, with the N-DRC linked to inner arm I1/f. One of four outer arm repeat is structurally connected to inner arm I1/f via a linker, and this linker is likely to provide signals from the central pair/radial spokes to the outer arms for regulation (Barber, Heuser, Carbajal-González, Botchkarev, & Nicastro, 2011; K. H. Bui et al., 2008).

1.4.6 Outer dynein arm proteins

Depending on the species, the ODA could possess one to three heavy chains that are responsible for the motor activities (I. R. Gibbons & Rowe, 1965). Dynein arms also consist of two intermediate chains, numerous light chains, and docking complex proteins (Figure 1.6 A). Unlike the cytoplasmic and IFT dyneins formed by homodimers of heavy chains, ODA heavy arms are encoded by different genes with distinctive ATPase and motor properties. The amino-terminal of axonemal heavy arms requires binding to two WD-repeat intermediate chains and light chains subcomplexes. This subcomplex belongs to three different classes, namely, LC8 (S. M. King & Patel-King, 1995), Tctex1 (Harrison, P, & King, 1998), and LC7 (Bowman et al., 1999), and are required for assembly of dynein motor. Mutants for ODA WD-repeat intermediate chains show that ODA subunits cannot be incorporated into the axoneme (Mitchell & Kang, 1991; Wilkerson, King, Koutoulis, Pazour, & Witman, 1995).

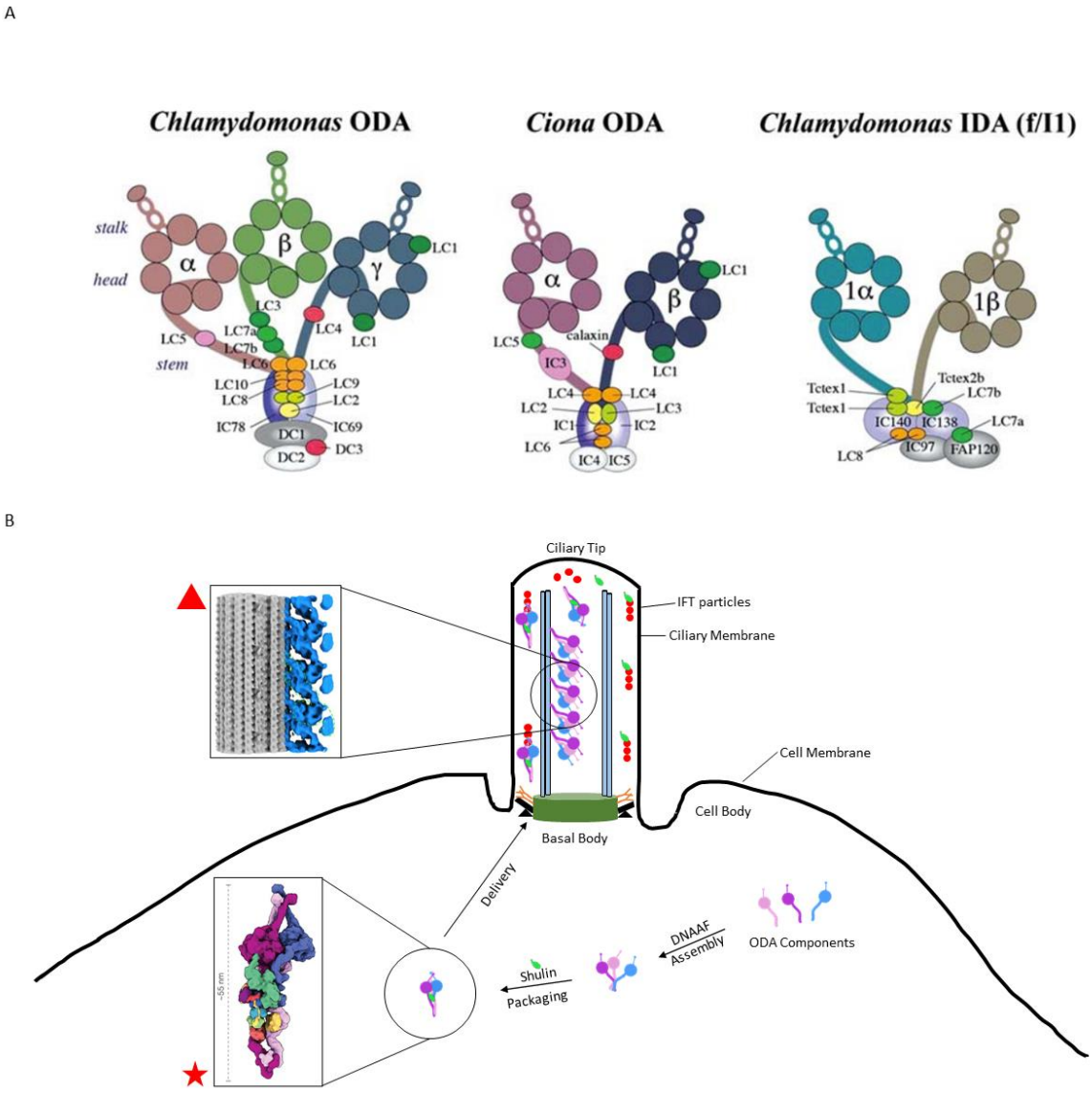

Figure 1.6 *Chlamydomonas* and *Ciona* ODA and diagram for ODA assembly in *Tetrahymena*

A. Schematic of *Chlamydomonas* and *Ciona* Outer Dynein Arm (ODA) and Inner Dynein Arm (IDA). Diagram borrowed from Inaba, 2011, Mol Hum Reproduction, with permission.

B. Diagram showing the assembly of ODA in cytoplasm and activation of ODA complex inside the cilium. Initially, in cytoplasm, after translation of ODA proteins, they are assembled by dynein axonemal assembly factors (DNAAFs). Then, it is packaged by Shulin, a regulatory protein. Red star show the surface rendering view of ODA complex with Shulin bound (adapted from Kubo et al., 2021, EMBO Report with permission). After packaging the ODA is delivered into the cilium

by IFT trains, and then later activated as it docks onto the doublet microtubules with Shulin destabilized to leave. The activated ODA complex forms a row on doublet microtubules, illustrated by Red Triangle, the 24 nm structure of ODA-doublet microtubules at 18 Å, from *Tetrahymena* K40R doublets. The unbound Shulin gets transported back to the cell body via IFT.

Each dynein heavy chain contains approximately 4500 residues and is estimated to take at least 13 minutes for each eukaryotic ribosome (Ingolia, Lf, & Weissman, 2011). Many assembly factors in the cytoplasm are required to stabilize and maintain large, heavy chain proteins to prevent aggregation (Figure 1.6B). Some of these factors are ODA7 (Duquesnoy et al., 2009), PIH domain proteins (Omran et al., 2008; Yamamoto, Hirono, & Kamiya, 2010), and Dyx1c1 which interact with Hsp70 and Hsp90 for help folding dynein components (Tarkar et al., 2013). Each of the dynein components (such as light chains and WD-repeat intermediate chains) are then assembled into discrete subcomplexes further associated with heavy chains and regulatory light chains to become a complete dynein arm complex (Fowkes & Mitchell, 1998). At this stage, the ODA needs to be transported into the cilium via IFT.

Prior to IFT, ODA needs to be held together in an inactive form for intraflagellar transport from the cell body into the cilium (Figure 1.6B), on the basis that active ODA probably interact with doublet microtubules and its traffic at the ciliary base (minus end) (Stephen M. King, 2016). This inactivation was supported in *Chlamydomonas* that FBB18 (C21orf59 in Zebrafish), an assembly factor, is likely to keep the ODA in its inactive conformation before being incorporated into the doublet microtubules (Austin-Tse et al., 2013). In *Tetrehymena*, Mali et al. (2021) showed that a regulatory protein, Shulin, binds to newly synthesized ODA and keeps the complex inactive during

IFT (Figure 1.6B star). Before IFT, the ODA complex needs to interact with specific adaptor proteins that help its attachment to IFT proteins. In *Chlamydomonas*, the ODA16 protein helps to target the ODA complex specifically to IFT46 protein during transport into the cilium (Ahmed et al., 2008).

In *Chlamydomonas* and *Tetrahymena*, the ODA is at least 1.2~2 MDa complex, containing three heavy chains and 11 light chains (G.J., Agrin, Walker, & Witman, 2006; Sakato & King, 2004). As shown in the Figure 1.6B (triangle), these ODA form a 24-nm repeating row on doublet microtubules via the docking complex (Khanh Huy Bui et al., 2012; T. Oda, T. Abe, H. Yanagisawa, & M. Kikkawa, 2016; Owa et al., 2014). The docking complex has a flexible conformation and mediate ODA binding to the doublet microtubule. ODAs get released from the doublet microtubule when the docking complex is absent under low ionic strength conditions, suggesting that the docking complex helps to stabilize the ODA by strengthening the electrostatic interactions (T. Oda, T. Abe, H. Yanagisawa, & M. Kikkawa, 2016). However, it is unclear about the mechanism of action for the interaction between the docking complex and doublet microtubules.

The heads from heavy chains of each ODA complex contain AAA+ for ATP hydrolysis. Since ODA contains three heavy chains, the three head motor domains would be aligned parallel to another to easily interact with the adjacent doublet microtubules when the dynein arm is in an active conformation. In inactive conformation, cryo-electron microscopy (cryo-EM) shows that the three ODA heads are joined together by a tail region containing dynein accessory chain

interaction sites (Mali et al., 2021b). Shulin binds to the ODA tail to make bridging contact for clustering the three motor domains together. Thus, Shulin could compact the three heads and perform an inhibitory function by transforming the ODA from an open to a closed state. Compaction by Shulin is likely necessary due to the transport of the ODA complex from the cytoplasm into the cilium, and a closed conformation is preferable when the ODA motor activity is shut down (Mali et al., 2021b). However, the closed conformation bound by Shulin is different from the active conformation when the three motor domains are in parallel. Therefore, it is unclear how the ODA incorporates into the ciliary axoneme and how ODA undergo conformational changes from inactive to active.

1.5 Post-translational modification of the axoneme

1.5.1 Post-translational modification of singlet microtubules

Microtubules are involved in many important cellular functions, such as mitosis, motility, cell shape (cytoskeleton), and signalling. Though microtubules were assembled from just α- and β-tubulin, they can bind and interact with many other proteins. Post-translational modifications (PTMs) of tubulin allow a different function to be performed or a variety of MAPs to be bound via modification of localization sites on parts of microtubules. Many types of PTMs could happen in or on the microtubule, usually concurrently, with other types of PTMs simultaneously (Figure 1.7A).

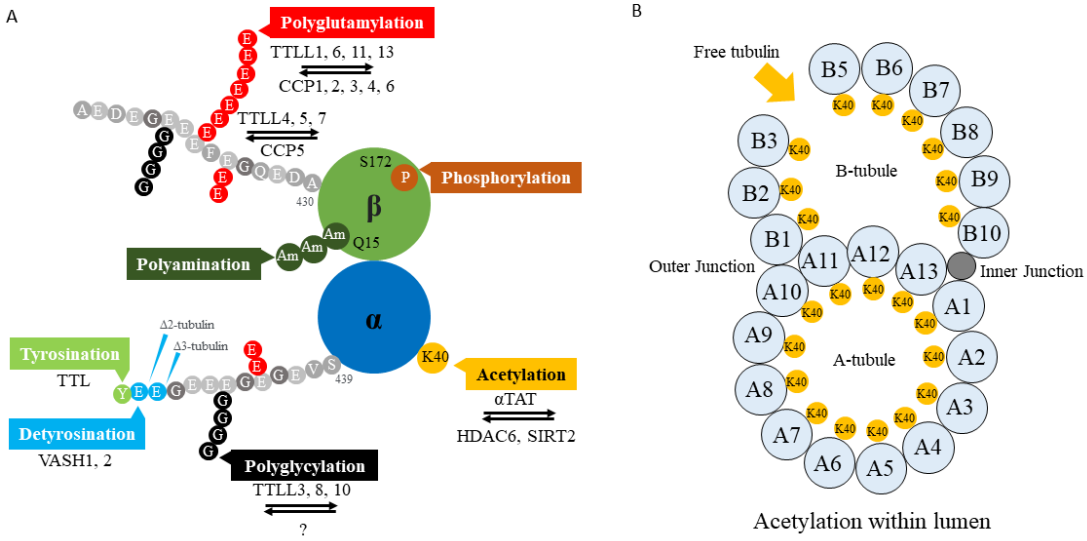

Figure 1.7 Typical types of post-translational modification for doublet microtubules.

A. Cartoon to show tyrosination (lime green), detyrosination (sky blue) to remove glutamate residues for producing Δ2-tubulin and Δ3-tubulin, polyglycylation (black) for addition of glycine onto glutamates, acetylation (yellow) of K40 on α-tubulin, polyamination (Am) of Q15 on β-tubulin, phosphorylation (P) of S172 on β-tubulin, and polyglutamylation (red) to produce long

chains of glutamates. Note that TTLL4, 5, 7 prefers the initiation of polyglutamylation, while TTLL1, 6, 11, 13 are more specific to the elongation process.

B. Cartoon to show that the acetylation of K40 within lumen of α-tubulin in both A-tubule and B-tubule. Acetylated K40 may help to stabilize cracks in the microtubule lattice by restricting motion and lower the disorder of K40 loop to maintain structure integrity, such that free tubulin has time to fill-in and repair the cracked structure.

1.5.1.1 Acetylation of microtubules

One of the most-studied PTM in tubulin is the acetylation of lysine 40 (K40) on singlet and doublet microtubules. Acetylation is catalyzed by α-acetyltransferase 1 (αTAT1), also known as MEC-17, and is 100 times more active on polymerized tubulins than the unpolymerized state (Figure 1.7B). ATAT2 has only been seen in *Caenorhabditis elegans*. Deacetylation is usually carried out by HDAC6 and SIRT2. Acetylation of K40 takes place inside the lumen of microtubules on α-tubulins. Because it is inside the lumen, the acetylation site is away from the outer surface of microtubules, where most MAPs and motor protein binding takes place. Logically, this probably makes acetylation less likely to regulate MAPs and motor proteins. But Hammond et al. (2010) has shown that acetylation could affect the motility rate of motor proteins kinesin-1 in axons (Hammond et al., 2010). Acetylation could slow down the kinesin-1 motility rate and binds weakly in mutant ciliary axoneme without acetylation in neurites (Reed et al., 2006). However, it was suggested enriching the acetylation level itself does not change the activity of kinesin-1 (Hammond et al., 2010; W. J. Walter, V., Fischermeier, & Diez, 2012). Acetylation does allow preferred binding of kinesin-1 walking on acetylated microtubules but does not affect the motor-based transport rate (Kaul, Soppina, & Verhey, 2014; W. J. Walter et al., 2012). In polarized neuronal cells, perhaps acetylation works with other PTMs. Detyrosination and polyglutamylation achieve a combined effect for performing cellular functions (Hammond et al., 2010). Other suggested acetylation sites could be K60 and K370 in α-tubulin and K103 in β-tubulin (Eshun-Wilson et al., 2019; N. Liu et al., 2015).

Acetylation may prolong the lifespan of microtubule in cells (G., LeDizet, & Chang, 1987; H., K., & Rosenbaum, 1986; M. & Piperno, 1986). It was proposed based on the observation that stabilization of microtubules led to their acetylation because increasing tubulin acetylation level did not increase microtubule stability. Recent observations suggest that acetylation may have a role in protecting microtubules from breaking and mechanical ageing (Portran, Schaedel, Xu, Théry, & Nachury, 2017; Xu et al., 2017). Microtubules in the cell are constantly exposed to stress such as mechanical forces and bending, so these motions would likely damage the microtubule lattice, leading to microtubule breakage. Acetylation was proposed to increase flexibility in the microtubule such that they are better suited for mechanical stress (Xu et al., 2017). Xu et al. (2017) observed that most hotspots for acetylation were found at microtubules bends or curvatures, which correlate to regions that had stress-induced cracks. This result also suggests a possible mechanism for αTAT1 to enter the lumen is via cracks and openings in the microtubule lattice when they are introduced (Schaap, Carrasco, de Pablo, MacKintosh, & Schmidt, 2006). Once αTAT1 enters the lumen, it could acetylate sites and help the damaged region more resistant to mechanical forces. Meanwhile, free tubulin dimers come to self-repair the opening and prolong the microtubule lifespan by restoring the microtubule's original stiffness (Schaedel et al., 2015). Other hypotheses exist for αTAT1 localization into the lumen, such as through open microtubule ends but unlikely because the ends of a microtubule inside a living cell are likely obstructed by proteins (Coombes et al., 2016). To summarize, acetylation of microtubules exists as a self-repair mechanism for increasing microtubule's adaptation to mechanical stresses.

The structure of K40 in microtubules was not visualized because it is highly disordered and flexible. However, recently, doublet microtubule assembled *in vitro* show that once the microtubules are

acetylated, the range of motion for the K40 loop is restricted, while the loop extends deeper into the microtubule lumen in a deacetylated state (Eshun-Wilson et al., 2019). Thus, the loop could have more conformation in the deacetylated state and likely influence lateral contacts between MIPs.

1.5.1.2 Detyrosination of microtubules

Tyrosination is a conserved PTM process among eukaryotes that involves incorporating tyrosine into α-tubulin and reversible via detyrosination (Figure 1.7A). Tubulin is usually tyrosinated, so that detyrosination would be the PTM in interest. The carboxypeptidase responsible for catalyzing detyrosination has not been discovered, which removes the carboxyl-terminal tyrosine to expose the penultimate glutamate residue in α-tubulin that can be further removed by deglutamylation by cytosolic carboxypeptidase to create a Δ2 α-tubulin (Arce & Barra, 1983; N & Flavin, 1981; Rogowski et al., 2010) (further discussed below). Tubulin tyrosine ligase (TTL) was identified to perform the function of tyrosination (Ersfeld et al., 1993; Schröder Hc - Wehland, Wehland J - Weber, & Weber, 1985). TTL modify free tubulin, and stable microtubules are mostly detyrosinated, suggesting that the detyrosination and tyrosination of microtubules are dependent on its dynamic instability (Prota et al., 2013; Schröder Hc - Wehland et al., 1985; Szyk, Deaconescu, Piszczek, & Roll-Mecak, 2011). Detyrosination is expected to enhance kinesin-1 in neurons (Hammond et al., 2010) and negatively regulate the activity of microtubule-depolymerizing kinesin (Peris et al., 2009).

1.5.1.3 Deglutamylation of microtubules

Deglutamylation occurs when cytosolic carboxypeptidase (CCP) removes side chains of glutamate (Es) that were added onto the glutamate residues in the protein sequence itself (Eddé et al., 1990). As shown in Figure 1.7A, the addition of these long chains of additional glutamates are known as poly-glutamylation, which occurs on several sites in the γ-carboxyl group of glutamates within the carboxyl-terminal tails (CTTs) of both tubulin dimers (Eddé et al., 1990; V. Redeker, Le Caer, Rossier, & Prome, 1991; V. Redeker, Melki R - Promé, Promé D - Le Caer, Le Caer Jp - Rossier, & Rossier, 1992). Polyglutamylation is catalyzed by tubulin tyrosine ligase-like family proteins (TTLLs), and the final polyglutamylation pattern is dependent on the specific TTLL (Janke et al., 2005). There are many types of TTLL, which differ in chain-initiating or elongating activities, on either α- or β-tubulins, have an autonomous activity or need associated activators (Janke et al., 2005; Suryavanshi et al., 2010; van Dijk et al., 2007; Wloga et al., 2008).

Polyglutamylation could regulate the electrostatic interaction between microtubules and proteins (Janke, K, & van Dijk, 2008; Tomohiro Kubo & Oda, 2017; Lacroix et al., 2010). This regulation could be done by changing the charges of carboxyl-terminal tails on tubulins to form a negatively charged “polymer brush” (Roll-Mecak, 2015). High levels of polyglutamylation were discovered on centrioles and ciliary axoneme, as the glutamylation level was increased on the central mitotic spindle and the midbody (Chelsea B. Backer, Gutzman, Pearson, & Cheeseman, 2012; Shinya Ohta, Mayako Hamada, Nobuko Sato, & Iyo Toramoto, 2015). However, unregulated glutamylation or hyper-glutamylation could lead to neurodegeneration in mouse

Purkinje cells (M. Magiera et al., 2018). *Tetrahymena* cells overexpressing TTLL6 results in hyper-glutamylation of cytoplasmic microtubules that are resistant to depolymerization (Wloga et al., 2010).

1.5.1.4 Poly-glycylation, poly-amination, phosphorylation in microtubules

Poly-glycylation creates chains of glycine on glutamate residues of both tubulin dimers (Figure 1.7A). Glycylases and polyglutamylation enzymes are both in the TTLL family, but not much is known about the function of glycylation in cytoplasmic microtubules (Rogowski et al., 2019).

Poly-amination is the irreversible addition of amines to glutamine residues on free tubulin and microtubules, done by a transglutaminase (Figure 1.7A). Poly-aminated microtubules are stable under cold or calcium-induced depolymerization experiments, with poly-amination sites found close to GTP-binding site for β-tubulin or dimer boundary (Song et al., 2013).

Tubulin could be phosphorylated, but only one site has been identified on S172 of β-tubulin (Figure 1.7A). During mitosis, cyclin-dependent kinase 1 (CDK1) catalyze phosphorylation on serine 172 of β-tubulin, results in impaired GTP binding and interaction between tubulin dimers (Fourest-Lieuvin et al., 2006). Furthermore, transient transfection tubulin mutants that mimic phosphorylated tubulin also impair tubulin dimer interaction, suggesting that tubulin phosphorylation by CDK1 could potentially regulate microtubule dynamics during cell division (Fourest-Lieuvin et al., 2006).

Other types of PTM in tubulin exist, such as ubiquitination for misfolded tubulin (Ren, 2003). In addition, palmitoylation regulates microtubule-membrane via hydrophobic interactions (Caron,

1997; Zambito & Wolff, 1997). glycosylation, arginylation, methylation and sumoylation have been reported, but additional research is needed to study their function and sites on tubulin.

1.5.2 Conservation of PTMs in doublet microtubules

Like microtubules in the cytoplasm, doublet microtubules also undergo several types of PTMs conserved among ciliated organisms. It was speculated that PTMs might have co-evolved with the evolution of cilia (Janke et al., 2005), an example being αTAT1 which is highly conserved in modifying K40 of α-tubulin in 9+0 and 9+2 axonemes (Shida et al., 2010). In *Caenorhabditis elegans*, MEC-17 (homolog of αTAT1) was initially identified as a BBSome-associated protein expressed in touch receptor neurons (Jin et al., 2010; Loktev et al., 2008; Y. Zhang et al., 2002). A paralog, αTAT-2, is expressed in touch receptor neurons and ciliated neurons (Shida et al., 2010). *Caenorhabditis elegans* lacking MEC-17 and its paralog αTAT-2 leads to decreased sensitivity in touch. Transgenic expression of α-tubulin (K40Q) that mimics acetylation could restore touch sensation (Shida et al., 2010). Depletion of αTAT1 in RPE-hTERT cells when entering quiescence delayed the construction of primary cilia, as αTAT1 is responsible for acetylation of both cytoplasmic microtubules and ciliary doublet microtubules (Shida et al., 2010). These results suggest that PTMs, such as acetylation, may play an important role in the conserved function of ciliogenesis and mechanosensation. Due to the important biological roles of PTMs, PTM activities would be conserved during evolution.

1.5.3 Can PTMs affect each other?

Traditionally, antibodies that recognize PTMs were used to detect cilia (M. M. Magiera & Janke, 2013), but functional roles of PTMs in cilia were not examined until recently. It is interesting to note that the levels of PTMs may be different inside the cilium. For example, in *Tetrahymena* cells, shorter cilia labelled with antibodies have higher levels of polyglutamylation and lower levels of poly-glycylation when compared to longer cilia in the same cell (Sharma et al., 2007). This phenotype is likely caused due to a proposed mechanism called "tubulin code" (Verhey, 2007), where PTMs of tubulin can selectively generate marks or codes that can be read by motor proteins, MAPs, or severing factors that interact with the microtubule.

PTMs may work in conjunction or competitively to help doublet microtubules perform functions in the cilium that may be related or identical to functions outside the cilium. Multiple PTMs could be found on the same CTT of axonemal tubulins, such as detyrosination, polyglutamylation, and poly-glycylation (Virginie Redeker et al., 2005). As such, microtubule effector activity could be dependent on multiple PTMs on the same CTT to amplify its functions rather than individual PTM (Verhey, 2007). Each of these PTM could influence the activity rate of another PTM. For example, in mice that lack a noncatalytic subunit of α-tubulin polyglutamylation, α-tubulin tyrosination was detected while α-tubulin acetylation and β-polyglutamylation stayed the same (Koji Ikegami et al., 2007). PTM could also have a "trans-tail" effect that affects modifications on neighbouring CTTs. For example, PTMs may have a cross-talk when site-directed mutagenesis of glycylation sites in *Tetrahymena* tubulin affected

the level of glutamylation and glycylation in both mutated and non-mutated tubulin subunits (Virginie Redeker et al., 2005).

1.5.4 Detyrosination of α-tubulin

Inside the cilia, tubulin detyrosination takes place on the B-tubules of doublet microtubules (Johnson, 1998). Furthermore, detyrosination could increase the velocity of kinesin-2 *in vitro* (Sirajuddin et al., 2014). This result is consistent with the electron microscopy findings that anterograde IFT trains are travelling on the B-tubules and suggest that IFT could be a collision-free process between the basal body and tip of the cilium (Jordan & Pigino, 2019; Stepanek & Pigino, 2016).

1.5.4 Poly-glutamylation in cilia

Glutamylation has important functions in *Tetrahymena* cilia and is highly enriched on the B-tubule of the nine outer doublet microtubules in motile cilia (Tomohiro Kubo, Yanagisawa, Yagi, Hirono, & Kamiya, 2010; Lechtreck & Geimer, 2000; Suryavanshi et al., 2010). It is not clear why the B-tubules are highly saturated with glutamylation, perhaps because the A-tubule surface is full of dynein arms and radial spokes (T. Ishikawa, 2015). Substitution of glutamates (positions 437–442 EEEEGE) to nonmodifiable aspartates (Ds) on the CCT of β-tubulin could lead to severe axonemes assembly defects such as short cilia, loss of central pair, and loss of B-tubules (Xia et al., 2000). This failure in axoneme assembly caused by the substitution of glutamates (Es) on the CTT of β-tubulin could be rescued by placing α-tubulin CTT with the corresponding protein sequence (Duan & Gorovsky, 2002; Xia et al., 2000). These mutation and rescue experiments suggest that at least two of the four consecutive glutamates are needed for cells to survive, and Es by itself will result in lethal phenotypes, whereas the exact placement of Es on the CTT is not important (Xia et al., 2000).

Glutamylation on α-tubulin is not essential to cell survival as substitution of all the glutamates on CTT of α-tubulin did not result in lethal phenotypes (Wloga et al., 2008). However, glutamylation on α-tubulin is required for assembly and function of some microtubule-based-organelle, as disruption of glutamyl ligase enzymes (TTLL1 and TTLL9) disrupted proper docking of basal bodies at the plasma membrane (Wloga et al., 2008). Interestingly, in *Tetrahymena* cilia, doublet microtubules are glutamylated, but the central microtubules are not (Suryavanshi et al., 2010).

Another important function for TTLLs is the assembly and stability of doublet microtubules in mammalian sperm. Male mice that lack TTLL1 are infertile and have abnormal development of sperm flagella with truncated axonemes (Campbell et al., 2002; Regnard et al., 2003). Mice that lack TTLL5 are sometimes missing doublet number 4 in sperm (G. S. Lee et al., 2013). Deficiency of TTLL9 results in losing a distal portion of doublet microtubule number 7 in mouse sperm (Konno et al., 2016). These axonemal defects in sperm could be due to instability or misassembled doublet microtubule, as hyper-glutamylation of cytoplasmic microtubules are resistant to depolymerization in conjunction with increased K40-acetylation (Wloga et al., 2010). Tubulin glutamylation could promote colocalization of centriole and spindle associate proteins (CSAP) that increase the stability of microtubules in cilia, centrioles, and the mitotic spindle (C. B. Backer, Gutzman Jh - Pearson, Pearson Cg - Cheeseman, & Cheeseman, 2012; S. Ohta, M. Hamada, N. Sato, & I. Toramoto, 2015). CSAP is proposed to be a tubulin code reader to recognize and stabilize poly-glutamylated microtubules in cytoplasm and cilia (Wloga, Joachimiak, Louka, & Gaertig, 2017b).

Hyper-glutamylation could have positive and negative effects in the same cilium, namely for its role in disassembly and shortening cilia. CCP1 is a deglutamylase. Hyperglutamylation caused by loss of CCP1 could increase IFT speed but results in loss of B-tubules and a progressive age-dependent defect of cilia axoneme (O'Hagan et al., 2011). Loss of CCP in mice also results in degeneration of Purkinje neurons (M. Magiera et al., 2018). Likewise, overexpression of glutamylase, such as TTLL6 in *Tetrahymena*, results in rapid shortening of cilia and fragmentation

of the axoneme, possibly due to loss of B-tubules (Wloga et al., 2010). However, this depolymerization is axoneme specific as other cilia in the same cell could remain stabilized, possibly due to each cilium's different levels of expression (Wloga et al., 2010). As such, hyper-glutamylation is probably not a promotor of doublet microtubule assembly but activates or stimulates depolymerizers such as katanin to sever the axoneme (O'Hagan & Barr, 2012; Sharma et al., 2007). Spastin is another depolymerizer whose activity could be promoted with a small number of glutamates on the tubulin but inhibited when a large number of glutamates are present (Valenstein & Roll-Mecak, 2016).

Chlamydomonas mutants lacking IDAs, ODAs, or nexin-DRC often have short flagella (B., Piperno, & Luck, 1979; LeDizet & Piperno, 1995; Yamamoto et al., 2010), but reducing tubulin glutamylation level in cilia via loss of function TTLL9 or FAP234 (an associated protein of glutamylation transported by IFT) elongates the cilia and slow down disassembly of the flagella (T. Kubo, Hirono, Aikawa, Kamiya, & Witman, 2015). Therefore, it is hypothesized that tubulin polyglutamylation has a shortening effect in axonemes with incomplete A-tubule associated proteins. Protein complexes bound to A-tubule could stabilize the axoneme, but glutamylation destabilizes the axoneme. Furthermore, proteins in A-tubule could compete with axoneme shortening mediated by tubulin glutamylation, where hyper-glutamylation could destabilize the axoneme (Wloga et al., 2017b).

1.5.5 Poly-glycylation in cilia

Glycylation is carried out by a subset of TTLLs and is a potential competitor of glutamylation (Rogowski et al., 2019; Wloga et al., 2009), as both occur within the same cluster of glutamates (V. Redeker et al., 1994). Polyglycine sidechains have an extended conformation, whereas polyglutamate side chains form swollen coils due to the increased negative charges (Roll-Mecak, 2015). Not all ciliated species have tubulin glycylation. In most organisms, TTLL3 is an initiase, and TTLL10 is an elongase (K. Ikegami et al., 2008; K. Ikegami & Setou, 2009; Rogowski et al., 2019; Wloga et al., 2009), but in *Drosophila melanogaster,* poly-glycylated tubulin is generated by TTLL3 alone (Rogowski et al., 2019). Only a single glycine is added in primate and human cilia due to a mutation that affects TTLL10's catalytic center (Rogowski et al., 2019). Knocking out all six paralogs of TTLL3 in *Tetrahymena* causes cells to have shorter cilia and fail to elongate in the presence of paclitaxel (Wloga et al., 2009). In zebrafish, depletion of both TTLL3 and TTLL6 results in missing B-tubules, misplaced doublets, and supernumerary central pairs (Pathak, C.A., & Drummond, 2011). In mice, both glycylases TTLL3 and TTLL8 stabilize the ependymal cilia, and TTLL6 glutamylase is responsible for ciliary beating (Bosch Grau et al., 2013). Depletion of TTLL3 causes disassembly of already constructed motile cilia, whereas depletion of TTLL8 causes a reduction in the number of multi-ciliated cells (Bosch Grau et al., 2013). Because loss of glycylation resulted in increased glutamylation (Rogowski et al., 2019; Wloga et al., 2009), to further propose that glycylation and glutamylation could have different and, if not competitive biological effects. However, due to the shear amount of different glutamylase members, knocking out all these enzymes would be difficult. Depletion of some of these glutamylase by siRNA only resulted in reduced ciliary beating frequency, and not in decreased polyglutamylation level (Bosch

Grau et al., 2013). Therefore, additional research would be required to test the competition hypothesis between glycylation and glutamylation in higher eukaryotes.

1.5.6 Acetylation in cilia

Acetylation was first discovered in flagella of *Chlamydomonas reinhardtii* (M. & Piperno, 1987; S.W. & Rosenbaum, 1983), and is carried out by αTAT1 on K40 inside the lumen of doublet microtubules (Figure 1.7B). HDAC6 (Hubbert et al., 2002; Y. Zhang et al., 2003) and SIRT2 (North, B.L., Borra, Denu, & Verdin, 2003) are two deacetylases that could promote assembly of mammalian primary cilia, knockdown of either deacetylase results in longer primary cilia, and overexpression leads to shorter or fewer cilia (Bangs, Schrode, Hadjantonakis, & Anderson, 2015; Pugacheva et al., 2007; Ran, Yang, Li, Liu, & Zhou, 2015; Yang et al., 2014; Zhou et al., 2014). The effect of HDAC6 overexpression could be countered by overexpression of K40Q, α-tubulin that mimics acetylated-K. This result suggests that HDAC6 and possibly SIRT2 could have a doublet microtubule depolymerization effect by destabilizing the lattice (Cueva, J., & Huang, 2012). HDAC6 could also stimulate actin polymerization at the basal body of primary cilia, whereas inhibition of actin polymerization trigger disassembly of the cilium (Ran et al., 2015). It is interesting to note that ciliary disassembly due to lysine polyubiquitination is unlikely mediated by HDAC6 or SIRT2 because the polyubiquitinated α-tubulin are acetylated (Huang, Dr, & Rosenbaum, 2009).

In *Chlamydomonas*, the expression of K40R mutation for α-tubulin did not affect the biological phenotype. Acetylation of K40 is probably not essential in *Tetrahymena* (Gaertig et al., 1995) via analysis of a K40R single mutation construct. Another acetylation mutant was generated by disrupting the *MEC-17* gene using homologous DNA recombination to replace the coding region with neo4 marker in *Tetrahymena* (Akella et al., 2010). The K40R mutant has a minimal amount

of acetylated cilia, while the MEC17 strain detects no acetylated cilia if labelled using an acetyl-K antibody (Akella et al., 2010). Direct light microscopy observation of both *Tetrahymena* K40R and *MEC-17* mutants showed normal cilia compare to wild-type, but with altered sensitivities to taxol (Akella et al., 2010).

Mice lacking α-TAT1 are healthy, but their sperm beats with reduced bend amplitude and distorted gyrus (Kalebic et al., 2013; Kim et al., 2013). The interaction of acetylation with other PTMs is unknown, but it was shown that *Tetrahymena* mutants deficient in glycylation has increased acetyl-K40 in the ciliary axoneme (Wloga et al., 2009), whereas tubulin detyrosination is decreased in *α-TAT1* deleted cells (Xu et al., 2017). This result may suggest a compensatory mechanism that may exist to make up for the absence of acetyl-K40 in organisms that have lost this PTM and only show mild consequences (Wloga et al., 2017b).

1.5.7 Effects of post-translational modification on ciliary motility

The doublet microtubules undergo many types of post-translational modifications (PTM). Some of the PTMs could have effects on the ciliary motility of IDA and ODA. For example, as deacetylation by SIRT2 decreases, acetylation of Lysine-40 (K40) increases ODA activity on doublet microtubules *in vitro,* respectively (Alper et al., 2014). Cryo-electron tomography did not detect a difference between acetylated tubulin and non-acetylated tubulin inside the axoneme and how this would affect other proteins (Howes, GM, Shida, Nachury, & Nogales, 2014).

In model organisms such as mice, *Chlamydomonas, Tetrahymena,* Zebrafish, mammalian ependyma and sperm cell lines, losing glutamylation TTLL (TTLL1, 5, 6, 9) results in a disturbed waveform, beat frequency or stalled beating of motile cilia (Bosch Grau et al., 2013; K. Ikegami, Sato S - Nakamura, Nakamura K - Ostrowski, Ostrowski Le - Setou, & Setou, 2010; Konno et al., 2016; Tomohiro Kubo et al., 2010; Pathak et al., 2011; Suryavanshi et al., 2010). Glutamylation of tubulin has more effects on IDA than ODA. Glutamylation of doublet microtubule could affect ODAs: if TTLL6, a tubulin elongase, is absent, the beat frequency would decrease (Suryavanshi et al., 2010). In axoneme that lack ODA, TTLL6 or TTLL9 glutamylase deficiency would increase the velocity of microtubule sliding, in which forces are solely generated by IDAs (Tomohiro Kubo et al., 2010; Suryavanshi et al., 2010). However, *Chlamydomonas* double mutants lacking both ODAs and TTLL9 glutamylase is completely paralyzed, but mutant lacking ODA would only have reduced motility (relying on the force generated by IDA) (Tomohiro Kubo et al., 2010). This result suggests that glutamylation of the tubulin may be necessary for regulating IDA, which controls the waveform motion of cilia. In zebrafish, deglutamylases mutant *ccp5* resulted in hyper-

glutamylation of doublet microtubules, which show a reduced beat amplitude of pronephric cilia (Pathak, Austin-Tse, Liu, Vasilyev, & Drummond, 2014). These results suggest that tubulin glutamylation may have an inhibitory effect on IDA activity by restraining the net force IDA exerted on doublet microtubules.

Chlamydomonas loss of TTLL9 greatly reduces inner-arm dynein species' motility but slightly affects dynein e mutant (Tomohiro Kubo et al., 2010). Dynein e may be responsible for producing an initial force in the axoneme for sliding disintegration (a mechanism triggered when nexin-dynein regulatory complex (N-DRC) is digested, and dynein are treated with ATP such that microtubule doublets are sliding past each other). TTLL9 mutant with active ODA and inner-dynein species a–e and g show increased microtubule sliding disintegration velocity rather than decrease (Tomohiro Kubo et al., 2010). Besides, the microtubule-binding domain of dynein e contains positively charges patches that interact with polyglutamate side chains, which are negatively charged. Therefore, glutamylation of tubulin would increase the time dynein e is bound to the microtubule to potentially affect the interaction of dynein e with adjacent polyglutamated doublet microtubule and the N-DRC. These results suggest that dynein e could be one of the main targets of tubulin glutamylation for regulating axonemal motility (Tomohiro Kubo et al., 2010).

1.6 Ciliopathies

Ciliopathy is a collective name for diseases related to the cilia, or more specifically, disorders caused by mutations in ciliary proteins that contribute to abnormal structure or function of eukaryotic cilia and flagella (Figure 1.8A). There are many ciliopathies. As of July 12, 2017, 35 ciliopathies have been confirmed in humans (Reiter & Leroux, 2017), with an estimated 1 in 1000 people being affected ("Welcome to the Ciliopathy Alliance," 2020). In addition, there are over 240 proteins that are candidates to ciliopathy proteins, and another 180 are established ciliopathy-associated proteins (Reiter & Leroux, 2017).

Ciliopathies were overlooked as human cilia were thought to be a vestigial organelle for a century since its discovery in 1898 (Zimmermann, 1898). With government funding wasted in war efforts, space race, nuclear weapons testing, and red tape, the insufficient funding for basic research limited our understanding of cilia. Ciliopathies were initially thought of as parts of other diseases, such as cancer or congenital conditions. Patients diagnosed with *situs inversus* were thought to have an autosomal recessive condition, but now it is known that a portion of *situs inversus* patients could also have primary ciliary dyskinesia (PCD). Not all *situs inversus* patients have PCD, but 50% of PCD patients have *situs inversus* (Stillwell, Wartchow, & Sagel, 2011). Approximately 30-35% of PCD patients could have mutations in ODA genes *DNAI1* or *DNAH5* (Zariwala, Knowles, & Omran, 2007). With genomic sequencing, molecular biology, and microscopy techniques advancement in the late 20th century and 21st century, more ciliopathies are starting to be identified for finding better treatments in patients affected.

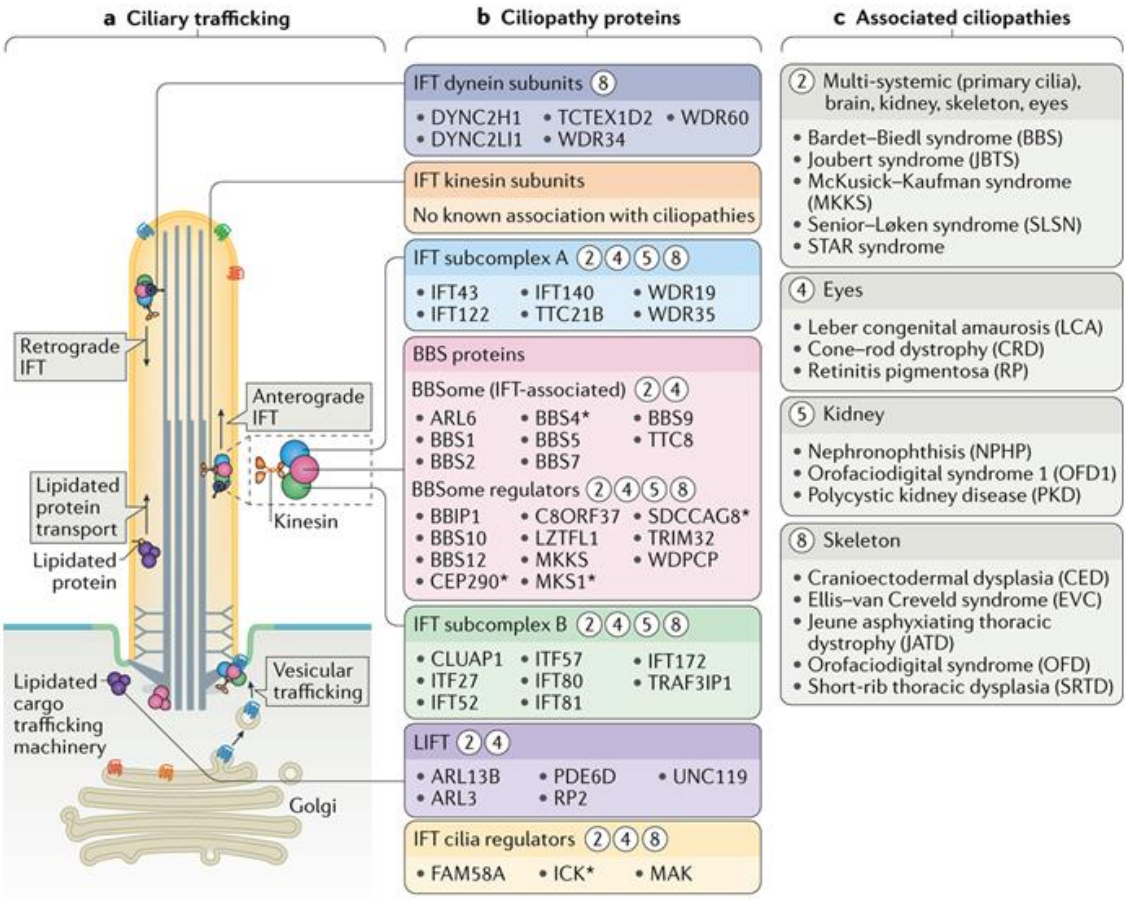

Figure 1.8 Overview of Ciliopathy.

a. Overview of ciliary trafficking by intraflagellar transport (IFT), lipidated protein intraflagellar targeting (LIFT), and molecular motors dynein-2 and kinesin-2 to and from cilia and Golgi.

b. Ciliary proteins that are associated with ciliopathies which is part of the IFT process, with regards to dynein, kinesin, IFT proteins, BBS proteins and regulators, and LIFT proteins.

c. Ciliopathies caused by defects of proteins listed in (b). Figure was borrowed from Reiter, J.F., and Leroux, M.R., 2017, Nature Reviews Molecular Cell Biology, with permission.

Previously, throughout this chapter, a few of the ciliopathies were identified that are caused by specific mutations in ciliary proteins. It is important to note that ciliopathies can have many

phenotypes, but some of these phenotypes are not caused by ciliopathies alone. For example, mutation in ODA and IFT proteins can lead to infertility, but not all infertile patients are caused by cilia and ciliary proteins malfunction. Infertility could also contribute to common factors such as chronic cigarette smoking, alcohol abuse, testicular cancer, or orchiectomy. This Section 1.6 would be dedicated to outlining human ciliopathies caused by mutations in IFT, ODA, inner junction proteins, and errors in PTMs of ciliary proteins.

1.6.1 Ciliopathy symptoms

Ciliopathies are characterized by a variety of clinical features, signs, and symptoms. In humans, some of these symptoms are cerebellar vermis hypoplasia, agenesis of the corpus callosum, situs inversus, polycystic kidneys, encephalocele (abnormal sac at brain posterior), polydactyly (supernumerary fingers or toes), loss of vision, and intellectual disability. Sometimes, additional phenotypes could also be associated with ciliopathies, though they could be a combination of other factors as well. These additional phenotypes include anencephaly (missing parts of the brain and skull), diabetes, exencephaly (brain located outside of the skull), hydrocephalus (accumulation of cerebrospinal fluid within the brain), hypotonia (low muscle tone), infertility, obesity, chronic respiratory tract infection and respiratory dysfunction, retinal degeneration, hearing loss, and spina bifida (incomplete closing of the spine). Generally, ciliopathies contain multiple symptoms from the lists above to form syndromes, with each symptom a result of a mutation in cilia-related genes. For example, a mutation in one or more *BBS* genes causes Bardet-Biedl syndrome that could have symptoms of vision loss, polydactyly, obesity, and hypogonadism (decreased production of sex hormones in gonads).

A unique ciliopathy is the Dandy-Walker syndrome that affects 1 in 25000 people (Stambolliu, Ioakeim-Ioannidou, Kontokostas, Dakoutrou, & Kousoulis, 2017). It is more accurately referred to as Dandy-Walker malformation (DWM), which describes an onset of clinical features rather than the syndrome itself. Unlike BBS, which is caused by BBS genes, DWM could be caused either by cilia-related genes or chromosomal abnormalities (trisomy 18, 13, 21, or 9). Using

medical ultrasound imaging, some cases of DWM could be diagnosed before birth, but the majority of cases are only identified after birth (Stambolliu et al., 2017). DWM is characterized by cerebellar vermis not fully forming such that both cerebellum hemispheres are not properly joined. In addition, the fourth ventricle and posterior fossa are enlarged and excessively filled with cerebrospinal fluid (Stambolliu et al., 2017). Some infants could also exhibit macrocephaly (due to hydrocephalus), slow motor development, intellectual and speech disabilities (Boddaert et al., 2003; Economou & Katsetos, 2012; Spennato et al., 2011). Comorbid ciliopathy genetic conditions in DWM patients include Joubert syndrome, Meckel-Gruber syndrome, Kallmann syndrome, Coffin-Siris syndrome, Fryns syndrome, oculocerebrocutaneous syndrome, Rubinstein–Taybi syndrome, and Walker–Warburg syndrome.

1.6.2 Ciliogenesis-related ciliopathies

A ciliogenesis-related ciliopathy in humans is the Alstrom syndrome, caused by a mutation in the ALMS1 protein. Mutation in the *ALMS1* gene may result in defective ciliogenesis. Alstrom syndrome patients have a loss of vision and hearing and suffer from obesity and type 2 diabetes mellitus (G. Li et al., 2007). The *ALMS1* gene is expressed in many fetal tissues, including the brain, eye, kidney, and skeletal muscle cells. Mutated *ALMS1* gene in older mice shows that kidney proximal tubule cells do not have cilium. In addition, knockdown of *Alms1* in mice prevents cell response to mechanical stimuli for increasing intracellular calcium signal (G. Li et al., 2007).

Meckel-Gruber syndrome (MGS) is a lethal disorder with phenotypes of cystic kidney dysplasia, polydactyly, developmental liver defects, and central nervous system malformation (Ahdab-Barmada & Claassen, 1990; Barker, Thomas, & Dawe, 2014). MGS can be further broken down into 10 different types, with the first six types associated with centrosome, basal body and ciliogenesis. Type 1 MGS is caused by MKS1 mutation (Kyttälä et al., 2006), part of the basal body. Type 2 and 3 MGS are caused by a mutation in TMEM216 and meckelin (Baala et al., 2007; A. Wang, 2011), respectively, which are transmembrane proteins in the basal body cilia. Defects in TMEM216 and meckelin could also cause Joubert syndrome (Baala et al., 2007). Type 4 MGS, Joubert syndrome, Leber congenital amaurosis and Senior-Løken syndrome could all be caused by a mutation in CEP290 (also known as nephrocystin-6), a centrosomal protein necessary for forming the basal body of cilium by binding microtubules to the cellular membrane (B. Chang et al., 2006; Drivas, Holzbaur, & Bennett, 2013; Sayer et al., 2006). RPGRIP1L associate with CEP290 at the basal body-centrosome complex, and mutation in this protein causes type 5 MGS

and Joubert syndrome (Delous et al., 2007). A mutation could cause the type 6 MGS and Joubert syndrome in CC2D2A, a coiled-coil protein with a calcium-binding domain (Tallila, Jakkula, Peltonen, Salonen, & Kestila, 2008).

1.6.3 Intraflagella transport ciliopathies

IFT is an important process in the maintenance of cilia and ciliary functions. Though IFT is not required for ciliogenesis, short cilia were be observed in IFT mutants to affect normal cellular function (Craft Van De Weghe et al., 2020). Mutation in most IFT genes will cause ciliopathy or abortion of the fetus, such as IFT122 (Walczak-Sztulpa et al., 2010), IFT43 (Arts et al., 2011), and IFT121 (Gilissen et al., 2010) to cause Sensenbrenner syndrome. Another interesting protein is IFT88, which is a tetratricopeptide repeat family protein. Mutation in IFT88 (aliases: DAF19, TG737, TTC10) could lead to diseased phenotype in many tissues in the human body, to list a few: starting with problems in ciliogenesis in photoreceptor cells to result in retinal degeneration (Chekuri et al., 2018; G. J. Pazour et al., 2002). In addition, IFT88 could regulate Hedgehog signaling resulting in misaligned kinocilium (C. F. Chang & Serra, 2013; Moon et al., 2020) and also affecting β-catenin activity in growth plates of chondrocytes (C. F. Chang & Serra, 2013). Elimination of IFT88 resulted in the deletion of motile cilia in the respiratory tract (Gilley et al., 2014). IFT88 could also play a role in the pathogenesis of cystic fibrosis and PCD in the lung (Stevens et al., 2020) and pulmonary fibrosis in primary cilia of the adult vasculature (Singh et al., 2020). IFT88 defects in newborn mice result in death shortly after birth as they are affected by polycystic kidney disease (G. J. Pazour et al., 2002).

1.6.4 Outer dynein arms ciliopathies

Missing either ODA or IDA results in a variety of ciliopathies. Figure 1.9A shows a cross-section view of normal human cilia, and Figure 1.9 B-H shows phenotypes of cilia when ODA or IDA is missing or defective. The most prevalent ciliopathy caused by ODA defects is PCD, affecting 1 in 10000 live births. Despite the name PCD, suggesting that this disease occurs in immotile primary cilia, PCD also affects motile cilia. About 15~20% of all PCD cases are caused by a mutation in the *DNAH5* gene (Failly et al., 2009; Olbrich et al., 2002; Omran et al., 2000), 10% of PCD cases by *DNAI1* gene (Failly et al., 2008; Pennarun et al., 1999; Zariwala et al., 2006), and 2% of PCD by *DNAI2* gene (Loges et al., 2008; Pennarun et al., 2000). These three genes encode proteins that are important for the ultrastructure of the ODA complex: dynein axonemal heavy chain 5 (HC5), dynein intermediate chain 1 (IC1), and axonemal dynein intermediate chain 2 (IC2), respectively. The latter two proteins, IC1 and IC2, were also studied using model organism *Chlamydomonas reinhardtii*. In human PCD patients, *situs inversus totalis*, neonatal respiratory distress, respiratory infection, *otitis media*, and bronchiectasis were observed in patients with HC5 and IC1 mutations. IC2 mutation results in all the above symptoms except for neonatal respiratory distress. Fertility defects were only observed in IC1 and IC2 mutation patients, though all three protein mutations have immotile cilia. These symptoms account for ~50% of human patients diagnosed with PCD (Praveen, Davis, & Katsanis, 2015).

In addition to these three proteins, there are also additional genes related to ODA that cause PCD, accounting for up to ~56% of PCD cases in a review paper by Praveen et al, (2015) *F1000Prime Reports*. Please note that PCD case statistics listed in this review paper may have two or more

gene mutations, so the statistics would likely overlap. For example, some PCD cases are caused by genes encoding proteins in docking complex to microtubule (eg. *ARMC4* (Hjeij et al., 2013; Onoufriadis et al., 2014), *CCDC114* (Knowles, M.W., et al., 2013; Onoufriadis et al., 2013), *DNAAF1* (Duquesnoy et al., 2009; Loges et al., 2009), *DNAAF2* (Omran et al., 2008), *LRRC6* (Kott et al., 2012; Serluca et al., 2009)). In addition, PCD cases can be affected by genes of both IDA and ODA for regulating their transcription (e.g. *ZNYND10* (Moore et al., 2013; Zariwala et al., 2013)), assembly (e.g. *SPAG1* (Knowles, L.E., et al., 2013), *DYX1C1 (Tarkar et al., 2013)*), and adaptor for transport into the cilium (*C21orf59/CFAP298* (Austin-Tse et al., 2013)). Additional PCD cases can be caused by mutated proteins in the central pair or nexin-dynein regulatory complex (Praveen et al., 2015).

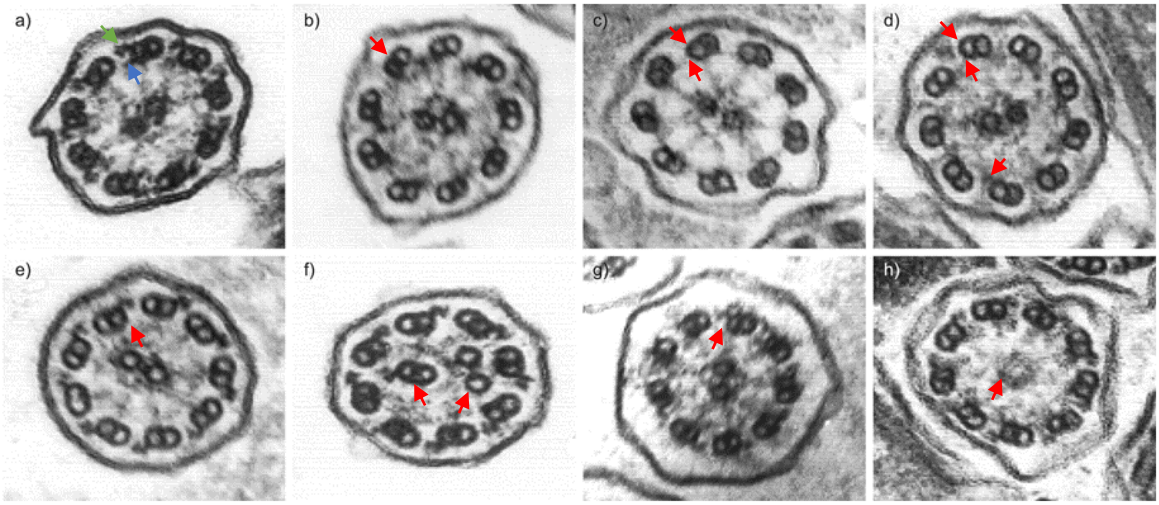

Figure 1.9 Phenotypes of ciliopathy caused by outer dynein arms and inner dynein arms.

a) Cross-section view of normal human cilia, characterized by 9+2 arrangement of microtubules and with outer dynein arms (green arrow) and inner dynein arms (blue arrow).
b) Outer dynein arms (ODA) missing (red arrow).
c) Both outer and inner dynein arms (IDA) are missing (red arrows).
d) ODA was missing, and IDA is only present on a few doublet microtubules (red arrows).
e) IDA missing but ODA present (red arrow).
f) Absence of IDA with axoneme being disorganized (red arrows).
g) IDA may be missing on some of the doublet microtubules, but ODAs were present (red arrow).
h) The central pair microtubules were missing (red arrow). Magnification 60000x. Images taken with permission from Papon J.F. et al., 2010, European Respiratory Journal.

1.6.5 Inner junction ciliopathies and parkinsonism

Proteins FAP52 and PACRG (parkin co-regulated gene) are important components of the inner junction region that are well-conserved across many organisms. Structurally, the knockout of FAP52 with FAP20 destabilizes the B-tubule and further damage the axoneme (Owa et al., 2019). Furthermore, deletion of FAP52 could lead to heterotaxy and *situs inversus totalis* in humans (Ta-Shma et al., 2015).

In *Tetrahymena,* two isoforms of PACRG exist. In mice, knocking out PACRG results in male infertility and hydrocephalus (Lorenzetti, Bishop, & Justice, 2004; Wilson et al., 2010). PACRG is a 30 kDa protein in humans and mice that is often co-expressed with parkin in many tissues, including the brain and heart (West, Lockhart, O'Farell, & Farrer, 2003). Screening of genomic DNA from human patients with isolated parkinsonism (age 6-62 years) and familial parkinsonism (age 7-81 years) show that deletion of gene promotor for parkin and PACRG resulted in the absence of expression, suggesting that parkin and PACRG deletion may cause early-onset parkinsonism (Lesage et al., 2007).

1.6.6 Post-translational modification ciliopathies

1.6.6.1 Ciliopathies associated with detyrosination

Meckel-Gruber syndrome (MGS) type 7, renal–hepatic–pancreatic dysplasia, and *situs inversus* could be caused by a mutation in nephrocystin-3 (NPHP3) (Bergmann et al., 2008). Human nephrocystin-3 contains an N-terminal coiled-coil domain that resembles that of nephrocystin-1 (T. Benzing et al., 2001), probably interacting with other coiled-coil domains to form protein homodimers. In addition, NPHP3 has eight C-terminal tetratricopeptide repeats (Thomas Benzing & Walz, 2008). The tetratricopeptide domains usually mediate protein-protein interaction and formation of complexes, with usual functions of transcriptional control, cell cycle regulation, neurogenesis, and protein folding. Importantly, at the center of the NPHP3 protein, there is a tubulin-tyrosine ligase domain. It was shown that these amino acids are highly conserved. A missense mutation resulted in cyst formation for causing polycystic kidney disease in mice (Olbrich et al., 2003), thus suggesting an important role tubulin-tyrosine ligase domain.

On the microtubule, a carboxypeptidase removes the C-terminal tyrosine of α-tubulin (Arce & Barra, 1983; N & Flavin, 1981), but tubulin tyrosine ligase can restore this tyrosine on free tubulin subunits (Ersfeld et al., 1993; Prota et al., 2013; Schröder Hc - Wehland et al., 1985; Szyk et al., 2011). In mice, disrupting tubulin-tyrosine ligase genes is lethal and shows problematic phenotypes in neuron networks, neurite outgrowth, and axon differentiation (Erck et al., 2005). A small portion of human patients with Joubert syndrome, characterized by abnormal cerebral development, could be caused by homozygous deletion of nephrocystin-1 (NPHP1) (Takano et al., 2003). NPHP1 interact with NPHP3 at the ciliary base (Olbrich et al., 2003). It is possible to

speculate a functional role of tubulin-tyrosine ligase in regulating neurite growth and neuron differentiation, but additional research is needed to study how a mutation in NPHP3 and its tubulin-tyrosine ligase domain contribute to Joubert syndrome.

1.6.6.2 Ciliopathies associated with glutamylation

Joubert syndrome could be caused by a mutation in CEP41, a protein that regulates the entry of tubulin poly-glutamylase TTLL6 (Tubulin Tyrosine Ligase Like 6). CEP41 does not have a tubulin tyrosine ligase domain, so it is probably not a glutamylase (van Dijk et al., 2007). In human male and female transfected *CEP41* mutant patient fibroblast cells, glutamylated tubulin was found in cilia's centriole and basal bodies but not found in the ciliary axoneme (J. E. Lee et al., 2012). In zebrafish, translation blocking morpholino antisense oligonucleotides was used to knock down TTLL6 and resulted in ciliopathy phenotypes such as a curved tail, the abnormal orientation of ear otolith, cystic kidney, and peripheral cardiac edema (J. E. Lee et al., 2012). Lee et al. (2012) further suggested that CEP41 could mediate transport of TTLL6 at the basal ciliary body by controlling transport into the cilium (J. E. Lee et al., 2012). Besides, hyper-glutamylation is linked to retinal dystrophy in humans (I et al., 1985) or photoreceptor degeneration in mice (Bosch Grau et al., 2017).

1.6.6.3 Ciliopathies associated with glycylation and colorectal cancer

In *Tetrahymena* cells, the knockout of all six paralogs of TTLL3 cause the cells to grow poorly and have shorter cilia (Wloga et al., 2009). Many TTLLs generate glycylation in eukaryotes, but in *Drosophila melanogaster*, TTLL3 is the only enzyme TTLL that facilitates tubulin poly-glycylation, and depletion using RNAi would create sterile male (Rogowski et al., 2019). Deletion of both TTLL3 and TTLL6 results in curved body axes and pronephric cysts resembling ciliopathy, probably due to reduced beat frequency or even paralysis of pronephric cilia (Pathak et al., 2011). In mice, the absence of both glycylases TTLL3 and TTLL8 leads to ciliary disassembly in ependymal cells (Bosch Grau et al., 2013) and shortening of cilia in photoreceptor cells to result in retinal degradation (Bosch Grau et al., 2017).

TTLL3 is the only glycylase in the colon in mice, and knockout promotes faster tissue turnover (Rocha et al., 2014). In humans, somatic mutation of the *TTLL3* gene was linked to colon cancer patients (Sjoblom et al., 2006). Furthermore, decreased level of TTLL3 expression was also found in human colorectal adenomas samples (Rocha et al., 2014). Additional data show that suppression of TTLL3 leads to decreased number of primary cilia and enhanced colon carcinogenesis (Rocha et al., 2014). As such, tubulin glycylation in primary cilia in the colon could potentially be linked to colon cancer development by its control of epithelial cell proliferation, or perhaps a link between primary cilia and the role of tubulin glycylation in the regulation cell cycle.

1.6.6.4 Ciliopathies associated with acetylation

Errors in acetylation and deacetylation of cytoplasmic microtubules and doublet microtubules or its regulation by ciliary proteins could lead to ciliopathy. KIF7 is a ciliary protein that regulates Hedgehog signalling (Figure 1.1F and G) (Dafinger et al., 2011; Goetz & Anderson, 2010). KIF7 knockdown in hTERT-RPE1 cells result in cilia malformation, abnormal centrosomal duplication, Golgi apparatus fragmentation, and a decreased acetylation level in cytoplasmic microtubules (Dafinger et al., 2011). Furthermore, KIF7 could co-precipitate with nephrocystin-1, and deletion of KIF7 causes Joubert syndrome in humans and mice (Dafinger et al., 2011). These results suggest that KIF7 loss of function could potentially contribute to the decreased acetylation level, later resulting in Joubert syndrome.

BBIP10, a Bardet-Biedl syndrome (BBS) protein, could only be found in ciliated organisms and is required for the proper assembly of primary cilia (Loktev et al., 2008). Knockdown of BBIP10, BBS1, BBS5 and PCM1 using siRNA in retinal pigment epithelial cells show that the ability to ciliogenesis was significantly reduced. In BBIP10 depleted cells, the cytoplasmic microtubule density and acetylation levels decreased, but free α-tubulin levels increased. However, the level of detyrosination and polyglutamylation remains the same. Overexpression of BBIP10 increased microtubule acetylation. With the addition of taxol, the level of acetyl-α-tubulin did not increase in BBIP10-depleted cells, but detyrosinated tubulin (Glu-tubulin) increased. The level of acetyl-α-tubulin in BBIP10-depleted cells could be restored by inhibition of HDAC6. Furthermore, depletion of BBIP10 in zebrafish resulted in BBS-like phenotypes (Loktev et al., 2008). It was shown that HDAC6 might indirectly influence the reabsorption of cilia by deacetylating doublet

microtubules (Pugacheva et al., 2007). Since the deacetylase HDAC6 is likely inhibited by the activity of BBIP10, it could be hypothesized that BBIP10 regulates HDAC6 by preventing premature ciliary disassembly.

At least 0.1% of the worldwide population is affected by autosomal dominant polycystic kidney disease (ADPKD), with 85% of cases caused by a mutation in the *Pkd1* gene in humans (Boucher & Sandford, 2004; Thivierge et al., 2006). The *PKD1* gene encodes polycystin-1, and its overexpression could cause ADPKD (Thivierge et al., 2006). The knockdown of the *Pkd1* gene could increase the SIRT2 level, decrease tubulin acetylation, and result in abnormal centrosome amplification and polyploidy (Zhou et al., 2014). SIRT2 is a nicotinamide adenine dinucleotide-dependent deacetylase (Afshar & Murnane, 1999; Frye, 1999). SIRT2 can regulate ciliogenesis in renal epithelial cells, as its overexpression would disrupt the formation of cilia (Zhou et al., 2014). However, knockdown of SIRT2 with siRNA blocks cilia disassembly during the cell cycle (Zhou et al., 2014). Conversely, loss of *Ift88* and *Kif3a* genes could cause hyperacetylation of cytoplasmic microtubules in immortalized renal collecting duct cell lines with ablated cilia (Berbari et al., 2013). A similar phenotype could be observed in kidneys from autosomal recessive polycystic kidneys patients (Berbari et al., 2013). These results suggest the cilia could influence the level of acetylation and deacetylation for impacting the global microtubule acetylation in the cell, which further contributes to regulating cell cycle and cellular functions (He, Ling, & Hu, 2020).

Chapter 1 References

Please refer to the Chapter 4 Master Reference List

Chapter 2

"The Delphic Oracle said that I was the wisest of all the Greeks. It is because I, alone among the Greeks, know that I know nothing."

Socrates, Greek philosopher, 470 B.C.E. – 399 B.C.E.

A Chinese quote with similar ideology:

"三人行，必有我師焉；擇其善者而從之，其不善者而改之。"

Confucius, 孔子《論語・述而》, 前 551 年 －前 479 年

2.1 Preface

Questions remain about how ODAs are bound to the doublet microtubule, how Shulin leaves the ODA, and how the ODAs get activated. ODA is required for sliding the doublet microtubules to produce the bending motion in cilia that dictates the beat frequency. Thus, the mechanism of ODA activation is an essential piece of information to understand how cilia beat and function.

In this Chapter 2, I, with Shintaroh Kubo, a post-doctoral fellow in Khanh Huy Bui's lab, elucidated a cryo-electron microscopy (EM) structure of the ODAs (also known as outer arm dyneins) that were frozen-hydrated from *Tetrahymena thermophila* cilia. Using this *in vivo* structure of activated ODA forming in rows on doublet microtubules, and by using coarse-grained molecular dynamics (MD) simulations, we propose a model for how ODA activates in cilia.

Our cryo-EM results suggest that ODA are bound to doublet microtubules via tail domain, so that the heavy chain head of subsequent ODA can interact with the tail domain of the previous ODA to form a row. The coarse grain MD simulation suggests that attachment of ODA to the doublet microtubule triggers its activation as the docking complex catches the tail domain, remodelling of the tail domain results in destabilization of Shulin. Once Shulin detaches from the ODA, remodelling propagates towards the heavy chain heads. Here, the heads are in post-powerstroke conformations, which are now ready to exert force. Our model provides direct evidence on the activation of ODA to carry out ciliary bending.

2.2 Paper Title

Remodeling and activation mechanisms of outer arm dyneins revealed by cryo-EM

Shintaroh Kubo[1,2,Ψ], Shun Kai Yang[1,Ψ], Corbin Black[1], Daniel Dai[1], Melissa Valente[1], Jacek Gaertig[3], Muneyoshi Ichikawa[4,5,*], Khanh Huy Bui[1,6*]

Author affiliations

1. Department of Anatomy and Cell Biology, McGill University, Montréal, Québec H3A 0C7, Canada

2. JSPS Overseas Research Fellow

3. Department of Cellular Biology, University of Georgia, Athens, GA 30602, USA

4. Division of Biological Science, Graduate School of Science and Technology, Nara Institute of Science and Technology, Ikoma, Nara 630-0192, Japan

5. PRESTO, Japan Science and Technology Agency, Kawaguchi, Saitama, 332-0012, Japan

6. Centre de Recherche en Biologie Structurale, McGill University, Montréal, Québec H3A 0C7, Canada

[Ψ] These authors contributed equally

*Corresponding authors:

Muneyoshi Ichikawa, Division of Biological Science, Graduate School of Science and Technology, Nara Institute of Science and Technology, Ikoma, Nara 630-0192, Japan.

PRESTO, Japan Science and Technology Agency, Kawaguchi, Saitama, 332-0012, Japan

E-mail: michikawa@bs.naist.jp

Khanh Huy Bui, Department of Anatomy and Cell Biology, McGill University, Montréal, Québec H3A 0C7, Canada. E-mail: huy.bui@mcgill.ca

Key words: Cilia, Doublet microtubule, Outer arm dynein, Cryo-electron Microscopy

2.3 Abstract

Cilia are thin microtubule-based protrusions of eukaryotic cells. The swimming of ciliated protists and sperm cells is propelled by the beating of cilia. Cilia propagate the flow of mucus in the trachea and protect the human body from viral infections. The main force generators of ciliary beating are the outer dynein arms (ODAs) which attach to the doublet microtubules. The bending of cilia is driven by the ODAs' conformational changes caused by ATP hydrolysis. Here, we report the native ODA complex structure attaching to the doublet microtubule by cryo-electron microscopy. The structure reveals how the ODA complex is attached to the doublet microtubule via the docking complex in its native state. Combined with coarse-grained molecular dynamic simulations, we present a model of how the attachment of the ODA to the doublet microtubule induces remodeling and activation of the ODA complex.

2.4 Introduction

Motion is an important aspect of life. In eukaryotes, cilia and flagella are responsible for cell motility. These microscopic hair-like organelles bend several tens of times per second to generate fluid flows. Cilia in trachea generate the flow of mucus and protect our body from infectious agents such as viruses. There is a canonical axonemal 9+2 structure where the central pair microtubules are surrounded by nine doublet microtubules (Figure 2.1A). The propulsive force generators of cilia and flagella are the axonemal dyneins. As the molecular motors, the axonemal dyneins drive the sliding of doublet microtubules, which is then converted into the bending of the cilium. The axonemal dyneins consist of outer arm dyneins and inner arm dyneins. The outer dynein arm (ODA) regulates the beat frequency while the inner arm dyneins are important for the waveform of the cilium (Brokaw & Kamiya, 1987). Improper assembly of the ODA complex causes ciliopathies in humans (reviewed in Reiter & Leroux, 2017).

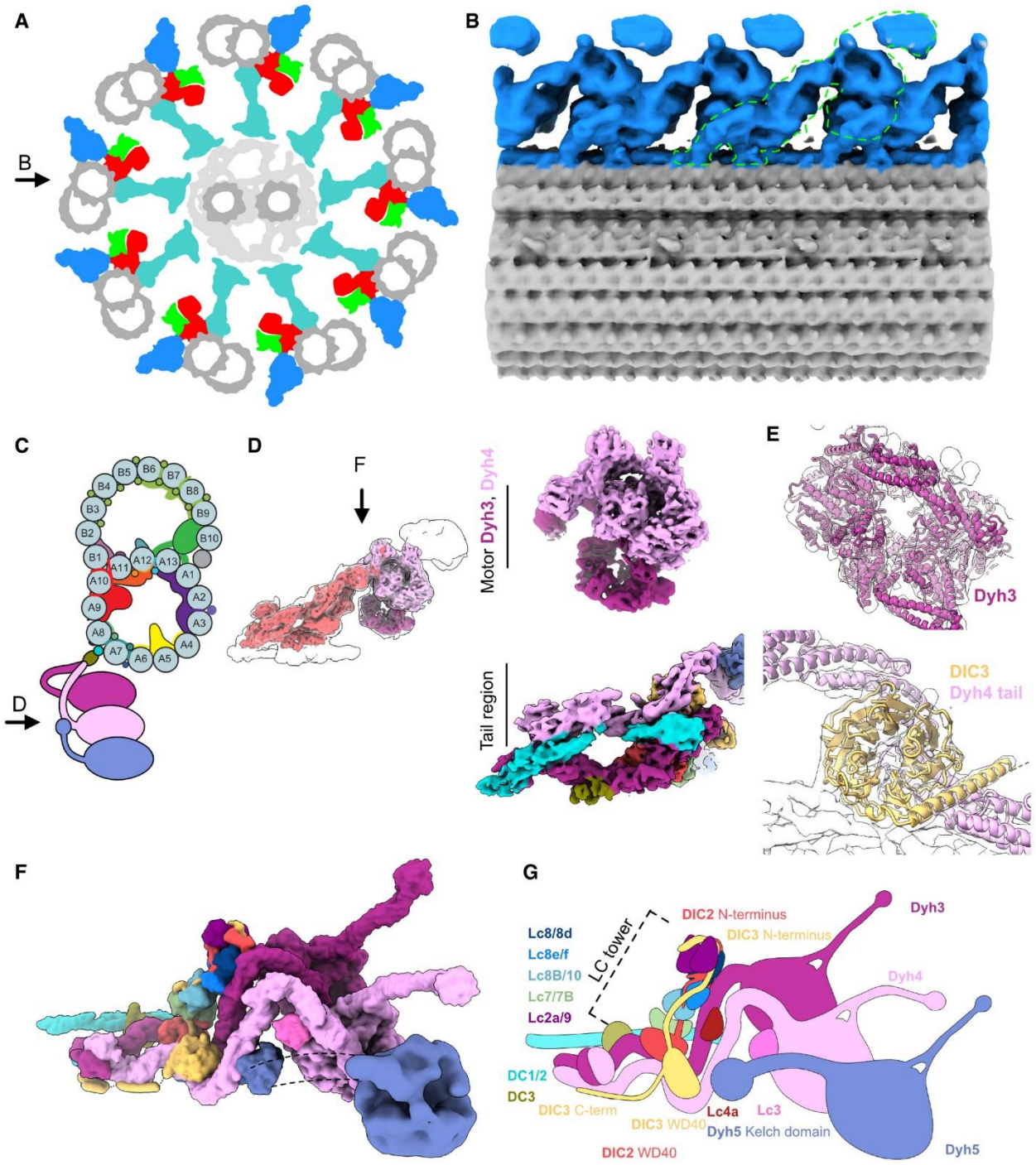

Figure 2.1 Cryo-EM structure of the ODA complex on the doublet microtubule

A. Schematic diagram of axoneme structure of cilia viewed from the base of the cilia. Doublet microtubule: gray; outer dynein arm: blue; inner dynein arm: red; dynein regulatory complex: green; radial spokes: cyan. Black arrow indicates the view in (B).

B. The 24-nm structure of the doublet microtubule from K40R mutant filtered to 18 Å showing the row of the ODA. The green outline indicates the single ODA complex.

C. A schematic cartoon of the doublet microtubule and the ODA complex. Arrow indicates the view in (D).

D. The focused refined maps of the tail and the heads of the ODA are shown within the map of the entire ODA complex (left). The focused refined maps of Dyh3 and Dyh4 heads and the tail (right).

E. Fitting of models into maps (Dyh3, top; DIC3 and Dyh4 tail, bottom). The α-helix part of the DIC3 was more structured in our map compared with that of the Shulin–ODA complex.

F, G. The surface render of the model (F) and the schematic cartoon (G) of the ODA with the docking complex. The Dyh5 is too flexible to resolve well by cryo-EM. The Dyh5 head is only shown as the 18-Å resolution surface render, and the Dyh5 tail is drawn as dotted lines. All the components (ICs, LCs, and DCs) are colored and indicated and will be used consistently in all the figures. C-terminal side of the DIC3 has more structured region along the Dyh4 HC tail on the doublet.

Unlike cytoplasmic dyneins which walk on microtubules while carrying cargos, axonemal dyneins are anchored firmly on the doublet microtubules (Goodenough & Heuser, 1982; Bui et al, 2008; Bui et al, 2009). The ODA complex is composed of two or three heavy chains (HCs) depending on the species (Diamant & Carter, 2013), two intermediate chains (ICs) and numerous light chains (LCs). For example, human cilia have two headed ODA (DNAH5 and DNAH9) while ODA of *Tetrahymena* contain three heavy chains (Dyh3, 4 and 5). Dynein HCs are the most important force producing components and each HC has a head domain and a tail domain. The three head domains are coupled together at the level of the tail domain. Within the head domain of each ODA HC, there is an AAA+ ring (composed of AAA1 to AAA6 subdomains) where ATP is hydrolyzed to exert force. The ODA complex is stably attached to the A-tubule of the doublet microtubule and produces force while interacting with the B-tubule of the neighboring doublet microtubule. The

docking of the ODA complex to the A-tubule of the doublet is mediated by the HC tail domain. The interaction with B-tubule of the neighboring doublet is mediated by the microtubule binding domain (MTBD) at the tip of the stalk which extends from the AAA+ ring. ICs and LCs have various regulatory roles (reviewed in King, 2012). Most of the ICs and LCs interact with the tail domain. However, LC1 is bound to the MTBD of the Dyh3 head (Ichikawa et al, 2015; Toda et al, 2020).

By conventional quick-frozen deep-etch replicas and cryo-electron tomography (cryo-ET) works, ODAs were shown to form a 24-nm repeating row on the doublet microtubules (Goodenough & Heuser, 1982; Nicastro et al, 2006; Bui et al, 2012; Lin & Nicastro, 2018). The ODA complex is proposed to be attached via the docking complex (DC) (Owa et al, 2014; Oda et al, 2016a). Within each ODA complex, the three heads are aligned parallel to each other so that all three head domains can interact with the adjacent doublet microtubule in a proper orientation. The architecture of ODA complex has been studied by negative staining EM using purified ODA complexes (Ichikawa et al, 2015), or cryo-electron tomography (cryo-ET) of the intact axoneme (Oda et al, 2016b). However, the resolutions were limited in these studies and the modeling of the protein subunits was not possible. Recently, a cryo-EM structure of the inactive *Tetrahymena* ODA complex (before its incorporation into cilia) was obtained (Mali et al, 2021). In the inactive form, three head domains are packed together by a regulator protein, Shulin. This conformation is markedly different from the active conformation observed in the axoneme where the three heads are in parallel arrangement. The subunit architecture was also revealed in high resolution for the inactive Shulin-ODA complex (Mali et al, 2021). However, to understand how ODA is incorporated into

the axoneme structure and activated, it was crucial to obtain a high-resolution structure of the ODA complex in the context of the doublet microtubule.

Here, we revealed the *Tetrahymena* ODA complex on the doublet microtubule at 5.5-7 Å resolutions. Our structure showed in detail how the *Tetrahymena* ODA complex is attached to the doublet, including its interaction with the DC complex. Very recently, high-resolution structure of *Chlamydomonas* ODA complex attached to the doublet microtubule was also reported by cryo-EM (Walton et al, 2021). This enabled us to compare the ODA structure from different species. Combined with coarse-grained molecular dynamics (MD) simulations, we have revealed how the ODA complex undergoes an activating rearrangement when it is docked onto the doublet microtubule.

2.5 Results

2.5.1 Cryo-EM structure of the ODA attached to the doublet microtubule

In our previous studies of the doublet microtubule structures, the ODA complexes were removed by high-salt treatment from doublets (Ichikawa et al, 2017; Ichikawa et al, 2019; Khalifa et al, 2020). Here, to obtain the native structure of the ODA complex on the doublet, we tried to obtain a wild-type (WT) *Tetrahymena* doublet microtubule structure without a salt wash (Figure 2.2A). The individual doublet microtubules were separated from the rest of the axoneme induction of microtubule sliding using ATP. However, in the disintegrated WT axonemes, the ODAs tended to detach from the doublet (Figure 2.2B) and we were not able to obtain the high resolution structure of the ODA by single particle analysis (Figure 2.2D and E). We noticed that the sliding of doublets in the ATP-reactivated K40R (Gaertig et al, 1995) or MEC17-KO mutant *Tetrahymena* axonemes (Akella et al, 2010) was less efficient as compared to the WT *Tetrahymena* axonemes, possibly due to different levels of post-translational modifications of tubulin. This enabled us to obtain cryo-EM images of partially split doublet microtubules with attached ODA complexes (Figure 2.2C). Using the cryo-EM images, we first obtained a 24-nm doublet microtubule unit structure as previously described (Ichikawa et al, 2017; Ichikawa et al, 2019; Khalifa et al, 2020) at a 3.9 Å resolution (Figure 2.3A). However, the resolution of the ODA part was not high enough due to its flexibility. Therefore, we performed signal subtraction of the doublet and obtained the ODA structure with a 7.8 Å resolution. From here, different regions of the ODA were further revealed by focused refinement. The tail region's resolution was improved to 5.5 Å, the Dyh3 head part to 5.8 Å and Dyh4 head part to 7 Å (Figure 2.3B). The resolution of the Dyh5 head remained at 17 Å since it was furthest from the doublet and more flexible. The head domains were in a parallel configuration (Figure 2.1B) as previously shown by cryo-ET studies (Bui et al, 2008; Lin &

Nicastro, 2018). Our structure fits well with previous cryo-ET structure of the intact axoneme, thereby confirming it is a physiological structure of the ODA complex (Figure 2.2F).

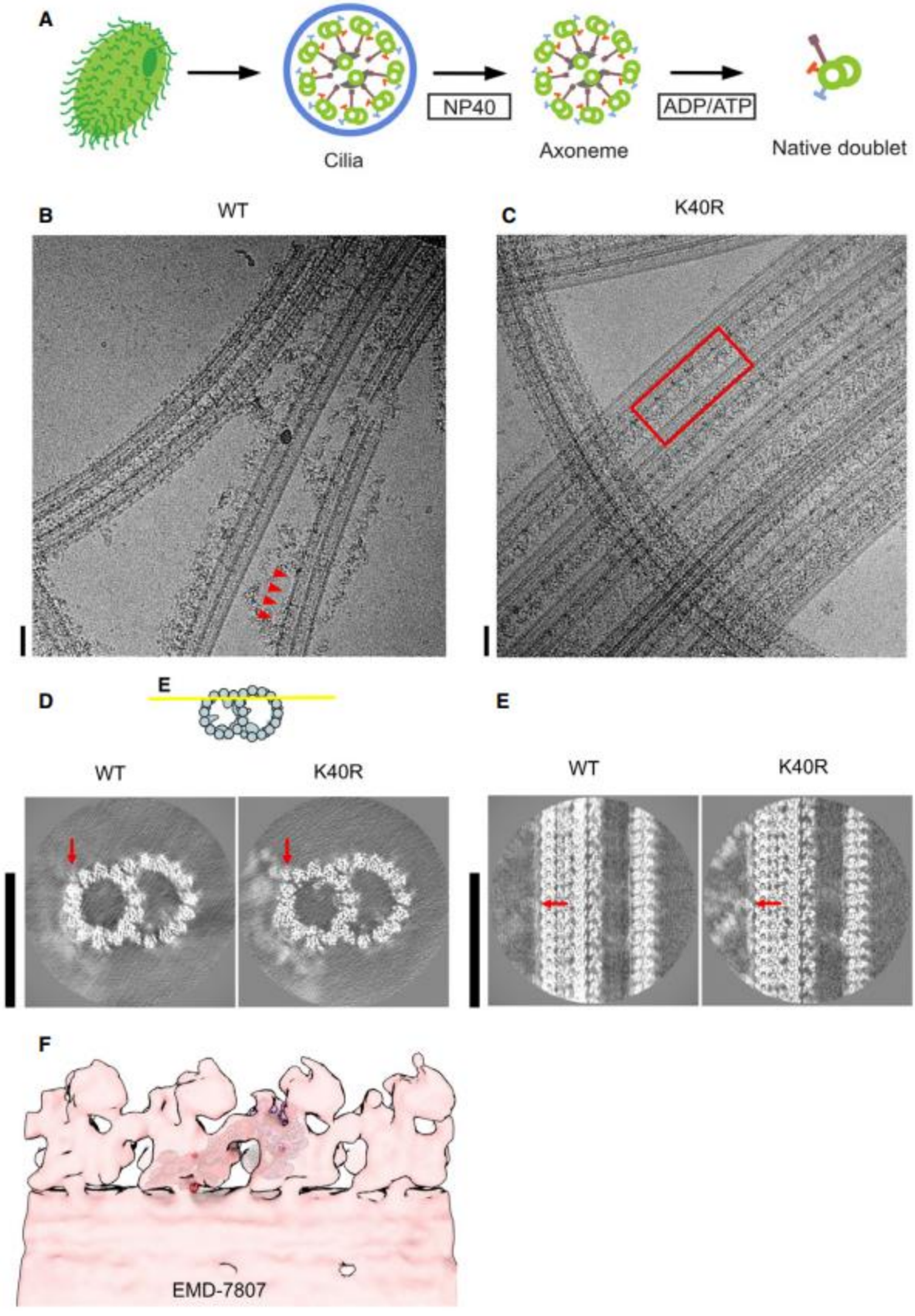
A
Cilia
NP40
Axoneme
ADP/ATP
Native doublet
B
WT
C
K40R
D
E
WT
K40R
E
WT
K40R
F
EMD-7807

Figure 2.2. Sample preparation and cryo-EM of the doublet microtubules.

A. The schematic of our isolation strategy for the intact doublet microtubules.

B., C. Micrographs of doublet microtubules from *Tetrahymena* WT (B) and K40R mutant (C). The red arrowheads indicate the ODA complex falling off from the doublet. The red rectangle indicates the row of intact ODA in the K40R mutant. Scale bars represent 50 nm.

D., E. 24 nm structure of doublet from WT and K40R showing the DC is intact in both cases while ODA is clearly present only in K40R. Red arrows indicate the docking complex. Scale bars, 50 nm.

F. Fitting of our high-resolution structure into the tomographic map of *Tetrahymena* showing it is physiological (DRib72B mutant rescued with Rib72B-GFP) (EMD7807, Stoddard et al, 2018).

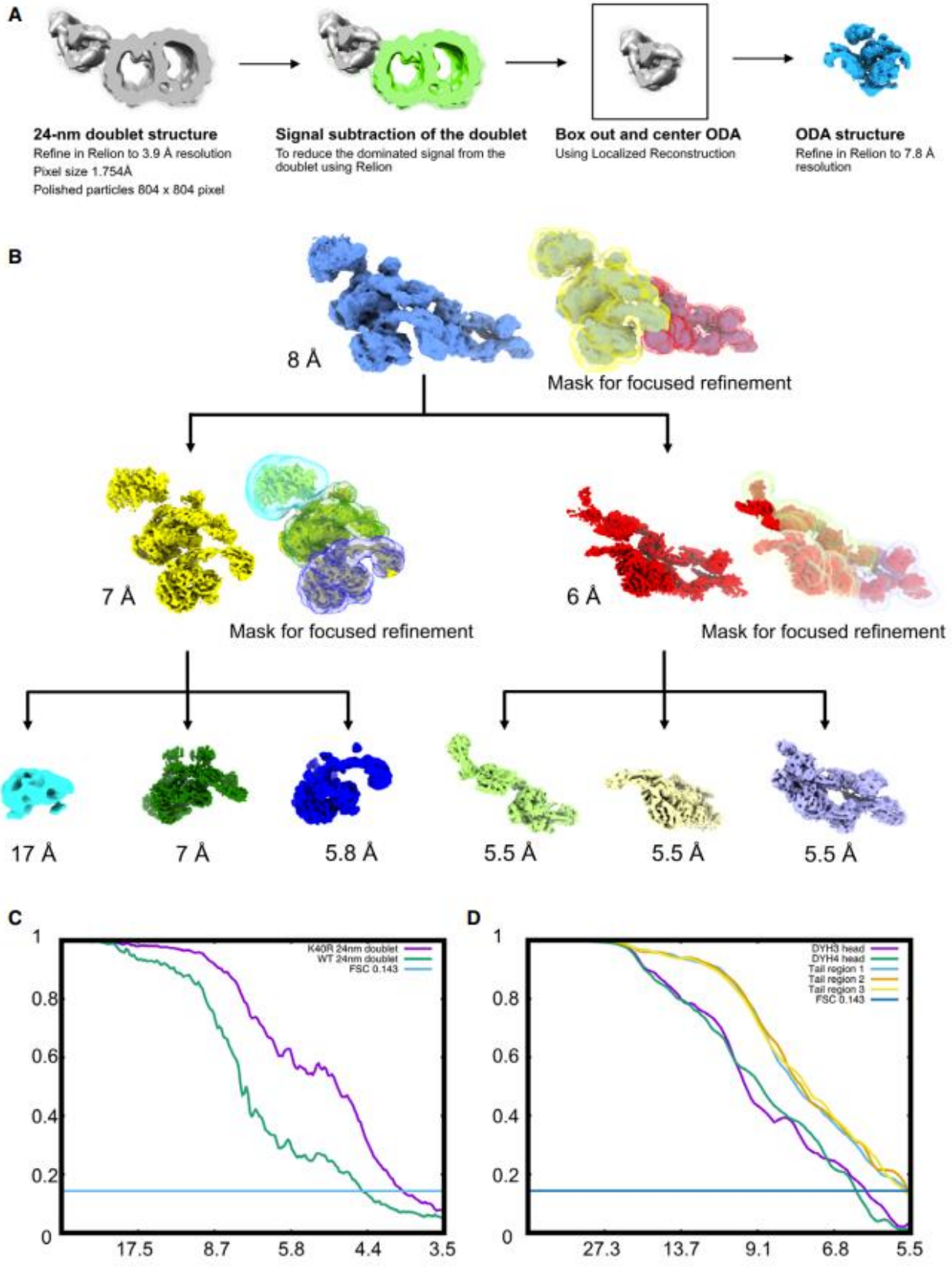
A
24-nm doublet structure
Refine in Relion to 3.9 Å resolution
Pixel size 1.754Å
Polished particles 804 x 804 pixel
Signal subtraction of the doublet
To reduce the dominated signal from the doublet using Relion
Box out and center ODA
Using Localized Reconstruction
ODA structure
Refine in Relion to 7.8 Å resolution
B
8 Å
Mask for focused refinement
7 Å
Mask for focused refinement
6 Å
Mask for focused refinement
17 Å
7 Å
5.8 Å
5.5 Å
5.5 Å
5.5 Å
C
K40R 24nm doublet
WT 24nm doublet
FSC 0.143
1
0.8
0.6
0.4
0.2
0
17.5
8.7
5.8
4.4
3.5
D
DYH3 head
DYH4 head
Tail region 1
Tail region 2
Tail region 3
FSC 0.143
1
0.8
0.6
0.4
0.2
0
27.3
13.7
9.1
6.8
5.5

Figure 2.3. Cryo-EM processing strategy.

A. Alignment strategy for ODA particles. First, we obtained the 24-nm doublet structures. After that, we performed signal subtraction of the doublet microtubule. We centered and boxed out the ODA particles and performed refinement of the entire ODA particles.

B. Focus refinement strategy for different regions of the ODA complex. The Dyh5 seems to be too flexible; therefore, we can only obtain Dyh4 head at 17 Å resolution.

C. Fourier Shell Correlation of the doublet of WT and K40R & MEC17 combined data.

D. Fourier Shell Correlation of the different regions of the ODA complex by focus refinement.

Using the recent Shulin-ODA complex structure from *Tetrahymena* as a starting model, we were able to build in all the components of the ODA complex except for Dyh5's head (Figure 2.1C-G). Since Dyh5 is not conserved in vertebrates (Ueno et al, 2014; Lin et al, 2014), an atomic model for conserved part of the ODA complex on the doublet was obtained. The ICs and LCs were also assigned to the density map. The majority of LCs were forming the LC tower as earlier observed in the Shulin-ODA complex (discussed below). Compared with the Shulin-ODA complex, there were some parts of ICs which were structured in our map and modeled (Figure 2.1E-G). There was a density not observed in the Shulin-ODA complex associated with Dyh4, and LC4 was tentatively assigned to this region (Figure 2.1F and G). Very recently, *Tetrahymena* ODA model based on cryo-EM structure of reconstituted ODA array on the doublet was reported (Rao et al, 2020). Our model was similar with obtained reconstituted ODA complex validating our model. When we compare our *Tetrahymena* ODA structure with recent *Chlamydomonas* ODA structure attached to the doublet (Walton et al, 2021), both structures appeared strikingly similar in general

(Figure 2.4). In our structure, there was also an additional density of two segments of coiled coil with a globular domain at the end which is running along the tail domain of the ODA (cyan parts in Figure 2.1D, F and G) (discussed later).

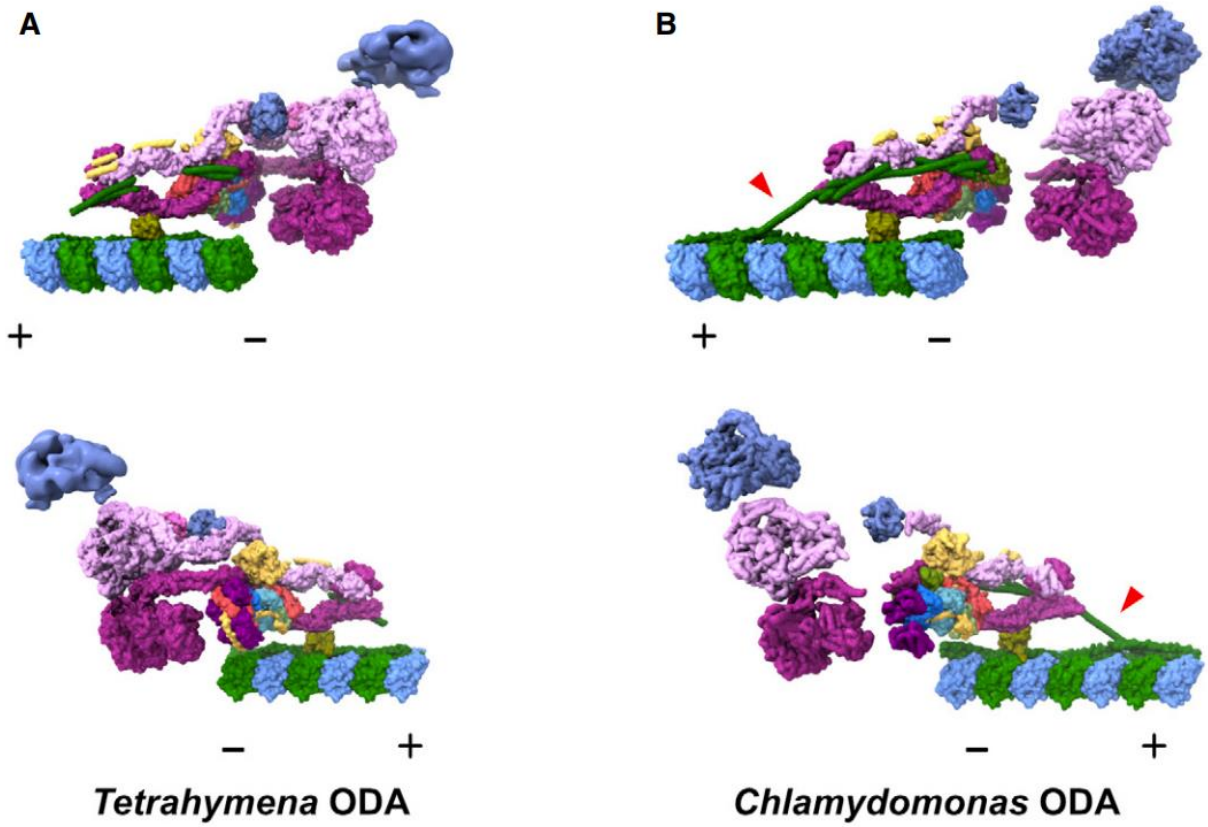

Figure 2.4. Comparison of the ODA structures obtained by cryo-EM.

A., B. The model of our *Tetrahymena* ODA complex (A) and *Chlamydomonas* ODA complex (PDB ID: 7KZM, Walton et al, 2021) (B) viewed from different sides. The Dyh5 head of *Tetrahymena* ODA is shown as 18-A resolution surface rendering. a-Tubulin is shown in green and b-tubulin is shown in blue. The polarities of the doublet microtubules are indicated by + and . In our *Tetrahymena* model, there is more modeled region around the linker region. In contrast, there is more modeled region in DC in the *Chlamydomonas* model from Walton et al

(2021), especially the region connecting the DC1/2 on the doublet surface and the extended coiledcoil region associated with the ODA complex (red arrowheads). These differences could relate to different properties of the *Tetrahymena* and *Chlamydomonas* ODA or different ways of sample preparation.

2.5.2 Attachment of the ODA complex to the doublet via the docking complex.

The part of DC on the doublet was also visualized in our structure which allowed us to understand how the ODA complex is attached to the doublet (Figure 2.5 and Figure 2.6A). We identified *Tetrahymena* proteins Q22T00, Q233H6 and I7M2C6 as DC1/2 and 3 following the names of the counterparts of *Chlamydomonas* (Figure 2.6B and C, see Materials & Methods for details). Along the doublet, DC1/2 forms a 24-nm repeating unit, the same periodicity as the repeating unit of the ODA complex. DC3 is associated with the DC1/2 coiled coil region on the doublet serving as a marker for the ODA attachment (Figure 2.5C and Figure 2.6A) as previously proposed (Ma et al, 2019). The α-helix bundle-3 of Dyh3-HC was interacting with the DC3 (Figure 2.5C). The tethering of the ODA to the doublet microtubule is mediated by Dyh3 alone and ICs/LCs are not involved with the microtubule. The DC1/2 also appears to connect to the coiled-coil density with a gap associated with the neighboring ODA tail domain (dashed line in Figure 2.5A, and Figure 2.6H). This model is consistent with the coiled coil prediction of DC1/2 with a gap (Figure 2.6B) and the previous tagging results of DC2 of *Chlamydomonas reinhardtii* by cryo-ET in Oda et al, (2016a) (Figure 2.6D-G, Figure 2.7). Therefore, the density associated with the tail domain corresponds to the C-terminal side of DC1/2 (Figure 2.6I and J). This is also consistent with recent *Chlamydomonas* ODA structure model (Figure 2.4).

The ODA complex is anchored to the doublet by the above-mentioned two sites: DC1/2 and DC3. Over these docking sites, there is a layer composed of Dyh3 HC, DIC2's WD domain, LC tower and the C-terminal side of DC1/2. Another layer of Dyh4 and DIC3 is further built onto this layer (Figure 2.5A and B). The three head domains are stacked together in a parallel configuration. The stacking of both the tail and the head domains is important for the proper attachment of the ODA onto the doublet.

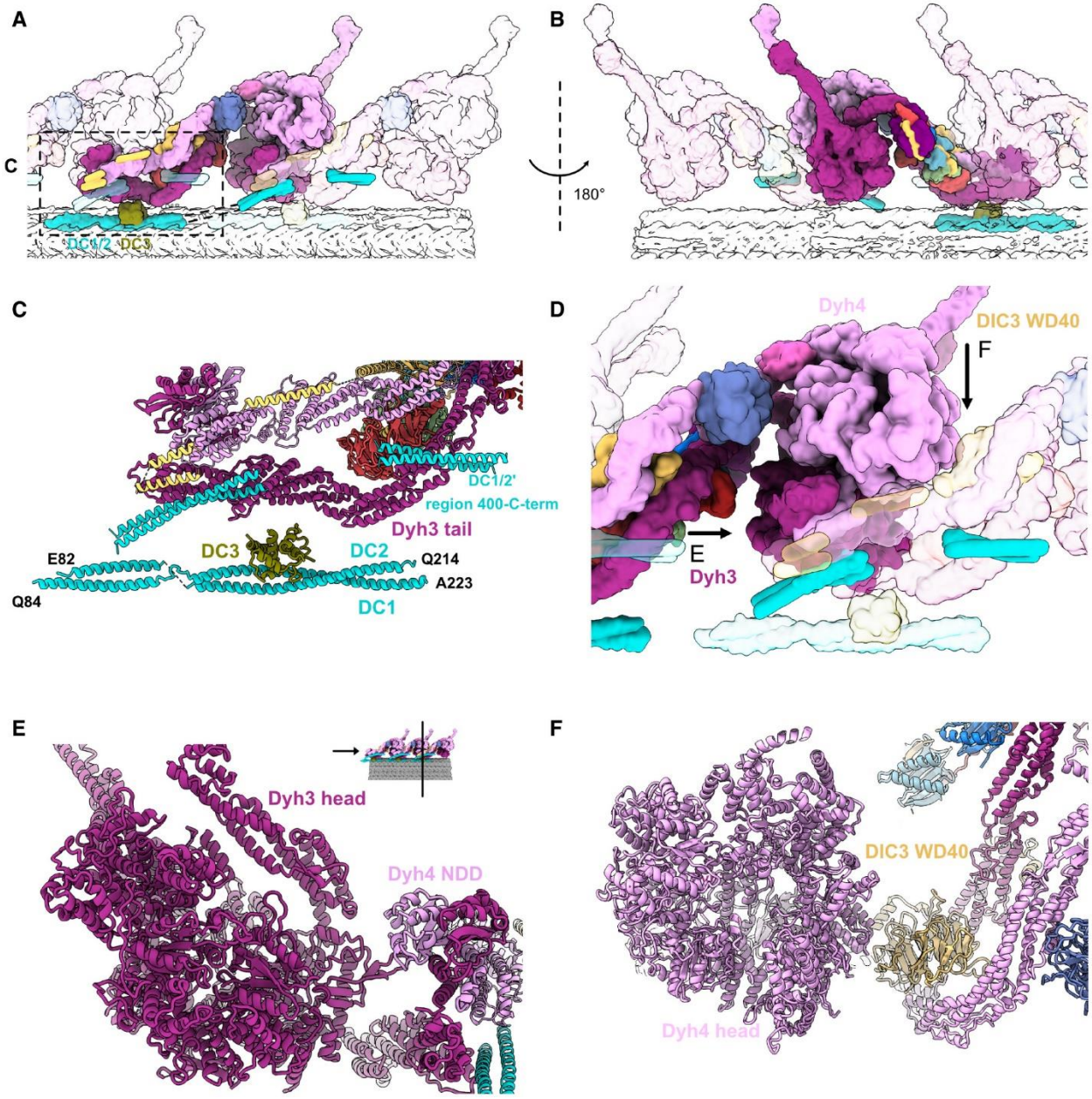

Figure 2.5. Interactions between the ODA complex and the DC

A, B. The stacking of the ODA complex in the axoneme viewed from inside (A) and outside (B) the cilia. All the components belonging to the middle ODA complex are shown in color. The proximal and distal ODA complexes are shown in transparent.

C. Model of the DC and the tail of the ODA.

D. The interaction of the head of the ODA complex with the tail of the next ODA complex unit. Dyh3 head interacts with the dimerization domain NDD of the proximal Dyh4. The Dyh4

head interacts with the DIC3 WD40 of the proximal ODA complex. Arrows indicate the views in (E) and (F).

E. Model view of the interaction between the Dyh3 head with the dimerization domain NDD of the proximal ODA complex.

F. Model view of the interaction between the Dyh4 head with the DIC3 WD40 of the proximal ODA complex.

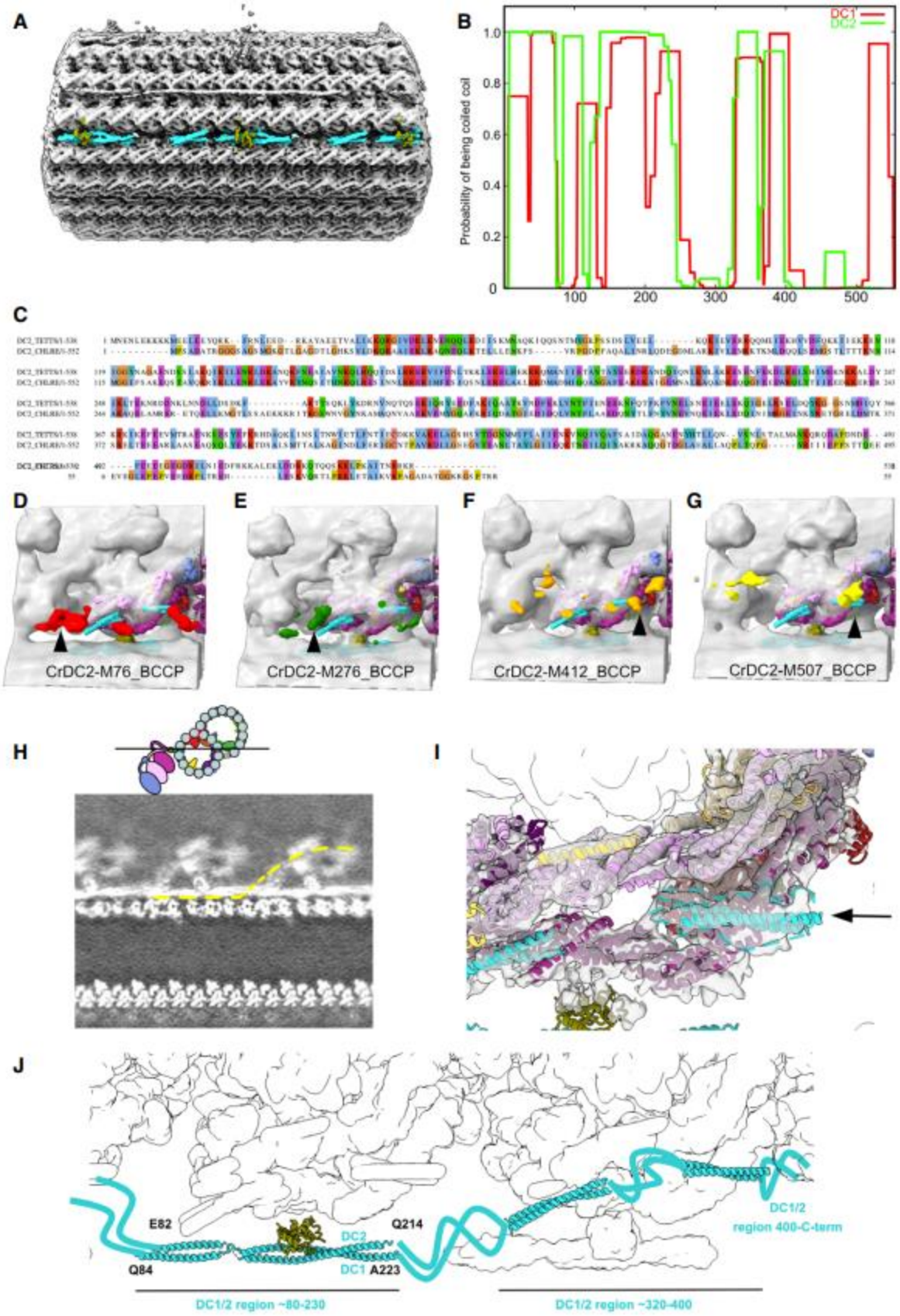
A
B
DC1
DC2
Probability of being coiled coil
1.0
0.8
0.6
0.4
0.2
0
100
200
300
400
500
C
D
E
F
G
CrDC2-M76_BCCP
CrDC2-M276_BCCP
CrDC2-M412_BCCP
CrDC2-M507_BCCP
H
I
J
E82
Q84
Q214
DC2
DC1 A223
DC1/2
region 400-C-term
DC1/2 region ~80-230
DC1/2 region ~320-400

Figure 2.6. Modeling of the docking complex.

A. The DC density on the doublet microtubule between PFs-A7 and A8.

B. Prediction of coiled coil for DC1 and DC2 using COILS with a window size of 28 (Lupas et al, 1991).

C. Sequence alignment of *Chlamydomonas* DC1 and *Tetrahymena* CCDC151 homolog (Q22T00).

D.–G. Structures of *Chlamydomonas* ODA reconstituted on microtubules with biotin carboxyl carrier protein (BCCP) tagged in different regions of DC2 (residue 76, 276, 412, and 507) from Oda et al (2016a) (EMD-6508, 6509, 6510, 6511). The enhanced signals of BCCP-tag are indicated in colors.

H. Slice from a density map showing the docking complex (position indicated in the cartoon). The yellow line indicates one continuous DC1/2. I The globular density at the end of the coiled coil of DC1/2 (black arrow and dotted line).

J. The model of the DC based on our analysis.

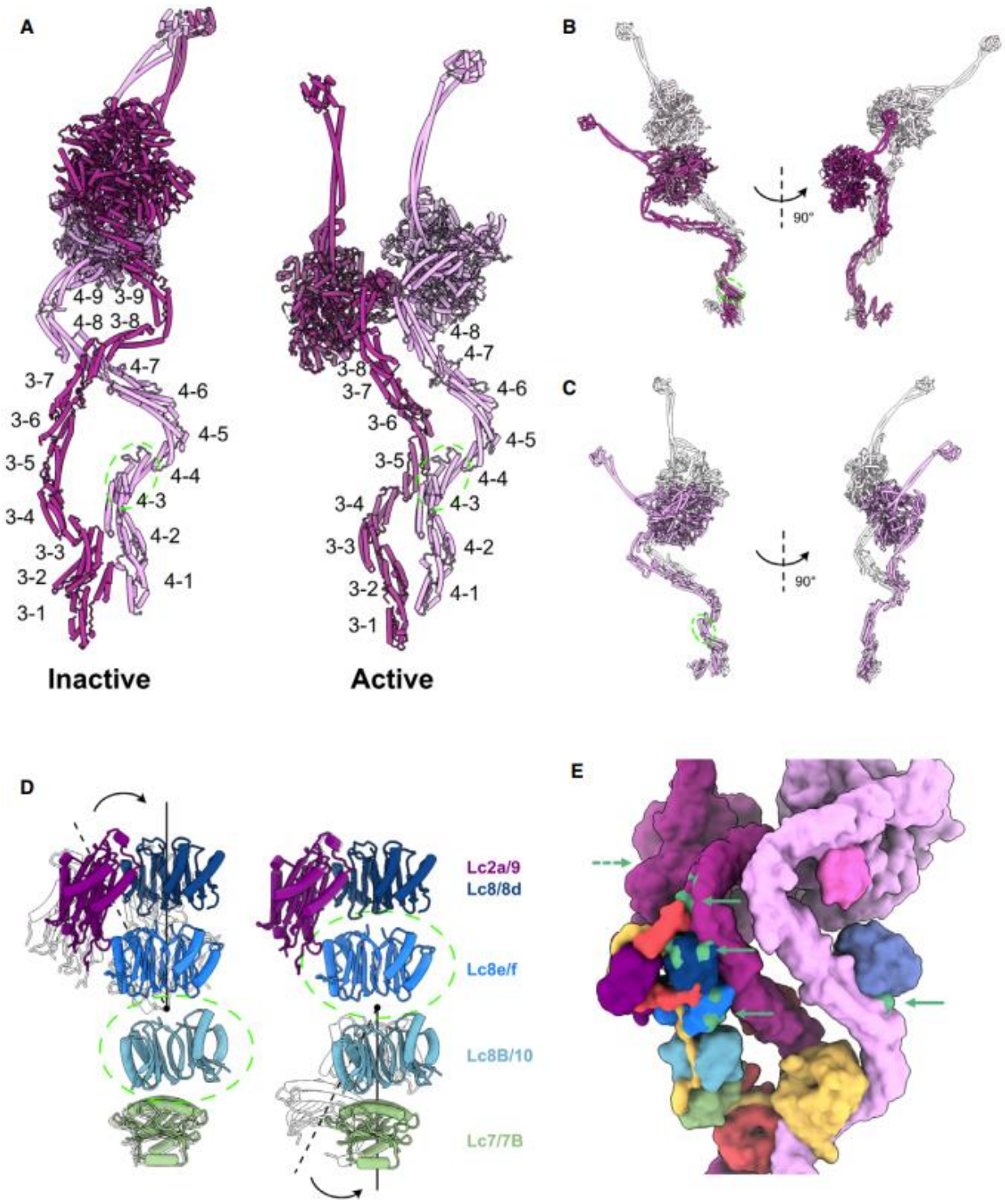

Figure 2.7. Data related to the remodeling of the ODA complex.

A. The labeling of helix bundles in the inactive and active Dyh3 and Dyh4. Inactive and active structures are aligned on helix bundle 4 of Dyh4 (residues 414–513).

B. Alignment of the inactive and active Dyh3 at helix bundle 3 (residue 448–536) showing ~ 90-degree rotation of the head domain (top).

C. Alignment of inactive and active Dyh4 at helix bundle 3 (residue 414–513) showing compressing conformational changes (bottom).

D. Bending conformational change in the LC tower. LC tower from the active ODA complex is in colors, and the LC tower from the Shulin–ODA is shown in transparent. LC towers are aligned based on either Lc8B/10 (left) or Lc8e/f (right) as indicated by green dashed circles.

E. Regions of the ODA that interact with Shulin in the inactive conformation (green regions with green arrowhead) are spread out in the active conformation. The dash arrow indicates the region of Dyh3 head interacting with C3 domain of Shulin, now at the back of the view.

While the ODA complex is not directly in contact with the doublet microtubule in its native state, ODAs can be reconstituted on preassembled singlet microtubules or doublets lacking DCs with 24-nm periodicity (Ueno et al, 2008; Owa et al, 2014). Our structure suggests that the ODA can be reconstituted on the microtubule without DCs by the interaction of the ODA heads with the proximal neighboring ODA tail domains (Figure 2.1B and Figure 2.5D-F). More specifically, the head of Dyh3 seems to interact with the N-terminal dimerization domain (NDD) of the proximal ODA Dyh4 tail while the Dyh4 head interacts with DIC3 WD40 domain of the proximal ODA. These interactions probably enable the spontaneous alignment and stacking of the ODA complexes on the doublet microtubule without the help of the DCs. Similar tail-to-head interaction was recently observed in reconstituted ODA array on the doublet microtubule (Rao et al, 2020). Since our structure is the native structure of ODA on the doublet, our structure validated their model of the interaction. The interactions between head and tail of neighboring ODA complexes were also observed in *Chlamydomonas* ODA (Walton et al, 2021).

2.5.3 Remodeling of the tail and the head.

It has been recently proposed that the ODA complex, before its assembly on the doublet, is in an inactive form with the regulatory protein Shulin (Mali et al, 2021). To understand how ODA rearranges into an active form on the doublet, we compared the structures of the Shulin-ODA complex with our ODA complex on the doublet (Figure 2.8 and Figure 2.7). The overall appearance of the active ODA complex on the doublet was quite different from that of the inactive Shulin-ODA complex, which has a more elongated conformation (Figure 2.8A). The elongated conformation of the inactive Shulin-ODA complex stems from the positions of the motor domains which are fixed in pre-powerstroke conformations (discussed later). The most unchanged region was the base region of the Dyh4 HC up to the bundle-4 region where the DIC3's WD40 domain resides (Figure 2.8B and Figure 2.7A). Dyh3 HC, DIC2 and LC tower were rotating together about ~90 degree relative to the Dyh4's base region (Figure 2.8B). With this configuration change, Dyh3 and Dyh4 HCs are no longer crossed to each other and freed. In the active conformation, DIC2's WD40 domain interacts with Dyh4 HC, and the WD40 domain of DIC3 is docked onto Dyh3 HC. Within the HCs, there were also conformational changes. The Dyh3 showed more change in configuration with ~90 degree rotation of the head compared with the inactive form whereas Dyh4 HC showed rather a compressing movement of the head side compared with Shulin-ODA structure (Figure 2.7A-C). These conformational changes are mediated by hinge-like motions between the α-helical bundles (Figure 2.8C). The center region (bundle 4-8) of Dyh3 showed a milder conformational change compared with other regions of the Dyh3 (Figure 2.8C) since the LC tower

is associated with this region. In detail, there is a slight change in conformation of both Dyh3 and LC tower (Figure 2.8D and Figure 2.7D). The conformational change was due to the association of α-helix bundle 8 of the Dyh3 with LC8/8d. This interaction was hindered in the Shulin-ODA complex since Shulin is keeping Dyh3's bundle 8 away from LC8/8d. These tail rearrangements align the head domains to parallel configuration on the doublet (discussed later).

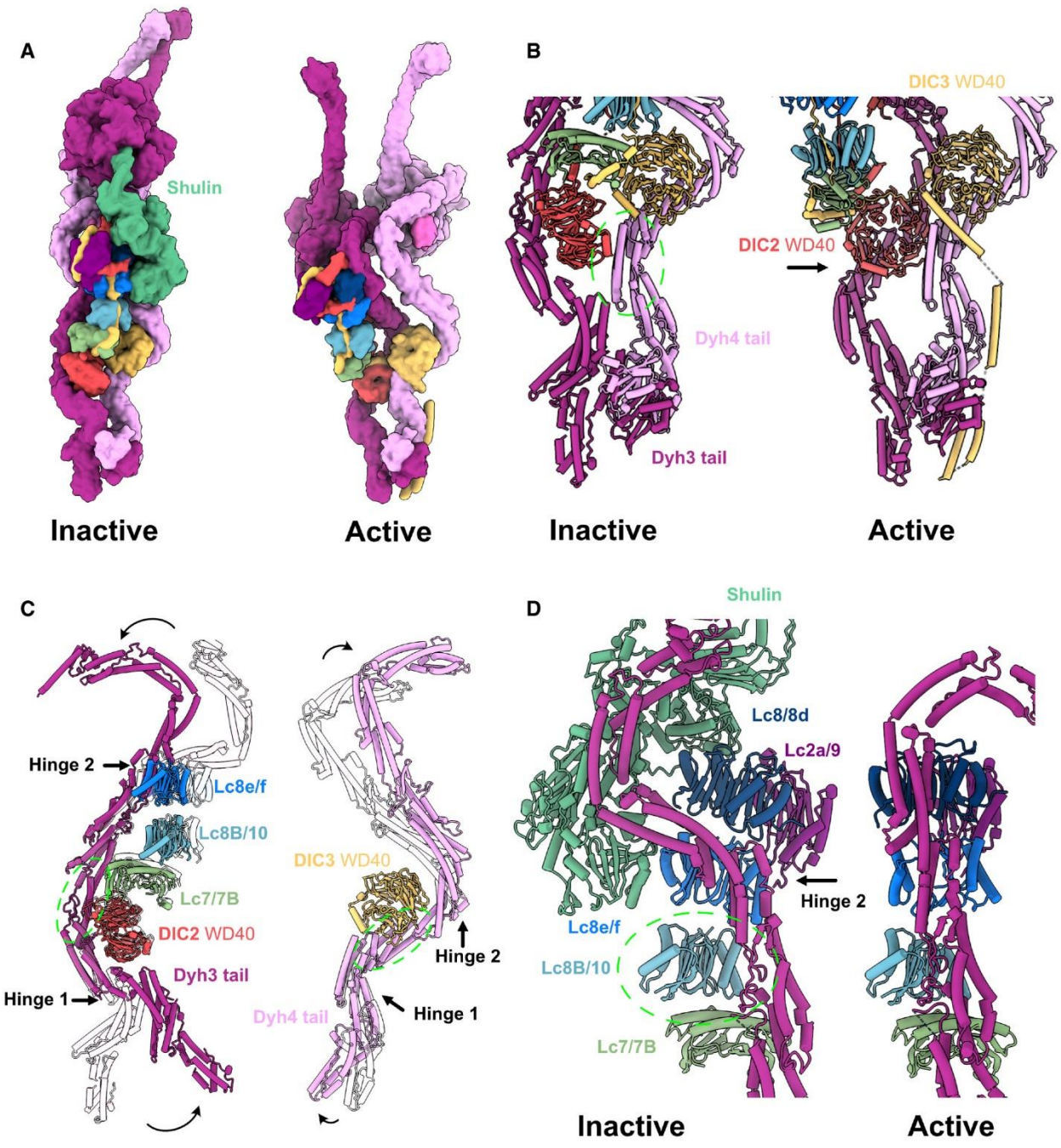

Figure 2.8. Comparison of the active ODA complex structure on the doublet and the inactive Shulin–ODA complex structure

A. The surface rendering of the inactive ODA model (with bound Shulin in green) and the active ODA model. Dyh5 is not shown.

B. Remodeling of Dyh3 and Dyh4 tails and associated IC/LCs. The green circle indicates the region of alignment (Dyh4 residues 414–513, helix bundle 3). Dyh4 tail does not exhibit large conformational change while Dyh3 rotates almost 90 degrees, evident by the rotation of DIC2 WD40 domain.

C. Superimposition of Dyh3 and Dyh4 tails between the inactive (transparent) and the active ODA (Dyh3 is aligned based on res. 535–646, helix bundle 5 while Dyh4 is aligned on res. 414–513, helix bundle 4). The Dyh3 tail exhibits two hinges with larger rotations while the Dyh4 tail also exhibits two hinges with smaller rotations.

D. The changes in interaction between Dyh3 tail and the LC tower due to the remodeling of inactive (with Shulin in green) to active conformations (two structures are aligned based on Lc8b/10). The conformations of Dyh3 bundle 8, Lc8/8d, and Lc2a/9 are significantly different. The release of the Shulin leads to the rotation of the Dyh3 tail, which causes the different interaction pattern between Dyh3 and LC8/8d.

2.5.4 Head domain structure of the ODA on the doublet.

In the Shulin-ODA complex, the heads are fixed in the pre-powerstroke positions (Figure 2.9A). In our active ODA complex structure, the linkers are in the post-powerstroke configuration both in the Dyh3 and Dyh4 heads. Therefore, the heads are ready to go through transition to next ATPase cycle with Shulin detached. Linker of the Dyh3 head was in a canonical post-powerstroke conformation (Figure 2.9A). As for the Dyh4 head, LC3 was docked onto the AAA+ ring in the post-powerstroke configuration of the linker. LC3 was interacting with AAA4 of the binding position of the Dyh4 AAA+ ring. However, the binding scheme was different from that of Lis1 which also binds to the AAA3 of cytoplasmic dynein (Toropova et al, 2014) (Figure 2.9B). LC3 still interacts with AAA4 but it was closer to AAA3. LC1 was previously shown to bind to the MTBD of Dyh3 head (Ichikawa et al, 2015; Toda et al, 2020). LC3 is the second component found to be associated with the head domain of the ODA complex. Since LC3 was interacting with both linker and the AAA+ ring, we carefully examined the linker position of Dyh4. The linker was

going at the middle of the apo state and the ADP state and slightly leaning toward AAA4 (Figure 2.9C). This is a novel configuration of dynein linker. To perform powerstroke, LC3 is thought to be detached from the AAA+ ring (Figure 2.9D).

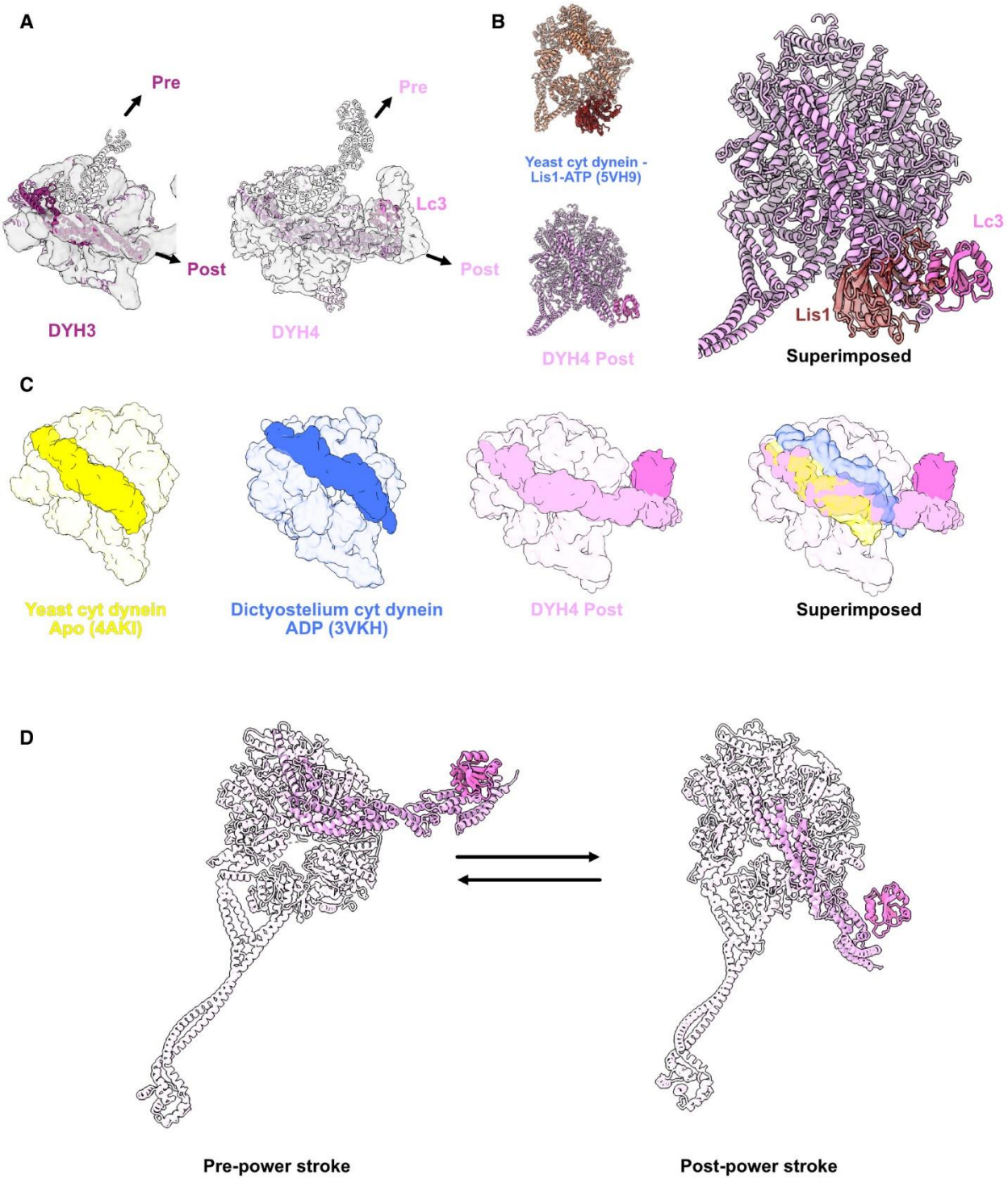

Figure 2.9. Structure of the head domain in ODA on the doublet

A. Models of the Dyh3 and Dyh4 heads in post-powerstroke conformations are fitted in the cryo-EM maps of the ODA on the doublet. The Dyh3 and Dyh4 linkers in pre-powerstroke conformations in the inactive Shulin–ODA model are also superimposed (shown in transparent).

B. Comparison of yeast cytoplasmic dynein bound to Lis1 (PDB:5VH9) with the Dyh4 bound to LC3. LC3 also binds to the AAA+ ring but in an opposite site from Lis1.

C. Comparison of the linker of Dyh4 in post-powerstroke conformation with the yeast cytoplasmic dynein in apostate and dictyostelium cytoplasmic dynein in ADP state reveals that the Dyh4 linker is positioned in between of the linker positions in apo and ADP states. The structures are aligned based on the AAA+ ring without linker.

D. Model for the conformation changes from pre-powerstroke to post-powerstrokes in Dyh4.

2.5.5 Docking of the ODA complex to the DC induces the remodeling

How the regulatory protein Shulin detaches from the ODA complex? When Shulin-ODA structure was docked onto the doublet microtubule, the Shulin region did not show a steric clash (Figure 2.10A). Therefore, we then examined the Shulin binding sites in the ODA complex on the doublet. Even though there was no other structure covering the Shulin binding sites, the regions involved in the interaction with Shulin were dispersed due to the rearrangement of the tail domain as well as the head domains (Figure 2.7E). From these results, the remodeling of the ODA itself likely causes the detachment of Shulin. To understand the cause of the remodeling of the ODA complex, we focused on the region where ODA binds to the doublet. As mentioned above, the base region of the Dyh4 tail did not change significantly (Figure 2.10A). In contrast, the tail region of Dyh3 remodeled and was located closer to the doublet (Figure 2.10A and B). This remodeled region coincides with the part which interacts with DC3. In addition, the remodeled Dyh3 interacted with extended coiled-coil region of DC1/2 (Figure 2.10C). The interaction between the head and the neighboring tail also thought to pull the Dyh3 HC.

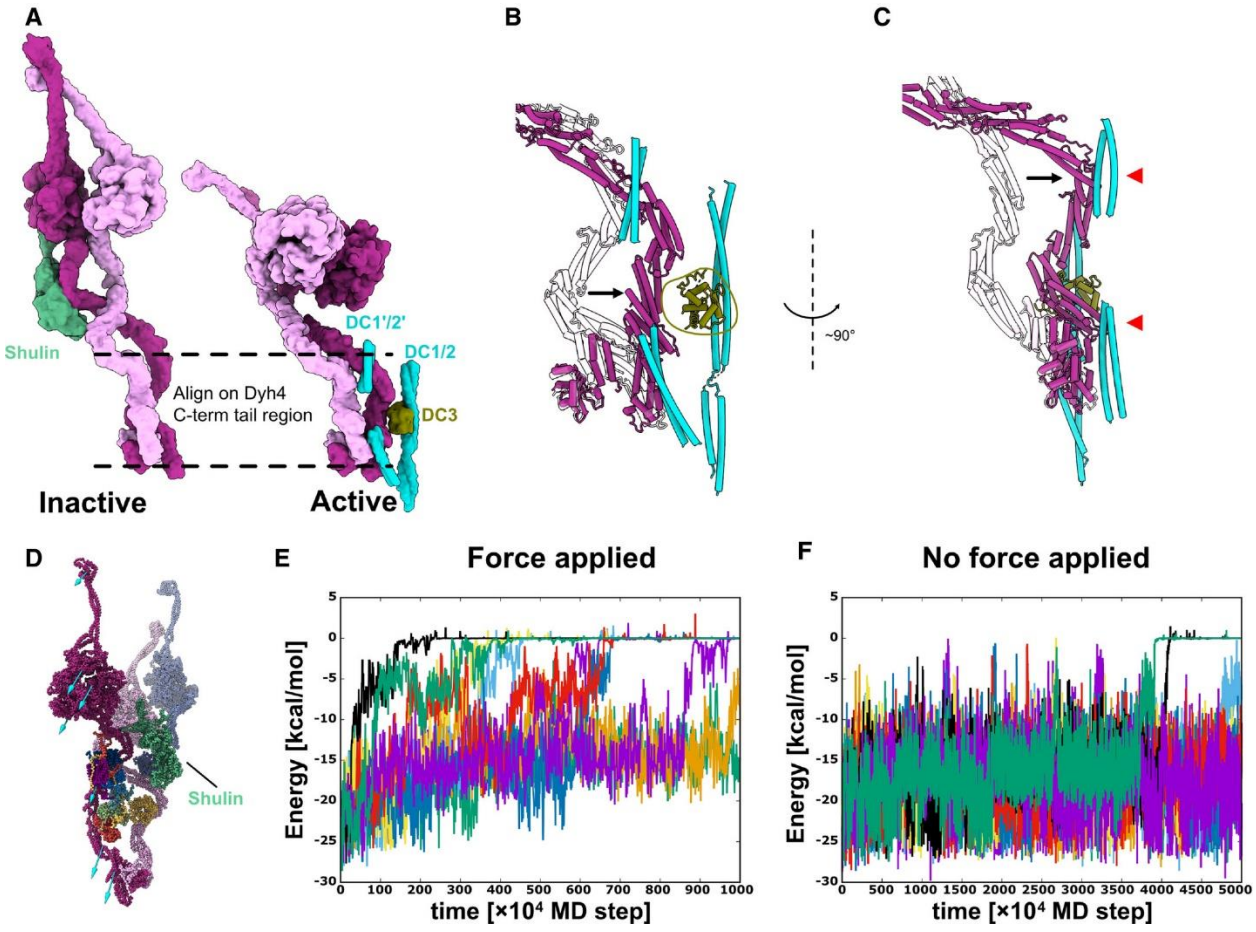

Figure 2.10. Remodeling of the tail domain and detachment of Shulin

A. Models of the inactive and the active ODA. Dyh3 and Dyh4 parts from the models are shown with Shulin and docking complex, respectively. The two structures are aligned based on the Dyh4 residues 414–513 (helix bundle 3).

B, C. Detailed comparison of the Dyh3 before and after the remodeling. With the two structures aligned as in (A), Dyh3 tail in the active conformation indicates significant shift toward DC3 (B). Similarly, the Dyh3 tail in the active conformation indicates a significant shift toward the extended coiled-coil region of DC1/2 (˜ 320–400 aa). Red arrowheads indicate the interaction sites of Dyh3 with the extended coiled-coil region of DC1/2.

D. Coarse grain molecular dynamics of the inactive Shulin–ODA complex. External force was applied in the direction of the arrow to simulate the remodeling of Dyh3 upon binding to the doublet microtubule. Shulin is shown in green.

E, F. Energy trajectories between Shulin and the ODA complex with (E) and without (F) external force applied to Dyh3. 8 out of 10 setups showed detachment of Shulin (energy = 0) with external force in 1,000 × 104 MD steps, which roughly corresponds to 10 μs. (E). In contrast, only two out of 10 trajectories showed Shulin detachment without applied force even with 5,000 × 104 MD steps, which approximately corresponds to 50 μs. (F). It should be noted that our coarse-grained MD simulation is performed in the condition where Shulin binding to the ODA complex is weakened, but it still showed the difference in detachment rate of Shulin in response to the global conformational change in the ODA complex.

To test if the remodeling of the Dyh3 HC causes the detachment of Shulin, we performed a coarse-grained MD simulation. Here, coarse-grained MD simulation was chosen over all-atom simulation for below reasons. First, the dynein is a huge protein complex and therefore the all-atom simulation was unfavorable. Previous all-atom simulation has shown dynein molecule's stability and flexibility (Kamiya et al, 2016; Can et al, 2019), however, it is difficult to track conformational change of dynein complex by all-atom simulation. Secondly, previous coarse-grained MD simulation has successfully captured the conformational change of cytoplasmic dynein, and it clarified the allosteric conformational change cascade of dynein's motor domain (Kubo et al, 2017; Goldtzvik et al, 2018). Lastly, we intended to understand the relationship between the global conformational change of the ODA and detachment of Shulin rather than the details of the residues. Thus, we have performed a coarse-grained MD simulation in the presence of external force. External force was applied to Dyh3 of the Shulin-ODA complex to mimic the remodeling of Dyh3 (Figure 2.10D, see Materials & Methods for the details). The coarse-grained MD simulation was performed from $1{,}000\times10^4$ to $5{,}000\times10^4$ MD steps. This time scale was chosen since the allosteric conformational change of dynein was captured with $1{,}000\times10^4$ MD steps in the previous MD simulation using AICG2+ (Kubo et al, 2017). Though the correspondence of MD step with the

real time is weak, one MD step roughly corresponds to ~1 ps. Thus, each trajectory corresponds to approximately 10-50 μs. To see the detachment of Shulin in these time scale, the interaction between Shulin and the ODA complex was weakened (see Materials and Methods for the details). In the presence of applied force, in eight out of ten MD trajectories, Shulin detached within $1{,}000\times10^4$ MD steps (Figure 2.10E, Movie EV1). In contrast, without external force applied, only two out of ten trajectories showed detachment within $5{,}000\times10^4$ MD steps, which is a five times longer time frame than the case with external force (Figure 2.10F). Therefore, the attraction by DCs and the adjacent ODA is likely to be important for Shulin detachment.

2.6 Discussion

Our structure presents a physiological binding state of the *Tetrahymena* ODA to the doublet via the DC complex in an unprecedented resolution. The *Tetrahymena* ODA complex is docked onto the doublet by two-sites via DCs. In addition, the ODA interacts with the neighboring ODA complex. These interactions are crucial for the stable attachment of the ODA to the doublet, and therefore, force generation by the ODA complex within cilia. The ODA is bottomed up by DC "heals" so that it can associate with the neighboring doublet properly. In different species, DCs might tune the ODA interaction schemes. DC3 in *Tetrahymena* and *Chlamydomonas* contains several EF-hand motifs. We speculate that the interaction of DC3 to the ODA can change based on the intracellular calcium ion concentration, leading to the regulation of ODA activity. In *Chlamydomonas*, high concentration of calcium ions is proposed to induce a symmetric waveform instead of the normal asymmetric breaststroke waveform (Bessen et al, 1980). The docking sites of the *Tetrahymena* ODA to the DC1/2 and 3 were similar with those of *Chlamydomonas* ODA (Walton et al, 2021). In contrast, the density connecting the DC1/2 regions on the doublet and the ODA complex was more prominent in *Chlamydomonas* ODA (Walton et al, 2021) (red arrowheads in Figure 2.4B). The coiled coil density of this region in *Tetrahymena* ODA was weaker and we could not model this region (Figure 2.4A). This could reflect the different properties of the DCs from different species.

DC3 is not conserved in vertebrates. In humans, the DC assembly affects CCDC114, CCDC151 and ARMC4 (Hjeij et al, 2014). Therefore, ARMC4 might act as DC3 in humans. However, ARMC4 (1,044 aa) is a significantly larger protein than DC3 (309 aa in *Tetrahymena*). Comparing

the tomography maps of human cilia and *Tetrahymena*, the human ODA also docks on the doublet at two sites (Figure 2.11B) (Stoddard et al, 2018; Lin et al, 2014a). However, both docking sites are different from the *Tetrahymena* ODA. The docking site close to *Tetrahymena* DC3 docking site is shifted (Figure 2.11B), while the other docking site attaches to PF-A7, instead of attaching to the DC1/2 between PFs-A7 and A8 as is the case in *Tetrahymena*. In humans, mutations leading to early termination or frameshift of CCDC151 (p.Glu109X, p.Glu309X and p.Ser419X) and CCDC114 (p.Ala248Serfs52 and p.Ser432Argfs*7) cause primary ciliary dyskinesia (Hjeij et al, 2014; Knowles et al, 2013; Zhang et al, 2019) (Figure 2.11A). These mutations map to both the regions of the DC1/2 of *Tetrahymena* binding site to the doublet and also binding to the Dyh3 tails as proposed by our structures. This implies the importance of the extended coiled-coil region of DC1/2 for the assembly of the ODA and for the remodeling of the ODA.

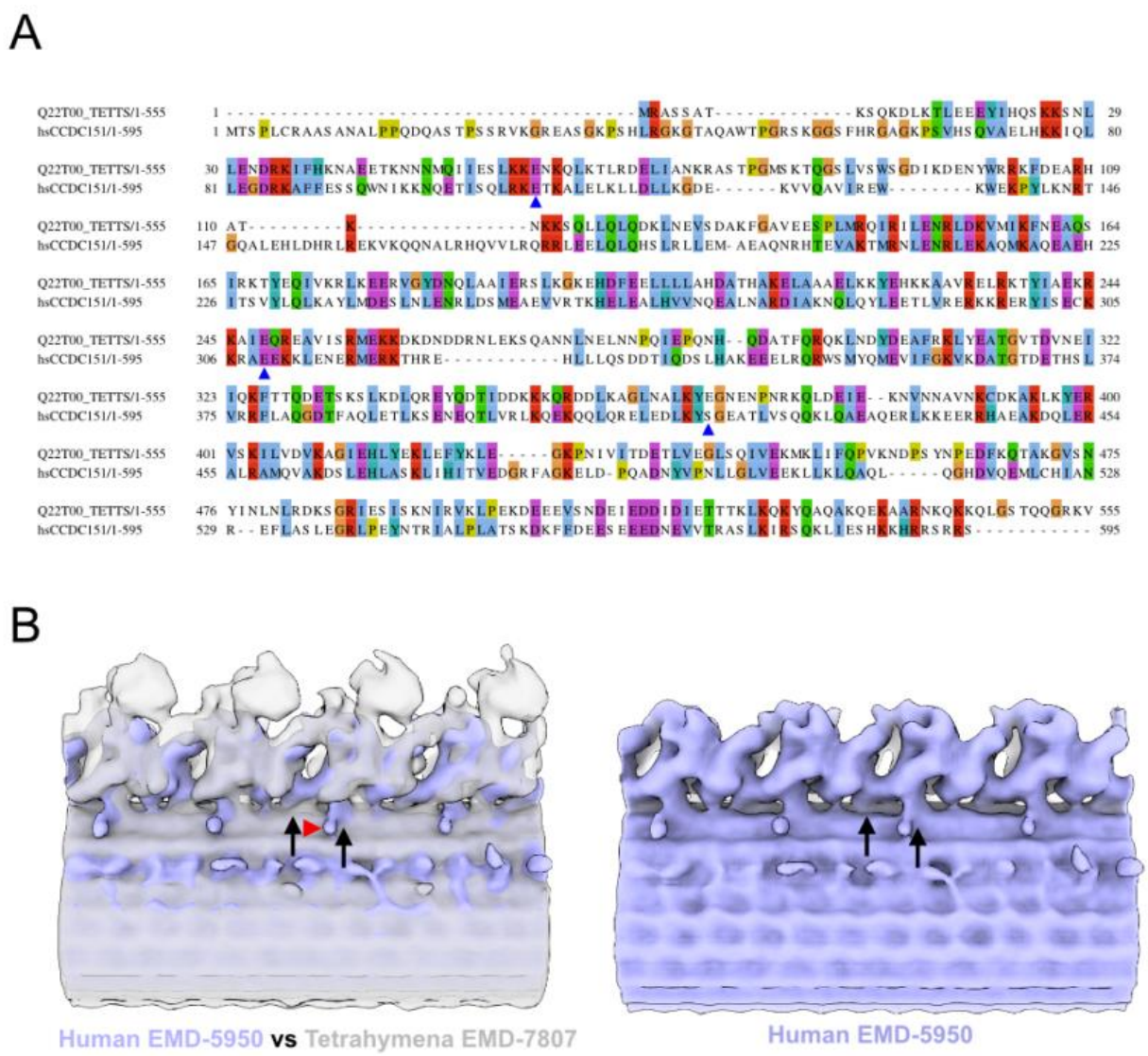

Figure 2.11. Data related to Docking complex

A. Sequence alignment of *Tetrahymena* DC1 (Q22T00_TETTS) and human CCDC151. Blue arrowhead indicates the residues at which early terminations are found in patients with ciliopathy (Hjeij, R. et al., 2014).

B. Overlapping of the tomographic structure of the axonemes from *Tetrahymena* (EMD-7807, Stoddard, D.et al., 2018) and human (EMD-5950, Lin, J. et al., 2014) (left panel) and the human axoneme alone (right). The two maps are aligned based on the radial spokes on the opposite sides. It is clear that the docking point of the human ODA (black arrows) are different from *Tetrahymena* ODA. In addition, there is an extra density protruding from the docking complex of humans (red arrowhead).

By comparing the active ODA complex structure with the recently obtained inactive form of the ODA complex, we were able to reveal the details of the remodeling of the ODA complex. The observed docking of the LC3 to the AAA+ ring of Dyh4 in the active ODA complex was surprising. Previous cryo-ET studies revealed that the βHC of the sea urchin sperm (equivalent to the Dyh4 of *Tetrahymena*) can undergo an ATPase cycle (Lin et al, 2014b). Therefore, in the ATP cycle of the Dyh4, the linker detaches from and re-attaches to the AAA+ ring (Figure 2.9D). LC3 is a thioredoxin component which was proposed to regulate the ODA activity in response to redox state of the cilia (Wakabayashi & King, 2006). Since LC3 was shown to interact with other proteins within the cilia depending on the redox state, LC3 might recruit other regulatory proteins to the Dyh4 AAA+ ring to modulate its motor activity. In the recent *Chlamydomonas* ODA structure, the linker of the β-HC, which corresponds to *Tetrahymena* Dyh4, is in a canonical post-powerstroke configuration (Walton et al, 2021). Furthermore, the *Chlamydomonas* γ-HC (equivalent to *Tetrahymena* Dyh3) showed the linker configuration similar to that of *Tetrahymena* Dyh4. This suggests that there is a complex regulatory mechanism of the ATPase cycle in the ODA complex.

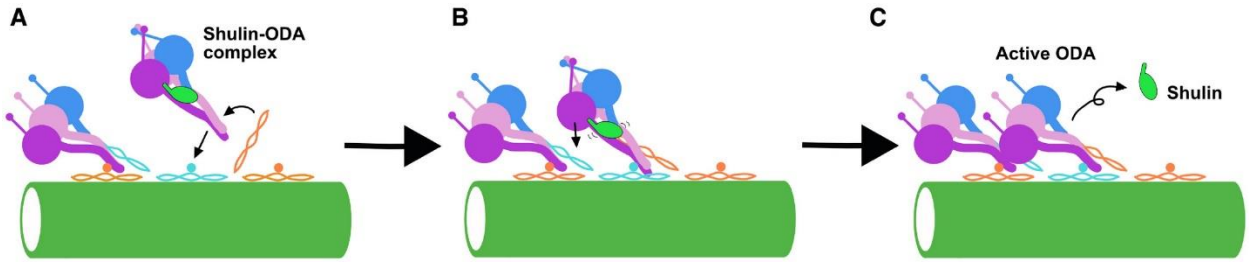

Figure 2.12. Model of the activation mechanism of the ODA

A. Shulin–ODA docks on the doublet through interaction between the tail region of Dyh3 and the DC3.

B. Extended coiled-coil region of the DC1/2 catches the ODA complex at the tail domain and facilitates the remodeling of the tail. Head domain of Dyh3 also interacts with the neighboring ODA complex's tail. Therefore, the Dyh3 is “pulled” toward the doublet and binding of the Shulin destabilizes.

C. Shulin detaches from the ODA complex and the head domains are remodeled and aligned parallel to each other. Head domains are also in post-powerstroke conformations and ready to exert force.

Though our coarse-grained MD simulation was performed with weakened Shulin interaction, it captured the effects of conformational change of ODA complex with Shulin detachment. Based on our structure and coarse-grained MD simulation, we present a model of how the ODA attachment induces remodeling and activation of the ODA complex (Figure 2.12). First, the Shulin-ODA complex docks onto the doublet using DC3 as a marker (Figure 2.12A). Next, the Dyh3 tail region starts to remodel. The extended coiled-coil region of DC1/2 catches the Dyh3 tail domain and facilitates the remodeling of the Dyh3 tail region (Figure 2.12B). Due to the remodeling in the Dyh3 tail region, the binding of Shulin becomes destabilized. After Shulin detaches, the remodeling of the ODA complex is propagated toward the heads (Figure 2.12C).

Without Shulin, the head domains would be released to be in a parallel configuration. Furthermore, the linker would be in post-powerstroke configurations and ready to exert force in cilia. Interaction of the head domain and the neighboring ODA complex would enhance this process. Our model illustrates a simple yet robust activation mechanisms of the ODA complex which does not require other external factors.

The remodeling of the tail involves an interaction with the extended coiled-coil part of DC1/2. This is the reminiscence of the cytoplasmic dynein's case. Cytoplasmic dynein-1 takes inactive conformation with two heads stacked together (Torisawa et al, 2014), when it binds to dynactin and adaptor proteins, such as BICD2, BICDR1 and HOOK3, the tail domain remodels and the two heads becomes separated (Zhang et al, 2017; Urnavicius et al, 2018). These adaptor proteins are also coiled-coil proteins and interact with the cytoplasmic dynein heavy chain by two sites to stabilize the remodeled conformation. In the cytoplasmic dynein, one of the ICs' WD domain interacts with the other remodeled HC similarly observed in the ODA's ICs. Thus, similar mechanisms are exploited for cytoplasmic dynein-1 and the ODA for the activation. The stacking of the head is also conserved with cytoplasmic dynein-2 (IFT dynein) (Toropova et al, 2017; Toropova et al, 2019). Thus, it would be interesting to clarify if there are similar adaptor proteins to remodel the tail when dynein-2 is working in the retrograde intraflagellar transport. The heterodimeric inner arm dynein-f has different subunit components and head arrangement compared with the ODA (Heuser et al, 2012). Therefore, future study is needed to show whether the same mechanism is exploited with two-headed axonemal dynein-f when incorporated to the doublet.

In conclusion, we have shown the ODA complex structure on the doublet by cryo-EM and obtained insights into how the ODA is activated inside the cilia. Our findings would be the important foundation to understand the generation of ciliary structure.

2.7 Materials & Methods

2.7.1 Growth of *Tetrahymena* cells for isolation

1 ml of the saturated *Tetrahymena* cells in SPP media (Gorovsky et al, 1975) was transferred into 50 ml liquid SPP and grown overnight with shaking at 150 rpm at 30℃ in the shaker incubator (ThermoFisher MAXQ8000). The overnight 50 ml culture was added to 900 ml of SPP and grown for approximately two days with shaking at 150 rpm at 30℃ (MAXQ8000) until the cell density reached an OD at 600 nm of 0.7.

2.7.2 Cilium isolation by dibucaine treatment

The *Tetrahymena* culture was centrifuged at 700g for 10 min at 22°C with slow deceleration (Avanti, Rotor JLA-8.1000). The cell pellet was resuspended with 10 ml of SPP and the volume was adjusted to 24 ml. The cell suspension was transferred to a 250 ml Erlenmeyer flask on ice. 1 ml dibucaine in SPP at 25 mg/ml was added to the flask to make a final concentration of 1 mg/ml, and the cell suspension was gently swirled over ice for exactly 60 seconds. 75 ml of ice-cold liquid SPP media was immediately added, and the 100 ml cilia suspension was then split into two 50 ml conical tubes. The cell suspension was centrifuged at 2,000g for 10 min at 4°C with slow deceleration (Sorvall ST 16R, Rotor 75003181). The cilia-containing supernatant was transferred to 4 centrifuge tubes for the Beckman Coulter JA 25.50 rotor, approximately 20 ml per tube. The tubes containing the cilia-containing supernatant were centrifuged at 17,000g for 40 min at 4℃ with slow deceleration (Avanti, Rotor JA25.50). The supernatants were discarded, and the pellets were carefully washed with the ice-cold Cilia Wash Buffer (50 mM HEPES at pH 7.4, 3 mM

$MgSO_4$, 0.1 mM EGTA, 1 mM DTT, 250 mM sucrose), before resuspension in 250 uL of the ice-cold Cilia Wash Buffer. The cilia were pelleted by centrifugation with 16,000xg for 10 min at 4°C in a microfuge, flash-frozen with liquid nitrogen and stored in the -80°C.

2.7.3 Purification of intact doublet microtubule

The thawed cilia pellet was resuspended in 250 µl ice-cold Cilia Final Buffer (50 mM HEPES at pH 7.4, 3 mM MgSO4, 0.1 mM EGTA, 1 mM DTT, 0.5% Trehalose, 1 mM PMSF). The concentration of total protein was measured using the Bradford Assay. The resuspended cilia sample was centrifuged at 16,000g for 10 min at 4°C in a microfuge (Eppendorf, Centrifuge 5415D). The supernatant was discarded, and the pellet was resuspended once more with 250 µl Cilia Final Buffer. NP-40 alternative (Millipore Sigma, 492016) was added to the final concentration of 15% and the total solution was resuspended. The samples were incubated on ice for 30 min before the demembraned cilia were centrifuged at 16,000g for 10 min at 4°C in a microfuge (Eppendorf, Centrifuge 5415D). The supernatant was discarded, and the axoneme-containing pellet was resuspended to 245 µl of Cilia Final Buffer. Final concentration of 1 mM ADP was added to the axonemes and incubated at room temperature for 10 minutes. Then, final concentration of 0.1 mM ATP was added to the solution and incubated at the room temperature for 10 minutes.

2.7.4 Cryo-EM sample preparation

Wild-type, K40R and MEC17-KO doublet concentrations were adjusted to 3 mg/ml. Quantifoil R2/2 (Electron Microscopy Sciences, #Q2100CR2) were treated with chloroform overnight and then glow discharged (30 seconds at 25 mAh). 3.5 μl of axoneme were applied to the pretreated grids and blotted by the Vitrobot Mark IV using blot force 3, blot time of 5 seconds, and drain time of 0.5 seconds.

2.7.5 Cryo-EM data acquisition

Movies of the doublet microtubules were acquired at 64kx nominal magnification (calculated pixel size of 1.370 Å/pixel) with counting mode using Titan Krios 300 kV FEG electron microscope (Thermo Fisher Scientific) with the direct electron detector K3 Summit (Gatan, Inc.) and the Bioquantum energy filter (Gatan, Inc.). The data were acquired using SerialEM (Mastronarde, 2005). The WT and MEC-17 datasets were collected using a total dose of 45 electrons per $Å^2$ over 40 frames. The K40R dataset was with a total dose of 73 electrons per $Å^2$ per frame over 30 frames. The defocus range was between -1.0 and -3.0 μm.

2.7.6 Cryo-EM image processing

The movies were motion corrected and dose-weighted using MotionCor2 (Zheng et al, 2017) implemented in Relion3 (Zivanov et al, 2018) and the contrast transfer function parameters were estimated using Gctf (Zhang, 2016). After discarding micrographs with apparent drift and ice contamination, bad contrast transfer function estimation (3,074, 2,410, 4,283 micrographs for WT, K40R and MEC17 data, respectively). K40R and MEC17 data were merged since the ODA structures were the same in both mutants (Yang et al, manuscript in preparation). The filaments were picked using e2helixboxer (Tang et al, 2007).

The particles of 512 x 512 pixels were initially picked with 8-nm periodicity, binned twice and pre-aligned using a modified version of the Iterative Helical Real Space Reconstruction script (Egelman, 2007) in SPIDER (Frank et al, 1996) to work with non-helical symmetry. After that, the alignment parameters were transferred to Frealign and the particles were aligned by Frealign for 6 iterations (Grigorieff, 2007). The alignment parameters were then converted into Relion 3.0. The particles were scaled to 1.744 Å/pixel (box size 402 pixel) for image processing to reduce memory usage. The 8-nm particles then underwent iterative per-particles-defocus refinement and Bayesian polishing in Relion 3.

The signal of the tubulin lattice was subtracted from each particle. The subtracted particles were subjected to 3D classification into three classes to obtain the 24-nm repeat particles with the ODA in the center. The 24-nm particles were then refined, resulting in resolution of 4.3 and 3.9 Å for WT, and K40R & MEC17 combined data from 71,462 and 139,548 particles, respectively. At this

point, it is clear that the WT doublet did not retain a lot of ODA, only the docking complex (Figure 2.2D and E). Therefore, we continued the next step with the K40R and MEC17 combined dataset.

The 24-nm particles were boxed out at a box size of 804 pixel at 1.744 Å/pixel and underwent Bayesian polishing. The ODA are then centered and boxed out of the imaging using the Localized Reconstruction in Scipion (De la Rosa-Trevín et al, 2016; Abrishami et al, 2020). The particles containing the ODA were then refined using Relion3 and cryoSPARC (Zivanov et al, 2018; Punjani et al, 2017). We first refined a single entire ODA region (Figure 2.3A). Then, we refined the ODA tail and head regions separately using focus refinement with masks for different regions (Figure 2.3B). The resolutions for different regions of the ODA are in the range of 5.5–7Å (Figures 2.3, 2.4, 2.6, 2.7).

2.7.7 Model building of the ODA complex on the doublet.

First, the Shulin-ODA complex model was separated into two regions: (1) Dyh3 & IC/LC tower region and (2) Dyh4, 5 & DIC3's WD domain. These two regions were rigid-body fitted into the active ODA map based on the tail region. Then, ICs and LCs were rigid-body fitted one by one to our cryo-EM map. Dyh3 and Dyh4 were segmented into several regions and further fitted to the density. Since the IC and LC regions were fitted quite well to our map at this point, the density corresponding to ICs and LCs were subtracted from the whole tail map and then the HC regions were fitted to the map more precisely. For the head part, the whole head domains were fitted to our cryo-EM map. We noticed that the linker parts of the Shulin-ODA complex were sticking out

since our maps are in post-powerstroke conformations. Thus, the linker part was segmented and fitted separately. For Dyh4, the linker region and LC3 were fitted together to our map and then fitted further separately. Finally, the model was integrated, and refined by Coot (Emsley et al, 2010) in our map and real space refined using Phenix (Adams et al, 2010).

2.7.8 Docking Complex Modelling

DC2 (Q233H6) and DC3 (I7M2C6) of *Tetrahymena* were found by blasting UniProt database using the *Chlamydomonas* DC2 (A8JF70) and DC3 (Q7Y0H2). Their initial models were constructed by MODELLER 9.19 using the AutoModel class with GA341 and DOPE model assessment (Šali & Blundell, 1993) from the DC2 and DC3 structure (PDB 6U42). Q233H6 and I7M2C6 were then modified in Coot (Emsley et al, 2010) in the density of the 24-nm average doublet microtubule structure to make them consistent with the density map (Figure 2.6A), in which the docking complex density is clearer. In our map, the density of helices of the docking complex are reliable but side chain densities are not very clear.

DC1 from *Chlamydomonas* (A8IPZ5) did not yield a homolog in *Tetrahymena* by blasting UniProt database. Since we could clearly see a density at the place of DC1 in the density map and DC1 from *Chlamydomonas* is not conserved in humans, we reasoned that there is another coiled coil protein in place of DC1. In humans, CCDC151 is known to be important for the docking complex and causes ciliopathy similar to CCDC114 (human DC2 homolog) (Hjeij et al, 2014; Zhang et al, 2019). The human CCDC151 localizes to respiratory ciliary axonemes and interacts with

CCDC114 (DC2 homolog). The proposed homolog of CCDC151 in *Chlamydomonas* is ODA10. While this protein is important for the ODA assembly in *Chlamydomonas* (Dean & Mitchell, 2013), it does not seem to localize in the axoneme like DC1/2 from the MS pattern (Pazour et al, 2005).

Using BLAST on UniProt database, Q22T00 was identified as a homolog for CCDC151. To see the MS profile of Q22T00, MS analyses were performed for untreated and salt-treated doublet samples as described in Dai et al, (2020). The MS profiles of Q22T00 were similar to DC2 and DC3 (Table 2.13). The coiled coil prediction of Q22T00 using COILS program (Lupas et al, 1991) also coincided with *Chlamydomonas* DC1 (Figure 2.6B). Therefore, we concluded that despite the weak conservation, Q22T00 is the DC1 in *Tetrahymena*. We constructed the initial model of Q22T00 to the DC1 using MODELLER. Q22T00 was then modelled by Coot in the density of the 24-nm average doublet microtubule structure (Figure 2.6A). The secondary prediction of Q22T00 fitted well with helical density observed in the density map. For the extended coiled-coil part of DC1/2, poly-alanine model was generated based on two regions of the coiled-coil of BICDR1 model (105-161 and 202-245 aa from PDB: 6F1T) and fitted to our cryo-EM map.

2.7.9 Visualization

The maps and models are visualized using ChimeraX (Goddard et al, 2018).

2.7.10 MD simulation

The inactive Shulin-ODA structure (PDB ID: 6ZYW) had some missing residues. For MD simulation, we modelled loops for missing regions by MODELLER (Šali & Blundell, 1993). At the same time, two intermediated parts of Dyh5 (531-636, 3,270-3,382), and both ends of the Dic2 and Dic3 sequences (1-74, 636-667, and 1-17, 511-670, respectively) were removed. Then, we did a coarse-grained MD simulation using this model. In the model, 1 amino-acid was treated as 1 bead and each bead located at the Cα position. The force field for observing dynamics used is AICG2+ (Li et al, 2012; Li et al, 2014). By using AICG2+, the coarse-grained MD approaches have been successfully employed to study large-scale protein dynamics, such as the bending motion of microtubules (Ichikawa et al, 2019), the rotational movement of F_0-motor of the yeast ATP synthase (Kubo et al, 2020), and the scheme of conformational change of cytoplasmic dynein (Kubo et al, 2017). Here, we aimed to gain insights into the relationship between global conformational change and detachment of Shulin. In the AICG2+, the reference structure was assumed as the most stable conformation, and their parameters are defined from the reference of all-atom structures. First, by comparing the inactive Shulin-ODA model with the active ODA structure on the doublet, chains that keep their binding and chains which change their binding schemes were determined by visual inspection. Based on this information, we adjusted the parameters that determine the attraction between the chains (see Figure 2.14 for the equation and the parameters). First, since Dyh3, 4, and 5 clearly have a different contact style, we set the attraction force between these chains to be 0.5 times of the default. Next, since the contacts between Dyh3, Dic2, and the LC tower were not significantly changed, we increased the attraction by a factor of 10 in order to treat this chain as a rigid body. Also, since there was no significant difference between Dyh4 and Dic3 contacts, we increased the force of attraction by a factor of 10.

Lastly, the attractive force between Shulin and others was decreased by 0.3 times the default in order to observe the Shulin detachment in a reasonable simulation time. After that, we run the simulations on several systems. When we applied the force, the force strength and direction was as follows: force direction, Dyh4 370th residue to Dyh3 480th residue; force power, f(x)=0.0001184, f(y)=0.0002144, f(z)=0.0003164. (CafeMol Unit); force type, PULL_UNIT_CF (see CafeMol Manual, Kenzaki et al, 2011). We performed 10 simulations for all systems using CafeMol version 2.1 (Kenzaki et al, 2011). Each MD simulation took $1{,}000 \times 10^4$ MD steps with external force and $5{,}000 \times 10^4$ MD steps without external force. The simulations were conducted by the underdamped Langevin dynamics at 300K temperature. We set the friction coefficient to 0.02 (CafeMol unit) and default values were used for others.

2.8 Data Availability

The data produced in this study are available in the following databases:

- Cryo-EM map: EMDB EMD-23926

  (https://www.emdataresource.org/EMD-23926)

- Model coordinates: PDB 7MOQ

  (https://www.rcsb.org/structure/7MOQ)

- Mass spectrometry data: DataDryad: doi:10.5061/dryad.p2ngf1vqv

  (https://doi.org/10.5061/dryad.p2ngf1vqv)

2.9 Acknowledgements

We thank Drs. Kaustuv Basu, Kelly Sears, Mike Strauss (Facility for Electron Microscopy Research), Ferdos Abid Ali and Andrew P. Carter for helping with data collection, processing and modelling. This work was supported by JST, PRESTO Grant Number JPMJPR20E1, JSPS KAKENHI Grant Numbers JP19K23726 and JP20K15733, and the Foundation for Nara Institute of Science and Technology (R2290001) to MI. SK is supported by JSPS Overseas Research Fellowships. KHB is supported by the grants from Canadian Institutes of Health Research (PJT-156354), Natural Sciences and Engineering Research Council of Canada (RGPIN-2016-04954) and Canadian Institute for Advanced Research (Arzieli Global Scholar Program).

2.10 Author Contributions

KHB and MI conceived the project and designed the experiments. JG generated mutant *Tetrahymena* strains. SKY and CB performed culture of the cells, purification of microtubule fractions from cilia with the help of DD and MV. SKY and CB performed vitrification of the grids, collected data. SKY, SK and KHB performed the cryo-EM data analysis of the doublet. SK, KHB and MI generated a model of the ODA complex on the doublet. SK performed the MD simulation. SK, MI and KHB interpreted the structure. All authors were involved in the manuscript writing process.

2.11 Conflicts of Interest

The authors declare no conflicts of interest.

2.12 Additional Figures and Tables

Table 2.13: Mass spectrometry of ODA complex components.

MS total spectrum count of ODA components from *Tetrahymena* WT, K40R doublet using native purification and NaCl treatment. In the NaCl treated doublet, most of the DC components were washed out.

Name	Name	UniprotID	K40R	WT	WT (NaCl)
Heavy chain	Dyh3	Q22A67	239,232,229	263,250,245	1,0,0
	Dyh4	I7M9J2	259,241,247	264,255,240	0,0,0
	Dyh5	I7M6H4	223,215,199	239,241,218	2,2,0
Intermediate chain	Dic2	I7M008	36,32,31	38,37,32	6,10,9
	Dic3	Q23FU1	40,38,37	38,39,35	15,11,12
Light chain	Lc3	A4VD75	9,9,7	7,7,6	0,0,0
	Lc4a	Q22C78	5,5,3	3,3,2	0,0,0
	Lc1	I7M1N7	22,22,20	19,17,18	0,0,0
	Lc2a	Q1HGH8	4,4,4	5,5,5	1,3,0
	Lc9	A4VEB3	4,3,3	5,5,3	0,0,0
	Lc8	W7XJB1	5,4,4	3,4,3	0,0,0
	Lc8d	Q24CE5	7,6,5	7,7,5	0,0,0
	Lc8e	Q24DI9	3,2,3	1,3,2	0,0,0
	Lc8f	Q22R86	4,4,5	3,4,5	0,0,0

	Lc10	I7MCM8	2,0,2	0,2,0	0,0,0
	Lc8b	A4VE64	6,6,6	2,2,0	0,0,0
	Lc7	I7MHB1	8,8,8	6,7,7	0,3,3
	Lc7b	Q1HFX1	6,4,5	5,5,4	0,0,0
	Lc7a*	Q1HFX2	4,4,4	3,3,3	0,0,0
	Lc2b*	I7M0N9	4,6,6	4,4,4	0,0,0
	Tct1a*	I7MGG2	0,0,0	0,0,0	0,0,0
	Tct1b*	Q231T5	2,2,2	0,0,0	0,0,0
Docking Complex	DC1	Q22T00	29,26,28	27,26,22	0,0,2
	DC2	Q233H6	20,19,17	24,25,24	0,3,2
	DC3	I7M2C6	15,13,11	17,16,17	4,3,4

* Components do not present in ODA according to Mali et al, (2021).

$$V_{AICG2+}(R|R_0) = \sum_i K_{b,i}\left(b_i - b_{i,0}\right)^2 + V_{loc}^{flp} + \sum_{j=i+2} \varepsilon_{loc,ij}\, exp\left(-\frac{\left(r_{ij} - r_{ij0}\right)^2}{2W_{ij}^2}\right) + \sum_{j=i+3} \varepsilon_{loc,ij}\, exp\left(-\frac{\left(\phi_{ij} - \phi_{ij0}\right)^2}{2W_{\phi,ij}^2}\right) + \sum_{i<j-3}^{nat\ contact} \varepsilon_{go,ij}\left[5\left(\frac{r_{ij0}}{r_{ij}}\right)^{12} - 6\left(\frac{r_{ij0}}{r_{ij}}\right)^{10}\right] + \sum_{i<j-3}^{non-native} \varepsilon_{ev}\left(\frac{d}{r_{ij}}\right)^{12}$$

b_i: bond length beween i-th and i+1-th residues.

V_{loc}^{flp}: (Terakawa et al., Biophys J 2011)

r_{ij}: distance between i-th and j-th residues.

ϕ_{ij}: dihedral angle defined as i-th, i+1-th, i+2-th, and i+3-th residues.

$W_{ij}^2, W_{\phi,ij}^2$: widths of the attractive interaction

$K_{b,i}, \varepsilon_{loc,ij}, \varepsilon_{go,ij}$: determined by AMBER force field

ε_{ev}, d: determined from a structural servay.

Figure 2.14 The equation for the AICG2+ potential is above.

Each term represents, the elasticity of the virtual bond, the sequence-dependent angle- and dihedral-angle potential, the structure-based local potential between i-th and i+2-th residues, the structure-based local potential for dihedral angles, the Go potential for non-local natively interacting pairs, and the generic repulsion for the rest of the non-local pairs. The vector R represents the $3n_{aa}$-dimensional Cartesian coordinates of the simulated protein where n_{aa} is the number of the protein amino acids. R_0 is the corresponding coordinates in the reference structure. All variables with the subscript 0 refer to parameters defined by the reference structure (initial structure). The attraction factor mentioned in the main text is “The Go potential for non-local natively interacting pairs” in the AICG2+ equation. The Go potential is already well estimated for the intra-chain interactions, but it needs to be edited for the inter-chain interactions, so we changed these parameters.

The CafeMol manual are written the meaning and the default values of these parameters (http://www.cafemol.org).

2.13 Chapter 2 References

Abrishami, V., Ilca, S. L., Gomez-Blanco, J., Rissanen, I., de la Rosa-Trevín, J. M., Reddy, V. S., Carazo, J.-M., & Huiskonen, J. T. (2020). Localized reconstruction in scipion expedites the analysis of symmetry mismatches in Cryo-EM data. *Progress in biophysics and molecular biology*. *160*, 43-52

Adams, P. D., Afonine, P. V., Bunkóczi, G., Chen, V. B., Davis, I. W., Echols, N., Headd, J. J., Hung, L.-W., Kapral, G. J., Grosse-Kunstleve, R. W., McCoy, A. J., Moriarty, N. W., Oeffner, R., Read, R. J., Richardson, D. C., Richardson, J. S., Terwilliger, T. C., & Zwart, P. H. (2010). PHENIX: a comprehensive Python-based system for macromolecular structure solution. *Acta crystallographica section D: biological crystallography*, *66*(2), 213-221.

Akella, J. S., Wloga, D., Kim, J., Starostina, N. G., Lyons-Abbott, S., Morrissette, N. S., Dougan, S. T., Kipreos, E. T., & Gaertig, J. (2010). MEC-17 is an α-tubulin acetyltransferase. *Nature*, *467*(7312), 218-222.

Bessen, M., Fay, R. B., & Witman, G. B. (1980). Calcium control of waveform in isolated flagellar axonemes of Chlamydomonas. *The journal of cell biology*, *86*(2), 446-455.

Brokaw, C. J., & Kamiya, R. (1987). Bending patterns of Chlamydomonas flagella: IV. Mutants with defects in inner and outer dynein arms indicate differences in dynein arm function. *Cell motility and the cytoskeleton*, *8*(1), 68-75.

Bui, K. H., Sakakibara, H., Movassagh, T., Oiwa, K., & Ishikawa, T. (2008). Molecular architecture of inner dynein arms in situ in Chlamydomonas reinhardtii flagella. *Journal of cell biology*, *183*(5), 923-932.

Bui, K. H., Sakakibara, H., Movassagh, T., Oiwa, K., & Ishikawa, T. (2009). Asymmetry of inner dynein arms and inter-doublet links in Chlamydomonas flagella. *Journal of cell biology*, *186*(3), 437-446.

Bui K. H. , Yagi T., Yamamoto R., Kamiya R., Ishikawa T. (2012). Polarity and asymmetry in the arrangement of dynein and related structures in the Chlamydomonas axoneme. *Journal of cell biology*, *198*(5): 913-925

Can S., Lacey S., Gur M., Carter A. P., Yildiz A. (2019). Directionality of dynein is controlled by the angle and length of its stalk. *Nature*, 566: 407-410

Dai, D., Ichikawa, M., Peri, K., Rebinsky, R., & Bui, K. H. (2020). Identification and mapping of central pair proteins by proteomic analysis. *Biophysics and physicobiology*, *17*, 71-85.

Dean, A. B., & Mitchell, D. R. (2013). Chlamydomonas ODA10 is a conserved axonemal protein that plays a unique role in outer dynein arm assembly. *Molecular biology of the cell*, *24*(23), 3689-3696.

De la Rosa-Trevín, J. M., Quintana, A., Cano, L. D., Zaldívar, A., Foche, I., Gutiérrez, J., Gómez-Blanco, J., Burguet-Castell, J., Cuenca-Alba, J., Abrishami, V., Vargas, J., Otón, J., Sharov, G., Vilas, J. L., Navas, J., Conesa, P., Kazemi, M., Marabini, R., Sorzano, C. O. S., &

Carazo, J. M. (2016). Scipion: A software framework toward integration, reproducibility and validation in 3D electron microscopy. *Journal of structural biology*, *195*(1), 93-99.

Diamant A. G., Carter A. P. (2013). Dynein Family Classification. In *Encyclopedia of Biophysics*, Roberts GCK (ed) pp. 552-572. Springer

Egelman, E. H. (2007). The iterative helical real space reconstruction method: surmounting the problems posed by real polymers. *Journal of structural biology*, *157*(1), 83-94.

Emsley, P., Lohkamp, B., Scott, W. G., & Cowtan, K. (2010). Features and development of Coot. *Acta crystallographica section D: biological crystallography*, *66*(4), 486-501.

Frank, J., Radermacher, M., Penczek, P., Zhu, J., Li, Y., Ladjadj, M., & Leith, A. (1996). SPIDER and WEB: processing and visualization of images in 3D electron microscopy and related fields. *Journal of structural biology*, *116*(1), 190-199.

Goldtzvik, Y., Mugnai, M. L., & Thirumalai, D. (2018). Dynamics of allosteric transitions in dynein. *Structure*, *26*(12), 1664-1677. E1665.

Goodenough, U. W., & Heuser, J. E. (1982). Substructure of the outer dynein arm. *The journal of cell biology*, 95(3), 798-815.

Gorovsky, M. A., Yao, M. C., Keevert, J. B., & Pleger, G. L. (1975). Isolation of micro-and macronuclei of *Tetrahymena* pyriformis. *Methods in cell biology* (Vol. 9, pp. 311-327). Academic Press.

Grigorieff, N. (2007). FREALIGN: high-resolution refinement of single particle structures. *Journal of structural biology*, *157*(1), 117-125.

Heuser, T., Barber, C. F., Lin, J., Krell, J., Rebesco, M., Porter, M. E., & Nicastro, D. (2012). Cryoelectron tomography reveals doublet-specific structures and unique interactions in the I1 dynein. *Proceedings of the national academy of sciences*, *109*(30), E2067-E2076.

Hjeij, R., Onoufriadis, A., Watson, C. M., Slagle, C. E., Klena, N. T., Dougherty, G. W., Kurkowiak, M., Loges, N. T., Diggle, C. P., Morante, N. F. C., Gabriel, G. C., Lemke, K. L., Li, Y., Pennekamp, P., Menchen, T., Konert, F., Martin, J. K., Mans, D. A., Letteboer, S. J. F., Werner, C., Burgoyne, T., Westermann, C., Rutman, A., Carr, I. M., O'Callaghan, C., Moya, E., Chung, E. M. K., Consortium, U., Sheridan, E., Nielsen, K. G., Roepman, R., Bartscherer, K., Burdine, R. D., Lo, C. W., Omran, H., & Mitchison, H. M., (2014). CCDC151 mutations cause primary ciliary dyskinesia by disruption of the outer dynein arm docking complex formation. *The American journal of human genetics*, *95*(3), 257-274.

Ichikawa, M., Saito, K., Yanagisawa, H.A., Yagi, T., Kamiya, R., Yamaguchi, S., Yajima, J., Kushida, Y., Nakano, K., Numata, O., & Toyoshima, Y. Y. (2015). Axonemal dynein light chain-1 locates at the microtubule-binding domain of the γ heavy chain. *Molecular biology of the cell*, *26*(23), 4236-4247.

Ichikawa, M., Liu, D., Kastritis, P. L., Basu, K., Hsu, T. C., Yang, S. K., & Bui, K. H. (2017). Subnanometre-resolution structure of the doublet microtubule reveals new classes of microtubule-associated proteins. *Nature communications*, *8*, 15035.

Ichikawa, M., Khalifa, A. A. Z., Kubo, S., Dai, D., Basu, K., Maghrebi, M. A. F., Vargas, J., & Bui, K. H. (2019). Tubulin lattice in cilia is in a stressed form regulated by microtubule inner proteins. *Proceedings of the national academy of sciences*, *116*(40), 19930-19938.

Kamiya, N., Mashimo, T., Takano, Y., Kon, T., Kurisu, G., & Nakamura, H. (2016). Elastic properties of dynein motor domain obtained from all-atom molecular dynamics simulations. *Protein engineering, design and selection*, *29*(8), 317-325.

Kenzaki, H., Koga, N., Hori, N., Kanada, R., Li, W., Okazaki, K. I., Yao, X.-Q., & Takada, S. (2011). CafeMol: A coarse-grained biomolecular simulator for simulating proteins at work. *Journal of chemical theory and computation*, *7*(6), 1979-1989.

Khalifa, A. A. Z., Ichikawa, M., Dai, D., Kubo, S., Black, C. S., Peri, K., McAlear, T. S., Veyron, S., Yang, S. K., Vargas, J., Bechstedt, S., Trempe, J.-F., & Bui, K. H. (2020). The inner junction complex of the cilia is an interaction hub that involves tubulin post-translational modifications. *Elife*, *9*, e52760.

King, S.M. (2012). Integrated control of axonemal dynein AAA (+) motors. *Journal of structural biology*, *179*(2), 222-228.

Knowles, M. R., Leigh, M. W., Ostrowski, L. E., Huang, L., Carson, J. L., Hazucha, M. J., Yin, W., Berg, J. S., Davis, S. D., Dell, S. D., Ferkol, T. W., Rosenfeld, M., Sagel, S. D., Milla, C. E., Olivier, K. N., Turner, E. H., Lewis, A. P., Bamshad, M. J., Nickerson, (2013). Exome sequencing identifies mutations in CCDC114 as a cause of primary ciliary dyskinesia. *The American journal of human genetics*, *92*(1), 99-106.

Kubo, S., Li, W., & Takada, S. (2017). Allosteric conformational change cascade in cytoplasmic dynein revealed by structure-based molecular simulations. *PLoS computational biology*, *13*(9), e1005748.

Kubo, S., Niina, T., & Takada, S. (2020). Molecular dynamics simulation of proton-transfer coupled rotations in ATP synthase FO motor. *Scientific reports*, 10, 8225.

Li, W., Terakawa, T., Wang, W., & Takada, S. (2012). Energy landscape and multiroute folding of topologically complex proteins adenylate kinase and 2ouf-knot. *Proceedings of the national academy of sciences*, *109*(44), 17789-17794.

Li, W., Wang, W., & Takada, S. (2014). Energy landscape views for interplays among folding, binding, and allostery of calmodulin domains. *Proceedings of the national academy of sciences*, *111*(29), 10550-10555.

Lin, J., Okada, K., Raytchev, M., Smith, M. C., & Nicastro, D. (2014). Structural mechanism of the dynein power stroke. *Nature cell biology*, *16*(5), 479-485.

Lin, J., Yin, W., Smith, M. C., Song, K., Leigh, M. W., Zariwala, M. A., Knowles, M. R., Ostrowski, L. E., & Nicastro, D. (2014). Cryo-electron tomography reveals ciliary defects underlying human RSPH1 primary ciliary dyskinesia. *Nature communications*, *5*, 5727.

Lin, J., & Nicastro, D. (2018). Asymmetric distribution and spatial switching of dynein activity generates ciliary motility. *Science*, *360*(6387), eaar1968.

Lupas A., Van Dyke M., Stock J. (1991). Predicting coiled coils from protein sequences. *Science*, *252*(5009): 1162-1164

Ma, M., Stoyanova, M., Rademacher, G., Dutcher, S. K., Brown, A., & Zhang, R. (2019). Structure of the decorated ciliary doublet microtubule. *Cell*, *179*(4), 909-922.

Mali, G. R., Ali, F. A., Lau, C. K., Begum, F., Skehel, M., & Carter, A. P. (2021). Shulin packages axonemal outer dynein arms for ciliary targeting. *Science*, *371*(6532), 910-916.

Mastronarde, D. N. (2005). Automated electron microscope tomography using robust prediction of specimen movements. *Journal of structural biology*, *152*(1), 36-51.

Nicastro, D., Schwartz, C., Pierson, J., Gaudette, R., Porter, M.E., & McIntosh, J. R. (2006). The molecular architecture of axonemes revealed by cryoelectron tomography. *Science*, *313*(5789), 944-948.

Oda T., Abe T., Yanagisawa H. A., Kikkawa M. (2016). Docking-complex-independent alignment of Chlamydomonas outer dynein arms with 24-nm periodicity in vitro. *Journal of Cell Science*, 129: 1547-1551

Oda, T., Abe, T., Yanagisawa, H. A., & Kikkawa, M. (2016). Structure and function of outer dynein arm intermediate and light chain complex. *Molecular biology of the cell*, *27*(7), 1051-1059.

Owa, M., Furuta, A., Usukura, J., Arisaka, F., King, S. M., Witman, G. B., Kamiya, R., & Wakabayashi, K.I. (2014). Cooperative binding of the outer arm-docking complex underlies the regular arrangement of outer arm dynein in the axoneme. *Proceedings of the national academy of sciences*, *111*(26), 9461-9466.

Pazour, G. J., Agrin, N., Leszyk, J., & Witman, G. B. (2005). Proteomic analysis of a eukaryotic cilium. *Journal of cell biology*, *170*(1), 103-113.

Punjani, A., Rubinstein, J. L., Fleet, D.J., & Brubaker, M. A. (2017). cryoSPARC: algorithms for rapid unsupervised cryo-EM structure determination. *Nature methods*, *14*(3), 290-296.

Rao, Q., Wang, Y., Chai, P., Kuo, Y. W., Han, L., Yang, R., Yang, Y., Howard, J. & Zhang, K. (2020). Cryo-EM structures of outer-arm dynein array bound to microtubule doublet reveal a mechanism for motor coordination. *bioRxiv* doi: https://doi.org/10.1101/2020.12.08.415687 [PREPRINT]

Reiter, J. F., & Leroux, M. R. (2017). Genes and molecular pathways underpinning ciliopathies. *Nature reviews molecular cell biology*, *18*(9), 533-547.

Šali, A., & Blundell, T. L. (1993). Comparative protein modelling by satisfaction of spatial restraints. *Journal of molecular biology*, *234*(3), 779-815.

Stoddard, D., Zhao, Y., Bayless, B. A., Gui, L., Louka, P., Dave, D., Suryawanshi, S., Tomasi, R. F. X., Dupuis-Williams, P., Baroud, C. N., Gaertig, J., & Nicastro, D. (2018). *Tetrahymena* RIB72A and RIB72B are microtubule inner proteins in the ciliary doublet microtubules. *Molecular biology of the cell*, *29*(21), 2566-2577.

Tang, G., Peng, L., Baldwin, P. R., Mann, D. ., Jiang, W., Rees, I., & Ludtke, S. J. (2007). EMAN2: an extensible image processing suite for electron microscopy. *Journal of structural biology*, *157*(1), 38-46.

Toda, A., Nishikawa, Y., Tanaka, H., Yagi, T., & Kurisu, G. (2020). The complex of outer-arm dynein light chain-1 and the microtubule-binding domain of the γ heavy chain shows how axonemal dynein tunes ciliary beating. *Journal of biological chemistry*, *295*(12), 3982-3989.

Torisawa, T., Ichikawa, M., Furuta, A., Saito, K., Oiwa, K., Kojima, H., Furuta, K., Toyoshima, Y. Y. (2014). Autoinhibition and cooperative activation mechanisms of cytoplasmic dynein. *Nature cell biology*, *16*(11), 1118-1124.

Toropova, K., Zou, S., Roberts, A. J., Redwine, W. B., Goodman, B. S., Reck-Peterson, S. L., & Leschziner, A. E. (2014). Lis1 regulates dynein by sterically blocking its mechanochemical cycle. *Elife*, *3*, e03372.

Toropova, K., Mladenov, M., & Roberts, A. J. (2017). Intraflagellar transport dynein is autoinhibited by trapping of its mechanical and track-binding elements. *Nature structural & molecular biology*, *24*(5), 461.

Toropova, K., Zalyte, R., Mukhopadhyay, A. G., Mladenov, M., Carter, A. P., & Roberts, A. J. (2019). Structure of the dynein-2 complex and its assembly with intraflagellar transport trains. *Nature structural & molecular biology*, *26*(9), 823-829.

Ueno, H., Yasunaga, T., Shingyoji, C., & Hirose, K. (2008). Dynein pulls microtubules without rotating its stalk. *Proceedings of the national academy of sciences*, *105*(50), 19702-19707.

Ueno, H., Bui, K. H., Ishikawa, T., Imai, Y., Yamaguchi, T., & Ishikawa, T. (2014). Structure of dimeric axonemal dynein in cilia suggests an alternative mechanism of force generation. *Cytoskeleton*, *71*(7), 412-422.

Urnavicius, L., Lau, C. K., Elshenawy, M. M., Morales-Rios, E., Motz, C., Yildiz, A., & Carter, A.P. (2018). Cryo-EM shows how dynactin recruits two dyneins for faster movement. *Nature*, *554*(7691), 202-206.

Wakabayashi, K., & King, S. M. (2006). Modulation of Chlamydomonas reinhardtii flagellar motility by redox poise. *The journal of cell biology*, *173*(5), 743-754.

Walton, T., Wu, H., & Brown, A. (2021). Structure of a microtubule-bound axonemal dynein. *Nature communications*, *12*, 477.

Zhang, K. (2016). Gctf: Real-time CTF determination and correction. *Journal of structural biology*, *193*(1), 1-12.

Zhang, K., Foster, H. E., Rondelet, A., Lacey, S.E., Bahi-Buisson, N., Bird, A. W., & Carter, A. P. (2017). Cryo-EM reveals how human cytoplasmic dynein is auto-inhibited and activated. *Cell*, *169*(7), 1303-1314.

Zhang, W. Z., Li, D. P., Wei, S. J., Guo, T., Wang, J., Luo, H., Yang, Y. F., & Tan, Z. P. (2019). Whole-exome sequencing identifies a novel CCDC151 mutation, c. 325G> T (p. E109X),

in a patient with primary ciliary dyskinesia and situs inversus. *Journal of human genetics*, *64*(3), 249-252.

Zheng, S. Q., Palovcak, E., Armache, J. P., Verba, K. A., Cheng, Y., & Agard, D. A. (2017). MotionCor2: anisotropic correction of beam-induced motion for improved cryo-electron microscopy. *Nature methods*, *14*(4), 331-332.

Zivanov, J., Nakane, T., Forsberg, B.O., Kimanius, D., Hagen, W. J., Lindahl, E., & Scheres, S. H. (2018). New tools for automated high-resolution cryo-EM structure determination in RELION-3. *Elife*, *7*, e42166.

Chapter 3

"There is nothing like a dream to create the future."

Victor-Marie Hugo, 1802-1885 C.E., *Les Misérables*

«Il n'y a rien de mieux qu'un rêve pour créer le futur.»

Victor-Marie Hugo, 1802 - 1885 E.C., *Les Misérables*

A Chinese quote with similar ideology:

"夫哀莫大於心死，而人死亦次之。"

Zhuang Zhou，莊子《莊子·田子方》,前 369 年－前 286 年

3.1 Preface

PTM is an important mechanism to maintain and regulate cilia, such as to help with the functions of ODA. When the acetylation level of K40 increases, the motility rate of ODA increases. In contrast, deacetylation decreases the motility rate of ODA on microtubules *in vitro* (Alper et al., 2014). However, questions remain about how PTM, such as acetylation, acts at a molecular level to facilitate the structure of ODA and the axoneme. The mechanism of how different types of PTM work and interact is important to allow our understanding of ciliary processes such as ciliogenesis, ciliary beating and bending, and IFT.

In this Chapter 3, I elucidated a cryo-EM structure of acetylated and nonacetylated doublet microtubules (DMT) from *Tetrahymena thermophila*. Using this structure and molecular dynamics (MD) simulations, we propose a model for the functional role of acetylation in cilia.

Our cryo-EM results resolved the acetylated and deacetylated K40 loops at 3.5 – 4.5 Å. No significant differences were noticed between that of the Wild-type (WT) CU428 and acetylation mutant density maps at this resolution. However, coarse grain MD simulation show that acetylated K40 loops have less flexibility and lower energy levels than those of the deacetylated K40 loops. Our results also show that K40 loop stabilize binding with the Microtubule inner proteins (MIPs), and that acetylation would have a cumulative effect on the DMT stability.

3.2 Paper Title

Effect of alpha tubulin acetylation on the doublet microtubule structure and microtubule inner proteins

Shun Kai Yang[1,Ψ], Shintaroh Kubo[1, Ψ], Katya Peri[1], Corbin Black[1], Daniel Dai[1], Zhe Fan[1], Melissa Valente[1], Khanh Huy Bui[1,2*]

Author affiliations

1. Department of Anatomy and Cell Biology, McGill University, Montréal, Québec H3A 0C7, Canada

2. Centre de Recherche en Biologie Structurale, McGill University, Montréal, Québec H3A 0C7, Canada

[Ψ] These authors contributed equally

*Corresponding author:

Khanh Huy Bui, Department of Anatomy and Cell Biology, McGill University, Montréal, Québec H3A 0C7, Canada. E-mail: huy.bui@mcgill.ca

Key words: Cilia, Doublet microtubule, Acetylation, Cryo-electron Microscopy

3.3 Abstract

Tubulin acetylation was first discovered in the cilia and later found in all kinds of long-lived and stable microtubules in the cells. Alongside other post-translational modifications such as polyglutamylation and detyrosination, acetylation is used to modulate the property of the microtubule. Acetylated microtubules are more stable and resistant to damage. Although the deacetylation of microtubules can lead to aberrant microtubule phenotypes in the cells, acetylation does not affect the survival of the cells. In contrast to other types of post-translational modification, acetylation of the lysine 40 of alpha-tubulin is the only luminal PTM site in the microtubule. The luminal location of the acetylated lysine 40 suggests that it might be used to tune the lateral interaction of protofilaments inside the microtubule. In this study, we examined the effect of tubulin acetylation on the doublet microtubule and microtubule inner proteins in the cilia of the ciliate *Tetrahymena thermophila* using a combination of cryo-electron microscopy, molecular dynamics, and mass spectrometry. We found that acetylation exerts a small-scale but cumulative effect on the doublet microtubule structure and stability. In addition, mass spectrometry indicates an interconnect between acetylation and phosphorylation in the cilia.

3.4 Introduction

Cilia have diverse roles in motility, sensory function, cellular signaling, and growth control. Motile cilia drive the flow of fluid, including human sperm (Lehti & Sironen, 2017), mucus clearance in lung and olfactory epithelium (Bustamante-Marin, M., & Ostrowski, 2017; Shang, Inthavong, & Tu, 2019), and cerebrospinal fluid circulation (Djenoune & Wyart, 2017; Orts-Del'Immagine & Wyart, 2017). Non-motile primary cilia are found in rod cells for transmitting chemical signals converted from light (De Robertis, 1956, 1960; Sjostrand, 1953; Tokuyasu K - Yamada & Yamada, 1959), and in kidney cells where cilia function as mechanosensors for transmitting flow signals into chemical signaling pathways (Kotsis et al., 2007; Yoder, 2007). At the core, motile and primary cilia share the same cytoskeleton structure, namely, the axoneme (Porter & Sale, 2000). The axoneme is composed of a bundle of nine outer doublet microtubules (DMT), each composed of protofilaments (PFs) of tubulins that form into a hollow cylinder A-tubule and an incomplete cylinder B-tubule (Fig. 3.1). Inside the lumen of the DMT, there is a weaving network of microtubule inner proteins (MIPs), which serves as additional support for the DMT to stabilize its structure (Ichikawa et al., 2019; Ichikawa et al., 2017; Khalifa, 2020; Ma et al., 2019).

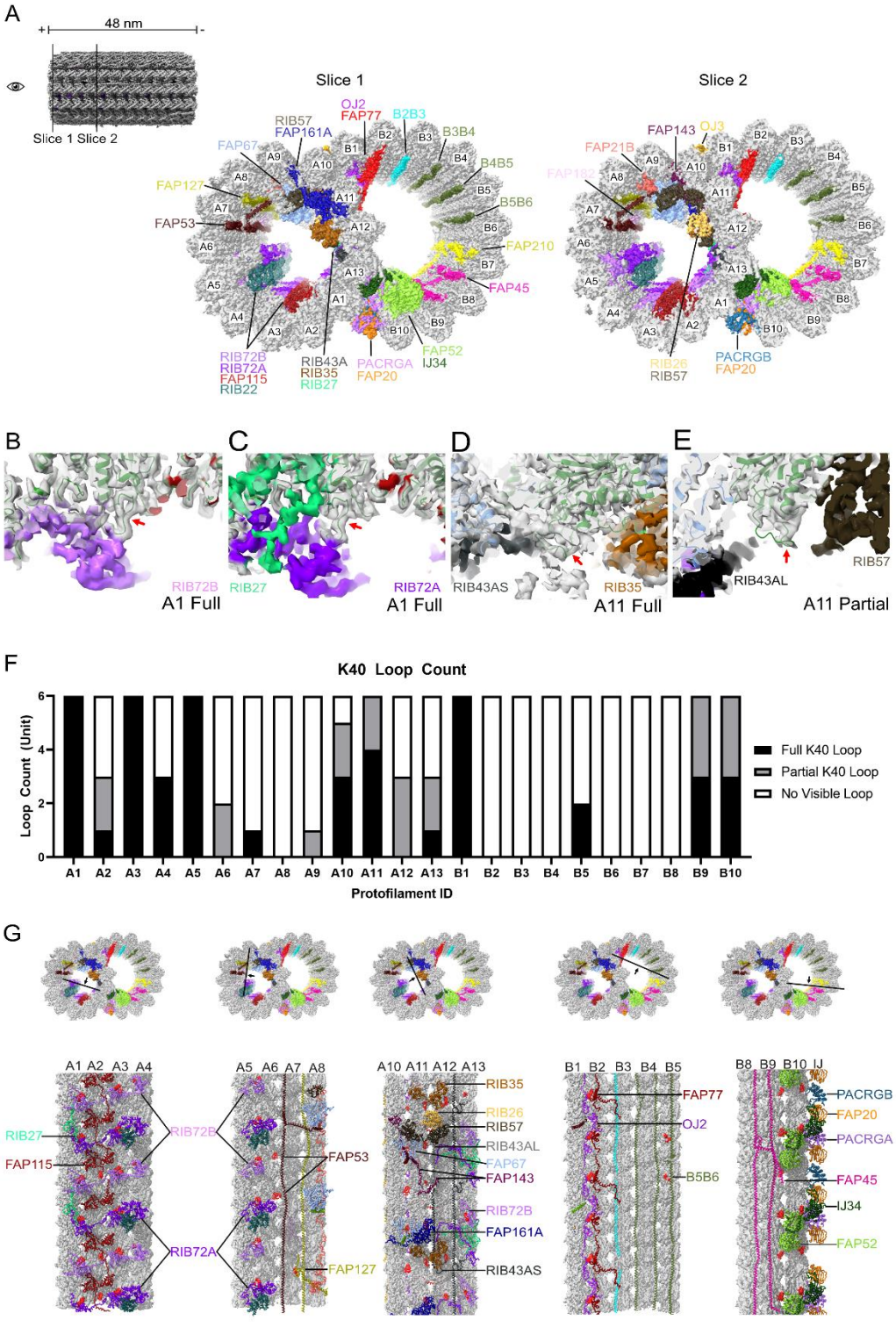

Figure 3.1. Cryo-EM map of the DMT show that αK40 closely interact with MIPs

A. Surface rendering view of the DMT from the tip of the cilia, with MIPs colored in the 48-nm repeat cryo-EM electron density map of *Tetrahymena*.

B.-C. Cryo-EM map and models of the full αK40 loops in protofilament A1, the red arrow points to the location of the loop.

D.-E. Cryo-EM map and models of the full (D) and partial (E) αK40 loops in protofilament A11, the red arrow points to the location of the loop.

F. Bar graph showing the composition of visible full and partial loops in both the A- and B-tubules.

G. 48-nm repeat surface rendering view of selected protofilaments with MIPs that interact with visible full and partial αK40 loops colored in red, indicating that αK40 loops are structured in regions with many MIPs.

Tubulins in the DMT undergo different post translational modifications (PTM) to provide different functions (Verhey, 2007). This mechanism of regulation is called ‘tubulin code”, in which PTMs can modulate the property of the microtubule directly or indirectly through the binding of microtubule associated proteins (MAPs). The common and well-studied tubulin PTMs are phosphorylation, detyrosination, glutamylation, glycylation and acetylation (Wloga, Joachimiak, Louka, & Gaertig, 2017a). The DMT contains a unique signature of PTM, which includes cilia specific PTM such as glycylation. For example, the B-tubule of the DMT is enriched in glutamylated and detyrosinated tubulins while A-tubule tubulins are mostly unmodified. In the cilia, PTM is a fine tune for ciliary function rather than a biphasic switch. Glutamylation could regulate inner dynein arm activities which controls the waveform motion of cilia (Tomohiro Kubo et al., 2010). Hyper-glutamylation due to depletion of deglutamylases can improve intraflagellar transport in ift88-deficient zebrafish (Pathak et al., 2014). Lack of glycylation could result in abnormal pre-powerstroke and post-powerstroke conformations of dynein arms in mouse sperms

(Gadadhar et al., 2021). The loss of glycylation will sometimes lead to an increase in glutamylation, probably by increased intraflagellar transport activity carrying glutamylase (T. Kubo et al., 2015; Rogowski et al., 2019; Rogowski et al., 2010; Wloga et al., 2009).

One of the most intriguing PTM in the cilia is acetylation, which occurs inside the lumen of the DMT on lysine 40 residue of α-tubulins (αK40). Acetylation was first identified in the cilia of *Chlamydomonas reinhardtii* (M. & Piperno, 1987; S.W. & Rosenbaum, 1983). Acetylation was later found on microtubules in the cells, such as in the neurons in *C. elegans* (Fukushige, Hendzel, Bazett-Jones, & McGhee, 1999; Shida et al., 2010). Acetylation could also take place on K60 and K370 residues of α-tubulin, and K58 of β-tubulin (N. Liu et al., 2015). Acetylation is particularly interesting because the αK40 loop is the only PTM site located inside the lumen (Eshun-Wilson et al., 2019; Kaul et al., 2014). The αK40 loop is structurally flexible (Eshun-Wilson et al., 2019), and almost 100% completely acetylated in cilia (Akella et al., 2010). Acetylated αK40 enhances microtubule stability and longevity (Schaedel et al., 2015). Zebrafish embryos lacking acetyl-K40 had fewer microtubules in neurons (Akella et al., 2010).

The main enzyme responsible for αK40 acetylation is alpha-acetyltransferase-1 (αTAT1). Deacetylation are carried out by Histone deacetylase 6 (HDAC6) (Hubbert et al., 2002; Y. Zhang et al., 2003) and NAD-dependent deacetylase sirtuin 2 (SIRT2) (North et al., 2003), which could promote disassembly of mammalian primary cilia. In *T. thermophila*, K40R (lysine to arginine) and MEC17 (αTAT1-knock out) mutant often led to short microtubules and fewer in numbers (Akella et al., 2010). Mice that lack αTAT1 have defective flagellar beat (Kalebic et al., 2013), and C. elegans become touch insensitive without αTAT1 (Akella et al., 2010; Shida et al., 2010).

Motor proteins travel preferentially on acetyl-K40 microtubules due to higher binding affinity (Garnham & Roll-Mecak, 2012; Reed et al., 2006), but research also showed that acetylation might work in conjunction with detyrosination to affect Kinesin-1 motility in a more complex mechanism (Kaul et al., 2014; W. J. Walter et al., 2012). Overexpression of HDAC6 or SIRT2 could lead to short cilia (Ran et al., 2015; Zhou et al., 2014), but cilia-shortening effect of HDAC6 could be countered by an acetyl-K mimic α-tubulin suggest that it may destabilize the microtubule lattice (Cueva et al., 2012). HDAC6 destabilize the doublet microtubule lattice to trigger cilia reabsorption into the cell as part of the cell cycle (Cueva et al., 2012), but HDAC6 could activated by Aurora Kinase A to upregulate tubulin glutamylation resulting in ciliary disassembly (Hubbert et al., 2002; Ki et al., 2020; Pugacheva et al., 2007).

Structurally, αK40 is located at a looped region in the lumen of α-tubulin, close to the tubulin lateral interaction interface. The αK40 loop is functionally important, but it is structurally flexible and disordered even in the 96% acetylated reconstituted microtubule (Eshun-Wilson et al., 2019; Howes et al., 2014). Cryo-EM and molecular dynamic studies of acetylated microtubules suggests that acetylation activity restrict the motion of αK40 loop by disturbing the electrostatic interaction energy, which weakens the lateral contacts to produce conformational changes that reduce disorder within the loop, and in turn stabilize the microtubule lattice (Eshun-Wilson et al., 2019). When lysine 40 is replaced with arginine, a charged residue that cannot be acetylated, the interfilament angle will change the salt bridge formation to result in elliptical microtubules that have decreased number of protofilament (Cueva et al., 2012).

Interestingly, many αK40 loops are fully structured as visualized in the cryo-EM structure of the DMT from the ciliate and green algae (Khalifa, 2020; Ma et al., 2019). Within the inner junction

of *Chlamydomonas* DMT, αK40 loops at protofilament B9 and B10 (Khalifa, 2020) clamp the microtubule inner protein (MIP) FAP52, a protein whose homolog causes ciliopathy in human (Ta-Shma et al., 2015). These results suggest that the αK40 loop may have an important role in recognizing and binding with different MIPs to stabilize cilia, and disruption of acetylation may disrupt the αK40 loop's interaction with MIPs.

Therefore, in this work we aimed to study the structural effect of acetylated and de-acetylated tubulin on the DMT and the MIPs from *Tetrahymena thermophila* wild-type, mutants devoid of acetylation (MEC17) and K40 specific de-acetylation (K40R) (Akella et al., 2010) by a combination of cryo-EM, molecular dynamics and mass spectrometry.

3.5 Results

3.5.1 Acetylated K40 loops are structured when interacting with MIPs

We first examined a 48-nm repeat cryo-EM density map at 3.5 Å resolution from the native doublet microtubules of *Tetrahymena* WT (CU428 strain) cilia of the (Figure 1A, manuscript in preparation). The DMT from the WT cilia are intact, except for the loss of outer dynein arms. With this map, we modelled all the tubulins within the 48-nm repeat of the DMT and identified all the visible αK40 loops within the structure. Most known *Tetrahymena* MIPs have been localized and identified in this map in our other works (manuscript in preparation). The tubulins in the DMT of *Tetrahymena* are almost 100% acetylated (Akella et al., 2010). In contrast to the acetylated singlet microtubule structure (Eshun-Wilson et al., 2019), we observed many fully-structured αK40 loops in the DMT (Fig. 3.1B-F). In certain protofilaments such as A1, A3, A5, A11, and B1, all the αK40 loops are structured. However, structured αK40 loops are a lot less present in the B-tubule (Fig. 3.1F). We discovered a pattern as to the location of structured αK40 loops: fully structured αK40 loops are visible where many MIPs and tubulin interact but are difficult to be resolved in places with little or no MIPs due to its flexibility. (Fig. 3.1G, Table 3.2). Notably, in A1, where Rib72A and Rib72B are in contact with the αK40 (Fig. 3.1B, C), all αK40 loops are fully structured due to the 8-nm alternating pattern of Rib72A and Rib72B (Fig. 3.1G). This pattern is consistent with previous observation of the αK40 loop in the green algae *Chlamydomonas reinhardtii* DMT (Khalifa, 2020; Ma et al., 2019). It also explained that the B-tubule has fewer numbers of structured αK40 compared to the A-tubule which has more MIPs.

Table 3.2. Count of full, partial, and missing αK40 loops. Based upon the K40R cryo-EM density maps, along with possible MIPs interaction for αK40 loops in each protofilament.

Protofilament ID (48-nm Internal Repeat)	Full K40 Loop Count	Partial K40 Loop Count	Possible MIP Interaction
A1	6	0	IJ34, Rib72a, Rib72b, FAP115, RIB27
A2	0	3	Rib72a, Rib72b, FAP115
A3	6	0	Rib72a, Rib72b, FAP115
A4	3	0	Rib72a, Rib72b, FAP22
A5	6	0	Rib72a, Rib72b, FAP22
A6	0	2	Rib72a, Rib72b, FAP53
A7	1	0	FAP127, FAP53, FAP182
A8	0	0	FAP127, FAP53, FAP21b, FAP182
A9	0	1	FAP127, FAP53, FAP21b, FAP67, FAP143, FAP161, RIB57
A10	3	2	FAP53, FAP67, FAP141, FAP143, FAP161, RIB57, RIB35
A11	4	2	FAP53, Rib43aL, FAP143, FAP161, RIB26, RIB57, RIB35
A12	0	3	Rib72a, Rib43aS, Rib43aL, FAP143, RIB27, RIB26, RIB57, RIB35
A13	1	2	Rib72a, Rib72b, Rib43aS, RIB27
B1	6	0	Rib72a, Rib72b, FAP77, OJ2, OJ3, FAP53, FAP141
B2	0	0	FAP77, FAP112
B3	0	0	FAP112, B3B4
B4	0	0	B3B4, B4B5
B5	2	0	B4B5
B6	0	0	FAP210
B7	0	0	FAP210, FAP45
B8	0	0	FAP210, FAP45
B9	3	3	FAP45, FAP52
B10	3	3	FAP52, FAP20, PACRGA, PACRGB, IJ34

It was reported that acetylated αK40 loops adopted more rigid conformations (Eshun-Wilson et al., 2019). Therefore, we compared the conformations of all the αK40 loops observed in our DMT

structure. Interestingly, the αK40 loops in its respective protofilaments do not have the same exact conformation (Fig. 3.3A). Each protofilament may undergo various angle restraints and compaction as it makes up the DMT. The shapes of αK40 loops adapt to the location of different protofilaments to facilitate MIPs interactions and for maintaining axonemal structure. We did not observe any conformations where the acetylated αK40 involved in potential lateral interaction (Fig. 3.3A, Fig. 3.1B-E).

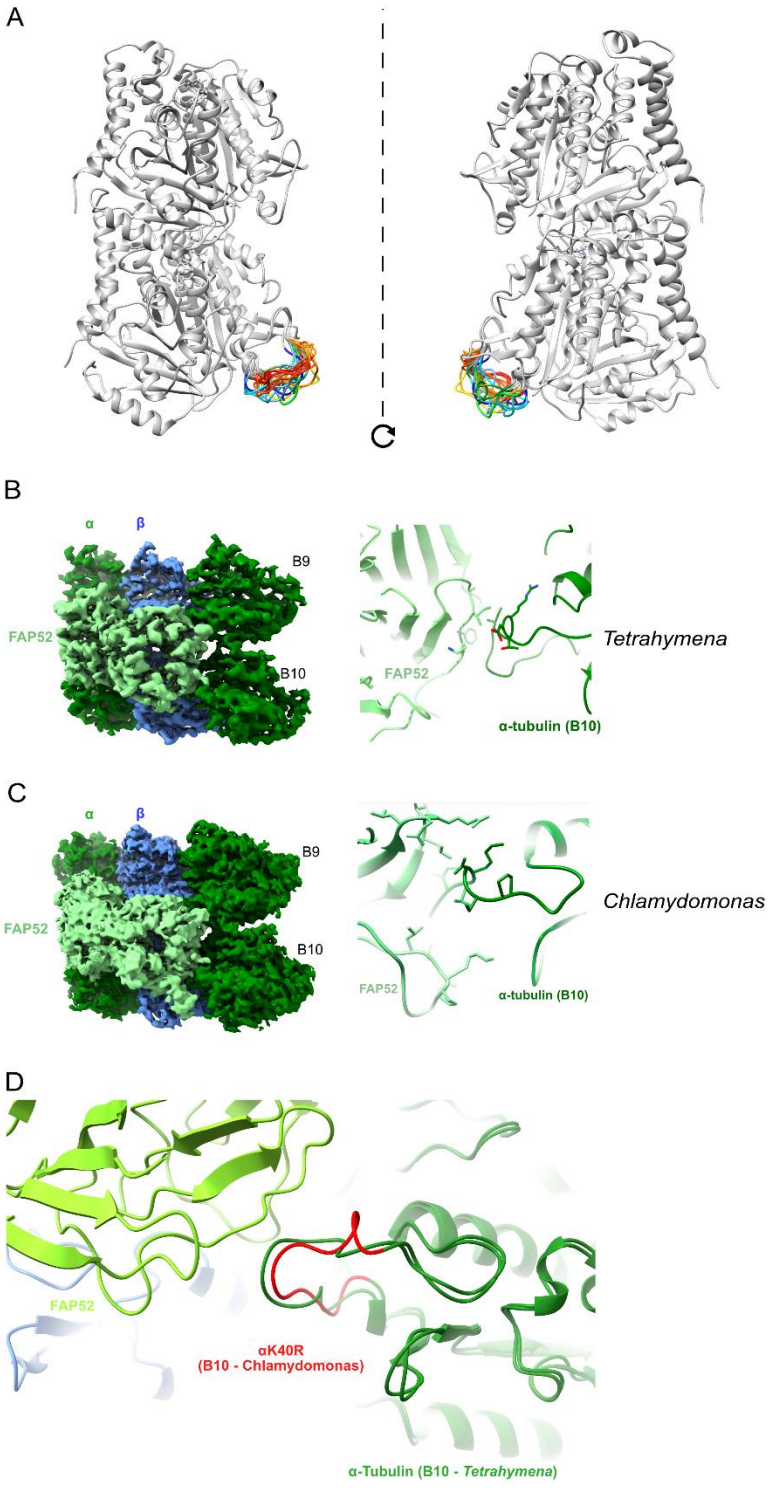
A
B
α
β
B9
FAP52
B10
FAP52
α-tubulin (B10)
Tetrahymena
C
α
β
B9
FAP52
B10
FAP52
α-tubulin (B10)
Chlamydomonas
D
FAP52
αK40R
(B10 - Chlamydomonas)
α-Tubulin (B10 - Tetrahymena)

Figure 3.3 Superimposed atomic models from *Tetrahymena* and *Chlamydomonas* at the αK40 loop and inner junction

A. Superimposed view of all the orientations of all the visible full and partial αK40 loops, showing their orientation.

B. Cryo-EM map (left) and model (right) of the cryo-EM density map from the inner junction region of *Tetrahymena* to show interaction of the full αK40 loop with FAP52.

C. Cryo-EM map (left) and model (right) of the cryo-EM density map from the inner junction region of *Chlamydomonas* to show interaction of the full αK40 loop with FAP52.

D. Superimposed view of the *Chlamydomonas* αK40 loop (colored in red) onto the inner junction model of *Tetrahymena*.

In addition, we also compared conformations of the αK40 loops at the same PF positions from two different species, *Tetrahymena thermophila* and *Chlamydomonas reinhardtii* (Fig. 3.3B-D). At the inner junction region, the αK40 loop from B9 and B10 are visible in both *Tetrahymena* and *Chlamydomonas* providing support to the FAP52, a conserved MIP. The conformations of the αK40 loops are very similar between two species. These results suggest that the conformation of αK40 can be tuned toward its interactions with the MIPs and form similar conformations.

3.5.2 De-acetylated DMT has the same structure as acetylated DMT

With our observation that acetylated αK40 adopting fixed conformation when interacting with MIPs, we want to evaluate whether de-acetylation will affect the MIPs interaction and hence the

DMT structure. Therefore, we obtained the structures of the DMT from MEC17 and K40R mutants. MEC17, a homolog of α-TAT1, is knocked out to abolish any acetylation in the DMT, and K40 is mutated to arginine to prevent microtubule acetylation (Akella et al., 2010). Comparing these two mutants to WT, we could examine the effect of total deacetylation and specific de-acetylation of αK40 residue. The structures of the DMT from K40R and MEC17 are at 3.5 and 4.5 Å resolution, respectively.

Our first observation is that all the MIPs look intact in both the MEC17 and K40R mutants (Fig. 3.4A of WT vs MEC17 vs K40R). This observation is consistent with the phenotypes that the MEC17 and K40R cilia looks similar to that of the WT cilia despite mutants being less stable (Akella et al., 2010).

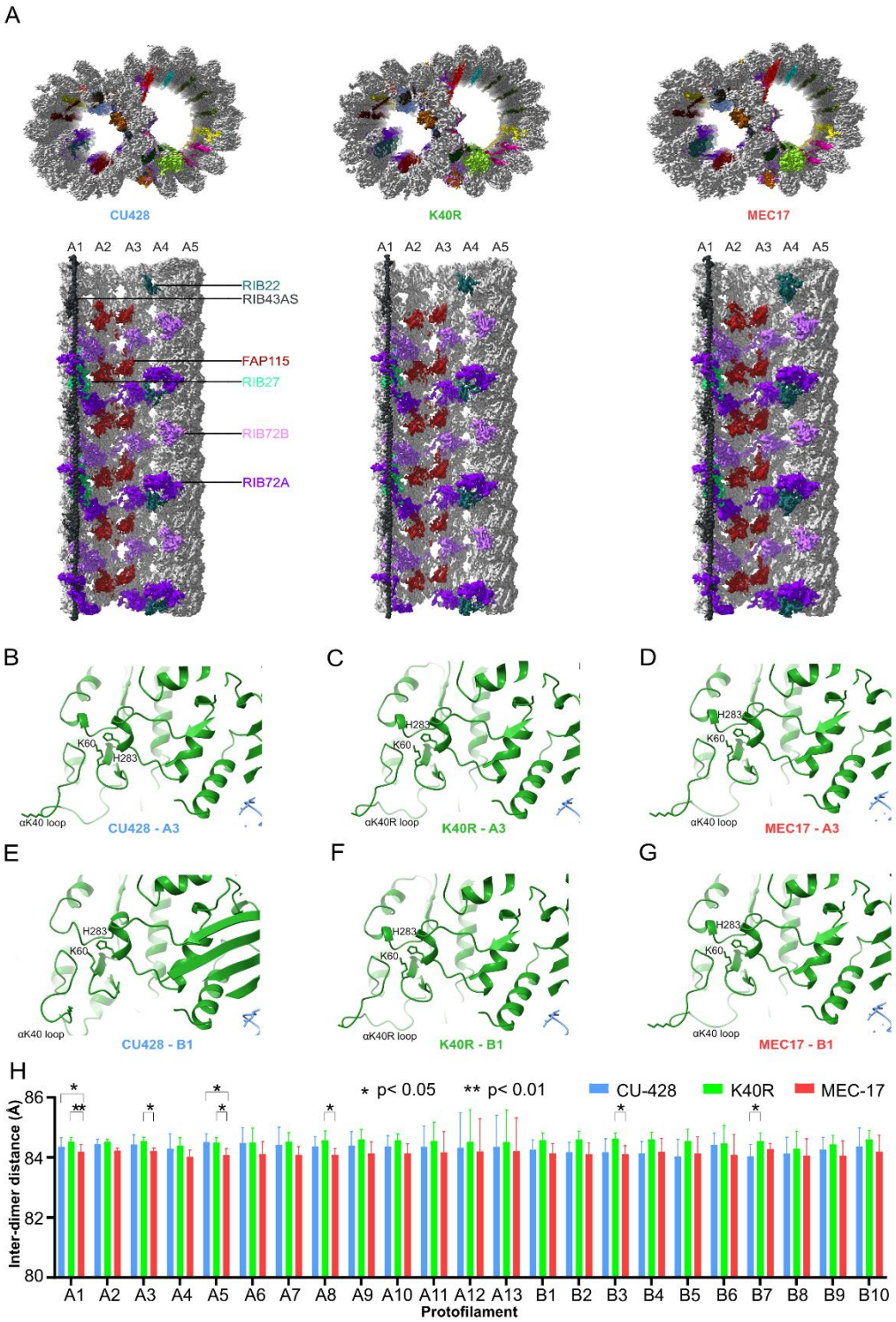
A
CU428
K40R
MEC17
A1 A2 A3 A4 A5
RIB22
RIB43AS
FAP115
RIB27
RIB72B
RIB72A
B
C
D
K60
H283
αK40 loop
CU428 - A3
αK40R loop
K40R - A3
MEC17 - A3
E
F
G
CU428 - B1
K40R - B1
MEC17 - B1
H
* p< 0.05
** p< 0.01
CU-428
K40R
MEC-17
Inter-dimer distance (Å)
86
84
82
80
A1 A2 A3 A4 A5 A6 A7 A8 A9 A10 A11 A12 A13 B1 B2 B3 B4 B5 B6 B7 B8 B9 B10
Protofilament

Figure 3.4 Cryo-EM maps from WT, K40R, and MEC17 show MIPs are intact and the αK40 loop are similar

A. Comparison of the cryo-EM density maps of the 48-nm repeat of DMT from CU428 (WT), K40R, and MEC17 strains of *Tetrahymena* to show that the MIPs are intact in all three species.

B.-D. Models of the full αK40 loops in protofilament A3 from CU428, K40R, and MEC17 species.

E.-G. Models of the full αK40 loops in protofilament B1 from CU428, K40R, and MEC17 species.

H. Bar graph showing the mean interdimer distance within each protofilament from all three species, indicating statistical significance (ANOVA, *: $p<0.05$, **: $p<0.05$, n=6).

Next, we compared the structures of the αK60 and αK40 loops at PF A3 and B1 to see any difference. Previously, it was reported that acetylation of tubulins leads to the reduction of interaction distance of K60 with the M-loop of the adjacent tubulin from 12 Å to 8 Å. Our comparison does not yield any large differences in both the acetylated and deacetylated αK40 and αK60 cases. However, this result does not rule out a change in αK40 and αK60 conformation, which is too small to observe at our resolution.

Since the tubulin lattice is sensitive to the nucleotide states of tubulins and microtubule stability (Ichikawa et al., 2019; R. Zhang, Alushin, Brown, & Nogales, 2015), tubulin lattice changes in deacetylated doublet microtubule mutant might correlate with stability. Therefore, we performed the tubulin dimer distance and inter-protofilament angle measurement of WT and the two acetylation mutants. While the dimer distance is almost similar for most PFs, there are statistically significant changes in inter-dimer distance in PFA1, A3, A5, A8, B3 and B7 between WT and

mutants (Fig. 3.4). Interestingly, the changes in the tubulin lattice are clearly observed in PFs A1, A3, A5 with MEC17 mutants, where the αK40 loops are fully observed along the PFs (Fig. 3.4D, G, H). Therefore, it is possible that the structural effect of deacetylation is more significant in the case of all residues instead of only deacetylated K40 and when the αK40 loop interacts with MIPs. This observation is consistent with the phenotypes observed in MEC17 and K40R mutants, in which MEC17 has more labile cilia. Our analysis also shows that tubulin lattice changes can be used as an indication for microtubule stability. On the other hand, the inter-protofilament angles in both MEC17 and K40R do not show any deviation from the WT (Figure 3.5).

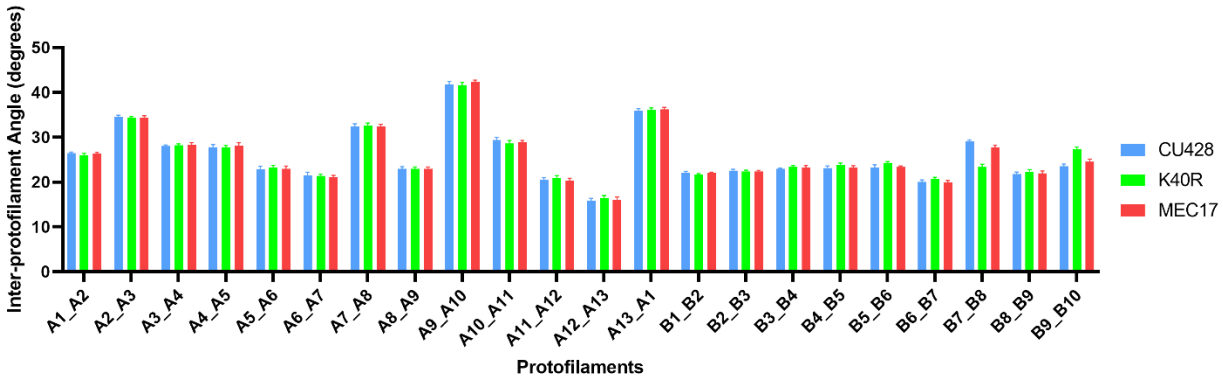

Figure 3.5. Inter-protofilament angles between subsequent protofilament, gathered from cryo-EM density maps of CU428 (WT), K40R, and MEC17 *Tetrahymena* species.

3.5.3 Acetylated αK40 loops are less flexible

Since we did not observe a clear structural difference between acetylated and non-acetylated DMT, we wanted to observe the structural difference using molecular dynamics. We performed an all-atom simulation for α-tubulin with acetylated and deacetylated αK40 to see whether acetylation changes the loop behavior (Fig 4A, B). To determine how acetylation of αK40 affects the structural change of the K40-loop, we used the K-means clustering method for the K40-loop region. The K-means algorithm is based on the position of Cα particles used for clustering. The whole trajectory with acetylated αK40 and the deacetylated αK40 were mixed and eight clusters were created from all of them (Fig. 3.6A). Then, the cluster with the most instantaneous structures (more than 30%) and the cluster with the second most instantaneous structures (more than 15%) were both derived from trajectories with acetylated αK40. On the other hand, the instantaneous structure obtained from the trajectory with deacetylated αK40 is composed of six clusters (less than 15% ~ 5%). Thus, the K40 acetylation has reduced αK40-loop structural conformation. For the first and the second largest majority cluster corresponding to acetylated αK40, the mean intra-cluster RMSD values for the clusters were about 1 and 2, respectively. On the other hand, other clusters' mean RMSD values were 2 to 6 (Fig. 3.6B). Therefore, from the RMSDs', we can say that the acetylated αK40 loop adopts more fixed conformations. Our result is very similar to the finding of molecular dynamics of acetylated and de-acetylated tubulins (Eshun-Wilson et al., 2019) despite the difference in the molecular dynamic set up of porcine and ciliate tubulins and the clustering methods.

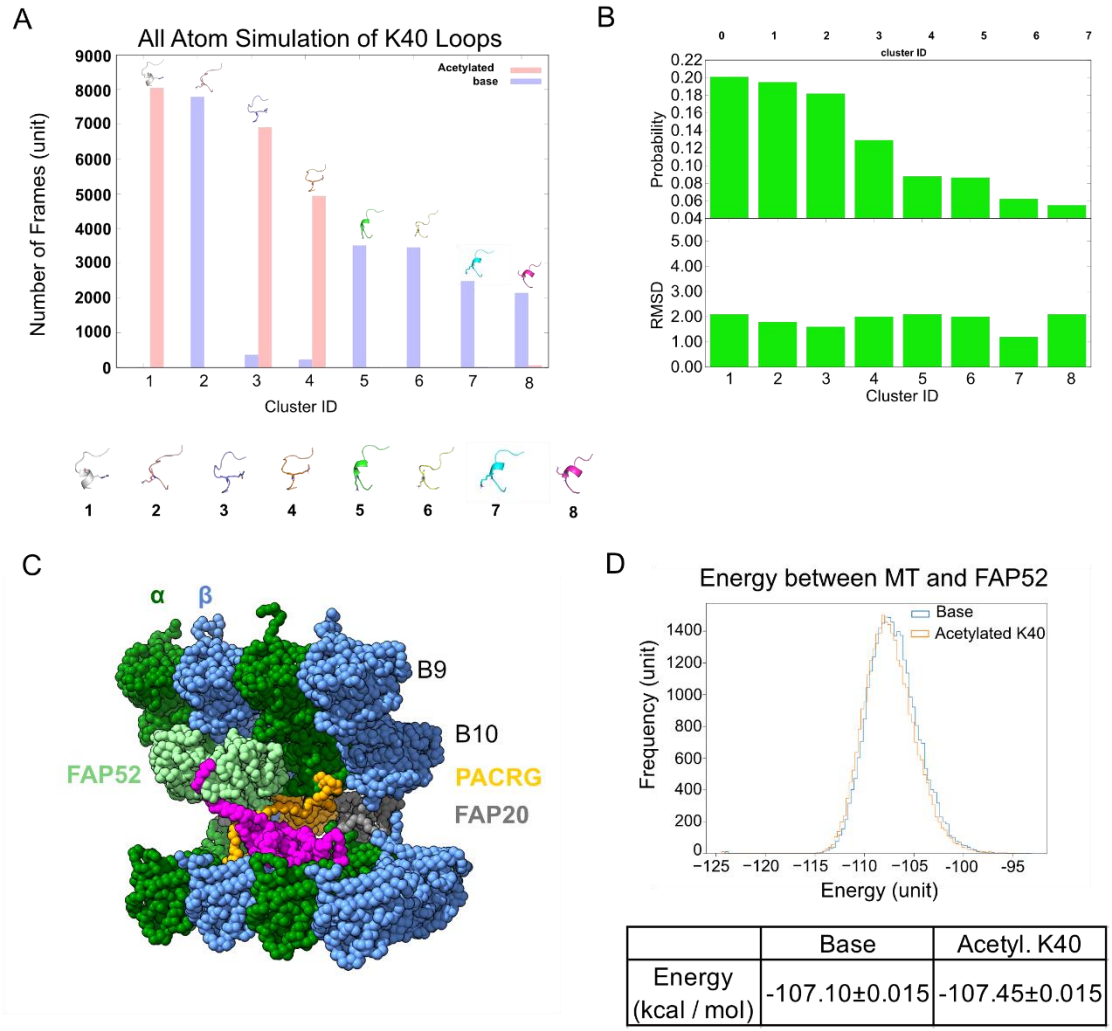

	Base	Acetyl. K40
Energy (kcal / mol)	-107.10±0.015	-107.45±0.015

Figure 3.6 Molecular dynamic simulation show that acetylated αK40 loops are less flexible and more stable

A. All atom simulation of αK40 loop clusters in different conformations of acetylated (pink) and base/non-acetylated (blue). Indicating that acetylated confirmations adopt in higher frames and are less flexible.

B. RMSD and probability of each cluster simulated in A.

C. Molecular dynamics coarse grain model of the inner junction region of *Tetrahymena*, each amino acid is 1 bead.

D. Graph showing the energy difference (in kcal / mol) between base (non-acetylated) and acetylated αK40, to indicate that each acetylated αK40 has slightly lower energy than the non-acetylated.

3.5.4 Acetylated αK40 stabilizes the binding with MIPs

Since we did not see any changes in MIPs in Mec17 and K40R mutants, we want to see whether the interaction between the K40 loop and MIP is affected by acetylation and deacetylation. We set up the coarse gain simulation to compare the energy between DMT and FAP52 with the acetylated αK40 and the deacetylated αK40 structure (Fig. 3.7).

We found that both acetylated and deacetylated αK40 have a stabilization effect when binding to FAP52. Calculating the mean and standard error of the energy between DMT and FAP52 from the entire trajectory, the energy of acetylated αK40 case is lower than that of deacetylated αK40 case (Fig. 3.7). Therefore, the acetylation of αK40 improves the interaction with FAP52. This, in turn, can have an impact on the stability of the DMT itself.

While the energy difference between acetylated and de-acetylated tubulin within a single FAP52 protein is small, the effect can be significantly multiplied in the periodic structures of the DMT with a lot of MIPs. As indicated in our observation of the visible αK40 loops (Fig. 3.1), there are 65 interactions between αK40 loops and MIPs out of a total of 138 tubulin dimers in a 48-nm repeat of the DMT. Therefore, acetylation of total αK40 can significantly improve the stability of the DMT, hence, the cilia. Therefore, despite no significant structural difference observed between WT, K40R and MEC17, K40R and MEC17 mutants show phenotypes of weaker cilia (Akella et al., 2010).

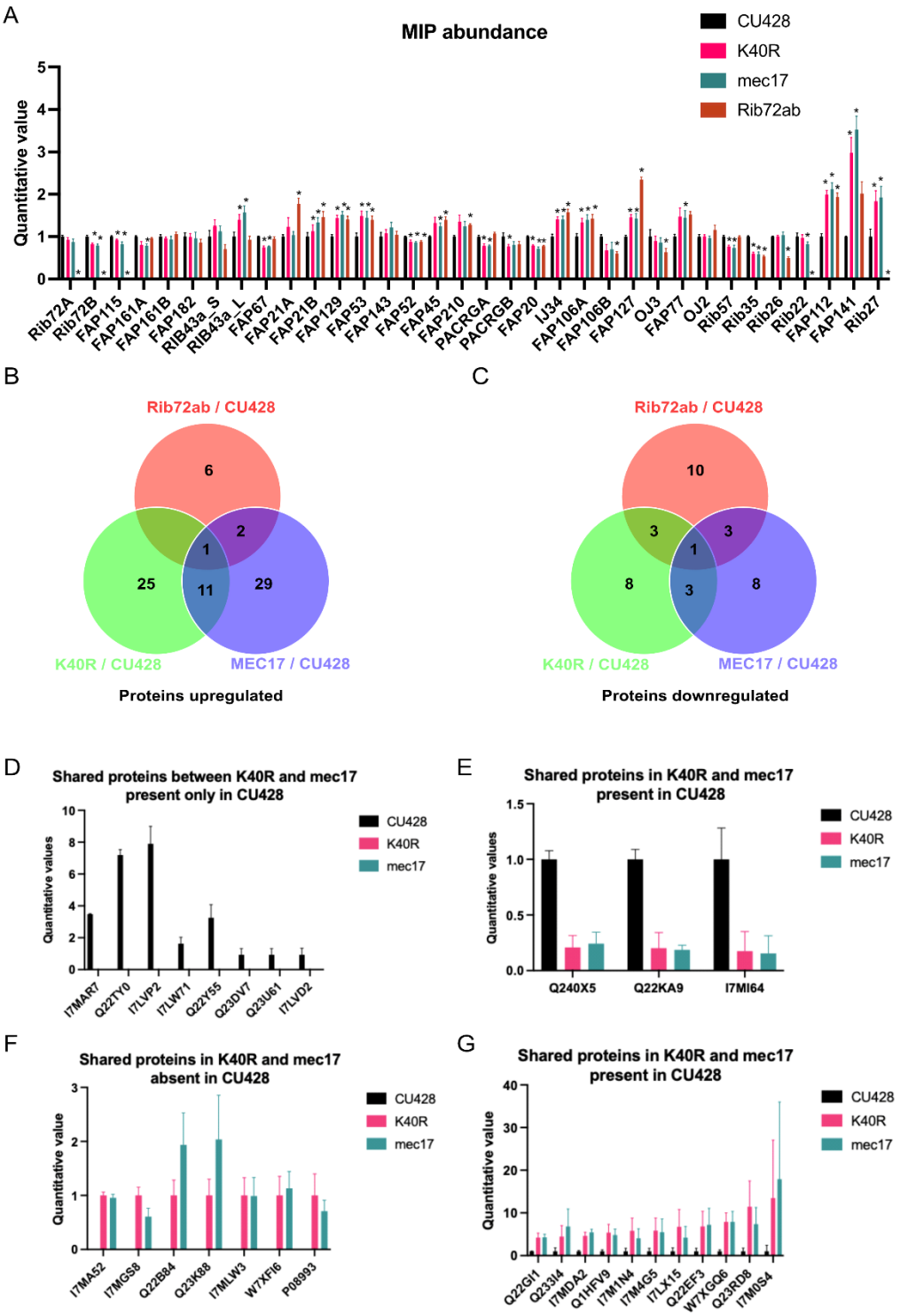
A
MIP abundance
CU428
K40R
mec17
Rib72ab
Quantitative value
Rib72A
Rib72B
FAP115
FAP161A
FAP161B
FAP182
RIB43a_S
RIB43a_L
FAP67
FAP21A
FAP21B
FAP129
FAP53
FAP143
FAP52
FAP45
FAP210
PACRGA
PACRGB
FAP20
IJ34
FAP106A
FAP106B
FAP127
OJ3
FAP77
OJ2
Rib57
Rib35
Rib26
Rib22
FAP112
FAP141
Rib27
B
Rib72ab / CU428
6
2
1
25
11
29
K40R / CU428
MEC17 / CU428
Proteins upregulated
C
Rib72ab / CU428
10
3
3
1
8
3
8
K40R / CU428
MEC17 / CU428
Proteins downregulated
D
Shared proteins between K40R and mec17 present only in CU428
Quantitative values
CU428
K40R
mec17
I7MAR7
Q22TY0
I7LVP2
I7LW71
Q22Y55
Q23DV7
Q23U61
I7LVD2
E
Shared proteins in K40R and mec17 present in CU428
Quantitative values
CU428
K40R
mec17
Q240X5
Q22KA9
I7MI64
F
Shared proteins in K40R and mec17 absent in CU428
Quantitative value
CU428
K40R
mec17
I7MA52
I7MGS8
Q22B84
Q23K88
I7MLW3
W7XFI6
P08993
G
Shared proteins in K40R and mec17 present in CU428
Quantitative value
CU428
K40R
mec17
Q22GH1
Q233I4
I7MDA2
Q1HFV9
I7M1N4
I7M4G5
I7LX15
Q22EF3
W7XGQ6
Q23RD8
I7M0S4

Figure 3.7 Mass spectrometry results showing the expression levels of proteins in mutant strains compared to WT.

A. Bar graph showing the abundance of MIPs based upon quantitative values (normalized total spectra) from mass spectrometry.

B. Proteins upregulated in Rib72ab, K40R, and MEC17 mutants when compared against the CU428 (WT).

C. Proteins downregulated in Rib72ab, K40R, and MEC17 mutants when compared against the CU428 (WT).

D. Proteins only found in the mass spectrometry of CU428 (WT) when compared with K40R and MEC17 mutants.

E. Downregulated proteins in both K40R and MEC17 mutants compared to CU428 (WT).

F. Proteins in both K40R and MEC17 mutants but are absent in CU428 (WT).

G. Upregulated proteins in both K40R and MEC17 mutants compared to CU428 (WT).

3.5.5 MS reveals the specific effect of de-acetylation

Our analysis so far shows that while there are significant phenotype differences (Akella et al., 2010), there is not significant difference in MIPs within the structure DMT of WT, K40R and MEC17 mutant. Therefore, we used mass spectrometry to analyze the changes in the ciliary proteome of the strains. In this mass spectrometry analysis, we specifically target changes in proteins which bind to the axoneme by performing mass spectrometry on the same DMT samples used for cryo-EM. In addition, to investigate the specific effect of acetylation, we performed MS of the Rib72ab and Rib72b mutants to exclude the proteome change downstream because of instability of the DMT (Tables 3.8-3.11). Rib72ab lacks both Rib72 and Rib72b, which leads to a significant number of MIPs missing and slower swimming speed (Stoddard et al., 2018).

Table 3.8. Proteins in common between K40R and Rib72ab mutants when compared against CU428

Gene name	Gene ID	Uniprot ID	Protein Levels	Homolog in *Chlamydomonas reinhardtii*	Homolog in *Homo sapiens*
Dynein light chain 4	TTHERM_00716250	I7MCM8	Downregulated	NA	NA
Glutathione S-transferase, amine-terminal domain protein	TTHERM_00602870	Q22YK8	Downregulated	NA	P09488
Uncharacterized protein	TTHERM_00455660	I7MI64	Downregulated	NA	NA

Table 3.9. Proteins in common between K40R and Rib72b mutants when compared against CU428

Gene name	Gene ID	Uniprot ID	Protein Levels	Homolog in *Chlamydomonas reinhardtii*	Homolog in *Homo sapiens*
Dynein light chain 4	TTHERM_00716250	I7MCM8	Downregulated	NA	NA
Glutathione S-transferase, amine-terminal domain protein	TTHERM_00602870	Q22YK8	Downregulated	NA	P09488
Tetratricopeptide repeat protein	TTHERM_00313720	Q22KA9	Downregulated	A8ITN7	Q8N4P2
CGMP-dependent kinase 5-1	TTHERM_00046530	Q23DN8	Downregulated	NA	NA

Table 3.10. Proteins in common between MEC17 and Rib72ab mutants when compared against CU428

Gene name	Gene ID	Uniprot ID	Protein Levels	Homolog in *Chlamydomonas reinhardtii*	Homolog in *Homo sapiens*
Uncharacterized protein	TTHERM_00732900	Q245C1	Upregulated	NA	NA
Cyclic nucleotide-binding domain protein	TTHERM_00143540	I7M0S4	Upregulated	NA	NA
Metallo-beta-lactamase family protein	TTHERM_00128670	I7M1D2	Downregulated	NA	NA
Intraflagellar transporter-like protein, putative	TTHERM_00149230	I7LWB4	Downregulated	IFT74	IFT74
Uncharacterized protein	TTHERM_00455660	I7MI64	Downregulated	NA	NA

Table 3.11. Proteins in common between MEC17 and Rib72b mutants when compared against CU428

Gene name	**Gene ID**	**Uniprot ID**	**Protein Levels**	**Homolog in *Chlamydomonas reinhardtii***	**Homolog in *Homo sapiens***
Uncharacterized protein	TTHERM_00388510	Q23RD8	Upregulated	NA	NA
Uncharacterized protein	TTHERM_00732900	Q245C1	Upregulated	NA	NA
Cyclic nucleotide-binding domain protein	TTHERM_00143540	I7M0S4	Upregulated	NA	NA
Tetratricopeptide repeat	TTHERM_00313720	Q22KA9	Downregulated	A8ITN7	Q8N4P2
Intraflagellar transporter-like protein TTHERM_00648910	TTHERM_00648910	I7LT74	Downregulated	IFT52	IFT52
Uncharacterized protein TTHERM_01106190	TTHERM_01106190	Q22BD8	Downregulated	NA	NA
Intraflagellar transporter-like protein, putative	TTHERM_00149230	I7LWB4	Downregulated	IFT74	IFT74

We first validated our observation with MIPs by analyzing the relative quality of MIPs in all the strains. As expected, most MIPs show no significant fold change (less than 1.5 fold changes) except for FAP112, FAP141 and Rib27 (Fig. 3.7A), and in particular, FAP141 showing 3 fold changes in K40R and MEC17. However, we did not observe the difference in periodicity of Rib27, FAP141 and FAP112 in the cryo-EM maps of WT, K40R and MEC17. We performed a control by analyzing fold changes in radial spoke proteins (Fig. 3.12). There is no significant fold change shown as expected.

A

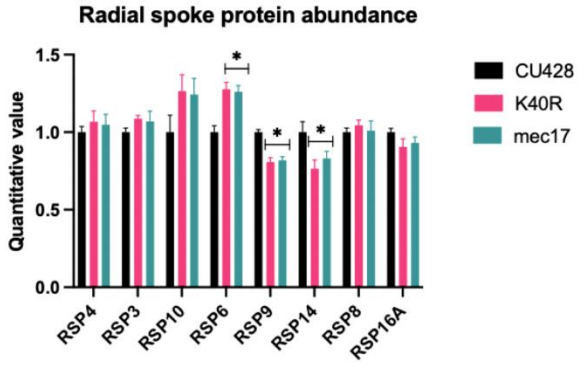
Radial spoke protein abundance
Quantitative value
1.5
1.0
0.5
0.0
CU428
K40R
mec17
RSP4
RSP3
RSP10
RSP6
RSP9
RSP14
RSP8
RSP16A

B

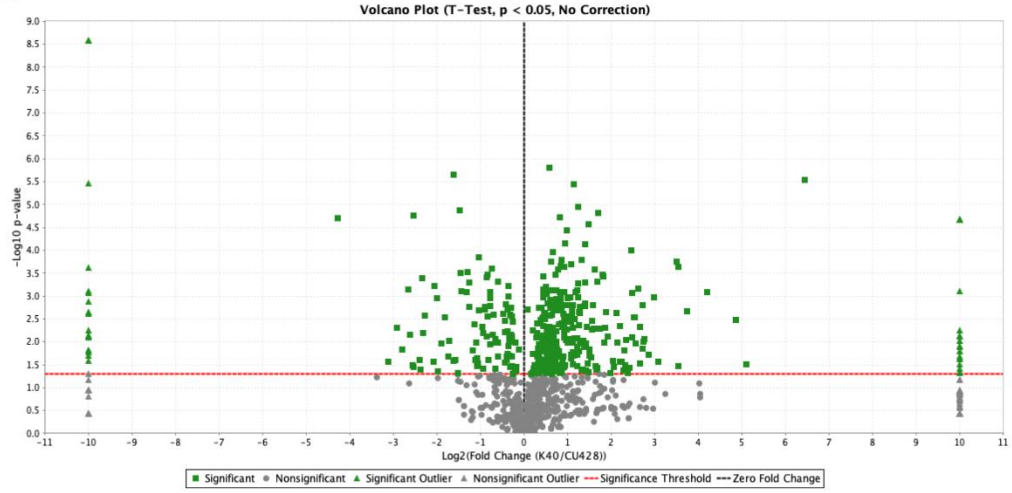
Volcano Plot (T-Test, p < 0.05, No Correction)
-Log10 p-value
Log2(Fold Change (K40/CU428))
Significant
Nonsignificant
Significant Outlier
Nonsignificant Outlier
Significance Threshold
Zero Fold Change

C

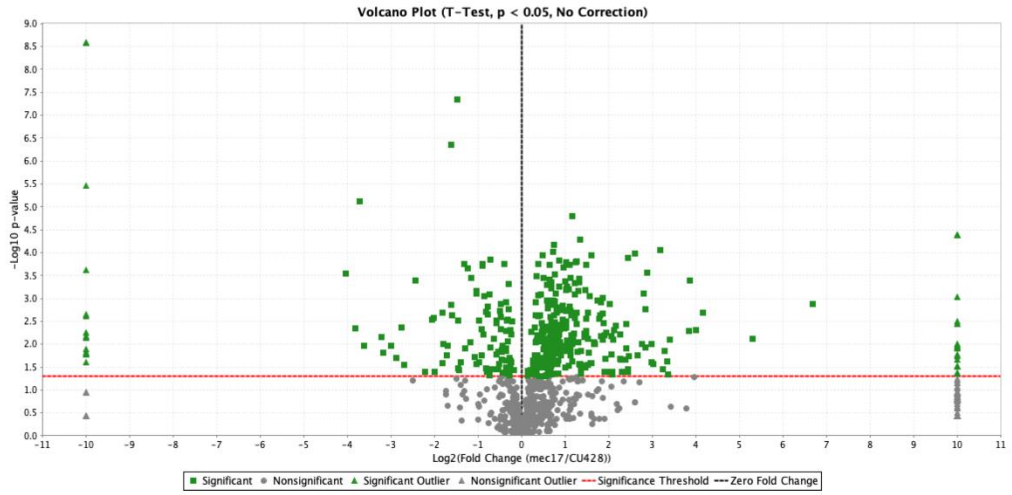
Volcano Plot (T-Test, p < 0.05, No Correction)
-Log10 p-value
Log2(Fold Change (mec17/CU428))
Significant
Nonsignificant
Significant Outlier
Nonsignificant Outlier
Significance Threshold
Zero Fold Change

Figure 3.12. Radial spoke protein abundance in mass spectrometry and volcano plots of proteins in K40R and MEC17 compared to WT

A. Radial spoke protein abundance in mass spectrometry triplicates of CU428 (WT), K40R, and MEC17 *Tetrahymena* species.

B. Volcano plot showing up and down regulated proteins in K40R mutants compared against CU428, y-axis showing the -Log10 p-values, and x-axis showing the Log2 fold change where negative and positive values suggest potential downregulation and upregulation, respectively.

C. Volcano plot showing up and down regulated proteins in MEC17 mutants compared against CU428.

There are 11 proteins significantly upregulated in both K40R and MEC17 by four folds compared to CU428 (Fig. 3.7B). By excluding protein significantly upregulated in Rib72ab vs. CU428, 10 proteins are significantly upregulated and shared between K40R and MEC17 (Fig. 3.7B, F, G). Similarly, we found three proteins significantly reduced in K40R and MEC17 but not in Rib72ab (Fig. 3.7C). This consistent pattern of upregulated and downregulated proteins in K40R and MEC17 against Rib72ab mutant shows that deacetylation of αK40 leads to a consistent response in proteome change in *Chlamydomonas* (Elam et al., 2011). Among the proteins that are missing in K40R and MEC17, there are protein phosphatase 2A related proteins such as regulatory subunit A (TTHERM_00766530, uniprot ID: I7MAR7), PP2C (TTHERM_00316330, uniprot ID: I7LW71), and PP2A (TTHERM_00355160, uniprot ID: Q22Y55) as shown in Fig. 3.7D. Furthermore, two kinase-like proteins are down-regulated in MEC17 and K40R (Fig. 3.7E) (TTHERM_00623090, uniprot ID: Q240X5, and TTHERM_00455660, uniprot ID: I7MI64). It was previously reported that knockdown of phosphatase inhibitor 2 reduces the acetylation of tubulin in primary cilium of human retinal epithelial cells(W. Wang & Brautigan, 2008). Inhibition

of protein phosphatase (1 and 2A) with calyculin A in the phosphatase inhibitor 2 knockdown cells partially rescued the acetylation of the ciliary microtubules. These results indicate that either the lack of acetylation at αK40 position or acetyltransferase can lead to a reduction of protein phosphatase 2A. Therefore, we can conclude that acetylation and phosphorylation have an interconnected relationship.

3.6 Discussion

In this work, we performed structural characterization of the structures of the DMT from two acetylation mutants K40R and MEC17 and compared to that of WT (CU428 strain). We showed that the αK40 loop of tubulin is structured when they interact with MIPs. On the other hand, the αK40 loop does not show significant structural alteration with either no acetylation of the loop (K40R) and totally deacetylation of the cilia. On the other hand, our molecular dynamic simulation shows that acetylation of αK40 improves the interaction with MIPs. This result indicates that the DMT is assembled first and formed structured αK40 loop binding to MIPs. Then, acetyltransferases come and acetylate the αK40 and other sites such as αK60. With many acetylation sites at MIP interaction sites, the DMT becomes more stable. Lack of acetylation destabilizes the DMT and leads to some tubulin lattice alteration and instability. Our result again demonstrates that the tubulin lattice can be a read-out for DMT stability (Ichikawa et al., 2019). In addition, the flexible αK40 is a region of αK40 that can be fine-tuned for the interaction with luminal proteins such as MIPs.

Similar to a recent study (Eshun-Wilson et al., 2019), our all-atom molecular dynamics simulation shows that the acetylated αK40 loop adopts less conformation. That study indicates that the acetylated αK40 leads to change in the lateral interaction in the microtubule. In our case, we did not observe any difference between WT and acetylation mutants in our cryo-EM maps. In particular, the acetylated αK40 that interacts with MIPs does not seem to be involved in lateral interaction. However, since we cannot observe the acetylated αK40 in many tubulins in the DMT and our all-atom MDs are set up quite differently, it is possible that acetylated αK40 loops can

impact the lateral interactions. Regardless, our study supports the notion that acetylation of tubulin is not a biphasic switch but a fine tuning to tubulin that impacts its stability.

Since both acetylation mutants lack protein phosphatase 2A and regulator units, it indicates an interconnection between tubulin acetylation and protein phosphatase 2A. TGF-β-activated kinase 1 (TAK1) is an important activator of αTAT1 in mice (N. Shah et al., 2018). We speculate that tubulin acetylase might require a balance of kinase and protein phosphatase for proper function in the cilia. Once the tubulin acetylase is not recruited properly into the cilia due to knock out or mutations in αK40, the balance of phosphatases (protein phosphatase 2A in this case) and kinase is affected. Interestingly, HDAC6 de-acetylase is also regulated by interaction with multiple kinases (Du, Seibenhener, Yan, Jiang, & Wooten, 2015). This again highlights the inter-dependence of phosphorylation and acetylation, two post translational modifications in the cilia. Previously, it was shown that the tubulin band is shifted in 2D gel in MEC-17 mutant (Akella et al., 2010) to suggest that tubulins have greater polyglutamylation in the case of deacetylation. In Fig. 3.7E, our MS results show that a tetratricopeptide repeat protein (TTHERM_00313720, Uniprot ID: Q22KA9), is downregulated in MEC17 and K40R. Protein BLAST found a homolog in *Homo sapiens* as Tetratricopeptide repeat protein 30B/IFT70 (uniprot ID: Q8N4P2), a protein required for the polyglutamylation of axonemal tubulin (Pathak, Obara, Mangos, Liu, & Drummond, 2007). Since acetylation is decreased in K40R and MEC17 mutants, the level of polyglutamylation could also be affected. Together with our results and others (Akella et al., 2010; T. Kubo et al., 2015; Rogowski et al., 2010; Wloga et al., 2008; Wloga et al., 2009), it is suggested that the PTM in the cilia is in a balancing act. Changing one type of PTM can shift the balance of other types of PTM.

3.7 Materials & Methods

3.7.1 Growth of *Tetrahymena* cells for isolation

Bean media (Williams et al., 1980) was used to store *Tetrahymena* cells, with 4 μL of the cell culture transferred into 40 mL of liquid SPP media. The cells were grown for 7 days at room temperature and then transferred into 50 mL of SPP liquid media for overnight growth at 30 °C, 150 RPM shaking in the Thermo Fisher MAXQ8000 incubator. Then, 50 mL of this overnight culture was added into 900 mL of liquid SPP media and grown at 30 °C (MAXQ8000) at 150 RPM for two days, or until OD600 is at 0.7.

3.7.2 Flagella isolation via dibucaine treatment

To harvest *Tetrahymena* cells, overnight culture was centrifuged at 700 g for 10 minutes with slow deceleration, at 22°C in the Avanti Centrifuge (Rotor JLA-8.1000). With 10 mL of room temperature SPP media added with DTT was used to resuspend the cell pellet and then adjusted to a final volume to 24 mL, followed by transfer to a ice cold 250 mL Erlenmeyer flask. Immediately, 1 mL of dibucaine (dissolved in distilled water at 25 mg/mL) was added to the flask and gently swirled for exactly 60 seconds in an ice water bath. To stop the reaction, 75 mL of ice cold SPP media (added with 1 mM EGTA) was immediately added to the Erlenmeyer flask, and then split into two conical 50 mL tubes for centrifugation at 2000 g for 10 minutes at 4°C with no deceleration (Sorvall ST 16R, Rotor 75003181). The supernatant that contains cilia was transferred to centrifuge tubes for the Beckman Coulter JA 25.50 rotor, approximately 30 mL per tube, for centrifugation at 17000 g for 40 minutes at 4°C with slow deceleration (Avanti, Rotor

JA25.50). The supernatant was discarded, with pellet gently washed with Cilia Wash Buffer (50 mM HEPES at pH 7.4, 3 mM MgSO4, 0.1 mM EGTA, 1 mM DTT, 250 mM sucrose), and flagella frozen with liquid nitrogen for storage in the -80°C freezer.

3.7.3 Purification of doublet microtubule fraction

Cilia suspension was thawed on ice and then centrifuged at 16000 g, 4°C, 10 minutes, in a microfuge in a refrigerated room (Eppendorf, Centrifuge 5415 D). Then the supernatant was discarded, and the pellet resuspended in 250 µl of ice-cold Cilia Final Buffer (50 mM HEPES at pH 7.4, 3 mM MgSO4, 0.1 mM EGTA, 1 mM DTT, 0.5% trehalose, 1 mM PMSF). To clean the cilia, the resuspended cilia was centrifuged at 16000 g, 10 minutes, at 4°C in microfuge (Eppendorf, Centrifuge 5415 D), and followed by supernatant removed. Then the pellet was resuspended with 250 µl of Cilia Final Buffer [without trehalose but with 44.1ul of 10% NP-40 alternative (Millipore Sigma, 492016) added to a final concentration of 1.5% NP-40]. The sample was put on ice to incubate for 30 minutes before the de-membraned flagella supernatant was removed after centrifugation at at 16,000 g for 10 min at 4°C in a microfuge (Eppendorf, Centrifuge 5415 D). The pellet which contains the axoneme was resuspended with 245 µl of Cilia Final Buffer (without trehalose), and then added with 2.5 µl of 100 mM ADP (to a final concentration 1 mM ADP) for incubation at room temperature for 10 minutes. This was followed by addition of 2.5 µl of 10 mM ATP (to a final concentration of 1 mM ATP) for incubation at room temperature for 10 minutes. Bradford reagent (Bio-rad 5000201) was used to measure the total protein concentration, and with the final protein concentration adjusted to 3 mg/mL using Cilia Final Buffer (without trehalose).

3.7.4 Cryo-EM sample preparation

The concentration of WT, K40R, and MEC17 doublet microtubules were adjusted to 3 mg/ml. Quantifoil R2/2 grids (Electron Microscopy Sciences, #Q225CR-06) were treated using 1 mL of chloroform overnight followed by negative glow discharge (30 seconds at 25 mAh). Then, 3.5 µl of axoneme sample were applied to treated grids inside the Vitrobot Mark IV (Thermo Fisher) at blot force 3, blot time of 5 seconds, and drain time of 0.5 seconds, followed by plunge freezing into liquid ethane.

3.7.5 Cryo-EM data acquisition

Using the Titan Krios 300 keV FEG electron microscope (Thermo Fisher) with direct electron detector K3 Summit (Gatan, Inc.) and the BioQuantum energy filter (Gatan, Inc.), movies of the axoneme were acquired at 64kx nominal magnification (calculated pixel size of 1.370 Å/pixel) using SerialEM (Mastronarde, 2005). A total dose of 45 electrons per Å2 over 40 frames for the WT and the MEC17 dataset. A total dose of 73 electrons per Å2 per frame over 30 frames for the K40R dataset. The defocus range was between -1.0 and -3.0 µm at an interval of 0.25 µm.

3.7.6 Image processing

Motion correction and dose-weighting of the movies were done using MotionCor2 (Zhang et al., 2017) implemented in Relion 3 (Zivanov et al., 2018), and the contrast transfer function parameters were estimated using Gctf (Zhang, 2016). Micrographs with apparent drift, and ice contamination,

and bad contrast transfer function estimation were discarded (3,074, 2,410, 4,283 micrographs for WT, K40R and MEC17 data, respectively). The filaments were picked manually using e2helixboxer (Tang et al., 2007).

Eight nanometer periodicity was used to pick particles of 512 x 512 pixels, binned twice, and pre-aligned using a modified version of the Iterative Helical Real Space Reconstruction script (Egelman, 2007) in SPIDER (Frank et al., 1996) to work with non-helical symmetry. The alignment parameters were then transferred to Frealign for aligning the particles for 6 iterations in Frealign (Grigorieff, 2007), and then converted into Relion 3.0. For image processing the particles were scaled to 1.744 Å/pixel (box size 402 pixel) for reducing computation memory usage. In Relion 3, Iterative per-particles-defocus refinement and Bayesian polishing were done for the 80nm particles.

Each particle were subtracted of its tubulin lattice signal, and underwent 3D classification into into two classes to obtain the 16-nm repeat particles. The 16-nm repeat particles were then subjected to 3D classification into 3 classes to obtain the 48-nm repeat particles. The 48-nm particles were then refined.

To improve the local resolution for each of the protofilament during modelling, we performed focused refinements by using masks to cover adjacent protofilaments regions in the DMT.

The particles of 512 x 512 pixels were initially picked with 8-nm periodicity, binned twice and pre-aligned using a modified version of the Iterative Helical Real Space Reconstruction script (44) in SPIDER (45) to work with non-helical symmetry. After that, the alignment parameters were transferred to Frealign and the particles were aligned by Frealign for 6 iterations (46). The alignment parameters were then converted into Relion 3.0. The particles were scaled to 1.744 Å/pixel (box size 402 pixel) for image processing to reduce memory usage. The 8-nm particles then underwent iterative per-particles-defocus refinement and Bayesian polishing in Relion 3.

The signal of the tubulin lattice was subtracted from each particle. The subtracted particles were subjected to 3D classification into two classes to obtain the 16-nm repeat particles. The 16-nm repeat particles were then subjected to 3D classification into 3 classes to obtain the 48-nm repeat particles. The 48-nm particles were then refined, resulting in resolution of X, Y, Z Angstrom for WT, K40R and MEC-17 from A, B, C particles respectively. To improve the resolution of different regions of the DMT for modelling, we performed a focused refinement by using a mask covering the inner junction region.

3.7.7 Tubulin Modelling

Modeling of each tubulin subunits were done using UCSF Chimera (Petterson et al., 2004). The WT tubulin models 6U0H (Ichikawa et al., 2019) were first fitted into the higher-resolution K40R

cryo-EM maps, then locally modelled using Coot (Emsley et al, 2010) and real space refined in Phenix (Adams et al, 2010) for generation of the K40R tubulin model. The new WT and MEC17 tubulin models were generated by fitting the K40R tubulin model in WT and MEC17 cryo-EM maps, respectively, followed by refinement in Coot (Emsley et al, 2010) and Phenix (Adams et al, 2010). Each of the K40 loop region from WT, K40R, and MEC17 was locally modelled in focused refinement cryo-EM maps using Coot (Emsley et al, 2010) and Phenix (Adams et al, 2010). All the maps and model visualization were taken using ChimeraX (Goddard et al., 2018).

3.7.8 Coarse-grained MD simulation

Based on the atomic structures of the 4 tubulin dimers, Fap276, and Fap52, we performed coarse-grained MD simulation. The purpose of this simulation was to check the effect of acetylated K40 for binding stability of Fap52. In the coarse-grained model, each amino acid was represented as a single bead located as its Cα position. For observing their dynamics, we used the excluded volume effect, electrostatic interaction, and the energy function: AICG2+ (cite: W. Li, Terakawa, Wang, & Takada, 2012; W. Li, Wang, & Takada, 2014). In the AICG2+, the reference structure was assumed as the most stable conformation, and their parameters are modified from the reference. It is known that the intradimer interaction is much stronger than the interdimer interaction, and the interdimer interaction is much stronger than intra-PFs interaction, so we set interdimer and PFs' non-local native interaction force to 0.8 and 0.3 times the original value, respectively, while that of the intradimer was kept as the original value (1.0 times). Of note, three residues (PHE133, GLY308, and GLU401) of the B9-PF beta-tubulin at the plus end side were anchored in their position for convenience analysis. We performed the simulation 10 times with acetylated K40 and

deacetylated K40 structure using the CafeMol package version 2.1 (cite: Kenzaki et al., JCTC 2011). Each MD simulation took 3×10^7 MD steps, and they were conducted by the underdamped Langevin dynamics as 300K temperature. We set the friction coefficient to 0.02 (CafeMol unit) and default values were used for others.

3.7.9 How to treat the effect of acetylation

Normally, in dealing with electrostatic interactions, LYS and ARG, GLU and ASP, and other amino acids were given a charge of +1, -1, and 0, respectively. However, in this simulation, it was necessary to evaluate the electrostatic interaction as accurately as possible, so we calculated the surface charge density from the all-atom structure, and remapped the charge distribution using only Ca beads to reproduce the all-atom surface charge distribution. The technique is called RESPAC (cite: Terakawa et al., JCTC 2014). We applied RESPAC to the region without missing, such as K40-loop and E-hook. For the missing region (and so we did loop modeling by MODELLER (cite: Šali, A. and Blundell., T. L., 1993), we treat their charge by default definition. In the coarse-grained model, each amino acid is treated as a single bead, so we simply treated that if the K40 was acetylated, the charge of it is zero, while deacetylated K40 has +1 charge value.

3.7.10 All-atom MD simulation

The purpose of the all-atom MD simulation was to check acetylated K40 takes less K40-loop's conformation than the deacetylated K40 case. In the all-atom MD simulation using GROMACS (cite: Abraham MJ SoftwareX 2015, Pronk S et al. Bioinformatics 2013), we used the

GROMOS54a7 force field for protein (cite: N. Schmid, Eur. Biophys. J., 2011) and SPC for solvent water (cite: Jorgensen W. L., PNAS 2005). We added sodium and chloride ions to neutralize the system and to make the salt concentration approximately equal to 0.1M. The energy minimization by the steepest descent minimization algorithm was followed by equilibration with NVT and NPT for 100 ps at 300K. In the production run, we used NPT ensemble simulations with 1 atm and 300K. The production run consisted of 1 fs step for 180 ns. The α-tubulin at the plus end of B9-PF was used as a reference structure for the simulation. For modeling the structure of acetylated K40, Vienna-PTM 2.0 (cite: Margreitter C (2013) Nucleic Acids Research, Petrov D (2013) PLOS Computational Biology, Margreitter C (2017) Journal of Computational Chemistry) was used. The force field used (GROMOS54a7) had already been set up for the acetylated lysine.

3.7.11 Mass Spectrometry

Samples prepared for cryo-EM were used for MS analysis. Laemmli buffer at 4X (#1610747, Bio-Rad) was added to the microtubule fraction samples in HMDEKP buffer so that it will be 1x, and 25-30 μg protein was loaded on the SDS-PAGE gel. Electrophoresis was performed, but the run was terminated before the proteins entered the separation gel. A band containing all proteins in the sample was then cut out from the gel and subjected to in-gel digestion. Obtained peptides (~2 μg) were chromatographically separated on a Dionex Ultimate 3000 UHPLC. First, peptides were loaded onto a Thermo Acclaim Pepmap (Thermo, 75 μm ID × 2 cm with 3 μm C18 beads) precolumn, and then onto an Acclaim Pepmap Easyspray (Thermo, 75 μm × 25 cm with 2 μm C18

beads) analytical column and separated with a flow rate of 200 nl/min with a gradient of 2-35% solvent (acetonitrile containing 0.1% formic acid) over 2 hours. Peptides of charge 2+ or higher were recorded using a Thermo Orbitrap Fusion mass spectrometer operating at 120,000 resolution (FWHM in MS1, 15,000 for MS/MS). The data was searched against *Chlamydomonas reinhardtii* protein dataset from UniProt (https://www.uniprot.org/).

MS data were analyzed by Scaffold_4.8.4 (Proteome Software Inc.). Proteins with mean values of exclusive unique peptide count of 2 or more in the WT MS results were used for analysis. Raw MS data were normalized by total spectra. Student's *t*-test was applied to K40R and WT MS results using biological triplicates. Proteins exhibiting a minimum of two-fold increase/decrease and a statistical significance threshold ($p < 0.05$) in mutants compared to WT were identified as up- or down-regulated.

3.8 Acknowledgements

We thank Drs. Kelly Sears, Mike Strauss, Kaustuv Basu, and Jeannie Mui (Facility for Electron Microscopy Research at McGill University), for helping with data collection and maintenance of the electron microscopes. SK is supported by JSPS Overseas Research Fellowships. KHB is supported by the grants from Canadian Institutes of Health Research (PJT-156354), Natural Sciences and Engineering Research Council of Canada (RGPIN-2016-04954) and Canadian Institute for Advanced Research (Arzieli Global Scholar Program).

3.9 Author Contributions

KHB conceived the project. KHB, SKY, SK designed the experiments. SKY and CB performed culture of the cells with help from MVP, KP. SKY performed purification of microtubule fractions from cilia. SKY and CB performed vitrification of the grids, collected data. SKY, CB, SK and KHB performed the cryo-EM data analysis of the doublet with assist from ZF. SKY, KHB generated a model of the doublet. SK performed the MD simulation. DD, KP assist SKY in MS data analysis. SKY, SK and KHB interpreted the structure. All authors were involved in the manuscript writing process.

3.10 Conflicts of Interest

The authors declare no conflicts of interest.

3.11 Additional Figures and Tables

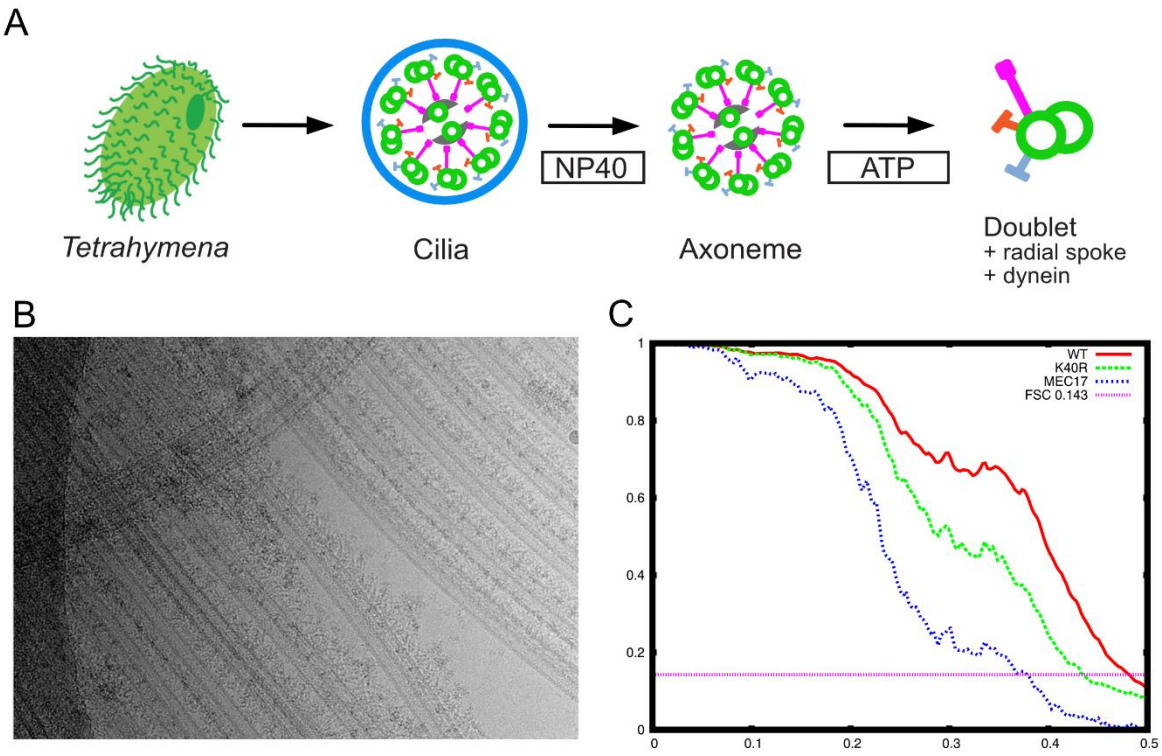

Figure 3.13. Purification schematic of axoneme and Gold-standard FSC of the cryo-EM maps.

A. Purification scheme of the axoneme in this study.

B. A typical cryo-EM image of the *Tetrahymena* DMT.

C. Gold-standard Fourier Shell Correlation of the 48 nm repeat cryo-EM maps of the WT (CU428), K40R, and MEC17 *Tetrahymena* strains.

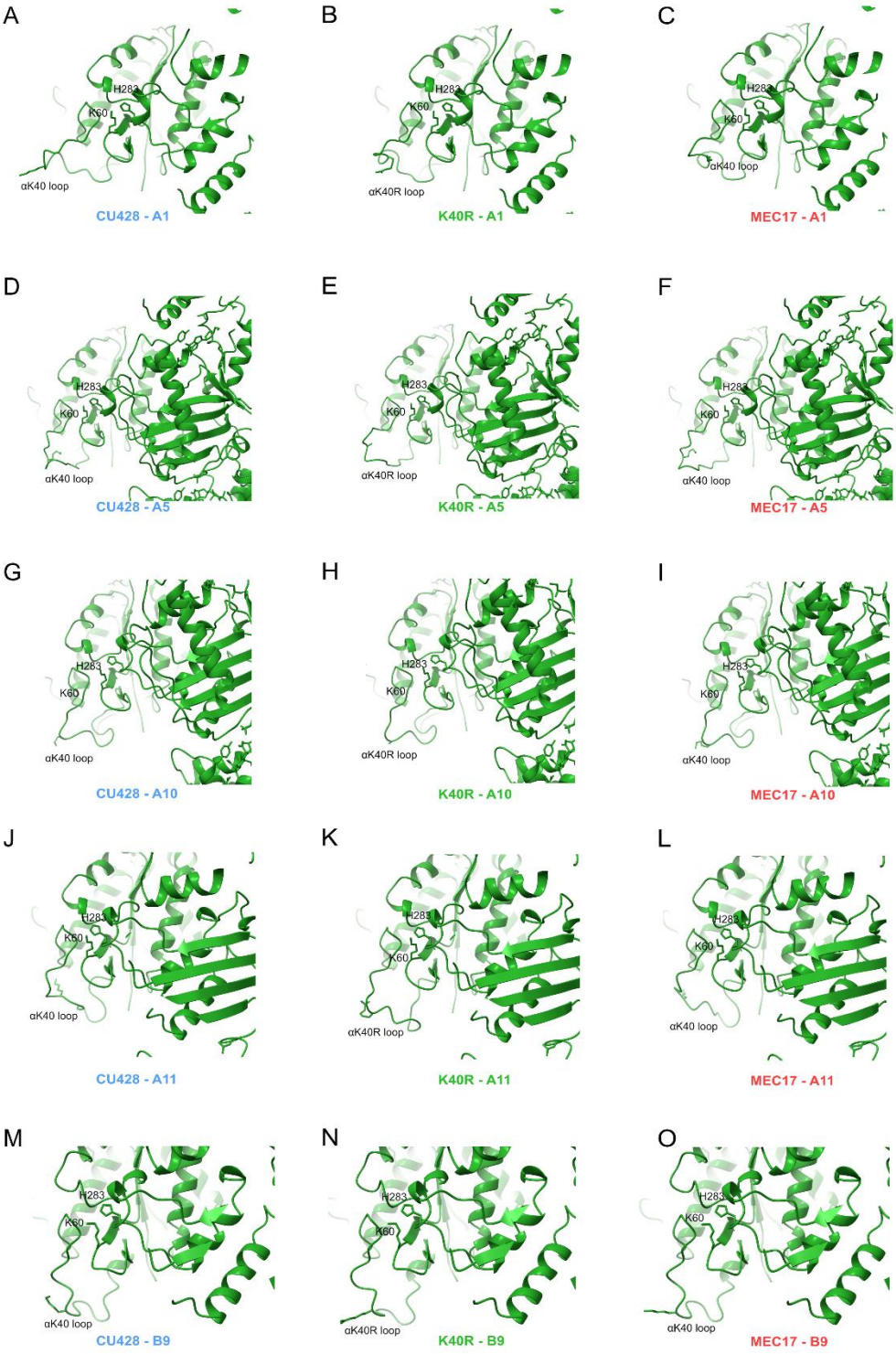
A
H283
K60
αK40 loop
CU428 - A1
B
H283
K60
αK40R loop
K40R - A1
C
H283
K60
αK40 loop
MEC17 - A1
D
H283
K60
αK40 loop
CU428 - A5
E
H283
K60
αK40R loop
K40R - A5
F
H283
K60
αK40 loop
MEC17 - A5
G
H283
K60
αK40 loop
CU428 - A10
H
H283
K60
αK40R loop
K40R - A10
I
H283
K60
αK40 loop
MEC17 - A10
J
H283
K60
αK40 loop
CU428 - A11
K
H283
K60
αK40R loop
K40R - A11
L
H283
K60
αK40 loop
MEC17 - A11
M
H283
K60
αK40 loop
CU428 - B9
N
H283
K60
αK40R loop
K40R - B9
O
H283
K60
αK40 loop
MEC17 - B9

Figure 3.14. Cryo-EM maps and models of selected full αK40 loops in A1 (A-C), A5 (D-F), A10 (G-I), A11 (J-L), and B9 (M-O) from CU428 (WT), K40R, and MEC17 *Tetrahymena* species.

Table 3.15. ANOVA test p-values and significance of the interdimer distance of tubulin subunits within each protofilaments, in CU428 (WT), K40R, and MEC17 *Tetrahymena* species.

Protofilaments	Interdimer distances from CU428 (Å) (mean ± SD, n = 6)	Interdimer distances from K40R (Å) (mean ± SD, n = 6)	Interdimer distances from MEC17 (Å) (mean ± SD, n = 6)	ANOVA p-values	p-value summary
A1	84.352 ± 0.276	84.518 ± 0.137	84.194 ± 0.221	0.097	ns
A2	84.453 ± 0.144	84.512 ± 0.083	84.222 ± 0.085	0.002	**
A3	84.426 ± 0.301	84.548 ± 0.113	84.218 ± 0.090	0.048	*
A4	84.300 ± 0.451	84.390 ± 0.244	84.016 ± 0.210	0.190	ns
A5	84.506 ± 0.268	84.493 ± 0.151	84.080 ± 0.195	0.009	**
A6	84.479 ± 0.473	84.495 ± 0.441	84.105 ± 0.388	0.305	ns
A7	84.418 ± 0.537	84.519 ± 0.282	84.091 ± 0.246	0.207	ns
A8	84.367 ± 0.298	84.575 ± 0.280	84.093 ± 0.191	0.034	*
A9	84.393 ± 0.428	84.603 ± 0.301	84.132 ± 0.351	0.157	ns
A10	84.364 ± 0.331	84.567 ± 0.195	84.141 ± 0.286	0.082	ns
A11	84.352 ± 0.639	84.546 ± 0.565	84.166 ± 0.636	0.629	ns
A12	84.323 ± 1.063	84.511 ± 0.989	84.198 ± 1.000	0.888	ns
A13	84.355 ± 0.957	84.506 ± 0.977	84.204 ± 1.018	0.890	ns
B1	84.253 ± 0.301	84.566 ± 0.226	84.136 ± 0.296	0.068	ns
B2	84.171 ± 0.302	84.592 ± 0.257	84.106 ± 0.343	0.046	*
B3	84.174 ± 0.413	84.617 ± 0.175	84.112 ± 0.255	0.034	*
B4	84.134 ± 0.359	84.607 ± 0.211	84.185 ± 0.417	0.085	ns
B5	84.036 ± 0.515	84.547 ± 0.368	84.133 ± 0.512	0.223	ns
B6	84.419 ± 0.358	84.473 ± 0.538	84.090 ± 0.617	0.465	ns
B7	84.042 ± 0.356	84.540 ± 0.252	84.271 ± 0.177	0.035	*
B8	84.129 ± 0.494	84.299 ± 0.525	84.061 ± 0.516	0.754	ns
B9	84.259 ± 0.371	84.432 ± 0.285	84.062 ± 0.446	0.321	ns
B10	84.359 ± 0.575	84.590 ± 0.281	84.194 ± 0.507	0.431	ns

Table 3.16. Inter-protofilament angle between subsequent protofilament obtained from cryo-EM maps of CU428 (WT), K40R, and MEC17 *Tetrahymena* species.

	CU428		K40R		MEC17	
Protofilaments	**Mean rotation angle (degrees) n = 7**	**Standard Deviation**	**Mean rotation angle (degrees) n = 7**	**Standard Deviation**	**Mean rotation angle (degrees) n = 7**	**Standard Deviation**
A1_A2	26.454	0.230	25.987	0.415	26.356	0.281
A2_A3	34.578	0.318	34.270	0.338	34.391	0.364
A3_A4	28.017	0.238	28.247	0.262	28.279	0.475
A4_A5	27.823	0.522	27.716	0.422	28.152	0.615
A5_A6	22.892	0.633	23.306	0.416	22.996	0.546
A6_A7	21.501	0.671	21.392	0.349	21.138	0.362
A7_A8	32.418	0.570	32.577	0.577	32.339	0.528
A8_A9	22.918	0.535	22.930	0.413	22.971	0.399
A9_A10	41.819	0.604	41.593	0.656	42.305	0.431
A10_A11	29.368	0.610	28.645	0.626	28.851	0.438
A11_A12	20.461	0.520	20.878	0.573	20.311	0.557
A12_A13	15.875	0.491	16.399	0.581	16.007	0.626
A13_A1	35.974	0.370	36.050	0.481	36.173	0.464
B1_B2	22.161	0.240	21.737	0.158	22.059	0.141
B2_B3	22.579	0.272	22.384	0.252	22.385	0.217
B3_B4	22.919	0.193	23.447	0.283	23.258	0.439
B4_B5	23.137	0.448	23.839	0.397	23.232	0.407
B5_B6	23.211	0.639	24.329	0.245	23.359	0.261
B6_B7	20.003	0.468	20.688	0.361	19.951	0.418
B7_B8	29.039	0.351	23.353	0.624	27.737	0.481
B8_B9	21.829	0.385	22.303	0.466	21.939	0.554
B9_B10	23.554	0.455	27.409	0.417	24.556	0.527

Table 3.17. Proteins at least two-folds upregulated in CU428 compared to both K40R and MEC17 mutants.

Gene name	Gene ID	Uniprot ID	Highest P-Value	Average Fold Change	Homolog in *Chlamydomonas reinhardtii*	Homolog in *Homo sapiens*
CAMP-dependent kinase, regulatory protein	TTHERM_00623090	Q240X5	0.003	4.5	A8ITN7	NA
Tetratricopeptide repeat protein	TTHERM_00313720	Q22KA9	0.006	5.2	NA	NA
Uncharacterized protein	TTHERM_00455660	I7MI64	0.035	6.1	NA	NA

Table 3.18. Proteins at least two-folds downregulated in CU428 compared to both K40R and MEC17 mutants.

Gene name	Gene ID	Uniprot ID	Highest P-Value	Average Fold Change	Homolog in *Chlamydomonas reinhardtii*	Homolog in *Homo sapiens*
Uncharacterized protein	TTHERM_00703420	Q22GI1	0.035	4.2	NA	NA
Uncharacterized protein	TTHERM_00392650	Q233I4	0.010	5.7	NA	NA
Uncharacterized protein	TTHERM_00548020	I7MDA2	0.005	5.0	NA	NA
Dynein light chain 8-like E	N/A	Q1HFV9	0.036	5.1	NA	NA
Uncharacterized protein	TTHERM_00483660	I7M1N4	0.041	5.0	NA	NA
Cyclic nucleotide-binding domain protein	TTHERM_00841230	I7M4G5	0.040	5.7	NA	NA
Hect domain and RCC1-like domain protein	TTHERM_00535910	I7LX15	0.041	5.5	NA	NA
Uncharacterized protein	TTHERM_00827160	Q22EF3	0.012	7.1	NA	NA
Uncharacterized protein	TTHERM_000732839	W7XGQ6	0.010	7.9	NA	NA
Uncharacterized protein	TTHERM_00388510	Q23RD8	0.000	9.2	NA	NA
Cyclic nucleotide-binding domain protein	TTHERM_00143540	I7M0S4	0.002	13.0	NA	NA

Table 3.19. Proteins at least two-folds downregulated in K40R mutant compared to CU428.

Gene name	Gene ID	Uniprot ID	Average CU428	Average K40R	p-value	Average fold change	Homolog in *Chlamydomonas reinhardtii*	Homolog in *Homo sapiens*
Dynein light chain 4	TTHERM_00716250	I7MCM8	12.080	3.057	0.001	0.300	NA	NA
Cell surface immobilization antigen SerH6, putative	TTHERM_00491130	Q23J59	14.630	3.516	0.001	0.200	A0A250XQN9	NA
CAMP-dependent kinase, regulatory protein	TTHERM_00623090	Q240X5	31.120	6.484	0.003	0.200	NA	NA
Tetratricopeptide repeat protein	TTHERM_00313720	Q22KA9	7.900	1.592	0.006	0.200	IFT70	Q8N4P2
CGMP-dependent kinase 5-1	TTHERM_00046530	Q23DN8	1.860	0.357	0.025	0.200	NA	NA
Glutathione S-transferase, amine-terminal domain protein	TTHERM_00602870	Q22YK8	6.730	1.172	0.000	0.200	NA	P09488
Heat shock 70 kDa protein	TTHERM_00105110	Q234I5	5.110	2.042	0.001	0.200	NA	NA
Uncharacterized protein	TTHERM_00455660	I7MI64	2.320	0.403	0.035	0.200	NA	NA

Table 3.20. Proteins at least two-folds upregulated in K40R mutant compared to CU428

Gene name	Gene ID	Uniprot ID	Avg CU428	Avg K40R	p-value	Average fold change	Homolog in *C. reinhardtii*	Homolog in *Homo sapiens*
WD domain, G-beta repeat protein	TTHERM_00006270	Q22SA9	1.160	4.649	0.047	4.000	NA	NA
Uncharacterized protein	TTHERM_00449680	Q238V2	0.460	1.932	0.026	4.200	NA	NA
Uncharacterized protein	TTHERM_00703420	Q22GI1	3.250	13.702	0.035	4.200	NA	NA
Uncharacterized protein	TTHERM_00392650	Q233I4	1.860	8.598	0.010	4.400	NA	NA
Uncharacterized protein	TTHERM_00548020	I7MDA2	1.860	8.598	0.005	4.600	NA	NA
SelT/selW/selH selenoprotein domain protein	TTHERM_00195980	Q23K36	0.460	2.289	0.042	4.900	NA	NA
FAM184 domain-containing protein	TTHERM_01321540	Q232U4	0.930	4.649	0.033	5.000	NA	Q8NB25
Calmodulin	NA	P02598	0.930	4.734	0.038	5.100	NA	Calmodulin 1,2,3
Dynein light chain 8-like E	NA	Q1HFV9	0.930	5.006	0.036	5.400	NA	P63167
Uncharacterized protein	TTHERM_00847020	Q22US8	0.700	3.927	0.008	5.600	NA	NA
Kinesin-like protein	TTHERM_01347910	Q229Q4	0.470	2.700	0.003	5.800	NA	Q2TAC6
Uncharacterized protein	TTHERM_00483660	I7M1N4	0.460	2.700	0.003	5.800	NA	NA
Cyclic nucleotide-binding domain protein	TTHERM_00841230	I7M4G5	0.460	2.700	0.003	5.800	NA	NA
Kinesin-like protein	TTHERM_00758880	Q23JL7	0.460	2.747	0.011	5.900	A0A2K3D1C7	A0A7I2V3N5
Scp-like extracellular protein, putative	TTHERM_00145900	I7MI85	1.620	10.088	0.001	6.200	NA	NA
Uncharacterized protein	TTHERM_00659030	I7M3P7	1.160	7.762	0.014	6.700	NA	NA
Hect domain and RCC1-like domain protein	TTHERM_00535910	I7LX15	0.700	4.696	0.010	6.800	NA	NA
Uncharacterized protein	TTHERM_00827160	Q22EF3	0.460	3.159	0.009	6.800	A0A2K3DZJ7	NA
Uncharacterized protein	TTHERM_000732839	W7XGQ6	0.930	7.341	0.001	7.900	NA	NA
Uncharacterized protein	TTHERM_00939090	Q22DN4	0.230	1.987	0.027	8.500	NA	NA
Uncharacterized protein	TTHERM_00388510	Q23RD8	1.160	13.239	0.000	11.000	NA	NA
B-box zinc finger protein	TTHERM_00112790	Q22Z92	0.230	2.692	0.033	12.000	NA	NA
Cyclic nucleotide-binding domain protein	TTHERM_00143540	I7M0S4	0.230	3.104	0.002	13.000	NA	NA
Uncharacterized protein	TTHERM_00497130	I7M4M1	0.230	4.284	0.000	18.000	NA	NA
EF hand protein	TTHERM_00833830	Q23A35	0.230	8.017	0.031	34.000	NA	NA

Table 3.21. Proteins at least two-folds downregulated in MEC17 mutant compared to CU428

Gene name	Gene ID	Uniprot ID	Avg CU428	Avg K40R	p-value	Average fold change	Homolog in *Chlamydomonas reinhardtii*	Homolog in *Homo sapiens*
CAMP-dependent kinase catalytic subunit	TTHERM_00433420	Q231B5	14.860	3.669	0.000	0.200	NA	NA
CAMP-dependent kinase, regulatory protein	TTHERM_00623090	Q240X5	31.120	7.513	0.003	0.200	NA	NA
Tetratricopeptide repeat	TTHERM_00313720	Q22KA9	7.900	1.471	0.000	0.200	A8ITN7	Q8N4P2
Uncharacterized protein	TTHERM_00455660	I7MI64	2.320	0.359	0.029	0.200	NA	NA
Metallo-beta-lactamase family protein	TTHERM_00128670	I7M1D2	9.530	1.418	0.004	0.100	NA	NA
Intraflagellar transporter-like protein	TTHERM_00648910	I7LT74	3.250	0.359	0.015	0.100	IFT54	IFT54
Uncharacterized protein	TTHERM_01106190	Q22BD8	4.410	0.359	0.011	0.080	NA	NA
Intraflagellar transporter-like protein, putative	TTHERM_00149230	I7LWB4	5.800	0.412	0.005	0.070	IFT74	IFT74

Table 3.22. Proteins least two-folds upregulated in MEC17 mutant compared to CU428

Gene name	Gene ID	Uniprot ID	Avg CU428	Avg K40R	p-value	Average fold change	Homolog in *C. reinhardtii*	Homolog in *H. sapiens*
Uncharacterized protein	TTHERM_00852750	Q24E65	4.180	16.987	0.001	4.100	NA	NA
Uncharacterized protein	TTHERM_00483660	I7M1N4	0.460	1.883	0.041	4.100	NA	NA
Uncharacterized protein	TTHERM_00219140	I7M2G4	1.620	6.778	0.007	4.200	NA	NA
Hect domain and RCC1-like domain protein	TTHERM_00535910	I7LX15	0.700	2.942	0.041	4.200	NA	NA
Uncharacterized protein	TTHERM_00703420	Q22GI1	3.250	13.940	0.008	4.300	NA	NA
Uncharacterized protein	TTHERM_00190760	I7M812	1.630	7.137	0.005	4.400	NA	NA
Dynein light chain 8-like E	NA	Q1HFV9	0.930	4.474	0.006	4.800	NA	P63167
Uncharacterized protein	TTHERM_00085240	Q236S4	0.230	1.121	0.021	4.800	NA	NA
Uncharacterized protein	TTHERM_00670810	I7LXT5	0.470	2.242	0.021	4.800	NA	NA
Uncharacterized protein	TTHERM_00468010	I7MAL9	0.930	4.536	0.022	4.900	NA	NA
Uncharacterized protein	TTHERM_00010960	Q22S36	0.690	3.415	0.040	4.900	NA	NA
Uncharacterized protein	TTHERM_00548020	I7MDA2	1.860	10.088	0.000	5.400	NA	NA
Kinesin-like protein	TTHERM_00794640	Q23VW7	0.470	2.592	0.018	5.500	NA	A0A7I2V3V3
Uncharacterized protein	TTHERM_00334380	I7M866	0.460	2.539	0.040	5.500	NA	NA
Cyclic nucleotide-binding domain protein	TTHERM_00841230	I7M4G5	0.460	2.539	0.040	5.500	NA	NA
Uncharacterized protein	TTHERM_00392650	Q233I4	0.700	4.772	0.010	6.800	NA	NA
Uncharacterized protein	TTHERM_00388510	Q23RD8	1.160	8.555	0.000	7.400	NA	NA
Uncharacterized protein	TTHERM_00827160	Q22EF3	0.460	3.354	0.012	7.200	NA	NA
Uncharacterized protein	TTHERM_000732839	W7XGQ6	0.930	7.329	0.010	7.900	NA	NA
Uncharacterized protein	TTHERM_00732900	Q245C1	0.460	3.669	0.024	7.900	NA	NA
Uncharacterized protein	TTHERM_001092361	W7X1T3	0.230	1.892	0.028	8.100	A0A2K3DJC4	NA
Uncharacterized protein	TTHERM_00825250	I7MCE2	0.230	1.892	0.028	8.100	NA	NA
Uncharacterized protein	TTHERM_00194430	Q23K92	0.930	8.555	0.000	9.200	NA	NA
Uncharacterized protein	TTHERM_01028860	Q23EF4	0.230	2.189	0.035	9.500	NA	NA
Uncharacterized protein	TTHERM_00078910	Q23FX3	0.470	4.536	0.014	9.700	NA	NA
Uncharacterized protein	TTHERM_00449080	Q239A7	0.470	4.728	0.024	10.000	NA	NA
Uncharacterized protein	TTHERM_01009900	Q23LQ6	0.230	3.363	0.000	15.000	NA	NA
Protein kinase	TTHERM_00497440	I7MB56	0.230	3.774	0.005	16.000	NA	NA
Cyclic nucleotide-binding domain protein	TTHERM_00143540	I7M0S4	0.230	4.124	0.002	18.000	NA	NA

3.12 Chapter 3 References

Akella, J. S., D., W., Kim, J., Starostina, N. G., Lyons-Abbott, S., Morrissette, N. S., Dougan, S. T., Kipreos, E. T., & Gaertig, J. (2010). MEC-17 is an alpha-tubulin acetyltransferase. Nature, 467(7312), 218-222. https://doi.org/10.1038/nature09324

Bustamante-Marin, M., X., & Ostrowski, L. E. (2017). Cilia and Mucociliary Clearance. Cold Spring Harbor perspectives in biology, 9(4), a028241. https://doi.org/10.1101/cshperspect.a028241

Cueva, J. G., J., H., & Huang, K. C. G., Miriam B. (2012). Posttranslational acetylation of α-tubulin constrains protofilament number in native microtubules. Curr Biol, 22(12), 1066-1074. https://doi.org/10.1016/j.cub.2012.05.012

De Robertis, E. (1956). Morphogenesis of the retinal rods; an electron microscope study. J Biophys Biochem Cytol., 2(4 Suppl), 209-218. https://doi.org/D - CLML: 5731:3597 OTO - NLM

De Robertis, E. (1960). Some observations on the ultrastructure and morphogenesis of photoreceptors. J Gen Physiol., 43(6), 1-13.

Djenoune, L., & Wyart, C. (2017). Light on a sensory interface linking the cerebrospinal fluid to motor circuits in vertebrates. J Neurogenet, 31(3), 113-127. https://doi.org/10.1080/01677063.2017.1359833

Du, Y., Seibenhener, M. L., Yan, J., Jiang, J., & Wooten, M. C. (2015). aPKC phosphorylation of HDAC6 results in increased deacetylation activity. PLOS ONE, 10(4), e0123191. https://doi.org/10.1371/journal.pone.0123191

Elam, C. A., Wirschell, M., Yamamoto, R., Fox, L. A., York, K., Kamiya, R., Dutcher, S. K., & Sale, W. S. (2011). An axonemal PP2A B-subunit is required for PP2A localization and flagellar motility. Cytoskeleton (Hoboken), 68(7), 363-372. https://doi.org/10.1002/cm.20519

Eshun-Wilson, L., Zhang, R., Portran, D., Nachury, M. V., Toso, D. B., Löhr, T., Vendruscolo, M., Bonomi, M., Fraser, J. S., & Nogales, E. (2019). Effects of α-tubulin acetylation on microtubule structure and stability. Proceedings of the National Academy of Sciences, 116(21), 10366. https://doi.org/10.1073/pnas.1900441116

Fukushige, T., Hendzel, M. J., Bazett-Jones, D. P., & McGhee, J. D. (1999). Direct visualization of the elt-2 gut-specific GATA factor binding to a target promoter inside the living Caenorhabditis elegans embryo. Proc Natl Acad Sci U S A, 96(21), 11883-11888. https://doi.org/10.1073/pnas.96.21.11883

Gadadhar, S., Viar, G. A., Hansen, J. N., Gong, A., Kostarev, A., Ialy-Radio, C., Leboucher, S., Whitfield, M., Ziyyat, A., Touré, A., Alvarez, L., Pigino, G., & Janke, C. (2021). Tubulin glycylation controls axonemal dynein activity, flagellar beat, and male fertility. Science, 371(6525), eabd4914. https://doi.org/doi:10.1126/science.abd4914

Garnham, C. P., & Roll-Mecak, A. (2012). The chemical complexity of cellular microtubules: tubulin post-translational modification enzymes and their roles in tuning microtubule functions. Cytoskeleton (Hoboken), 69(7), 442-463. https://doi.org/10.1002/cm.21027

Howes, S. C., GM, A., Shida, T., Nachury, M. V., & Nogales, E. (2014). Effects of tubulin acetylation and tubulin acetyltransferase binding on microtubule structure. Mol Biol Cell, 25(2), 257-266. https://doi.org/10.1091/mbc.E13-07-0387

Hubbert, C., A., G., Shao, R., Kawaguchi, Y., Ito, A., Nixon, A., Yoshida, M., Wang, X.-F., & Yao, T.-P. (2002). HDAC6 is a microtubule-associated deacetylase. Nature, 417(6887), 455-458. https://doi.org/DOI10.1038/417455a

Ichikawa, M., Khalifa, A. A. Z., Kubo, S., Dai, D., Basu, K., Maghrebi, M. A. F., Vargas, J., & Bui, K. H. (2019). Tubulin lattice in cilia is in a stressed form regulated by microtubule inner proteins. Proceedings of the National Academy of Sciences, 116(40), 19930-19938. https://doi.org/10.1073/pnas.1911119116

Ichikawa, M., Liu, D., Kastritis, P. L., Basu, K., Hsu, T. C., Yang, S., & Bui, K. H. (2017). Subnanometre-resolution structure of the doublet microtubule reveals new classes of microtubule-associated proteins. Nature Communications, 8(1), 15035. https://doi.org/10.1038/ncomms15035

Kalebic, N., S., S., Perlas, E., Bolasco, G., Martinez, C., & Heppenstall, P. A. (2013). αTAT1 is the major α-tubulin acetyltransferase in mice. Nat Commun, 4, 1962.

Kaul, N., Soppina, V., & Verhey, K. J. (2014). Effects of α-tubulin K40 acetylation and detyrosination on kinesin-1 motility in a purified system. Biophys J., 106(12), 2636-2643. https://doi.org/10.1016/j.bpj.2014.05.008

Khalifa, A. A. Z., Ichikawa, M., Dai, D., Kubo, S., Black, C.S., Peri, K., McAlear, T.S., Veyron, S., Yang, S.K., Vargas, J., Bechstedt, S., Trempe, J., Bui., K.H. . (2020). The inner junction complex of the cilia is an interaction hub that involves tubulin post-translational modifications. Elife, 9, e52760.

Ki, S. M., Kim, J. H., Won, S. Y., Oh, S. J., Lee, I. Y., Bae, Y. K., Chung, K. W., Choi, B. O., Park, B., Choi, E. J., & Lee, J. E. (2020). CEP41-mediated ciliary tubulin glutamylation drives angiogenesis through AURKA-dependent deciliation. EMBO Rep, 21(2), e48290. https://doi.org/10.15252/embr.201948290

Kotsis, F., R, N., Boehlke, C., Bashkurov, M., Walz, G., & Kuehn, E. W. (2007). Ciliary calcium signaling is modulated by kidney injury molecule-1 (Kim1). Pflugers Arch, 453(3), 819-829. https://doi.org/10.1007/s00424-006-0168-0

Kubo, T., Hirono, M., Aikawa, T., Kamiya, R., & Witman, G. B. (2015). Reduced tubulin polyglutamylation suppresses flagellar shortness in Chlamydomonas. Mol Biol Cell, 26(15), 2810-2822. https://doi.org/10.1091/mbc.E15-03-0182

Kubo, T., Yanagisawa, H.-a., Yagi, T., Hirono, M., & Kamiya, R. (2010). Tubulin Polyglutamylation Regulates Axonemal Motility by Modulating Activities of Inner-Arm

Dyneins. Current Biology, 20(5), 441-445. https://doi.org/https://doi.org/10.1016/j.cub.2009.12.058

Lehti, M. S., & Sironen, A. (2017). Formation and function of sperm tail structures in association with sperm motility defects. Biology of Reproduction, 97(4), 522-536. https://doi.org/10.1093/biolre/iox096

Liu, N., Xiong, Y., Li, S., Ren, Y., He, Q., Gao, S., Zhou, J., & Shui, W. (2015). New HDAC6-mediated deacetylation sites of tubulin in the mouse brain identified by quantitative mass spectrometry. Scientific Reports, 5(1), 16869. https://doi.org/10.1038/srep16869

M., L., & Piperno, G. (1987). Identification of an acetylation site of Chlamydomonas alpha-tubulin. Proc Natl Acad Sci U S A, 84(16), 5720-5724.

Ma, M., Stoyanova, M., Rademacher, G., Dutcher, S. K., Brown, A., & Zhang, R. (2019). Structure of the Decorated Ciliary Doublet Microtubule. Cell, 179(4), 909-922.e912. https://doi.org/https://doi.org/10.1016/j.cell.2019.09.030

North, B. J., B.L., M., Borra, M. T., Denu, J. M., & Verdin, E. (2003). The human Sir2 ortholog, SIRT2, is an NAD+-dependent tubulin deacetylase. Mol Cell, 11(2), 437-444. https://doi.org/Doi 10.1016/S1097-2765(03)00038-8

Orts-Del'Immagine, A., & Wyart, C. (2017). Cerebrospinal-fluid-contacting neurons. Curr Biol, 27(22), R1198-r1200. https://doi.org/10.1016/j.cub.2017.09.017

Pathak, N., Austin-Tse, C. A., Liu, Y., Vasilyev, A., & Drummond, I. A. (2014). Cytoplasmic carboxypeptidase 5 regulates tubulin glutamylation and zebrafish cilia formation and function. Mol Biol Cell, 25(13), 1836-1844. https://doi.org/10.1091/mbc.E13-01-0033

Pathak, N., Obara, T., Mangos, S., Liu, Y., & Drummond, I. A. (2007). The zebrafish fleer gene encodes an essential regulator of cilia tubulin polyglutamylation. Mol Biol Cell, 18(11), 4353-4364. https://doi.org/10.1091/mbc.e07-06-0537

Porter, M. E., & Sale, W. S. (2000). The 9 + 2 axoneme anchors multiple inner arm dyneins and a network of kinases and phosphatases that control motility. J Cell Biol, 151(5), F37-42. https://doi.org/10.1083/jcb.151.5.f37

Pugacheva, E. N., Jablonski, S. A., Hartman, T. R., Henske, E. P., & Golemis, E. A. (2007). HEF1-dependent Aurora A activation induces disassembly of the primary cilium. Cell, 129(7), 1351-1363. https://doi.org/10.1016/j.cell.2007.04.035

Ran, J., Yang, Y., Li, D., Liu, M., & Zhou, J. (2015). Deacetylation of α-tubulin and cortactin is required for HDAC6 to trigger ciliary disassembly. Sci Rep, 5, 12917.

Reed, N. A., Cai, D., Blasius, T. L., Jih, G. T., Meyhofer, E., Gaertig, J., & Verhey, K. J. (2006). Microtubule Acetylation Promotes Kinesin-1 Binding and Transport. Current Biology, 16(21), 2166-2172. https://doi.org/https://doi.org/10.1016/j.cub.2006.09.014

Rogowski, K., Francois, J., van Dijk, J., Wloga, D., Strub, J.-M., Levilliers, N., Thomas, D., Bré, M.-H., Van Dorsselaer, A., Gaertig, J., & Janke, C. (2019). Evolutionary divergence of enzymatic mechanisms for posttranslational polyglycylation. Cell, 137(6), 1076-1087.

Rogowski, K., van Dijk, J., Magiera, M. M., Bosc, C., Deloulme, J.-C., Bosson, A., Peris, L., Gold, N. D., Lacroix, B., Bosch Grau, M., Bec, N., Larroque, C., Desagher, S., Holzer, M., Andrieux, A., Moutin, M.-J., & Janke, C. (2010). A family of protein-deglutamylating enzymes associated with neurodegeneration. Cell, 143(4), 564-578. https://doi.org/10.1016/j.cell.2010.10.014

S.W., L. H., & Rosenbaum, J. L. (1983). Chlamydomonas alpha-tubulin is posttranslationally modified in the flagella during flagellar assembly. J Cell Biol. , 97(1), 258-263.

Schaedel, L., John, K., Gaillard, J., Nachury, M. V., Blanchoin, L., & Théry, M. (2015). Microtubules self-repair in response to mechanical stress. Nat Mater., 14(11), 1156-1163.

Shah, N., Kumar, S., Zaman, N., Pan, C. C., Bloodworth, J. C., Lei, W., Streicher, J. M., Hempel, N., Mythreye, K., & Lee, N. Y. (2018). TAK1 activation of alpha-TAT1 and microtubule hyperacetylation control AKT signaling and cell growth. Nat Commun, 9(1), 1696. https://doi.org/10.1038/s41467-018-04121-y

Shang, Y., Inthavong, K., & Tu, J. (2019). Development of a computational fluid dynamics model for mucociliary clearance in the nasal cavity. Journal of Biomechanics, 85, 74-83. https://doi.org/https://doi.org/10.1016/j.jbiomech.2019.01.015

Shida, T., Cueva, J. G., Xu, Z., Goodman, M. B., & Nachury, M. V. (2010). The major alpha-tubulin K40 acetyltransferase alphaTAT1 promotes rapid ciliogenesis and efficient mechanosensation. Proc Natl Acad Sci U S A, 107(50), 21517-21522. https://doi.org/10.1073/pnas.1013728107

Sjostrand, F. S. The ultrastructure of the outer segments of rods and cones of the eye as revealed by the electron microscope. (0095-9898 (Print)). https://doi.org/D - CLML: 5425:5456:294:405 OTO - NLM

Sjostrand, F. S. (1953). The ultrastructure of the innersegments of the retinal rods of the guinea pig eye as revealed by electron microscopy. J Cell Comp Physiol, 42(1), 45-70. https://doi.org/D - CLML: 5425:5457:294:405 OTO - NLM

Stoddard, D., Zhao, Y., Bayless, B. A., Gui, L., Louka, P., Dave, D., Suryawanshi, S., Tomasi, R. F.-X., Dupuis-Williams, P., Baroud, C. N., Gaertig, J., Winey, M., & Nicastro, D. (2018). Tetrahymena RIB72A and RIB72B are microtubule inner proteins in the ciliary doublet microtubules. Molecular Biology of the Cell, 29(21), 2566-2577. https://doi.org/10.1091/mbc.E18-06-0405

Ta-Shma, A., Perles, Z., Yaacov, B., Werner, M., Frumkin, A., Rein, A. J., & Elpeleg, O. (2015). A human laterality disorder associated with a homozygous WDR16 deletion. Eur J Hum Genet, 23(9), 1262-1265. https://doi.org/10.1038/ejhg.2014.265

Tokuyasu K - Yamada, E., & Yamada, E. (1959). The fine structure of the retina studied with the electron microscope. IV. Morphogenesis of outer segments of retinal rods. J Biophys Biochem Cytol., 6(2), 225-230.

Verhey, K. J. G., J. . (2007). The Tubulin Code. Cell Cycle, 6(17), 2152-2160. https://doi.org/10.4161/cc.6.17.4633

Walter, W. J., V., B., Fischermeier, E., & Diez, S. (2012). Tubulin acetylation alone does not affect kinesin-1 velocity and run length in vitro. PLOS ONE, 7(8), e42218.

Wang, W., & Brautigan, D. L. (2008). Phosphatase inhibitor 2 promotes acetylation of tubulin in the primary cilium of human retinal epithelial cells. BMC Cell Biol, 9, 62. https://doi.org/10.1186/1471-2121-9-62

Wloga, D., Joachimiak, E., Louka, P., & Gaertig, J. (2017). Posttranslational Modifications of Tubulin and Cilia. Cold Spring Harbor perspectives in biology, 9(6). https://doi.org/10.1101/cshperspect.a028159

Wloga, D., K., R., Sharma, N., Sharma N - Van Dijk J - Janke, C., Eddé, B., Bré, M.-H., Levilliers, N., Redeker, V., Duan, J., Gorovsky, M. A., Jerka-Dziadosz, M., & Gaertig, J. (2008). Glutamylation on alpha-tubulin is not essential but affects the assembly and functions of a subset of microtubules in Tetrahymena thermophila. Eukaryot Cell, 7(8), 1362-1372.

Wloga, D., Webster, D. M., Rogowski, K., Bre, M. H., Levilliers, N., Jerka-Dziadosz, M., Janke, C., Dougan, S. T., & Gaertig, J. (2009). TTLL3 Is a Tubulin Glycine Ligase that Regulates the Assembly of Cilia. Developmental Cell, 16(6), 867-876. https://doi.org/10.1016/j.devcel.2009.04.008

Yoder, B. K. (2007). Role of primary cilia in the pathogenesis of polycystic kidney disease. J Am Soc Nephrol, 18(5), 1381-1388. https://doi.org/10.1681/ASN.2006111215

Zhang, R., Alushin, G. M., Brown, A., & Nogales, E. (2015). Mechanistic Origin of Microtubule Dynamic Instability and Its Modulation by EB Proteins. Cell, 162(4), 849-859. https://doi.org/10.1016/j.cell.2015.07.012

Zhang, Y., Li, N., Caron, C., Matthias, G., Hess, D., Khochbin, S., & Matthias, P. (2003). HDAC-6 interacts with and deacetylates tubulin and microtubules in vivo. EMBO J, 22(5), 1168-1179. https://doi.org/10.1093/emboj/cdg115

Zhou, X., Fan, L. X., Li, K., Ramchandran, R., Calvet, J. P., & Li, X. (2014). SIRT2 regulates ciliogenesis and contributes to abnormal centrosome amplification caused by loss of polycystin-1. Hum Mol Genet, 23(6), 1644-1655. https://doi.org/10.1093/hmg/ddt556

Chapter 4

“The ultimate tragedy is not the oppression and cruelty by the bad people but the silence over that by the good people.”

Martin Luther King Jr., American Baptist minister and activist, 1929-1968 C.E.

«Le monde souffre beaucoup, non pas à cause de la violence des mauvaises personnes mais à cause du silence des bonnes personnes.»

Napoléon Bonaparte, 1769 - 1821 E.C.

4.1 Preface

In November 2019, our laboratory received two acetylation mutants, *Tetrahymena* strains K40R and MEC17, from Dr. Jacek Gaertig of the University of Georgia, USA. After discussion with Dr. Bui, we decided that a side project for obtaining a cryo-EM map of acetylation mutants would be medically relevant, as it would help us to understand the structural changes DMT undergoes in its acetylated and deacetylated states, which contributed to many human diseases (Discussed in Chapter 1).

We enlisted help from Dr. Shintaroh Kubo for the ODA research project, a new post-doctoral fellow who joined the lab. At the time of manuscript preparation, we learned that Dr. Andrew Carter had published a closed and inactive conformation of ODA (Mali et al., 2021a). We used this to support the development of our model because the ODA in our micrographs, which lined up into a row, would be in the open and activated conformation. Dr. Kubo did all the molecular dynamics simulations to help understand how the ODA undergo conformational changes from the inactive to active states, which become an integral part of our published manuscript.

Our initial hypothesis for the acetylation mutants was that the MIPs would detach or become missing without acetylation. This speculation was based on the results that K40 is the only PTM site within the lumen (Eshun-Wilson et al., 2019; Kaul et al., 2014) and phenotype results by Dr. Gaertig lab (Akella et al., 2010). Akella et al. (2010) showed that acetylation mutants would have more labile and fewer cilia than the WT and that decreased acetylation would have an increased polyglutamylation response. However, our structural analysis reveals that MIPs are intact in the

CU428 and acetylation mutants (K40R and MEC17). Using the K40R cryo-EM maps, we also noticed, for the first time, that there are new electron densities on the outside and inside the lumen of DMT which was also later observed in CU428 maps. These densities suggest that removing the NaCl treatment during the preparation was important for keeping these proteins intact.

We obtained a high-resolution cryo-EM map for our structural analysis of 3.5 Å for K40R DMT and 4.0 Å for CU428 maps. Our new hypothesis is that the αK40 loop of tubulin remains structured wherever they interact with MIPs. This hypothesis is supported by Figure 3.1F-G and Table 3.2, where full αK40 loops are visible where many MIPs interactions are present. In addition, Figures 3.1B-D and Figure 3.3A show that none of the αK40 loop model stands the same when superimposed. This result suggests that the αK40 loops may stabilize a conformation when binding with the MIP, which our MD results can further support that acetylation of αK40 can improve its interaction with MIPs (Fig. 3.6D).

4.2 General Discussion

We decided that it would be wise to obtain a structure of the WT strain (CU428) of *Tetrahymena thermophila*, as previously we used mucocyst-deficient strain (SB255) that is incapable of exocytosis (Satir, Reichman, & Orias, 1986). However, CU428 strain *Tetrahymena thermophila* secret thick mucous that is a technical challenge to obtain clean cilia sample after purification. Therefore, a cryo-EM study of the mucous strain (CU428) would prove to be useful in understanding the most native strain of *Tetrahymena*. I solved the mucous technical challenge of CU428, K40R and MEC17 strains by adding a centrifugation step using 50 mL tubes in a spinning bucket rotor at no deacceleration setting. I also decided to increase the concentration of ADP and ATP used to split the doublets and skip the NaCl treatment step done in previous work (Ichikawa et al., 2017).

My preliminary negative staining and cryo-EM screening on the Tecnai F20 (Thermo Fisher Scientific ®) showed interesting results that there is a row of densities lining up the DMT (Figure 2.2C and Figure 3.13B). Initial analysis of micrographs collected from the Titan Krios 300 keV (Thermo Fisher Scientific ®) microscope revealed that the row of densities was ODA complexes formed on the DMT (Fig. 2.2E). There were no previous high-resolution structures of the ODA at the time. Thus we decided to perform analysis of the ODA complexes and K40R mutant simultaneously. (In this chapter, I will first talk about the ODA and then the effect of acetylation).

4.3 Outer Dynein Arm

Our structure of ODA bound to the DMT was revolved at an unprecedented resolution at 5.5–7 Å. Though this resolution is not impressive for cryo-EM, we had the highest resolution for ODA at the time of publication because our intact ODA was a huge protein complex with many components. The molecular dynamic simulations show that the ODA is docked onto the DMT via the docking complex. Our ODA structure also shows that ODA can interact with neighbouring ODA complex, as it would provide stable attachments to the DMT for generating forces within the cilia (Fig 1.5B). We also speculate that ODA and DC3 interaction could be based on intracellular calcium concentrations, as high calcium ion concentration would result in a symmetric waveform of flagella in *Chlamydomonas* (Bessen , Fay , & Witman 1980). In future work, it would be most interesting to confirm and study this phenomenon at high and low calcium concentrations.

DC3 is not conserved in humans, as mutations could result in PCD by termination or frameshift of CCDC151 (p.Glu109X, p.Glu309X and p.Ser419X) and CCDC114 (p.Ala248Serfs52 and p.Ser432Argfs*7) (Figure 2.11A). (Hjeij et al., 2014; Knowles, M.W., et al., 2013; W. Zhang et al., 2019). In our structures, we propose that the DC1/2 binding to Dyh3 tails and the DMT are in locations of these mutations. This result further explains the importance of the extended coiled-coil region of DC1/2 for proper assembly and activation of ODA. Our results are supported by a cryo-EM structure of *Chlamydomonas* ODA (Walton, Wu, & Brown, 2021) and bovine ODA (M. Gui, Farley, et al., 2021), showing that DC3 is localized to the DC1/2 coiled-coil portion.

Comparing the inactive and active ODA complex from cryo-EM allows us to speculate that LC3 dock to the AAA+ ring of Dyh4 via an ATPase cycle (Figure 2.9D). Here, the Dyh4 can detach and re-attach to the AAA+ ring, and its motor activity could be regulated by LC3, which interacts with other ciliary proteins (Wakabayashi & King, 2006). In agreement with that from *Chlamydomonas* ODA (Walton et al., 2021), our results confirm that the ATPase cycle is an important mechanism of ODA complex activation. Also similar to our results, the conformational change of one dynein in *Chlamydomonas* (Walton et al., 2021) is a coordinated activity that relies on ATP to propagate to the neighbouring dynein.

What remains unclear is the structural interaction between nexin and dynein during the force generation by ATP in motile cilia. The nexin-dynein regulatory complex has a previous cryo-ET structure from *Chlamydomonas* (L. Gui et al., 2019), but the resolution is insufficient to answer how ATP affects nexin. Therefore, it would be interesting to perform cryo-ET collection from *Tetrahymena* to obtain a high-resolution structure, as *Tetrahymena* cells are easier to harvest cilia and manipulate by molecular genetics.

Our coarse-grained MD simulation with Shulin captured the conformational changes of the ODA complex as Shulin detaches. The MD results allow us to present a model for how ODA attachment to the DMT can cause a robust remodelling and activation of the ODA complex without external factors (Figure 2.12). However, questions remain on the mechanism of how Shulin structurally keeps the ODA inactivated, as most of our ODA is in its activated state. In the future, we would

do pull-down assays or reconstitution of Shulin bound to DMT followed by cryo-EM, to observe the activation and inactivation mechanism further when Shulin is present.

In conclusion, we have shown and proposed an activation mechanism of ODA inside the cilia using cryo-EM. We believe that these findings would shed light on the understanding of cilia, ciliary force generation, and ciliopathies in humans.

4.4 Acetylation of Doublet Microtubules

Our results show that acetylated and deacetylated αK40 would stabilize as they are bound to FAP52 in the inner junction. Acetylated αK40 would have lower energy than the non-acetylated αK40 (Fig. 3.6A), leading to stability of the tubulin lattice. Although the difference is small-scale for one specific α-tubulin, it would cause a large-scale stabilization via acetylation in a cilium that could be from 1 to 9 μm long (Dummer, Poelma, DeRuiter, Goumans, & Hierck, 2016). In our case, the energy difference between acetylated and non-acetylated is 0.35 kcal/mol. Assuming an average cilium length of 6 um, divided by 16 nm and multiplied by 0.35 kcal/mol, the difference between non-acetyl and acetylated energy in a cilium would be 131.25 kcal/mol. This summation would be an amount of energy for stabilizing the cilium structure in a large scale. What is unclear is the potential energy difference between the other MIPs in the A-tubule to the αK40 since our results show that MIPs facilitate interaction with αK40 at many sites in PF A1 to PF A13 (Fig 3.1). In the future, we would perform molecular dynamics to examine the energy difference of αK40 to both globular and filamentous MIPs in the A-tubule, such as that of FAP27, FAP115, Rib72 and Rib43A. This MD would help us confirm our hypothesis for the role of αK40 acetylation in stabilizing the tubulin lattice.

Our cryo-EM results are similar to a recent study (Eshun-Wilson et al., 2019) of acetylation on reconstituted microtubules that acetylated αK40 loop has fewer conformations than non-acetylated. This recent study found that acetylated αK40 has a more extended conformation into the lumen to facilitate lateral interactions. However, our results did not show a difference in the cryo-EM maps

of acetylated (CU428) and non-acetylated (K40R and MEC17). After downloading their map (EMD-0612–EMD-0615) and atomic models (PDB ID codes 602Q–602T) into UCSF Chimera, we do not observe the 8 Å difference of the non-acetylated αK40 loop interaction to H1'-S2 loop, compared to the acetylated counterpart.

Our results also indicate that αK40 does not facilitate any lateral interactions. It may be possible that we cannot observe these lateral interactions as we are limited by the current resolution of our acetylated (CU428) density map, as we can only observe a few full acetylated αK40 loops. However, in contrast to our study, Eshun-Wilson et al. (2019) used pulled-down tubulins and then reconstituted the microtubule, so many different tubulin isotypes would be used to interfere with results. In addition, MIPs would also be missing in reconstituted microtubules, so Eshun-Wilson et al. (2019) would not have the chance to observe the MIPs interaction with αK40 loops. Besides, our MD used various clusters of acetylated and non-acetylated αK40 loops (Fig. 3.6A-B), with RMSD indicating how each cluster includes different conformation types. Low RMSD indicates that structures belonging to the cluster is similar. Eshun-Wilson et al. (2019) only used a few conformations, which could not have captured the full sample variety of αK40 loops.

Our mass spectrometry results were done using three replicates for each species (CU428, K40R, MEC17 strains) to show a consistent response of acetylation within WT and acetylation mutants. Furthermore, knowing that Rib72a and Rib72b knockout strains show MIP1, MIP4, and MIP6 structures being missing (Stoddard et al., 2018), we performed mass spectrometry of Rib72ab and Rib72b mutant strains. Therefore, we can eliminate the possible factors of filamentous MIPs on

the stability of tubulin lattice and the absence of certain MIPs. By doing so, we are the first to show changes in the proteome of acetylation mutants by taking advantage of model organism *Tetrahymena thermophila* species that allow specific point-mutation of K40R and knockout of αTAT. These results allowed us to examine better the structural and proteomic consequences of acetylation for the stability of the tubulin lattice.

To conclude, we found that the lack of acetylation could lead to the tubulin lattice's alteration and instability. We are the first to link tubulin lattice instability to an imbalance of the level of PTM expression inside the cilia. A recent study shows that the cilia could synthesize proteins to maintain their functions (Hao, Chen, Yan, & Zhu, 2021); while our mass spectrometry also detected ribosomes, we could speculate that PTM plays a huge role in the maintenance of doublet microtubule structure. We show that the αK40 loop is flexible enough to interact and stabilize binding with MIPs and lower energy to stabilize the whole cilia. In addition, the level of PTMs in cilia could be subject to a balancing or compensatory mechanism to maintain ciliary stability and carry out ciliary functions. We have a reason to find other PTMs in the cilia because previous studies have found that the K40R mutant tubulins behave slightly differently from acetylated WT tubulins. Akella et al. (2010) show using 2D SDS–PAGE that MEC-17-KO α-tubulin isoforms are more basic than wild-type isoforms. In the future, additional research is needed to confirm the structural and proteomic effect of acetylation via double or triple PTM mutants (such as polyglutamylation and glycylation) in *Tetrahymena*. These new mutants may also help us examine this crosstalk between different types of PTM in the cilia and how they could compensate or balance to affect cilia's function, and if tubulin lattice alteration is a universal mechanism to control

PTM. Our study would pave the way for future research on the complex effects of PTM in cilia to analyze human diseases.

4.4 Master Reference List (Introduction, Chapter 1 & 4)

Afshar, G., & Murnane, J. P. (1999). Characterization of a human gene with sequence homology to Saccharomyces cerevisiae SIR2. *Gene, 24*(234), 161-168. doi:10.1016/s0378-1119(99)00162-6

Ahdab-Barmada, M., & Claassen, D. (1990). A distinctive triad of malformations of the central nervous system in the Meckel-Gruber syndrome. *J Neuropathol Exp Neurol., 49*(6), 610-620. doi:10.1097/00005072-199011000-00007

Ahmed, N. T., Gao C - Lucker, B. F., Bf., L., Cole, D. G., Dg., C., Mitchell, D. R., & Mitchell, D. R. (2008). ODA16 aids axonemal outer row dynein assembly through an interaction with the intraflagellar transport machinery. *J Cell Biol, 183*(313-22), 313-322. doi:10.1083/jcb.200802025

Akella, J. S., D., W., Kim, J., Starostina, N. G., Lyons-Abbott, S., Morrissette, N. S., . . . Gaertig, J. (2010). MEC-17 is an alpha-tubulin acetyltransferase. *Nature, 467*(7312), 218-222. doi:10.1038/nature09324

Alper, J. D., Decker, F., Agana, B., & Howard, J. (2014). The motility of axonemal dynein is regulated by the tubulin code. *Biophys J., 107*(12), 2872-2880. doi:10.1016/j.bpj.2014.10.061

Arce, C. A., & Barra, H. S. (1983). Association of tubulinyl-tyrosine carboxypeptidase with microtubules. *FEBS Lett., 157*(1), 75-78. doi:10.1016/0014-5793(83)81119-3

Arts, H. H., Bongers, E. M. H. F., Mans, D. A., van Beersum, S. E. C., Oud, M. M., Bolat, E., . . . Roepman, R. (2011). C14ORF179 encoding IFT43 is mutated in Sensenbrenner syndrome. *Journal of Medical Genetics, 48*(6), 390. doi:10.1136/jmg.2011.088864

Austin-Tse, C., J, H., Zariwala, M. A., Gilberti, R. M., Gee, H. Y., Hellman, N., . . . Hildebrandt, F. (2013). Zebrafish Ciliopathy Screen Plus Human Mutational Analysis Identifies C21orf59 and CCDC65 Defects as Causing Primary Ciliary Dyskinesia. *Am J Hum Genet., 93*(4), 672-686. doi:10.1016/j.ajhg.2013.08.015

B., H., Piperno, G., & Luck, D. J. (1979). Paralyzed flagella mutants of Chlamydomonas reinhardtii. Defective for axonemal doublet microtubule arms. *J Biol Chem, 254*(8), 3091-3099.

Baala, L., Romano, S., Khaddour, R., Saunier, S., Smith, U. M., Audollent, S., . . . Attie-Bitach, T. (2007). The Meckel-Gruber syndrome gene, MKS3, is mutated in Joubert syndrome. *American journal of human genetics, 80*(1), 186-194. doi:10.1086/510499

Backer, C. B., Gutzman Jh - Pearson, C. G., Pearson Cg - Cheeseman, I. M., & Cheeseman, I. M. (2012). CSAP localizes to polyglutamylated microtubules and promotes proper cilia function and zebrafish development. *Mol Biol Cell.*

Backer, C. B., Gutzman, J. H., Pearson, C. G., & Cheeseman, I. M. (2012). CSAP localizes to polyglutamylated microtubules and promotes proper cilia function and zebrafish development. *Molecular Biology of the Cell 23*(11), 2122-2130. doi:10.1091/mbc.e11-11-0931

Bangs, F. K., Schrode, N., Hadjantonakis, A. K., & Anderson, K. V. (2015). Lineage specificity of primary cilia in the mouse embryo. *Nat Cell Biol., 17*(2), 113-122. doi:10.1038/ncb3091

Barber, C. F., Heuser, T., Carbajal-González, B. I., Botchkarev, V. V., & Nicastro, D. (2011). Three-dimensional structure of the radial spokes reveals heterogeneity and interactions

with dyneins in Chlamydomonas flagella. *Molecular Biology of the Cell, 23*(1), 111-120. doi:10.1091/mbc.e11-08-0692

Barker, A. R., Thomas, R., & Dawe, H. R. (2014). Meckel-Gruber syndrome and the role of primary cilia in kidney, skeleton, and central nervous system development. *Organogenesis, 10*(1), 96-107. doi:10.4161/org.27375

Benzing, T., P., G., K., H., Hildebrandt, F., Kim, E., & Walz, G. (2001). Nephrocystin interacts with Pyk2, p130(Cas), and tensin and triggers phosphorylation of Pyk2. *Proc Natl Acad Sci USA, 98*(17), 9784-9789. doi:10.1073/pnas.171269898

Benzing, T., & Walz, G. (2008). Chapter 8 - Pathogenesis of Nephronophthisis and Medullary Cystic Kidney Disease. In D. B. Mount & M. R. Pollak (Eds.), *Molecular and Genetic Basis of Renal Disease* (pp. 131-140). Philadelphia: W.B. Saunders.

Berbari, N. F., N., S., Malarkey, E. B., Pieczynski, J. N., Boddu, R., Gaertig, J., . . . Yoder, B. K. (2013). Microtubule modifications and stability are altered by cilia perturbation and in cystic kidney disease. *Cytoskeleton (Hoboken), 70*(1), 24-31. doi:10.1002/cm.21088

Bergmann, C., M, F., Brüchle, N. O., Frank, V., Olbrich, H., Kirschner, J., . . . Omran, H. (2008). Loss of nephrocystin-3 function can cause embryonic lethality, Meckel-Gruber-like syndrome, situs inversus, and renal-hepatic-pancreatic dysplasia. *American journal of human genetics, 82*(4), 959-970. doi:10.1016/j.ajhg.2008.02.017

Bessen , M., Fay , R., & Witman , G. (1980). Calcium control of waveform in isolated flagellar axonemes of chlamydomonas. *Journal of Cell Biology, 86*(2), 446-455. doi:10.1083/jcb.86.2.446

Blackwell, R., Sweezy-Schindler, O., Edelmaier, C., Gergely, Z. R., Flynn, P. J., Montes, S., . . . Betterton, M. D. (2017). Contributions of Microtubule Dynamic Instability and Rotational Diffusion to Kinetochore Capture. *Biophysical Journal, 112*(3), 552-563. doi:10.1016/j.bpj.2016.09.006

Boddaert, N., Klein O - Ferguson, N., Ferguson N - Sonigo, P., Sonigo P - Parisot, D., Parisot D - Hertz-Pannier, L., Hertz-Pannier L - Baraton, J., . . . Brunelle, F. (2003). Intellectual prognosis of the Dandy-Walker malformation in children: the importance of vermian lobulation. *Neuroradiology, 45*(5), 320-324. doi:10.1007/s00234-003-0980-6

Bosch Grau, M., G, G. C., Rocha, C., Magiera, M. M., Marques Sousa, P., Giordano, T., . . . Janke, C. (2013). Tubulin glycylases and glutamylases have distinct functions in stabilization and motility of ependymal cilia. *J Cell Biol, 202*(3), 441-451.

Bosch Grau, M., Masson, C., Gadadhar, S., Rocha, C., Tort, O., Marques Sousa, P. V., S., . . . Janke, C. (2017). Alterations in the balance of tubulin glycylation and glutamylation in photoreceptors leads to retinal degeneration. *J Cell Sci, 130*(5), 938-949. doi:10.1242/jcs.199091

Boucher, C., & Sandford, R. (2004). Autosomal dominant polycystic kidney disease (ADPKD, MIM 173900, PKD1 and PKD2 genes, protein products known as polycystin-1 and polycystin-2). *European Journal of Human Genetics, 12*(5), 347-354. doi:10.1038/sj.ejhg.5201162

Bowman, A. B., Rs, P.-K., Benashski, S. E., McCaffery, J. M., Goldstein, L. S., & King, S. M. (1999). Drosophila roadblock and Chlamydomonas LC7: a conserved family of dynein-associated proteins involved in axonal transport, flagellar motility, and mitosis. *J Cell Biol, 146*(1), 165-180. Retrieved from https://www.ncbi.nlm.nih.gov/pubmed/10402468

Brokaw, C. J. (1975). Molecular mechanism for oscillation in flagella and muscle. *Proceedings of the National Academy of Sciences, 72*(8), 3102. doi:10.1073/pnas.72.8.3102

Brokaw, C. J. (2009). Thinking about flagellar oscillation. *Cell Motility, 66*(8), 425-436. doi:https://doi.org/10.1002/cm.20313

Brokaw, C. J., & Kamiya, R. (1987). Bending patterns of Chlamydomonas flagella: IV. Mutants with defects in inner and outer dynein arms indicate differences in dynein arm function. *Cell Motil Cytoskeleton, 8*(1), 68-75. doi:10.1002/cm.970080110

Brouhard, G., & Sept, D. (2012). Microtubules: Sizing Up the GTP Cap. *Current Biology, 22*(18), R802-R803. doi:https://doi.org/10.1016/j.cub.2012.07.050

Bui, K. H., H, S., Movassagh, T., Oiwa, K., & Ishikawa, T. (2008). Molecular architecture of inner dynein arms in situ in Chlamydomonas reinhardtii flagella. *J Cell Biol, 183*(5), 923-932. doi:10.1083/jcb.200808050

Bui, K. H., Yagi, T., Yamamoto, R., Kamiya, R., & Ishikawa, T. (2012). Polarity and asymmetry in the arrangement of dynein and related structures in the Chlamydomonas axoneme. *Journal of Cell Biology, 198*(5), 913-925. doi:10.1083/jcb.201201120

Burgess, S. A., Da, C., Dover, S. D., & Woolley, D. M. (1991). The inner dynein arm complex: compatible images from freeze-etch and thin section methods of microscopy. *J Cell Sci, 100*, 319-328. doi:10.1242/jcs.100.2.319

Burgess, S. A., Ml, W., Sakakibara, H., Knight, P. J., & Oiwa, K. (2003). Dynein structure and power stroke. *Nature, 421*(6924), 715-718. doi:10.1038/nature01377

Bustamante-Marin, M., X., & Ostrowski, L. E. (2017). Cilia and Mucociliary Clearance. *Cold Spring Harbor perspectives in biology, 9*(4), a028241. doi:10.1101/cshperspect.a028241

Campbell, P. K., Waymire, K. G., Heier, R. L., Sharer, C., Day, D. E., Reimann, H., . . . MacGregor, G. R. (2002). Mutation of a novel gene results in abnormal development of spermatid flagella, loss of intermale aggression and reduced body fat in mice. *Genetics, 162*(1), 307-320. doi:10.1093/genetics/162.1.307

Caron, J. M. (1997). Posttranslational modification of tubulin by palmitoylation: I. In vivo and cell-free studies. *Mol Biol Cell., 8*(4), 621-636. doi:10.1091/mbc.8.4.621

Cassidy-Hanley, D. M. (2012). Tetrahymena in the laboratory: strain resources, methods for culture, maintenance, and storage. *Methods in Cell Biology, 109*, 237-276. doi:10.1016/B978-0-12-385967-9.00008-6

Chang, B., H, K., Hawes, N., Jimeno, D., He, S., Lillo, C., . . . Swaroop, A. (2006). In-frame deletion in a novel centrosomal/ciliary protein CEP290/NPHP6 perturbs its interaction with RPGR and results in early-onset retinal degeneration in the rd16 mouse. *Hum Mol Genet, 15*(11), 1847-1857. doi:10.1093/hmg/ddl107

Chang, C. F., & Serra, R. (2013). Ift88 regulates Hedgehog signaling, Sfrp5 expression, and β-catenin activity in post-natal growth plate. *J Orthop Res, 31*(3), 350-356. doi:10.1002/jor.22237

Chekuri, A., Guru, A. A., Biswas, P., Branham, K., Borooah, S., Soto-Hermida, A., . . . Ayyagari, R. (2018). IFT88 mutations identified in individuals with non-syndromic recessive retinal degeneration result in abnormal ciliogenesis. *Hum Genet, 137*(6-7), 447-458. doi:10.1007/s00439-018-1897-9

Coombes, C., Yamamoto, A., McClellan, M., Reid, T. A., Plooster, M., Luxton, G. W. G., . . . Gardner, M. K. (2016). Mechanism of microtubule lumen entry for the α-tubulin acetyltransferase enzyme αTAT1. *Proceedings of the National Academy of Sciences, 113*(46), E7176. doi:10.1073/pnas.1605397113

Corbit, K. C., Aanstad, P., Singla, V., Norman, A. R., Stainier, D. Y. R., & Reiter, J. F. (2005). Vertebrate Smoothened functions at the primary cilium. *Nature, 437*(7061), 1018-1021. doi:10.1038/nature04117

Craft Van De Weghe, J., Harris, J. A., Kubo, T., Witman, G. B., & Lechtreck, K. F. (2020). Diffusion rather than intraflagellar transport likely provides most of the tubulin required for axonemal assembly in Chlamydomonas. *J Cell Sci, 133*(17), jcs249805.

Cruz, C., V., R., Kutejova, E., Cayuso, J., Lawson, V., Stevens, J., . . . Briscoe, J. (2010). Foxj1 regulates floor plate cilia architecture and modifies the response of cells to sonic hedgehog signalling. *Development, 137*(24), 4271-4282. doi:10.1242/dev.051714

Csaba, G., Kovács P - Pállinger, E., & Pállinger, E. (2004). Presence and localization of epidermal growth factor (EGF)- and EGF-receptor-like immunoreactivity in Tetrahymena. *Cell Biol Int, 28*(7), 491-496. doi:10.1016/j.cellbi.2004.04.002

Cueva, J. G., J., H., & Huang, K. C. G., Miriam B. (2012). Posttranslational acetylation of α-tubulin constrains protofilament number in native microtubules. *Curr Biol, 22*(12), 1066-1074. doi:10.1016/j.cub.2012.05.012

D.R., M., & Rosenbaum, J. L. (1985). A motile Chlamydomonas flagellar mutant that lacks outer dynein arms. *J Cell Biol, 100*(4), 1228-1234.

Dafinger, C., Liebau, M. C., Elsayed, S. M., Hellenbroich, Y., Boltshauser, E., Korenke, G. C., . . . Bolz, H. J. (2011). Mutations in KIF7 link Joubert syndrome with Sonic Hedgehog signaling and microtubule dynamics. *J Clin Invest, 121*(7), 2662-2667. doi:10.1172/JCI43639

De Robertis, E. (1956). Morphogenesis of the retinal rods; an electron microscope study. *J Biophys Biochem Cytol., 2*(4 Suppl), 209-218. doi:D - CLML: 5731:3597 OTO - NLM

De Robertis, E. (1960). Some observations on the ultrastructure and morphogenesis of photoreceptors. *J Gen Physiol., 43*(6), 1-13.

Dehmelt, L., & Halpain, S. (2005). The MAP2/Tau family of microtubule-associated proteins. *Genome Biol, 6*(1), 204. doi:10.1186/gb-2004-6-1-204

Delous, M., L., B., Salomon, R., Laclef, C., Vierkotten, J., Tory, K., . . . Saunier, S. (2007). The ciliary gene RPGRIP1L is mutated in cerebello-oculo-renal syndrome (Joubert syndrome type B) and Meckel syndrome. *Nat Genet, 39*(7), 875-881. doi:10.1038/ng2039

Dishinger, J. F., H.I., K., Jenkins, P. M., Fan, S., Hurd, T. W., Hammond, J. W., . . . Verhey, K. J. (2010). Ciliary entry of the kinesin-2 motor KIF17 is regulated by importin-beta2 and RanGTP. *Nat Cell Biol, 12*(7), 703-710.

Djenoune, L., & Wyart, C. (2017). Light on a sensory interface linking the cerebrospinal fluid to motor circuits in vertebrates. *J Neurogenet, 31*(3), 113-127. doi:10.1080/01677063.2017.1359833

Doolin, P. F., & Birge, W. J. (1966). Ultrastructural organization of cilia and basal bodies of the epithelium of the choroid plexus in the chick embryo. *The Journal of Cell Biology, 29*(2), 333-345. doi:10.1083/jcb.29.2.333

Drechsel, D. N., & Kirschner, M. W. (1994). The minimum GTP cap required to stabilize microtubules. *Curr Biol, 4*(12), 1053-1061. doi:10.1016/s0960-9822(00)00243-8

Drivas, T. G., Holzbaur, E. L. F., & Bennett, J. (2013). Disruption of CEP290 microtubule/membrane-binding domains causes retinal degeneration. *J Clin Invest, 123*(10), 4525-4539. doi:10.1172/JCI69448

Du, Y., Seibenhener, M. L., Yan, J., Jiang, J., & Wooten, M. C. (2015). aPKC phosphorylation of HDAC6 results in increased deacetylation activity. *PLOS ONE, 10*(4), e0123191. doi:10.1371/journal.pone.0123191

Duan, J., & Gorovsky, M. A. (2002). Both carboxy-terminal tails of alpha- and beta-tubulin are essential, but either one will suffice. *Curr Biol, 12*(4), 313-316. doi:10.1016/S0960-9822(02)00651-6

DuJardin, F. (1841). *Histoire Naturelle des Zoophytes (Infusoires).* Roret, Paris.

Dummer, A., Poelma, C., DeRuiter, M. C., Goumans, M.-J. T. H., & Hierck, B. P. (2016). Measuring the primary cilium length: improved method for unbiased high-throughput analysis. *Cilia, 5*(1), 7. doi:10.1186/s13630-016-0028-2

Duquesnoy, P., Estelle, E., Vincensini, L., Freshour, J., Bridoux, A.-M., Coste, A., . . . Amselem, S. (2009). Loss-of-function mutations in the human ortholog of Chlamydomonas reinhardtii ODA7 disrupt dynein arm assembly and cause primary ciliary dyskinesia. *American journal of human genetics, 85*(6), 890-896. doi:10.1016/j.ajhg.2009.11.008

Dymek, E. E., Lin, J., Fu, G., Porter, M. E., Nicastro, D., & Smith, E. F. (2019). PACRG and FAP20 form the inner junction of axonemal doublet microtubules and regulate ciliary motility. *Mol Biol Cell, 30*(15), 1805-1816. doi:10.1091/mbc.E19-01-0063

Economou, A., & Katsetos, C. D. (2012). Patterns of cognitive and fine motor deficits in a case of Dandy-Walker continuum. *J Child Neurol, 27*(7), 930-937. doi:10.1177/0883073811429500

Eddé, B., J, R., Le Caer, J. P., Desbruyères, E., Gros, F., & Denoulet, P. (1990). Posttranslational glutamylation of alpha-tubulin. *Science, 247*(4938), 83-85. doi:10.1126/science.1967194

Elam, C. A., Wirschell, M., Yamamoto, R., Fox, L. A., York, K., Kamiya, R., . . . Sale, W. S. (2011). An axonemal PP2A B-subunit is required for PP2A localization and flagellar motility. *Cytoskeleton (Hoboken), 68*(7), 363-372. doi:10.1002/cm.20519

Erck, C., Peris, L., Andrieux, A., Meissirel, C., Gruber, A. D., Vernet, M., . . . Wehland, J. (2005). A vital role of tubulin-tyrosine-ligase for neuronal organization. *Proceedings of the National Academy of Sciences, 102*(22), 7853. doi:10.1073/pnas.0409626102

Ersfeld, K., J, W., Plessmann, U., Dodemont, H., Gerke, V., & Weber, K. (1993). Characterization of the tubulin-tyrosine ligase. *J Cell Biol., 120*(3), 725-732. doi:10.1083/jcb.120.3.725

Eshun-Wilson, L., Zhang, R., Portran, D., Nachury, M. V., Toso, D. B., Löhr, T., . . . Nogales, E. (2019). Effects of α-tubulin acetylation on microtubule structure and stability. *Proceedings of the National Academy of Sciences, 116*(21), 10366. doi:10.1073/pnas.1900441116

Esteves, A. R., Palma, A. M., Gomes, R., Santos, D., Silva, D. F., & Cardoso, S. M. (2019). Acetylation as a major determinant to microtubule-dependent autophagy: Relevance to Alzheimer's and Parkinson disease pathology. *Biochimica et Biophysica Acta (BBA) - Molecular Basis of Disease, 1865*(8), 2008-2023. doi:https://doi.org/10.1016/j.bbadis.2018.11.014

Failly, M., A, S., Muñoz, A., Falconnet, E., Rossier, C., Santamaria, F., . . . Blouin, J.-L. (2008). DNAI1 mutations explain only 2% of primary ciliary dykinesia. *Respiration, 76*(2), 198-204. doi:10.1159/000128567

Failly, M., L, B., Letourneau, A., Munoz, A., Falconnet, E., Rossier, C., . . . Blouin, J. L. (2009). Mutations in DNAH5 account for only 15% of a non-preselected cohort of patients with primary ciliary dyskinesia. *J Med Genet, 120*(3), 725-732. doi:10.1136/jmg.2008.061176

Fourest-Lieuvin, A., L, P., Gache, V., Garcia-Saez, I., Juillan-Binard, C., Lantez, V., & Job, D. (2006). Microtubule regulation in mitosis: tubulin phosphorylation by the cyclin-dependent kinase Cdk1. *Mol Biol Cell., 17*(3), 1041-1050. doi:10.1091/mbc.e05-07-0621

Fowkes, M. E., & Mitchell, D. R. (1998). The role of preassembled cytoplasmic complexes in assembly of flagellar dynein subunits. *Mol Biol Cell, 9*(9), 2337-2347. doi:10.1091/mbc.9.9.2337

Frye, R. A. (1999). Characterization of five human cDNAs with homology to the yeast SIR2 gene: Sir2-like proteins (sirtuins) metabolize NAD and may have protein ADP-ribosyltransferase activity. *Biochem Biophys Res Commun, 260*(1), 273-279. doi:DOI 10.1006/bbrc.1999.0897

Fukushige, T., Hendzel, M. J., Bazett-Jones, D. P., & McGhee, J. D. (1999). Direct visualization of the elt-2 gut-specific GATA factor binding to a target promoter inside the living Caenorhabditis elegans embryo. *Proc Natl Acad Sci U S A, 96*(21), 11883-11888. doi:10.1073/pnas.96.21.11883

G., P., LeDizet, M., & Chang, X. J. (1987). Microtubules containing acetylated alpha-tubulin in mammalian cells in culture. *J Cell Biol, 104*(2), 289-302.

G.J., P., Agrin, N., Walker, B. L., & Witman, G. B. (2006). Identification of predicted human outer dynein arm genes: candidates for primary ciliary dyskinesia genes. *J Med Genet, 43*(1), 62-73.

Gadadhar, S., Viar, G. A., Hansen, J. N., Gong, A., Kostarev, A., Ialy-Radio, C., . . . Janke, C. (2021). Tubulin glycylation controls axonemal dynein activity, flagellar beat, and male fertility. *Science, 371*(6525), eabd4914. doi:doi:10.1126/science.abd4914

Gaertig, J., Ma, C., Bowen, J., Gu, L., Pennock, D. G., & Gorovsky, M. A. (1995). Acetylation of lysine 40 in alpha-tubulin is not essential in Tetrahymena thermophila. *J Cell Biol., 129*(5), 1301-1310.

Garnham, C. P., & Roll-Mecak, A. (2012). The chemical complexity of cellular microtubules: tubulin post-translational modification enzymes and their roles in tuning microtubule functions. *Cytoskeleton (Hoboken), 69*(7), 442-463. doi:10.1002/cm.21027

Gee, M. A., Heuser Je - Vallee, R. B., & Vallee, R. B. (1997). An extended microtubule-binding structure within the dynein motor domain. *Nature, 390*(6660), 636-639. doi:Doi 10.1038/37663

Gibbons, I. R. (1963). STUDIES ON THE PROTEIN COMPONENTS OF CILIA FROM TETRAHYMENA PYRIFORMIS. *Proc Natl Acad Sci U S A., 50*(5), 1002-1010. doi:10.1073/pnas.50.5.1002

Gibbons, I. R., & Rowe, A. J. (1965). Dynein: A Protein with Adenosine Triphosphatase Activity from Cilia. *Science, 149*(3682), 424-426.

Gilissen, C., Arts, H. H., Hoischen, A., Spruijt, L., Mans, D. A., Arts, P., . . . Brunner, H. G. (2010). Exome sequencing identifies WDR35 variants involved in Sensenbrenner syndrome. *American journal of human genetics, 87*(3), 418-423. doi:10.1016/j.ajhg.2010.08.004

Gilley, S. K., Ae, S., Pasek, R. C., Sas, K. M., Steele, S. L., Amria, M., . . . Bell, P. D. (2014). Deletion of airway cilia results in noninflammatory bronchiectasis and hyperreactive airways. *Am J Physiol Lung Cell Mol Physiol, 306*(2), L162-169. doi:10.1152/ajplung.00095.2013

Goetz, S. C., & Anderson, K. V. (2010). The primary cilium: a signalling centre during vertebrate development. *Nat Rev Genet, 11*(5), 331-344. doi:10.1038/nrg2774

Gui, L., Song, K., Tritschler, D., Bower, R., Yan, S., Dai, A., . . . Nicastro, D. (2019). Scaffold subunits support associated subunit assembly in the Chlamydomonas ciliary nexin-dynein regulatory complex. *Proceedings of the National Academy of Sciences, 116*(46), 23152. doi:10.1073/pnas.1910960116

Gui, M., Farley, H., Anujan, P., Anderson, J. R., Maxwell, D. W., Whitchurch, J. B., . . . Brown, A. (2021). De novo identification of mammalian ciliary motility proteins using cryo-EM. *Cell, 184*(23), 5791-5806.e5719. doi:https://doi.org/10.1016/j.cell.2021.10.007

Gui, M., Ma, M., Sze-Tu, E., Wang, X., Koh, F., Zhong, E. D., . . . Brown, A. (2021). Structures of radial spokes and associated complexes important for ciliary motility. *Nature Structural & Molecular Biology, 28*(1), 29-37. doi:10.1038/s41594-020-00530-0

H., M., K., G., & Rosenbaum, J. L. (1986). The acetylation of alpha-tubulin and its relationship to the assembly and disassembly of microtubules. *J Cell Biol, 103*(2), 571-579.

Habura, A., I, T., Chisholm, R. L., & Koonce, M. P. (1999). Interaction mapping of a dynein heavy chain. Identification of dimerization and intermediate-chain binding domains. *J Biol Chem, 274*(22), 15447-15453. doi:10.1074/jbc.274.22.15447

Hammond, J. W., Cf, H., Kaech, S., Jacobson, C., Banker, G., & Verhey, K. J. (2010). Posttranslational modifications of tubulin and the polarized transport of kinesin-1 in neurons. *Mol Biol Cell, 21*(4), 572-583. doi:10.1091/mbc.E09-01-0044

Hao, K., Chen, Y., Yan, X., & Zhu, X. (2021). Cilia locally synthesize proteins to sustain their ultrastructure and functions. *Nature Communications, 12*(1), 6971-6971. doi:10.1038/s41467-021-27298-1

Harrison, A., P, O.-C., & King, S. M. (1998). Identification of the t complex-encoded cytoplasmic dynein light chain tctex1 in inner arm I1 supports the involvement of flagellar dyneins in meiotic drive. *J Cell Biol, 140*(5), 1137-1147. doi:10.1083/jcb.140.5.1137

Haycraft, C. J., Banizs, B., Aydin-Son, Y., Zhang, Q., Michaud, E. J., & Yoder, B. K. (2005). Gli2 and Gli3 localize to cilia and require the intraflagellar transport protein polaris for processing and function. *PLoS genetics, 1*(4), e53-e53. doi:10.1371/journal.pgen.0010053

He, K., Ling, K., & Hu, J. (2020). The emerging role of tubulin posttranslational modifications in cilia and ciliopathies. *Biophysics Reports, 6*(4), 89-104. doi:10.1007/s41048-020-00111-0

Heuser, T., M, R., Krell, J., Porter, M. E., & Nicastro, D. (2009). The dynein regulatory complex is the nexin link and a major regulatory node in cilia and flagella. *J Cell Biol, 187*(6), 921-933. doi:10.1083/jcb.200908067

Hill, P., B, W., & Rüther, U. (2007). The molecular basis of Pallister Hall associated polydactyly. *Hum Mol Genet, 16*(17), 2089-2096. doi:10.1093/hmg/ddm156

Hirokawa, N., Tanaka, Y., Okada, Y., & Takeda, S. (2006). Nodal Flow and the Generation of Left-Right Asymmetry. *Cell, 125*(1), 33-45. doi:10.1016/j.cell.2006.03.002

Hjeij, R., A, L., Francis, R., Zariwala, M. A., Liu, X., Li, Y., . . . Omran, H. (2013). ARMC4 mutations cause primary ciliary dyskinesia with randomization of left/right body asymmetry. *Am J Hum Genet., 93*(2), 357-367. doi:10.1016/j.ajhg.2013.06.009

Hjeij, R., Onoufriadis, A., Watson, C. M., Slagle, C. E., Klena, N. T., Dougherty, G. W., . . . Mitchison, H. M. (2014). CCDC151 mutations cause primary ciliary dyskinesia by disruption of the outer dynein arm docking complex formation. *American journal of human genetics, 95*(3), 257-274. doi:10.1016/j.ajhg.2014.08.005

Howes, S. C., GM, A., Shida, T., Nachury, M. V., & Nogales, E. (2014). Effects of tubulin acetylation and tubulin acetyltransferase binding on microtubule structure. *Mol Biol Cell, 25*(2), 257-266. doi:10.1091/mbc.E13-07-0387

Hu, Q., L, M., Jin, H., Scott, M. P., Nachury, M. V., & Spiliotis, E. T. (2010). A septin diffusion barrier at the base of the primary cilium maintains ciliary membrane protein distribution. *Science, 329*(5990), 436-439. doi:10.1126/science.1191054

Huang, K., Dr, D., & Rosenbaum, J. L. (2009). The ubiquitin conjugation system is involved in the disassembly of cilia and flagella. *J Cell Biol, 186*(4), 601-613. doi:10.1083/jcb.200903066

Huangfu, D., A, L., Rakeman, A. S., Murcia, N. S., Niswander, L., & Anderson, K. V. (2003). Hedgehog signalling in the mouse requires intraflagellar transport proteins. *Nature, 502*(7470), 194-200. doi:10.1038/nature02061

Huangfu, D., & Anderson, K. V. (2005). Cilia and Hedgehog responsiveness in the mouse. *Proceedings of the National Academy of Sciences of the United States of America, 102*(32), 11325. doi:10.1073/pnas.0505328102

Hubbert, C., A., G., Shao, R., Kawaguchi, Y., Ito, A., Nixon, A., . . . Yao, T.-P. (2002). HDAC6 is a microtubule-associated deacetylase. *Nature, 417*(6887), 455-458. doi:DOI 10.1038/417455a

I, A., Curless, R. G., Holzman, B. H., Aballi, A. J., Ajmone-Marsan, C., Caram, I., & Lopez, P. F. (1985). Computerized tomography and electroencephalography in childhood coma: which test should be performed first? *J Fla Med Assoc., 72*(10), 843-845.

Ichikawa, M., Khalifa, A. A. Z., Kubo, S., Dai, D., Basu, K., Maghrebi, M. A. F., . . . Bui, K. H. (2019). Tubulin lattice in cilia is in a stressed form regulated by microtubule inner proteins. *Proceedings of the National Academy of Sciences, 116*(40), 19930-19938. doi:10.1073/pnas.1911119116

Ichikawa, M., Liu, D., Kastritis, P. L., Basu, K., Hsu, T. C., Yang, S., & Bui, K. H. (2017). Subnanometre-resolution structure of the doublet microtubule reveals new classes of microtubule-associated proteins. *Nature Communications, 8*(1), 15035. doi:10.1038/ncomms15035

Ikegami, K., D., H., Mukai, M., Livnat, I., MacGregor, G. R., & Setou, M. (2008). TTLL10 is a protein polyglycylase that can modify nucleosome assembly protein 1. *FEBS Lett, 582*(7), 1129-1134. doi:10.1016/j.febslet.2008.02.079

Ikegami, K., Heier, R. L., Taruishi, M., Takagi, H., Mukai, M., Shimma, S., . . . Setou, M. (2007). Loss of α-tubulin polyglutamylation in ROSA22 mice is associated with abnormal targeting of KIF1A and modulated synaptic function. *Proceedings of the National Academy of Sciences, 104*(9), 3213. doi:10.1073/pnas.0611547104

Ikegami, K., Sato S - Nakamura, K., Nakamura K - Ostrowski, L. E., Ostrowski Le - Setou, M., & Setou, M. (2010). Tubulin polyglutamylation is essential for airway ciliary function through the regulation of beating asymmetry. *Proc Natl Acad Sci U S A, 107*(23), 10490-10495. doi:10.1073/pnas.1002128107

Ikegami, K., & Setou, M. (2009). TTLL10 can perform tubulin glycylation when co-expressed with TTLL8. *FEBS Lett, 583*(12), 1957-1963. doi:10.1016/j.febslet.2009.05.003

Ingolia, N. T., Lf, L., & Weissman, J. S. (2011). Ribosome profiling of mouse embryonic stem cells reveals the complexity and dynamics of mammalian proteomes. *Cell, 147*(4), 789-802. doi:10.1016/j.cell.2011.10.002

Ishikawa, H., & Marshall, W. F. (2017). Intraflagellar Transport and Ciliary Dynamics. *Cold Spring Harb Perspect Biol., 9*(3), a021998. doi:10.1101/cshperspect.a021998

Ishikawa, H., Thompson, J., Yates, John R., & Marshall, Wallace F. (2012). Proteomic Analysis of Mammalian Primary Cilia. *Current Biology, 22*(5), 414-419. doi:https://doi.org/10.1016/j.cub.2012.01.031

Ishikawa, T. (2015). Cryo-electron tomography of motile cilia and flagella. *Cilia, 4*(1), 3. doi:10.1186/s13630-014-0012-7

Janke, C., K, R., & van Dijk, J. (2008). Polyglutamylation: a fine-regulator of protein function? 'Protein Modifications: beyond the usual suspects' review series. *EMBO Rep, 9*(7), 636-641.

Janke, C., K, R., Wloga, D., Regnard, C., Kajava, A. V., Strub, J.-M., . . . Eddé, B. (2005). Tubulin polyglutamylase enzymes are members of the TTL domain protein family. *Science, 308*(5729), 1758-1762. doi:10.1126/science.1113010

Jensen, V. L., Li, C., Bowie, R. V., Clarke, L., Mohan, S., Blacque, O. E., & Leroux, M. R. (2015). Formation of the transition zone by Mks5/Rpgrip1L establishes a ciliary zone of exclusion (CIZE) that compartmentalises ciliary signalling proteins and controls PIP2 ciliary abundance. *The EMBO Journal, 34*(20), 2537-2556. doi:https://doi.org/10.15252/embj.201488044

Jin, H., S.R., W., Shida, T., Schulz, S., Aguiar, M., Gygi, S. P., . . . Nachury, M. V. (2010). The conserved Bardet-Biedl syndrome proteins assemble a coat that traffics membrane proteins to cilia. *Cell, 141*(7), 1208-1219. doi:10.1016/j.cell.2010.05.015

Johnson, K. A. (1998). The axonemal microtubules of the Chlamydomonas flagellum differ in tubulin isoform content. *J Cell Sci, 111*, 313-320. doi:10.1242/jcs.111.3.313

Jordan, M. A., & Pigino, G. (2019). Chapter 9 - In situ cryo-electron tomography and subtomogram averaging of intraflagellar transport trains. In T. Müller-Reichert & G. Pigino (Eds.), *Methods in Cell Biology* (Vol. 152, pp. 179-195): Academic Press.

Kalebic, N., S., S., Perlas, E., Bolasco, G., Martinez, C., & Heppenstall, P. A. (2013). αTAT1 is the major α-tubulin acetyltransferase in mice. *Nat Commun, 4*, 1962.

Kamiya, R., & Okamoto, M. (1985). A mutant of Chlamydomonas reinhardtii that lacks the flagellar outer dynein arm but can swim. *Journal of Cell Science, 74*(1), 181-191. doi:10.1242/jcs.74.1.181

Kang, S., Jr, G. J. M., Olney, A. H., & Biesecker, L. G. (1997). GLI3 frameshift mutations cause autosomal dominant Pallister-Hall syndrome. *Nat Genet., 15*(3), 266-268. doi:10.1038/ng0397-266

Kaul, N., Soppina, V., & Verhey, K. J. (2014). Effects of α-tubulin K40 acetylation and detyrosination on kinesin-1 motility in a purified system. *Biophys J., 106*(12), 2636-2643. doi:10.1016/j.bpj.2014.05.008

Khalifa, A. A. Z., Ichikawa, M., Dai, D., Kubo, S., Black, C.S., Peri, K., McAlear, T.S., Veyron, S., Yang, S.K., Vargas, J., Bechstedt, S., Trempe, J., Bui., K.H. . (2020). The inner junction complex of the cilia is an interaction hub that involves tubulin post-translational modifications. *Elife, 9*, e52760.

Khanna, H. (2015). Photoreceptor Sensory Cilium: Traversing the Ciliary Gate. *Cell, 4*(4), 674-686. doi:10.3390/cells4040674

Ki, S. M., Kim, J. H., Won, S. Y., Oh, S. J., Lee, I. Y., Bae, Y. K., . . . Lee, J. E. (2020). CEP41-mediated ciliary tubulin glutamylation drives angiogenesis through AURKA-dependent deciliation. *EMBO Rep, 21*(2), e48290. doi:10.15252/embr.201948290

Kim, G. W., L., L., Ghorbani, M., You, L., & Yang, X.-J. (2013). Mice lacking α-tubulin acetyltransferase 1 are viable but display α-tubulin acetylation deficiency and dentate gyrus distortion. *J Biol Chem, 288*(28), 20334-20350. doi:10.1074/jbc.M113.464792

King, S. M. (2016). Axonemal Dynein Arms. *Cold Spring Harbor perspectives in biology, 8*(11), a028100. doi:10.1101/cshperspect.a028100

King, S. M., & Patel-King, R. S. (1995). The M(r) = 8,000 and 11,000 outer arm dynein light chains from Chlamydomonas flagella have cytoplasmic homologues. *J Biol Chem, 270*(19), 11445-11452.

Kinzel, D., K., B., Davis, E. E., Burtscher, I., Trümbach, D., Diplas, B., . . . Lickert, H. (2010). Pitchfork regulates primary cilia disassembly and left-right asymmetry. *Dev Cell, 19*(1), 66-77. doi:10.1016/j.devcel.2010.06.005

Knowles, M. R., L.E., O., Loges, N. T., Hurd, T., Leigh, M. W., Huang, L., . . . Zariwala, M. A. (2013). Mutations in SPAG1 cause primary ciliary dyskinesia associated with defective outer and inner dynein arms. *American journal of human genetics, 93*(4), 711-720. doi:10.1016/j.ajhg.2013.07.025

Knowles, M. R., M.W., L., Ostrowski, L. E., Huang, L., Carson, J. L., Hazucha, M. J., . . . Zariwala, M. A. (2013). Exome sequencing identifies mutations in CCDC114 as a cause of primary ciliary dyskinesia. *Am J Hum Genet., 92*(1), 99-106. doi:10.1016/j.ajhg.2012.11.003

Konno, A., Ikegami, K., Konishi, Y., Yang, H. J., Abe, M., Yamazaki, M., . . . Setou, M. (2016). Ttll9-/- mice sperm flagella show shortening of doublet 7, reduction of doublet 5 polyglutamylation and a stall in beating. *J Cell Sci, 129*(14), 2757-2766. doi:10.1242/jcs.185983

Kotsis, F., R, N., Boehlke, C., Bashkurov, M., Walz, G., & Kuehn, E. W. (2007). Ciliary calcium signaling is modulated by kidney injury molecule-1 (Kim1). *Pflugers Arch, 453*(3), 819-829. doi:10.1007/s00424-006-0168-0

Kott, E., P, D., Copin, B., Legendre, M., Dastot-Le Moal, F., Montantin, G., . . . Amselem, S. (2012). Loss-of-function mutations in LRRC6, a gene essential for proper axonemal assembly of inner and outer dynein arms, cause primary ciliary dyskinesia. *American journal of human genetics, 91*(5), 958-964. doi:10.1016/j.ajhg.2012.10.003

Kozminski, K. G., K.A., J., Forscher, P., & Rosenbaum, J. L. (1993). A motility in the eukaryotic flagellum unrelated to flagellar beating. *Proc Natl Acad Sci U S A, 90*(12), 5519-5523. doi:10.1073/pnas.90.12.5519

Kubo, T., Hirono, M., Aikawa, T., Kamiya, R., & Witman, G. B. (2015). Reduced tubulin polyglutamylation suppresses flagellar shortness in Chlamydomonas. *Mol Biol Cell, 26*(15), 2810-2822. doi:10.1091/mbc.E15-03-0182

Kubo, T., & Oda, T. (2017). Electrostatic interaction between polyglutamylated tubulin and the nexin–dynein regulatory complex regulates flagellar motility. *Molecular Biology of the Cell, 28*(17), 2260-2266. doi:10.1091/mbc.e17-05-0285

Kubo, T., Yanagisawa, H.-a., Yagi, T., Hirono, M., & Kamiya, R. (2010). Tubulin Polyglutamylation Regulates Axonemal Motility by Modulating Activities of Inner-Arm Dyneins. *Current Biology, 20*(5), 441-445. doi:https://doi.org/10.1016/j.cub.2009.12.058

Kyttälä, M., J., T., Salonen, R., Kopra, O., Kohlschmidt, N., Paavola-Sakki, P., . . . Kestilä, M. (2006). MKS1, encoding a component of the flagellar apparatus basal body proteome, is mutated in Meckel syndrome. *Nat Genet, 38*(2), 155-157.

Lacroix, B., van Dijk, J., Gold, N. D., Guizetti, J., Aldrian-Herrada, G., Rogowski, K., . . . Janke, C. (2010). Tubulin polyglutamylation stimulates spastin-mediated microtubule severing. *Journal of Cell Biology, 189*(6), 945-954. doi:10.1083/jcb.201001024

Lechtreck, K. F., & Geimer, S. (2000). Distribution of polyglutamylated tubulin in the flagellar apparatus of green flagellates. *Cell Motil Cytoskeleton, 47*(3), 219-235. doi:10.1002/1097-0169(200011)47:3<219::AID-CM5>3.0.CO;2-Q

LeDizet, M., & Piperno, G. (1995). The light chain p28 associates with a subset of inner dynein arm heavy chains in Chlamydomonas axonemes. *Mol Biol Cell., 6*(6), 697-711. doi:10.1091/mbc.6.6.697

Lee, G. S., Y., H., Dougherty, E. J., Jimenez-Movilla, M., Avella, M., Grullon, S., . . . Simons, S. S., Jr. (2013). Disruption of Ttll5/stamp gene (tubulin tyrosine ligase-like protein 5/SRC-1 and TIF2-associated modulatory protein gene) in male mice causes sperm malformation and infertility. *J Biol Chem, 288*(21), 15167-15180. doi:10.1074/jbc.M113.453936

Lee, J. E., Jl, S., Zaki, M. S., Schroth, J., Bielas, S. L., Marsh, S. E., . . . Gleeson, J. G. (2012). CEP41 is mutated in Joubert syndrome and is required for tubulin glutamylation at the cilium. *Nat Genet, 44*(2), 193-199. doi:10.1038/ng.1078

Lehti, M. S., & Sironen, A. (2017). Formation and function of sperm tail structures in association with sperm motility defects. *Biology of Reproduction, 97*(4), 522-536. doi:10.1093/biolre/iox096

Lesage, S., P, M., Lohmann, E., Lacomblez, L., Teive, H., Janin, S., . . . Brice, A. (2007). Deletion of the parkin and PACRG gene promoter in early-onset parkinsonism. *Hum Mutat. , 28*(1), 27-32. doi:10.1002/humu.20436

Li, G., R, V., Nelms, K., Gekakis, N., Goodnow, C., McNamara, P., . . . Glynne, R. (2007). A role for Alström syndrome protein, alms1, in kidney ciliogenesis and cellular quiescence. *PLoS Genet, 28*(1), 27-32. doi:10.1371/journal.pgen.0030008

Li, S., Fernandez, J.-J., Marshall, W. F., & Agard, D. A. (2012). Three-dimensional structure of basal body triplet revealed by electron cryo-tomography. *The EMBO Journal, 31*(3), 552-562. doi:https://doi.org/10.1038/emboj.2011.460

Liu, N., Xiong, Y., Li, S., Ren, Y., He, Q., Gao, S., . . . Shui, W. (2015). New HDAC6-mediated deacetylation sites of tubulin in the mouse brain identified by quantitative mass spectrometry. *Scientific Reports, 5*(1), 16869. doi:10.1038/srep16869

Liu, Y. X., Xue, B., Sun, W. Y., Wingfield, J. L., Sun, J., Wu, M., . . . Fan, Z. (2021). Bardet-Biedl syndrome 3 protein promotes ciliary exit of the signaling protein phospholipase D via the BBSome. *Elife, 10*, e59119. doi:10.7554/eLife.59119

Loges, N. T., H, O., Becker-Heck, A., Häffner, K., Heer, A., Reinhard, C., . . . Omran, H. (2009). Deletions and point mutations of LRRC50 cause primary ciliary dyskinesia due to dynein arm defects. *American journal of human genetics, 85*(6), 883-889. doi:10.1016/j.ajhg.2009.10.018

Loges, N. T., H, O., Fenske, L., Mussaffi, H., Horvath, J., Fliegauf, M., . . . Omran, H. (2008). DNAI2 mutations cause primary ciliary dyskinesia with defects in the outer dynein arm. *Am J Hum Genet., 83*(5), 547-558. doi:10.1016/j.ajhg.2008.10.001

Loktev, A. V., Q., Z., Beck, J. S., Searby, C. C., Scheetz, T. E., Bazan, J. F., . . . Nachury, M. V. (2008). A BBSome subunit links ciliogenesis, microtubule stability, and acetylation. *Dev Cell, 15*(6), 854-865. doi:10.1016/j.devcel.2008.11.001

Lorenzetti, D., Bishop, C. E., & Justice, M. J. (2004). Deletion of the Parkin coregulated gene causes male sterility in the quaking(viable) mouse mutant. *Proceedings of the National*

Academy of Sciences of the United States of America, 101(22), 8402. doi:10.1073/pnas.0401832101

M., L., & Piperno, G. (1986). Cytoplasmic microtubules containing acetylated alpha-tubulin in Chlamydomonas reinhardtii: spatial arrangement and properties. *J Cell Biol, 103*(1), 13-22.

M., L., & Piperno, G. (1987). Identification of an acetylation site of Chlamydomonas alpha-tubulin. *Proc Natl Acad Sci U S A, 84*(16), 5720-5724.

Ma, M., Stoyanova, M., Rademacher, G., Dutcher, S. K., Brown, A., & Zhang, R. (2019). Structure of the Decorated Ciliary Doublet Microtubule. *Cell, 179*(4), 909-922.e912. doi:https://doi.org/10.1016/j.cell.2019.09.030

Magiera, M., Bodakuntla, S., Žiak, J., Lacomme, S., Marques Sousa, P., Leboucher, S., . . . Janke, C. (2018). Excessive tubulin polyglutamylation causes neurodegeneration and perturbs neuronal transport. *EMBO J, 37*(23), e100440. doi:10.15252/embj.2018100440

Magiera, M. M., & Janke, C. (2013). Investigating tubulin posttranslational modifications with specific antibodies. *Methods Cell Biol, 115*, 247-267. doi:10.1016/B978-0-12-407757-7.00016-5

Mali, G. R., Ali, F. A., Lau, C. K., Begum, F., Boulanger, J., Howe, J. D., . . . Carter, A. P. (2021a). Shulin packages axonemal outer dynein arms for ciliary targeting. *Science, 371*(6532), 910. doi:10.1126/science.abe0526

Mali, G. R., Ali, F. A., Lau, C. K., Begum, F., Boulanger, J., Howe, J. D., . . . Carter, A. P. (2021b). Shulin packages axonemal outer dynein arms for ciliary targeting. *Science, 371*(6532), 910-916. doi:10.1126/science.abe0526

Marshall, W. F. (2008). Chapter 1 Basal Bodies: Platforms for Building Cilia. In *Current Topics in Developmental Biology* (Vol. 85, pp. 1-22): Academic Press.

Marshall, W. F., H., Q., Rodrigo Brenni, M., & Rosenbaum, J. L. (2005). Flagellar length control system: testing a simple model based on intraflagellar transport and turnover. *Mol Biol Cell, 16*(1), 270-278. doi:10.1091/mbc.e04-07-0586

Meves, F. (1899). Ueber den Einfluss der Zellteilung auf den Sekretionsvorgang, nach Beobachtungen an der Niere der Salamanderlarve. In *Festschrift zum Siebenzigsten Geburtstag von Carl von Kupffer* (pp. 57-62). Gustav Fischer, Jena.

Mitchell, D. R., & Kang, Y. (1991). Identification of oda6 as a Chlamydomonas dynein mutant by rescue with the wild-type gene. *J Cell Biol, 113*(4), 835-842. doi:DOI 10.1083/jcb.113.4.835

Molla-Herman, A., Ghossoub, R., Blisnick, T., Meunier, A., Serres, C., Silbermann, F., . . . Benmerah, A. (2010). The ciliary pocket: an endocytic membrane domain at the base of primary and motile cilia. *Journal of Cell Science, 123*(10), 1785-1795. doi:10.1242/jcs.059519

Moon, K., Ma, J. H., Min, H., Koo, H., Kim, H., Ko, H. W., & Bok, J. (2020). Dysregulation of sonic hedgehog signaling causes hearing loss in ciliopathy mouse models. *Elife, 9*, e56551. doi:10.7554/eLife.56551

Moore, D. J., A., O., Shoemark, A., Simpson, M. A., zur Lage, P. I., de Castro, S. C., . . . Mitchison, H. M. (2013). Mutations in ZMYND10, a gene essential for proper axonemal assembly of inner and outer dynein arms in humans and flies, cause primary ciliary dyskinesia. *Am J Hum Genet., 93*(2), 346-356. doi:10.1016/j.ajhg.2013.07.009

Müller, O. F. (1786). *Animalcula infusoria; fluvia tilia et marina, que detexit, systematice descripsit et ad vivum delineari curavit*: Molleri, Havniae.

N, K., & Flavin, M. (1981). Preferential action of a brain detyrosinolating carboxypeptidase on polymerized tubulin. *J Biol Chem, 256*(14), 7678-7686.

Nigg, E. A., & Raff, J. W. (2009). Centrioles, Centrosomes, and Cilia in Health and Disease. *Cell, 139*(4), 663-678. doi:10.1016/j.cell.2009.10.036

Norrander, J. M., A.M., d. C., Brown, J. A., Porter, M. E., & Linck, R. W. (2000). The Rib43a protein is associated with forming the specialized protofilament ribbons of flagellar microtubules in Chlamydomonas. *Mol Biol Cell, 11*(1), 201-215. doi:DOI 10.1091/mbc.11.1.201

North, B. J., B.L., M., Borra, M. T., Denu, J. M., & Verdin, E. (2003). The human Sir2 ortholog, SIRT2, is an NAD+-dependent tubulin deacetylase. *Mol Cell, 11*(2), 437-444. doi:Doi 10.1016/S1097-2765(03)00038-8

Numata, N., Kon, T., Shima, T., Imamula, K., Mogami, T., Ohkura, R., . . . Sutoh, K. (2008). Molecular mechanism of force generation by dynein, a molecular motor belonging to the AAA+ family. *Biochemical Society Transactions, 36*(1), 131-135. doi:10.1042/BST0360131

O'Hagan, R., B.P., P., Silva, M., Phirke, P., Nguyen, K. C. Q., Hall, D. H., . . . Barr, M. M. (2011). The tubulin deglutamylase CCPP-1 regulates the function and stability of sensory cilia in C. elegans. *Curr Biol, 21*(20), 1685-1694. doi:10.1016/j.cub.2011.08.049

O'Hagan, R., & Barr, M. M. (2012). Regulation of tubulin glutamylation plays cell-specific roles in the function and stability of sensory cilia. *Worm, 1*(3), 155-159. doi:10.4161/worm.19539

Oda, T., Abe, T., Yanagisawa, H., & Kikkawa, M. (2016). Docking-complex-independent alignment of Chlamydomonas outer dynein arms with 24-nm periodicity in vitro. *J Cell Sci, 129*(8), 1547-1551. doi:10.1242/jcs.184598

Oda, T., Abe, T., Yanagisawa, H., & Kikkawa, M. (2016). Structure and function of outer dynein arm intermediate and light chain complex. *Mol Biol Cell, 27*(7), 1051-1059. doi:10.1091/mbc.E15-10-0723

Oda, T., Yagi, T., Yanagisawa, H., & Kikkawa, M. (2013). Identification of the Outer-Inner Dynein Linker as a Hub Controller for Axonemal Dynein Activities. *Current Biology, 23*(8), 656-664. doi:https://doi.org/10.1016/j.cub.2013.03.028

Ogawa, K. (1991). Four ATP-binding sites in the midregion of the beta heavy chain of dynein. *Nature, 352*(6336), 643-645. doi:10.1038/352643a0

Ohta, S., Hamada, M., Sato, N., & Toramoto, I. (2015). Polyglutamylated Tubulin Binding Protein C1orf96/CSAP Is Involved in Microtubule Stabilization in Mitotic Spindles. *PLOS ONE*.

Ohta, S., Hamada, M., Sato, N., & Toramoto, I. (2015). Polyglutamylated Tubulin Binding Protein C1orf96/CSAP Is Involved in Microtubule Stabilization in Mitotic Spindles. *PLOS ONE, 10*(11), e0142798. doi:10.1371/journal.pone.0142798

Olbrich, H., K., H., Kispert, A., Völkel, A., Volz, A., Sasmaz, G., . . . Omran, H. (2002). Mutations in DNAH5 cause primary ciliary dyskinesia and randomization of left-right asymmetry. *Nat Genet, 30*(2), 143-144. doi:10.1038/ng817

Olbrich, H., M., F., Hoefele, J., Kispert, A., Otto, E., Volz, A., . . . Omran, H. (2003). Mutations in a novel gene, NPHP3, cause adolescent nephronophthisis, tapeto-retinal degeneration and hepatic fibrosis. *Nat Genet, 34*(4), 455-459. doi:10.1038/ng1216

Omran, H., D., K., Olbrich, H., Tsukahara, T., Loges, N. T., Hagiwara, H., . . . Takeda, H. (2008). Ktu/PF13 is required for cytoplasmic pre-assembly of axonemal dyneins. *Nature, 456*(7222), 611-616. doi:10.1038/nature07471

Omran, H., K., H., Völkel, A., Kuehr, J., Ketelsen, U. P., Ross, U. H., . . . Hildebrandt, F. (2000). Homozygosity mapping of a gene locus for primary ciliary dyskinesia on chromosome 5p and identification of the heavy dynein chain DNAH5 as a candidate gene. *Am J Respir Cell Mol Biol, 23*(5), 696-702.

Onoufriadis, A., A, S., Munye, M. M., James, C. T., Schmidts, M., Patel, M., . . . Mitchison, H. M. (2014). Combined exome and whole-genome sequencing identifies mutations in ARMC4 as a cause of primary ciliary dyskinesia with defects in the outer dynein arm. *J Med Genet, 51*(1), 61-67. doi:10.1136/jmedgenet-2013-101938

Onoufriadis, A., T., P., Antony, D., Shoemark, A., Micha, D., Kuyt, B., . . . Mitchison, H. M. (2013). Splice-site mutations in the axonemal outer dynein arm docking complex gene CCDC114 cause primary ciliary dyskinesia. *American journal of human genetics, 92*(1), 88-98. doi:10.1016/j.ajhg.2012.11.002

Orts-Del'Immagine, A., & Wyart, C. (2017). Cerebrospinal-fluid-contacting neurons. *Curr Biol, 27*(22), R1198-r1200. doi:10.1016/j.cub.2017.09.017

Owa, M., Furuta, A., Usukura, J., Arisaka, F., King, S. M., Witman, G. B., . . . Wakabayashi, K.-i. (2014). Cooperative binding of the outer arm-docking complex underlies the regular arrangement of outer arm dynein in the axoneme. *Proceedings of the National Academy of Sciences, 111*(26), 9461. doi:10.1073/pnas.1403101111

Owa, M., Uchihashi, T., Yanagisawa, H.-a., Yamano, T., Iguchi, H., Fukuzawa, H., . . . Kikkawa, M. (2019). Inner lumen proteins stabilize doublet microtubules in cilia and flagella. *Nature Communications, 10*(1), 1143. doi:10.1038/s41467-019-09051-x

Pan, J., Q., W., & Snell, W. J. (2004). An aurora kinase is essential for flagellar disassembly in Chlamydomonas. *Dev Cell, 6*(3), 445-451.

Pan, J., & Snell, W. J. (2005). Chlamydomonas shortens its flagella by activating axonemal disassembly, stimulating IFT particle trafficking, and blocking anterograde cargo loading. *Dev Cell, 9*(3), 431-438. doi:10.1016/j.devcel.2005.07.010

Parker, J. D., L.K., H., Diener, D. R., Rasi, M. Q., Mahjoub, M. R., Rosenbaum, J. L., & Quarmby, L. M. (2010). Centrioles are freed from cilia by severing prior to mitosis. *Cytoskeleton (Hoboken), 67*(7), 425-430. doi:10.1002/cm.20454

Pathak, N., Austin-Tse, C. A., Liu, Y., Vasilyev, A., & Drummond, I. A. (2014). Cytoplasmic carboxypeptidase 5 regulates tubulin glutamylation and zebrafish cilia formation and function. *Mol Biol Cell, 25*(13), 1836-1844. doi:10.1091/mbc.E13-01-0033

Pathak, N., C.A., A., & Drummond, I. A. (2011). Tubulin tyrosine ligase-like genes ttll3 and ttll6 maintain zebrafish cilia structure and motility. *J Biol Chem, 286*(13), 11685-11695. doi:10.1074/jbc.M110.209817

Pathak, N., Obara, T., Mangos, S., Liu, Y., & Drummond, I. A. (2007). The zebrafish fleer gene encodes an essential regulator of cilia tubulin polyglutamylation. *Mol Biol Cell, 18*(11), 4353-4364. doi:10.1091/mbc.e07-06-0537

Pazour, G. J., Agrin, N., Leszyk, J., & Witman, G. B. (2005). Proteomic analysis of a eukaryotic cilium. *The Journal of Cell Biology, 170*(1), 103-113. doi:10.1083/jcb.200504008

Pazour, G. J., S.A., B., Deane, J. A., Cole, D. G., Dickert, B. L., Rosenbaum, J. L., . . . Besharse, J. C. (2002). The intraflagellar transport protein, IFT88, is essential for vertebrate photoreceptor assembly and maintenance. *J Cell Biol, 157*(1), 103-113. doi:10.1083/jcb.200107108

Pedersen, L. B., M.S., M., Geimer, S., Leitch, J. M., Rosenbaum, J. L., & Cole, D. G. (2005). Chlamydomonas IFT172 is encoded by FLA11, interacts with CrEB1, and regulates IFT at the flagellar tip. *Curr Biol., 15*(3), 262-266. doi:DOI 10.1016/j.cub.2005.01.037

Pennarun, G., C., C., Escudier, E., Bridoux, A. M., Dastot, F., Cacheux, V., . . . Duriez, B. (2000). The human dynein intermediate chain 2 gene (DNAI2): cloning, mapping, expression pattern, and evaluation as a candidate for primary ciliary dyskinesia. *Hum Genet., 107*(6), 642-649.

Pennarun, G., E., E., Chapelin, C., Bridoux, A. M., Cacheux, V., Roger, G., . . . Duriez, B. (1999). Loss-of-function mutations in a human gene related to Chlamydomonas reinhardtii dynein IC78 result in primary ciliary dyskinesia. *Am J Hum Genet., 65*(6), 1508-1519. doi:10.1086/302683

Per Hellung-larsen, V. L., and Niels Tommerup. (1986). Chemoattraction in Tetrahymena: on the role of chemokinesis. *The Biological Bulletin, 170*(3), 357-367. doi:https://doi.org/10.2307/1541847

Peris, L., M, W., Lafanechère, L., Brocard, J., Moore, A. T., Kozielski, F., . . . Andrieux, A. (2009). Motor-dependent microtubule disassembly driven by tubulin tyrosination. *J Cell Biol, 41*(6), 546-553. doi:10.1083/jcb.200902142

Piao, T., M., L., Wang, L., Guo, Y., Li, D., Li, P., . . . Pan, J. (2009). A microtubule depolymerizing kinesin functions during both flagellar disassembly and flagellar assembly in Chlamydomonas. *Proc Natl Acad Sci U S A, 106*(12), 4713-4718. doi:10.1073/pnas.0808671106

Porter, M. E., & Sale, W. S. (2000). The 9 + 2 axoneme anchors multiple inner arm dyneins and a network of kinases and phosphatases that control motility. *J Cell Biol, 151*(5), F37-42. doi:10.1083/jcb.151.5.f37

Portran, D., Schaedel, L., Xu, Z., Théry, M., & Nachury, M. (2017). Tubulin acetylation protects long-lived microtubules against mechanical ageing. *Nat Cell Biol, 19*(4), 391-398. doi:10.1038/ncb3481

Praveen, K., Davis, E. E., & Katsanis, N. (2015). Unique among ciliopathies: primary ciliary dyskinesia, a motile cilia disorder. *F1000Prime Rep, 7*, 36. doi:10.12703/P7-36

Prota, A. E., Magiera, M. M., Kuijpers, M., Bargsten, K., Frey, D., Wieser, M., . . . Steinmetz, M. O. (2013). Structural basis of tubulin tyrosination by tubulin tyrosine ligase. *J Cell Biol, 200*(3), 259-270. doi:10.1083/jcb.201211017

Pugacheva, E. N., Jablonski, S. A., Hartman, T. R., Henske, E. P., & Golemis, E. A. (2007). HEF1-dependent Aurora A activation induces disassembly of the primary cilium. *Cell, 129*(7), 1351-1363. doi:10.1016/j.cell.2007.04.035

Ran, J., Yang, Y., Li, D., Liu, M., & Zhou, J. (2015). Deacetylation of α-tubulin and cortactin is required for HDAC6 to trigger ciliary disassembly. *Sci Rep, 5*, 12917.

Redeker, V., Le Caer, J. P., Rossier, J., & Prome, J. C. (1991). Structure of the polyglutamyl side chain posttranslationally added to alpha-tubulin. *J Biol Chem, 266*(34), 23461-23466. Retrieved from https://www.ncbi.nlm.nih.gov/pubmed/1720781

Redeker, V., Levilliers, N., Vinolo, E., Rossier, J., Jaillard, D., Burnette, D., . . . Bré, M.-H. (2005). Mutations of Tubulin Glycylation Sites Reveal Cross-talk between the C Termini of α- and β-Tubulin and Affect the Ciliary Matrix in Tetrahymena*. *Journal of Biological Chemistry, 280*(1), 596-606. doi:https://doi.org/10.1074/jbc.M408324200

Redeker, V., Melki R - Promé, D., Promé D - Le Caer, J. P., Le Caer Jp - Rossier, J., & Rossier, J. (1992). Structure of tubulin C-terminal domain obtained by subtilisin treatment. The major alpha and beta tubulin isotypes from pig brain are glutamylated. *FEBS Lett*

. *313*(2), 185-192. doi:Doi 10.1016/0014-5793(92)81441-N

Redeker, V., N., L., Schmitter, J. M., Le Caer, J. P., Rossier, J., Adoutte, A., & Bré, M. H. (1994). Polyglycylation of tubulin: a posttranslational modification in axonemal microtubules. *Science, 266*(5191), 1688-1691. doi:10.1126/science.7992051

Reed, N. A., Cai, D., Blasius, T. L., Jih, G. T., Meyhofer, E., Gaertig, J., & Verhey, K. J. (2006). Microtubule Acetylation Promotes Kinesin-1 Binding and Transport. *Current Biology, 16*(21), 2166-2172. doi:https://doi.org/10.1016/j.cub.2006.09.014

Regnard, C., Fesquet, D., Janke, C., Boucher, D., Desbruyeres, E., Koulakoff, A., . . . Edde, B. (2003). Characterisation of PGs1, a subunit of a protein complex co-purifying with tubulin polyglutamylase. *J Cell Sci, 116*(Pt 20), 4181-4190. doi:10.1242/jcs.00743

Reiter, J. F., Blacque, O. E., & Leroux, M. R. (2012). The base of the cilium: roles for transition fibres and the transition zone in ciliary formation, maintenance and compartmentalization. *EMBO reports, 13*(7), 608-618. doi:10.1038/embor.2012.73

Reiter, J. F., & Leroux, M. R. (2017). Genes and molecular pathways underpinning ciliopathies. *Nature Reviews Molecular Cell Biology, 18*(9), 533-547. doi:10.1038/nrm.2017.60

Ren, Y. Z., Jinghui; Feng, Jian. (2003). Parkin Binds to α/β Tubulin and Increases their Ubiquitination and Degradation. *The Journal of Neuroscience, 23*(8), 3316-3324.

Rocha, C., Papon, L., Cacheux, W., Marques Sousa, P., Lascano, V., Tort, O., . . . Janke, C. (2014). Tubulin glycylases are required for primary cilia, control of cell proliferation and tumor development in colon. *EMBO J, 33*(19), 2247-2260. doi:10.15252/embj.201488466

Rogowski, K., Francois, J., van Dijk, J., Wloga, D., Strub, J.-M., Levilliers, N., . . . Janke, C. (2019). Evolutionary divergence of enzymatic mechanisms for posttranslational polyglycylation. *Cell, 137*(6), 1076-1087.

Rogowski, K., van Dijk, J., Magiera, M. M., Bosc, C., Deloulme, J.-C., Bosson, A., . . . Janke, C. (2010). A family of protein-deglutamylating enzymes associated with neurodegeneration. *Cell, 143*(4), 564-578. doi:10.1016/j.cell.2010.10.014

Rohatgi, R., Milenkovic L - Scott, M. P., & Scott, M. P. (2007). Patched1 regulates hedgehog signaling at the primary cilium. *Science, 317*(5836), 372-376. doi:10.1126/science.1139740

Roll-Mecak, A. (2015). Intrinsically disordered tubulin tails: complex tuners of microtubule functions? *Semin Cell Dev Biol, 37*, 11-19. doi:10.1016/j.semcdb.2014.09.026

S.W., L. H., & Rosenbaum, J. L. (1983). Chlamydomonas alpha-tubulin is posttranslationally modified in the flagella during flagellar assembly. *J Cell Biol. , 97*(1), 258-263.

Sakato, M., & King, S. M. (2004). Design and regulation of the AAA+ microtubule motor dynein. *J Struct Biol, 146*(1-2), 58-71. doi:10.1016/j.jsb.2003.09.026

Samso, M., Radermacher, M., Frank, J., & Koonce, M. P. (1998). Structural characterization of a dynein motor domain. *J Mol Biol, 276*(5), 927-937. doi:10.1006/jmbi.1997.1584

Satir, B. H., Reichman, M., & Orias, E. (1986). Conjugation rescue of an exocytosis-competent membrane microdomain in Tetrahymena thermophila mutants. *Proc Natl Acad Sci U S A, 83*(21), 8221-8225. doi:10.1073/pnas.83.21.8221

Sayer, J. A., Otto, E. A., O'Toole, J. F., Nurnberg, G., Kennedy, M. A., Becker, C., . . . Hildebrandt, F. (2006). The centrosomal protein nephrocystin-6 is mutated in Joubert syndrome and activates transcription factor ATF4. *Nature Genetics, 38*(6), 674-681. doi:10.1038/ng1786

Schaap, I. A. T., Carrasco, C., de Pablo, P. J., MacKintosh, F. C., & Schmidt, C. F. (2006). Elastic Response, Buckling, and Instability of Microtubules under Radial Indentation. *Biophysical Journal, 91*(4), 1521-1531. doi:https://doi.org/10.1529/biophysj.105.077826

Schaedel, L., John, K., Gaillard, J., Nachury, M. V., Blanchoin, L., & Théry, M. (2015). Microtubules self-repair in response to mechanical stress. *Nat Mater., 14*(11), 1156-1163. doi:D - NLM: EMS64433 EDAT- 2015/09/08 06:00 MHDA- 2016/01/26 06:00 CRDT- 2015/09/08 06:00 PHST- 2014/12/11 00:00 [received] PHST- 2015/07/24 00:00 [accepted] PHST- 2015/09/08 06:00 [entrez] PHST- 2015/09/08 06:00 [pubmed] PHST- 2016/01/26 06:00 [medline] AID - nmat4396 [pii] AID - 10.1038/nmat4396 [doi] PST - ppublish

Schröder Hc - Wehland, J., Wehland J - Weber, K., & Weber, K. (1985). Purification of brain tubulin-tyrosine ligase by biochemical and immunological methods. *J Cell Biol, 100*(1), 276-281.

Serluca, F. C., Xu, B., Okabe, N., Baker, K., Lin, S. Y., Sullivan-Brown, J., . . . Burdine, R. D. (2009). Mutations in zebrafish leucine-rich repeat-containing six-like affect cilia motility and result in pronephric cysts, but have variable effects on left-right patterning. *Development, 136*(10), 1621-1631. doi:10.1242/dev.020735

Shah, A. S., Ben-Shahar, Y., Moninger, T. O., Kline, J. N., & Welsh, M. J. (2009). Motile cilia of human airway epithelia are chemosensory. *Science, 325*(5944), 1131-1134. doi:10.1126/science.1173869

Shah, N., Kumar, S., Zaman, N., Pan, C. C., Bloodworth, J. C., Lei, W., . . . Lee, N. Y. (2018). TAK1 activation of alpha-TAT1 and microtubule hyperacetylation control AKT signaling and cell growth. *Nat Commun, 9*(1), 1696. doi:10.1038/s41467-018-04121-y

Shang, Y., Inthavong, K., & Tu, J. (2019). Development of a computational fluid dynamics model for mucociliary clearance in the nasal cavity. *Journal of Biomechanics, 85*, 74-83. doi:https://doi.org/10.1016/j.jbiomech.2019.01.015

Sharma, N., Bryant, J., Wloga, D., Donaldson, R., Davis, R. C., Jerka-Dziadosz, M., & Gaertig, J. (2007). Katanin regulates dynamics of microtubules and biogenesis of motile cilia. *J Cell Biol, 178*(6), 1065-1079. doi:10.1083/jcb.200704021

Shida, T., Cueva, J. G., Xu, Z., Goodman, M. B., & Nachury, M. V. (2010). The major alpha-tubulin K40 acetyltransferase alphaTAT1 promotes rapid ciliogenesis and efficient mechanosensation. *Proc Natl Acad Sci U S A, 107*(50), 21517-21522. doi:10.1073/pnas.1013728107

Singh, S., Adam, M., Matkar, P. N., Bugyei-Twum, A., Desjardins, J. F., Chen, H. H., . . . Singh, K. K. (2020). Endothelial-specific Loss of IFT88 Promotes Endothelial-to-Mesenchymal Transition and Exacerbates Bleomycin-induced Pulmonary Fibrosis. *Sci Rep, 10*(1), 4466. doi:10.1038/s41598-020-61292-9

Sirajuddin, M., Rice, L. M., & Vale, R. D. (2014). Regulation of microtubule motors by tubulin isotypes and post-translational modifications. *Nat Cell Biol, 16*(4), 335-344. doi:10.1038/ncb2920

Sjoblom, T., Jones, S., Wood, L. D., Parsons, D. W., Lin, J., Barber, T. D., . . . Velculescu, V. E. (2006). The consensus coding sequences of human breast and colorectal cancers. *Science, 314*(5797), 268-274. doi:10.1126/science.1133427

Sjostrand, F. S. The ultrastructure of the outer segments of rods and cones of the eye as revealed by the electron microscope. (0095-9898 (Print)). doi:D - CLML: 5425:5456:294:405 OTO - NLM

Sjostrand, F. S. (1953). The ultrastructure of the innersegments of the retinal rods of the guinea pig eye as revealed by electron microscopy. *J Cell Comp Physiol, 42*(1), 45-70. doi:D - CLML: 5425:5457:294:405 OTO - NLM

Song, Y., Kirkpatrick, L. L., Schilling, A. B., Helseth, D. L., Chabot, N., Keillor, J. W., . . . Brady, S. T. (2013). Transglutaminase and polyamination of tubulin: posttranslational modification for stabilizing axonal microtubules. *Neuron, 78*(1), 109-123. doi:10.1016/j.neuron.2013.01.036

Sorokin, S. (1962). Centrioles and the formation of rudimentary cilia by fibroblasts and smooth muscle cells. *The Journal of Cell Biology, 15*(2), 363-377. doi:10.1083/jcb.15.2.363

Sorokin, S. P. (1968). Reconstructions of Centriole Formation and Ciliogenesis in Mammalian Lungs. *Journal of Cell Science, 3*(2), 207-230. doi:10.1242/jcs.3.2.207

Spennato, P., Mirone, G., Nastro, A., Buonocore, M. C., Ruggiero, C., Trischitta, V., . . . Cinalli, G. (2011). Hydrocephalus in Dandy-Walker malformation. *Childs Nerv Syst, 27*(10), 1665-1681. doi:10.1007/s00381-011-1544-4

Stambolliu, E., Ioakeim-Ioannidou, M., Kontokostas, K., Dakoutrou, M., & Kousoulis, A. A. (2017). The Most Common Comorbidities in Dandy-Walker Syndrome Patients: A Systematic Review of Case Reports. *Journal of Child Neurology, 32*(10), 886-902. doi:10.1177/0883073817712589

Stepanek, L., & Pigino, G. (2016). Microtubule doublets are double-track railways for intraflagellar transport trains. *Science, 352*(6286), 721-724. doi:10.1126/science.aaf4594

Stevens, E. M., Vladar, E. K., Alanin, M. C., Christensen, S. T., von Buchwald, C., & Milla, C. (2020). Ciliary Localization of the Intraflagellar Transport Protein IFT88 Is Disrupted in Cystic Fibrosis. *American Journal of Respiratory Cell and Molecular Biology, 62*(1), 120-123. doi:DOI 10.1165/rcmb.2018-0287LE

Stillwell, P. C., Wartchow, E. P., & Sagel, S. D. (2011). Primary Ciliary Dyskinesia in Children: A Review for Pediatricians, Allergists, and Pediatric Pulmonologists. *Pediatr Allergy Immunol Pulmonol, 24*(4), 191-196. doi:10.1089/ped.2011.0099

Stoddard, D., Zhao, Y., Bayless, B. A., Gui, L., Louka, P., Dave, D., . . . Nicastro, D. (2018). Tetrahymena RIB72A and RIB72B are microtubule inner proteins in the ciliary doublet microtubules. *Molecular Biology of the Cell, 29*(21), 2566-2577. doi:10.1091/mbc.E18-06-0405

Suryavanshi, S., Eddé, B., Fox, L. A., Guerrero, S., Hard, R., Hennessey, T., . . . Gaertig, J. (2010). Tubulin Glutamylation Regulates Ciliary Motility by Altering Inner Dynein Arm Activity. *Current Biology, 20*(5), 435-440. doi:https://doi.org/10.1016/j.cub.2009.12.062

Szyk, A., Deaconescu, A. M., Piszczek, G., & Roll-Mecak, A. (2011). Tubulin tyrosine ligase structure reveals adaptation of an ancient fold to bind and modify tubulin. *Nat Struct Mol Biol, 18*(11), 1250-1258. doi:10.1038/nsmb.2148

Ta-Shma, A., Perles, Z., Yaacov, B., Werner, M., Frumkin, A., Rein, A. J., & Elpeleg, O. (2015). A human laterality disorder associated with a homozygous WDR16 deletion. *Eur J Hum Genet, 23*(9), 1262-1265. doi:10.1038/ejhg.2014.265

Takano, K., Nakamoto, T., Okajima, M., Sudo, A., Uetake, K., & Saitoh, S. (2003). Cerebellar and brainstem involvement in familial juvenile nephronophthisis type I. *Pediatr Neurol, 28*(2), 142-144. doi:10.1016/s0887-8994(02)00619-7

Tallila, J., Jakkula, E., Peltonen, L., Salonen, R., & Kestila, M. (2008). Identification of CC2D2A as a Meckel syndrome gene adds an important piece to the ciliopathy puzzle. *American journal of human genetics, 82*(6), 1361-1367. doi:10.1016/j.ajhg.2008.05.004

Tanos, B. E., Yang, H. J., Soni, R., Wang, W. J., Macaluso, F. P., Asara, J. M., & Tsou, M. F. (2013). Centriole distal appendages promote membrane docking, leading to cilia initiation. *Genes & development, 27*(2), 163-168. doi:10.1101/gad.207043.112

Tarkar, A., Loges, N. T., Slagle, C. E., Francis, R., Dougherty, G. W., Tamayo, J. V., . . . Uk10k. (2013). DYX1C1 is required for axonemal dynein assembly and ciliary motility. *Nature Genetics, 45*(9), 995-+. doi:10.1038/ng.2707

Thivierge, C., Kurbegovic A - Couillard, M., Couillard M - Guillaume, R., Guillaume R - Coté, O., Coté O - Trudel, M., & Trudel, M. (2006). Overexpression of PKD1 causes polycystic kidney disease. *Mol Cell Biol, 26*(4), 1538-1548. doi:10.1128/MCB.26.4.1538-1548.2006

Tokuyasu K - Yamada, E., & Yamada, E. (1959). The fine structure of the retina studied with the electron microscope. IV. Morphogenesis of outer segments of retinal rods. *J Biophys Biochem Cytol., 6*(2), 225-230.

Tsao, C. C., & Gorovsky, M. A. (2008). Different effects of Tetrahymena IFT172 domains on anterograde and retrograde intraflagellar transport. *Mol Biol Cell, 19*(4), 1450-1461. doi:10.1091/mbc.E07-05-0403

Tynan, S. H., Gee, M. A., & Vallee, R. B. (2000). Distinct but overlapping sites within the cytoplasmic dynein heavy chain for dimerization and for intermediate chain and light intermediate chain binding. *Journal of Biological Chemistry, 275*(42), 32769-32774. doi:DOI 10.1074/jbc.M001537200

Valenstein, M. L., & Roll-Mecak, A. (2016). Graded Control of Microtubule Severing by Tubulin Glutamylation. *Cell, 164*(5), 911-921. doi:10.1016/j.cell.2016.01.019

van Dijk, J., Rogowski, K., Miro, J., Lacroix, B., Edde, B., & Janke, C. (2007). A targeted multienzyme mechanism for selective microtubule polyglutamylation. *Mol Cell, 26*(3), 437-448. doi:10.1016/j.molcel.2007.04.012

Verhey, K. J. G., J. . (2007). The Tubulin Code. *Cell Cycle, 6*(17), 2152-2160. doi:10.4161/cc.6.17.4633

Wakabayashi, K., & King, S. M. (2006). Modulation of Chlamydomonas reinhardtii flagellar motility by redox poise. *J Cell Biol, 173*(5), 743-754. doi:10.1083/jcb.200603019

Walczak-Sztulpa, J., Eggenschwiler, J., Osborn, D., Brown, D. A., Emma, F., Klingenberg, C., . . . Kuss, A. W. (2010). Cranioectodermal Dysplasia, Sensenbrenner Syndrome, Is a Ciliopathy Caused by Mutations in the IFT122 Gene. *American journal of human genetics, 86*(6), 949-956. doi:10.1016/j.ajhg.2010.04.012

Walter, L. (1929). Ciliogenesis in a cystically dilated hydatid of Morgagni. *Anat. Rec., 42*(2), 177-187. doi:DOI 10.1002/ar.1090420208

Walter, W. J., V., B., Fischermeier, E., & Diez, S. (2012). Tubulin acetylation alone does not affect kinesin-1 velocity and run length in vitro. *PLOS ONE, 7*(8), e42218.

Walton, T., Wu, H., & Brown, A. (2021). Structure of a microtubule-bound axonemal dynein. *Nature Communications, 12*(1), 477. doi:10.1038/s41467-020-20735-7

Wang, A. (2011). TMEM216 joins its ciliary cousins in ciliopathies. *Clin Genet, 79*(1), 45-47. doi:10.1111/j.1399-0004.2010.01556_2.x

Wang, B., Fallon, J. F., & Beachy, P. A. (2000). Hedgehog-regulated processing of Gli3 produces an anterior/posterior repressor gradient in the developing vertebrate limb. *Cell, 100*(4), 423-434. doi:10.1016/s0092-8674(00)80678-9

Wang, W., & Brautigan, D. L. (2008). Phosphatase inhibitor 2 promotes acetylation of tubulin in the primary cilium of human retinal epithelial cells. *BMC Cell Biol, 9*, 62. doi:10.1186/1471-2121-9-62

Welcome to the Ciliopathy Alliance. (2020). Retrieved from https://www.ciliopathyalliance.org/

West, A. B., Lockhart, P. J., O'Farell, C., & Farrer, M. J. (2003). Identification of a novel gene linked to parkin via a bi-directional promoter. *J Mol Biol, 326*(1), 11-19. doi:10.1016/s0022-2836(02)01376-1

Wilkerson, C. G., King, S. M., Koutoulis, A., Pazour, G. J., & Witman, G. B. (1995). The 78,000 M(r) intermediate chain of Chlamydomonas outer arm dynein isa WD-repeat protein required for arm assembly. *J Cell Biol, 129*(1), 169-178. doi:10.1083/jcb.129.1.169

Wilson, G. R., Wang, H. X., Egan, G. F., Robinson, P. J., Delatycki, M. B., O'Bryan, M. K., & Lockhart, P. J. (2010). Deletion of the Parkin co-regulated gene causes defects in ependymal ciliary motility and hydrocephalus in the quakingviable mutant mouse. *Human Molecular Genetics, 19*(8), 1593-1602. doi:10.1093/hmg/ddq031

Wloga, D., Dave, D., Meagley, J., Rogowski, K., Jerka-Dziadosz, M., & Gaertig, J. (2010). Hyperglutamylation of Tubulin Can either Stabilize or Destabilize Microtubules in the Same Cell. *Eukaryotic Cell, 9*(1), 184-193. doi:10.1128/Ec.00176-09

Wloga, D., Joachimiak, E., Louka, P., & Gaertig, J. (2017a). Posttranslational Modifications of Tubulin and Cilia. *Cold Spring Harbor perspectives in biology, 9*(6). doi:10.1101/cshperspect.a028159

Wloga, D., Joachimiak, E., Louka, P., & Gaertig, J. (2017b). Posttranslational Modifications of Tubulin and Cilia. *Cold Spring Harb Perspect Biol.*(1943-0264 (Electronic)).

Wloga, D., K., R., Sharma, N., Sharma N - Van Dijk J - Janke, C., Eddé, B., Bré, M.-H., . . . Gaertig, J. (2008). Glutamylation on alpha-tubulin is not essential but affects the assembly and functions of a subset of microtubules in Tetrahymena thermophila. *Eukaryot Cell, 7*(8), 1362-1372.

Wloga, D., Webster, D. M., Rogowski, K., Bre, M. H., Levilliers, N., Jerka-Dziadosz, M., . . . Gaertig, J. (2009). TTLL3 Is a Tubulin Glycine Ligase that Regulates the Assembly of Cilia. *Developmental Cell, 16*(6), 867-876. doi:10.1016/j.devcel.2009.04.008

Xia, L., Hai, B., Gao, Y., Burnette, D., Thazhath, R., Duan, J., . . . Gaertig, J. (2000). Polyglycylation of tubulin is essential and affects cell motility and division in Tetrahymena thermophila. *Journal of Cell Biology, 149*(5), 1097-1106. doi:DOI 10.1083/jcb.149.5.1097

Xu, Z. J., Schaedel, L., Portran, D., Aguilar, A., Gaillard, J., Marinkovich, M. P., . . . Nachury, M. V. (2017). Microtubules acquire resistance from mechanical breakage through intralumenal acetylation. *Science, 356*(6335), 328-332. doi:10.1126/science.aai8764

Yamamoto, R., Hirono, M., & Kamiya, R. (2010). Discrete PIH proteins function in the cytoplasmic preassembly of different subsets of axonemal dyneins. *J Cell Biol, 190*(1), 65-71. doi:10.1083/jcb.201002081

Yamamoto, R., Song, K. K., Yanagisawa, H., Fox, L., Yagi, T., Wirschell, M., . . . Sale, W. S. (2013). The MIA complex is a conserved and novel dynein regulator essential for normal ciliary motility. *Journal of Cell Biology, 201*(2), 263-278. doi:10.1083/jcb.201211048

Yanagisawa, H., Mathis, G., Oda, T., Hirono, M., Richey, E. A., Ishikawa, H., . . . Qin, H. M. (2014). FAP20 is an inner junction protein of doublet microtubules essential for both the planar asymmetrical waveform and stability of flagella in Chlamydomonas. *Molecular Biology of the Cell, 25*(9), 1472-1483. doi:10.1091/mbc.E13-08-0464

Yang, Y., Ran, J., Liu, M., Li, D., Li, Y., Shi, X., . . . Zhou, J. (2014). CYLD mediates ciliogenesis in multiple organs by deubiquitinating Cep70 and inactivating HDAC6. *Cell Res, 24*(11), 1342-1353. doi:10.1038/cr.2014.136

Ye, F., Nager, A. R., & Nachury, M. V. (2018). BBSome trains remove activated GPCRs from cilia by enabling passage through the transition zone. *J Cell Biol, 217*(5), 1847-1868. doi:10.1083/jcb.201709041

Yoder, B. K. (2007). Role of primary cilia in the pathogenesis of polycystic kidney disease. *J Am Soc Nephrol, 18*(5), 1381-1388. doi:10.1681/ASN.2006111215

Zambito, A. M., & Wolff, J. (1997). Palmitoylation of tubulin. *Biochem Biophys Res Commun, 239*(3), 650-654. doi:10.1006/bbrc.1997.7525

Zariwala, M. A., Gee, H. Y., Kurkowiak, M., Al-Mutairi, D. A., Leigh, M. W., Hurd, T. W., . . . Hildebrandt, F. (2013). ZMYND10 Is Mutated in Primary Ciliary Dyskinesia and Interacts with LRRC6. *American journal of human genetics, 93*(2), 336-345. doi:10.1016/j.ajhg.2013.06.007

Zariwala, M. A., Knowles, M. R., & Omran, H. (2007). Genetic defects in ciliary structure and function. *Annu Rev Physiol, 69*, 423-450. doi:10.1146/annurev.physiol.69.040705.141301

Zariwala, M. A., Leigh, M. W., Ceppa, F., Kennedy, M. P., Noone, P. G., Carson, J. L., . . . Knowles, M. R. (2006). Mutations of DNAI1 in primary ciliary dyskinesia: evidence of founder effect in a common mutation. *Am J Respir Crit Care Med, 174*(8), 858-866. doi:10.1164/rccm.200603-370OC

Zhang, F., Su, B., Wang, C., Siedlak, S. L., Mondragon-Rodriguez, S., Lee, H. G., . . . Zhu, X. (2015). Posttranslational modifications of alpha-tubulin in alzheimer disease. *Translational neurodegeneration, 4*, 9. doi:10.1186/s40035-015-0030-4

Zhang, Q., Seo, S., Bugge, K., Stone, E. M., & Sheffield, V. C. (2012). BBS proteins interact genetically with the IFT pathway to influence SHH-related phenotypes. *Hum Mol Genet, 21*(9), 1945-1953. doi:10.1093/hmg/dds004

Zhang, R., Alushin, G. M., Brown, A., & Nogales, E. (2015). Mechanistic Origin of Microtubule Dynamic Instability and Its Modulation by EB Proteins. *Cell, 162*(4), 849-859. doi:10.1016/j.cell.2015.07.012

Zhang, W., Li, D., Wei, S., Guo, T., Wang, J., Luo, H., . . . Tan, Z. (2019). Correction: Whole-exome sequencing identifies a novel CCDC151 mutation, c.325GT (p.E109X), in a patient with primary ciliary dyskinesia and situs inversus. *J Hum Genet, 64*(8), 829. doi:10.1038/s10038-019-0624-2

Zhang, Y., Li, N., Caron, C., Matthias, G., Hess, D., Khochbin, S., & Matthias, P. (2003). HDAC-6 interacts with and deacetylates tubulin and microtubules in vivo. *EMBO J, 22*(5), 1168-1179. doi:10.1093/emboj/cdg115

Zhang, Y., Ma, C., Delohery, T., Nasipak, B., Foat, B. C., Bounoutas, A., . . . Chalfie, M. (2002). Identification of genes expressed in C. elegans touch receptor neurons. *Nature, 418*(6895), 331-335. doi:10.1038/nature00891

Zhou, X., Fan, L. X., Li, K., Ramchandran, R., Calvet, J. P., & Li, X. (2014). SIRT2 regulates ciliogenesis and contributes to abnormal centrosome amplification caused by loss of polycystin-1. *Hum Mol Genet, 23*(6), 1644-1655. doi:10.1093/hmg/ddt556

Zhu, X., Wang, J., Li, S., Lechtreck, K., & Pan, J. (2021). IFT54 directly interacts with kinesin-II and IFT dynein to regulate anterograde intraflagellar transport. *EMBO J, 40*(5), e105781. doi:10.15252/embj.2020105781

Zimmermann, K. W. (1898). Beitrage zur Kenntniss einiger Drusen und Epithelien. *Arch. Mikrosk. Anat., 52*, 552-706.

"The way of heaven is to be forever rigorous and strong, so we must strive ceaselessly towards our goals."

"The earth's terrains are vast and diverse, so we must be kind, open minded and receptive to people, things, and events. "

Ji Chang, King Wen of Zhou, 1152 – 1056 B.C.E., *I Ching/Yi Jing*

"天行健，君子以自強不息"

"地勢坤，君子以厚德載物"

周文王姬昌《易經・周易》, 前 1152 年 －前 1056 年